Facultad de Ciencias

Departamento de Biología Molecular

Influence of *Trypanosoma cruzi* and host genetic variability on Chagas disease immunopathology

Doctoral Thesis

Cristina Poveda Cuevas

Madrid, 2016

The research leading to these results has received funding from the People Programme (Marie Curie Actions) of the European Union's Seventh Framework Programme FP7/2007-2013/ under REA grant agreement n°317057.

A mis padres, hermanos y Juan Sebastián por su apoyo incondicional.

A Núria y Manolo por dirigir este trabajo.

Y al 226 por acompañarme en el proceso.

CONTENTS

ABBREVIATIONS

APC	Antigen Presenting Cells
Arg-1	Arginase-1
BSA	Bovine Serum Albumin
COX-2	Cyclooxygenase 2
DAPC	Discriminant Analysis of Principal Components
DNA	Deoxyribonucleic
d.p.i.	Days post-infection
EAT2	Ewing's sarcoma-associated transcript 2
EEA	Early endosome antigen 1
FBS	Fetal Bovine Serum
FITC	Fluorescein Isothiocyanate
GIP	Glycosylphosphatidylinositol
GIPL	Glycoinositolphospholipid
h.p.i.	Hours post-infection
HSC	Hematopoietic Stem Cells
IC_{50}	Half Maximal Inhibitory Concentration
IFN	Interferon
Ig	Immunoglobulin
IgG	Immunoglobulin G
Il	Interleukin
iNOS	Inducible Nitric Oxide Synthase
Lin	Lineage
LPS	Lipopolysaccharide
MHC	Major Histocompatibility Complex
Min	Minute
Ml	Milliliter
MTT	3-(4,5-Dimethylthiazol-2-yl)-2,5-diphenyltetrazolium bromide
MDSCs	Myeloid-derived Suppressor Cells
MyD88	Myeloid-Differentiation primary response 88
NADPH	Nicotinamide Adenine Dinucleotide Phosphate
NI	Non-infected
ND	Non-detected
NO	Nitric Oxide
NOX	NADPH Oxidase
PAMPs	Pathogen-associated molecular patterns
PBS	Phosphate Buffered Saline
PCR	Polymerase Chain Reaction
PI3K	Phosphoinositide 3-kinase
PIP_3	Phosphatidylinositol (3,4,5)-trisphosphate

PRRs	Pattern-recognition receptors
qPCR	Quantitative Polymerase Chain Reaction
Rab5	Ras-related protein 5
RNA	Ribonucleic Acid
ROS	Reactive Oxygen Species
RQ	Relative Quantity
RT-PCR	Reverse Transcription PCR
SAP	(SLAM)–associated protein
SLAM	Signaling Lymphocytic Activation Molecule
SLAMF1	Signaling Lymphocytic Activation Molecule family member 1
Th	T helper
TGF-β	Transforming growth factor beta
TLR	Toll-Like Receptor
TNF	Tumor Necrosis Factor
WB	Western Blot
YAP1	Yes Associated Protein 1
μg	Microgram
μl	Microliter

ABSTRACT

ABSTRACT

Chagas disease is an important problem of public health in the Americas, is caused by the intracellular parasite *Trypanosoma cruzi.* It is a complex disease with great variety of reservoirs and vectors, different ways transmission and parasite high genetic variability. For this reason the immunopathology is still not completely understood and there is no efficient treatment. Due to its high genetic variability *T. cruzi* has been classified into six different Discrete Typing Units. Studies evaluating the immunopathology in Chagas disease have been performed using single *T. cruzi* strains, thus, the role of the genetic variability of the parasite has not been taken in account. On the other hand, studies using a unique parasite strain and different mouse genetic backgrounds showed numerous inconsistences. For this reason it is important to evaluate the role of parasite genetic variability and the mouse genetic background, to better understand the immunopathology of Chagas disease.

Previous studies in the laboratory demonstrated the importance of Toll-Like receptor 2 (TLR2) and Signaling Lymphocytic Activation Molecule Family 1 receptor (SLAMF1), during the infection with *T. cruzi in vivo* and *in vitro* using the Y parasite strain. The aim of this project was to evaluate the immunopathology of Chagas Disease using different reference strains of *T. cruzi in vivo* and *in vitro*, in mice with different mouse genetic background and deficient in the expression of TLR2 and SLAMF1 receptors.

We found that macrophages from C57BL/6 mice were more resistant to *in vitro* infection with all *T. cruzi* strains evaluated compared to BALB/c, being the rate of infection variable depending on the strain. TLR2 was crucial during the interaction phase of macrophages and all the different strains potentiating parasite internalization. In contrast, SLAMF1 played an important role as a microbial sensor by suppressing NAPDH oxidase 2 (NOX2) expression and Reactive Oxygen Species (ROS) production for all the *T. cruzi* strains evaluated, except for VFRA cl1.

I*n vivo* results with BALB/c and *Slamf1*$^{-/-}$ mice infected with Dm28c, Y and VFRA cl1 strains, where in agreement with *in vitro* results. Thus, *Slamf1* $^{-/-}$ mice infected Dm28c and Y were more resistant to infection compared with infected BALB/c mice, but more susceptible when infected with VFRA cl1 strain. Infections with the Y strain denoted the inverse correlation between the presence of Myeloid-derived Suppressor Cells (MDSCs) in the heart (denoted by expression of Arg-1, iNOS and COX-2 MDSCs markers) and mice survival, which was 30% and 100% in BALB/c and *Slamf1* $^{-/-}$ mice, respectively. Dm28c and VFRA cl1 parasite strains caused lower levels of MDSCs in heart, but higher immune response in spleen and liver, indicating a more efficient control of the infection that impedes infected MDSCs reaching the heart that as a "Trojan horse", deliver the parasites, causing cardiac damage and the death of the mice.

Finally, we showed for the first time that immune-responsive gene 1 (Irg1) levels were high in mice hearts during *T. cruzi* infection. *In vitro* studies using epimastigotes showed a high IC_{50} for itaconic acid, a metabolite produced by Irg1 that inhibits pathogen's isocitrate lyase, thus, the last constitutes a new drug target for Chagas disease treatment.

RESUMEN

La enfermedad de Chagas es importante problema de salud pública en Latino América, esta enfermedad es causada por el parasito intracelular *Trypanosoma cruzi.* La enfermedad de Chagas es una compleja enfermedad que involucra gran variedad de reservorios y vectores, tiene diferentes vías de transmisión además de que el parasito posee una alta variabilidad genética. Por estas razones la imunopatología aún no se ha esclarecido por completo. Recientemente, *T. cruzi* ha sido clasificado en seis diferentes unidades de tipificación debido a su alta variabilidad genética. Hasta el momento, la mayoría de los estudios imunopatológicos se han desarrollado únicamente empleado una cepa de parasito, ha sí que el papel de la variabilidad genética de *T. cruzi* no ha sido considerando hasta el momento. Por otro lado, estudios usando una única cepa en diferentes fondos genéticos de ratón muestran resultados contradictorios. Por esta razón es importante evaluar el papel de la variabilidad genética del parasito así como la variabilidad genética del hospedador para entender de una mejor manera la enfermedad de Chagas.

Estudios anteriores en el laboratorio han demostrado la importancia de los receptores Toll-like 2 (TLR2) y Signaling Lymphocytic Activation Molecule Family 1 receptor (SLAMF1), durante la infección con *T. cruzi in vivo* e *in vitro* utilizando la cepa Y. El propósito de este trabajo fue evaluar la imunopatología de la enfermedad de Chagas utilizando diferentes cepas de referencia de *T. cruzi in vivo* e *in vitro,* en ratones con diferente fondo genético y con deficiencia en la expresión de los receptores TLR2 y SLAMF1.

Hemos encontrado que los macrófagos de ratones C57BL/6 son más resistentes a la infección *in vitro* con todas cepas de *T. cruzi* evaluadas comparado con los BALB/c, siendo la tasa de infección variable dependiente de la cepa. TLR2 tuvo un papel crucial durante la fase de interacción en macrófagos potenciando la internalización de todas las cepas del parasito. En contraste, se observó que SLAMF1 juega un papel importante como sensor microbiano por la suprimiendo la expresión de la NADPH oxidasa 2 (NOX 2) y la producción del Reactive Oxygen Species (ROS) para todas las cepas excepto papara la VFRA cl 1.

Los resultados *in vivo* en ratones BALB/c y *Slamf1*$^{-/-}$ infectados con las cepas Dm28c, Y e VFRA cl1 confirmaron los resultados obtenidos en el *in vitro.* Los ratones *Slamf1*$^{-/-}$ infectados con Dm28c e Y fueron más resistentes a la infección comparados con los ratones BALB/c, pero más susceptibles cuando fueron infectados con la cepa VFRA cl1. La infecciones con la cepa Y mostraron una correlación inversa entre la presencia de Myeloid-derived Suppressor Cells (MDSCs) en el corazón (explicado por la expresión de Arg-1, iNOS y COX-2, marcadores de MDSCs) y la supervivencia en ratones, donde un 30% y 100% en BALB/c y *Slamf1*$^{-/-}$ sobrevivieron respectivamente. Las infecciones con Dm28c y VFRA cl1 causaron niveles más bajos de MDSCs en el corazón, pero una respuesta inmune más fuerte en bazo e hígado, indicando un control más eficiente impidiendo a las MDSCs alcanzar al corazón como un "caballo de Troya" , llevando a los parásitos, causando daño cardiaco y finalmente la muerte a los ratones.

Finalmente, hemos observado por primera vez que los niveles más altos del gene immune-responsive gene 1 (Irg1) en el corazón durante la infección de *T. cruzi.* El estudio *In vitro* utilizando epimastigotes mostraron un alto IC_{50} para el ácido itaconico, un metabolito producido por el IRG1 que inhibe la isocitrato liasa de los patógenos, por lo tanto esto contribuiría como una nueva diana de tratamiento en la enfermedad de Chagas.

INTRODUCTION

1 INTRODUCTION

1.1 CHAGAS DISEASE

Chagas disease or American trypanosomiasis is considered by the World Health Organization (World Health Organization, 2015) as a major problem in health and the fourth cause of death in Latin America. This parasitic disease caused by the protozoan *Trypanosoma cruzi*, was discovered in 1909 by the Brazilian physician Carlos Chagas (1879-1934), but the first evidence in human tissues of the Atacama mommies date to nearly 9 thousand years ago (Guhl *et al.*, 1999).

Chagas disease affects about 7 million individuals and 110 million are in risk of contracting the infection, given the vectors wide geographic distribution in the American continent (Rassi Jr. *et al.*, 2012). Every year 10-14 thousand people die for this disease. However, many aspects of the pathogenesis of Chagas Disease remain unknown and the treatments still are non-effective.

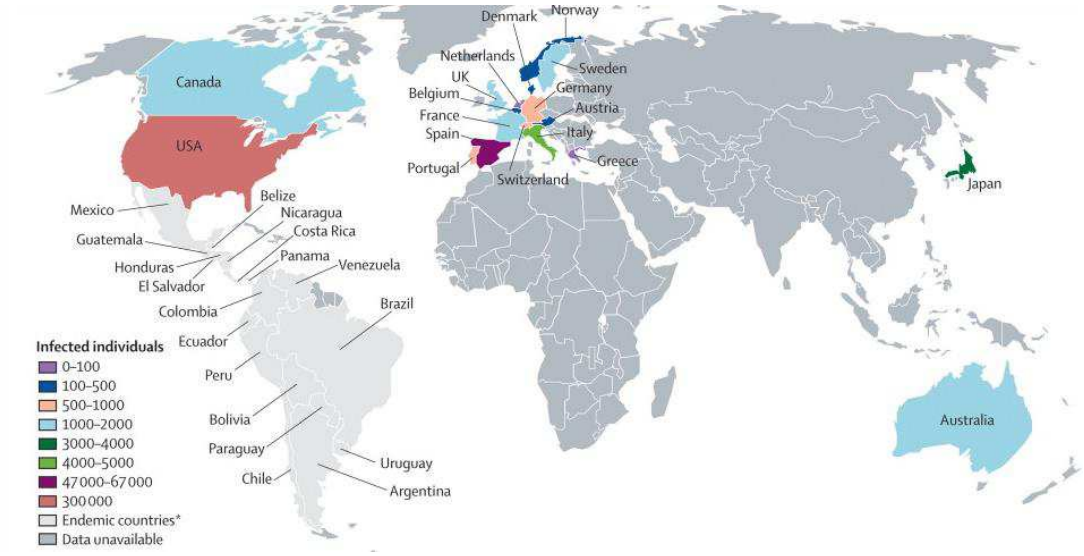

Figure 1. Map of the world distribution of Chagas disease. *Image taken from* (Rassi Jr *et al.*, 2010).

The main mechanism of transmission to humans is vectorial, by the infected feces of the blood sucking reduviidae bugs of the Triatominae subfamily. Transmission can also occur via blood transfusion, orally (contaminated food), by congenital transmission or laboratory accidents (Prata, 2001). The increment of cases in non-endemic countries is associated with the large number of Latin American immigrants, for this reason is considered an emergent problem in North America,

Europe and Japan (Parker and Sethi, 2011; Pérez-Ayala *et al.*, 2011). United States of America is the first non-endemic country with 300 thousand people infected (mostly from Mexico), followed by Spain with 47-67 thousand people (Rassi Jr *et al.*, 2010) (Figure 1).

Chagas disease is a very complex disease in almost all aspects. Among those, it can be transmitted to humans and more than 150 species of domestic and wild animals by more than 130 species of the blood-sucking reduviidae bugs. The most important vector species are *Triatoma infestant* in the sub-amazonia endemic regions (Southern South America), *Rhodnius prolixus* mainly in northern South America (Colombia and Venezuela) and *Triatoma dimidiata* also in the northern South America but also in Central America and Mexico.

1.2 TRANSMISSION CYCLE

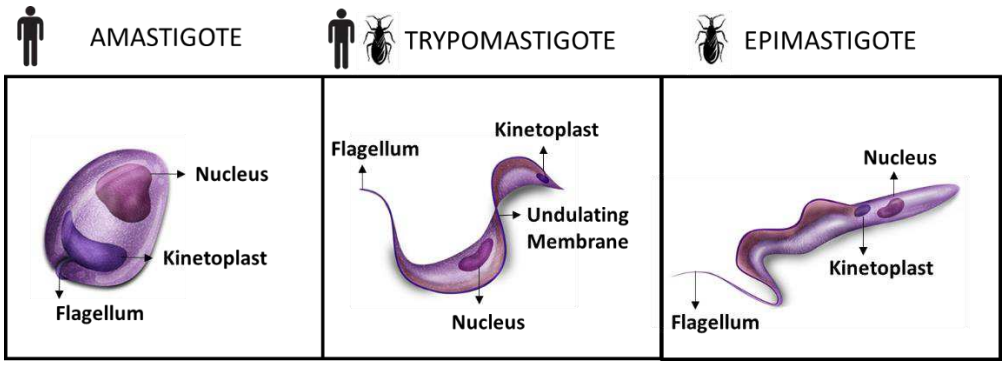

Figure 2. Trypanosoma cruzi morphology. *Amastigote: replicative form in the vertebrate host. Trypomastigote: infective form non-replicative in vertebrates and invertebrates. Epimastigote: replicative form in triatomines.*

T. cruzi is an intracellular protozoan that belongs to the order of kinetoplastidae order and *Trypanosomatidae* family. Is characterized by the presence of a flagellum that originates from the single mitochondrion in which is situated the kinetoplast, a specialized DNA-containing organelle. In its life cycle the parasite alternates between the bug vector and the vertebrate host. The life cycle stages are: trypomastigote, amastigote and epimastigote. These forms can be distinguished by the position of the kinetoplast relative to the nucleus and by the presence or absence of a free flagellum (Figure 2).

The epimastigote is the replicative flagellate form and is found in the hindgut of the triatomines. The trypomastigote is the flagellate and infective non-replicative form in the vector (metacyclic trypomastigotes) and the mammalian host (blood trypomastigote). The amastigote is the

aflagellate form and is localized intracellularly into the parasitophorous vacuoles of host cells where it multiplies inside the cell by binary fission (Brener, 1971).

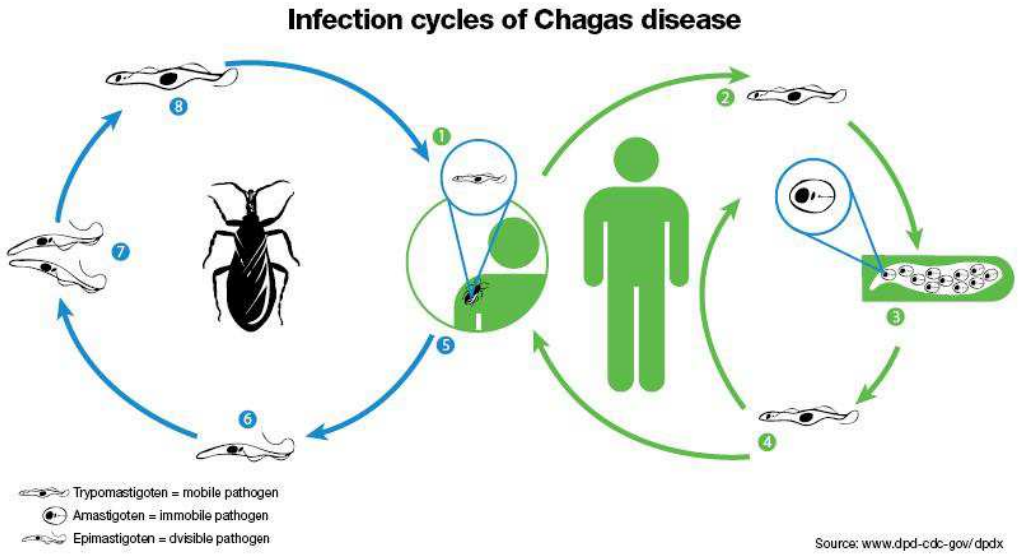

Figure 3. Life cycle of Trypanosoma cruzi, the causative parasite of Chagas disease. 1-5. *Steps in vertebrate host.* ***5-8.*** *Steps in invertebrate host (Triatomine).*
Image taken from (http://www.cdc.gov/parasites/chagas/biology.html)

T. cruzi presents a complex life cycle with different stages in the insect vector and the mammalian host. Figure 3 shows a brief summary of the infection cycle of Chagas Disease. **1.** Infected triatomine bug takes blood meal and defecate, metacyclic trypomastigotes are in the bug feces. These metacyclic trypomastigotes can enter by the bite wound or mucosal membrane (Conjunctiva). **2.** Metacyclic trypomastigote travel to the blood stream and can penetrate a wide variety of mammalian cells at the bite wound site. Inside the cells the trypomastigotes transform into amastigotes. **3.** Amastigotes multiply by binary fission in the host cell cytoplasm for ~ 5-6 times until they occupy most of the cell volume **4.** In this stage intracellular amastigotes transform into trypomastigotes, following by the rupture of the host cell plasma membrane releasing the trypomastigotes into the blood stream and where they are able to infect new cells or new tissues. **5.** The triatomine bug takes infected blood meal (metacyclic trypomastigote). **6.** Trypomastigotes transform to epimastigotes from the proboscides to the midgut of the triatomines. **7.** In the midgut the epismatigote multiplies. **8.** The epimastigote transforms again into trypomastigote, from the midgut to the hindgut. Finally, the cycle is completed when a new bug bite a new host (Brener, 1972; Costales and Rowland, 2007).

1.3 GENETIC VARIABILITY OF *T. CRUZI*

Trypanosoma cruzi is a very heterogeneous species presenting a high genetic variability. This genetic variability has been demonstrated using biological, biochemical and molecular technics, that allow their classification into at least six Discrete Typing Units (DTUs), named from TcI to TcVI (Zingales *et al.*, 2009; Zingales *et al.*, 2012). These DTUs are thought to be associated with the geographical distribution, the transmission cycle (domestic and sylvatic) and the clinical manifestation (Figure 4) with both homogeneous (TcI-TcII) groups and heterogeneous groups (TcIII–TcVI) that are considered hybrids due to ancestral recombination events (Westenberger *et al.*, 2006). The different DTUs are circulating among mammalian host and insect vector across Latin America. Recently a new genotype has been found, designated as TcBat due to its association with bats in Brazil, Panama and Colombia (Marcili *et al.*, 2009; Pinto Dias, 2013; Ramírez *et al.*, 2013).

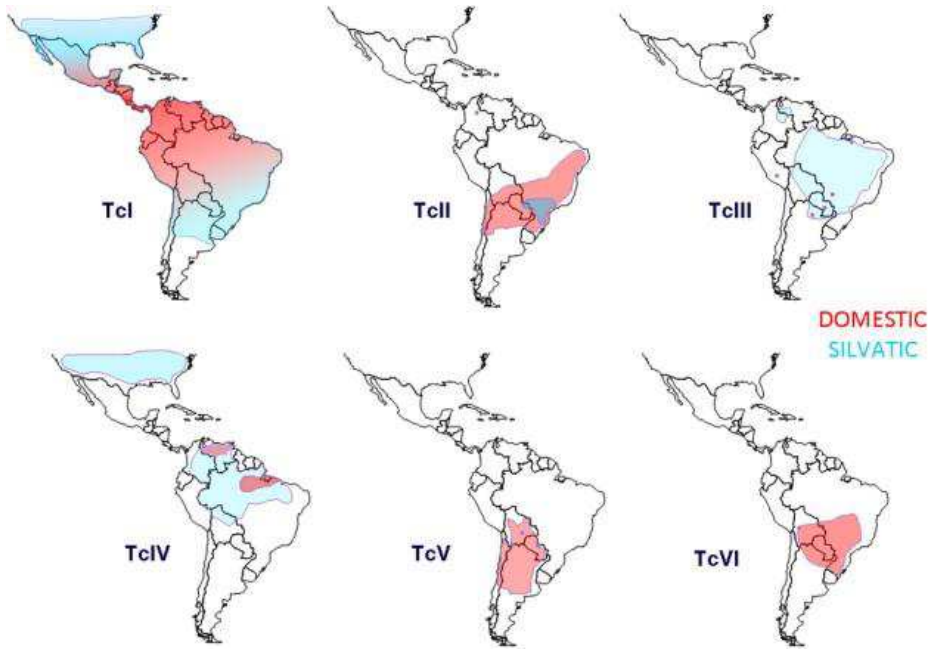

Figure 4. Distribution of the DTUs in South America. *Image taken from* (Zingales *et al.*, 2012)

The cardiac and megavisceral forms of Chagas disease in South America are associated with the DTUs TcI, TcII, TcV and TcVI. TcI is the most prevalent strain in countries at the north of the Amazon river basin (Colombia and Venezuela) where is associated with cardiomyopathy, whereas TcII–TcVI are the most prevalent in the southern cone countries; TcII is the principal agent of Chagas disease in the American Southern Cone and the vector is *Triatoma infestans*. For TcV y TcVI,

derived from the hybridization between TcII and TcIII/TcIV, the transmission cycle is mainly domestic (Zafra *et al.*, 2008; B. Zingales *et al.*, 2009). These DTUs are associated also with megavisceral syndromes. TcV is associated with congenital cases in Argentina (Burgos *et al.*, 2007; Diosque *et al.*, 2003). However, this distribution is not absolute, since all of them can be found across the continent. For the case of North America, only cardiac cases have been reported almost associated with the TcI and occasionally with the TcIV.

TcIII and TcIV are mostly associated with a sylvatic cycle and information about their geographical distribution is scarce. TcIII has not been associated in human cases and is found in domestic dogs and in peridomestics triatomines in Brazil. TcIV is associated with oral cases in the Amazon basin and Venezuela (Coura *et al.*, 2002; Marcili *et al.*, 2009).

1.4 Clinical Phases

Chagas disease presents three clinical phases: acute, indeterminate and chronic phase.

The **acute phase** lasts between 4-8 weeks, 90% of the patients in acute phase are asymptomatic. For this reason is very difficult to diagnose these patients and treat them. The other 10% present symptoms 1-2 weeks after exposure as fever, fatigue, body aches, headache, rash, loss of appetite, diarrhea and vomiting. The most recognized sing of acute phase is the Romaña's sign, which includes swelling of the eyelids on the side of the face near the bite wound or where the bug feces were deposited or accidentally rubbed into the eye. The acute phase is also characterized by a high parasitemia. 5-10% of the patients in acute phase present myocarditis. The mortality in this phase is around 1% as a result of severe myocarditis or meningoencephalitis. The treatment at this point will usually cure the patient, but because the difficult diagnosis many cases are not detected and thus not treated (Rassi Jr. *et al.*, 2012).

About 90% of the acute phase cases resolve spontaneously, even without the treatment. 60-70% of the patients never develop clinical manifestations; these patients have the **Indeterminate or asymptomatic form**. This phase is characterized by the presence of antibodies against *T. cruzi* in serum, low or undetectable parasitemia, and normal electrocardiogram and chest radiological examinations.

The remaining 30-40% of the Chagas Disease patients progress to the **chronic phase.** However, the clinical manifestations usually appear 10-30 year after the initial infection, involving the heart,

esophagus, colon or a combination, and are denominated: cardiomyopathy, megavisceral syndromes and cardiodigestive forms, respectively (Marin-Neto and Rassi, 2009). The cardiomyopathy is the most serious manifestation in Chagas disease, about the 20-30% of the chronic patients developed this clinical manifestation. The megavisceral syndromes are seen almost exclusively at the south of the Amazon basin (Argentina, Brazil, Chile and Bolivia), approximately 10-15% develop megaesophagus or megacolon or a combination. Finally, 2% developed cardiomyopathy and megavisceral syndromes.

1.5 IMMUNE RESPONSE

After the invasion of *T. cruzi* across the endothelium, an activation of different **innate immune system** defense mechanisms start associated with specialized cells that recognize the parasite, especially involving **macrophages**. The infected macrophages secret Interleukin 12 (IL-12) that activate the Natural Killers to produce pro-inflammatory interleukin Interferon γ (IFN-γ), which is crucial for further activation of macrophages. The high levels of IFN-γ promote the liberation of Nitric Oxide (NO), important for parasite killing (Machado *et al.*, 2008; Munoz-Fernandez *et al.*, 1992; Silva *et al.*, 1998). The lack of control in the production of IFN-γ by the natural killer is in part responsible for tissue damage in the chronic phase (Cunha-Neto *et al.*, 2005). On the other hand, *T. cruzi* also triggers immunosuppression of T lymphocytes and macrophages. This immunosuppression could be mediated by anti-inflammatory cytokines as IL-4, IL-10 and Transforming growth factor beta (TGF-β) to avoid excessive response by the pro-inflammatory cytokines in acute phase (Sanjabi *et al.*, 2009).

T. cruzi infected cells produce NO in response of IFN-γ. NO regulates the cardiac muscle and endothelium physiology but produced in excess cause damage in the myocardium and leads to alterations in cardiac functions. In mice infected with the Y strain of *T. cruzi,* it has been found an infiltration of myeloid cells which express Inducible Nitric Oxide Synthase (iNOS) and Arginase-1 (Arg-1), implicated in the suppression in the proliferation of T cells (Cuervo *et al.*, 2008). Cyclooxygenase 2 (COX-2) is also expressed by MDSCs and is responsible of prostaglandin-mediated cardiac inflammatory infiltration (Guerrero *et al.*, 2015). Also, the immunosuppression implicates AgC10 parasite antigen which negatively regulates the activation of T cells and macrophages (Kierszenbaum *et al.*, 1999).

After recognition of the parasite, the antigen presenting cell (APC) migrates to nearby lymph nodes, to present the antigens to the T lymphocytes (Gutierrez *et al.*, 2009). Antigen presentation is mediated by the interaction between the TCR (T cells receptors) and major histocompatibility complex I (MCH-I) in CD8+ lymphocytes or MCH-II in CD4+ lymphocytes. Once activated this complex promotes the recruitment of others inflammatory cells as B cells and neutrophils. Two main different **adaptive immune responses** may take place, namely Th1 and Th2.

In the acute phase the immune response is mainly Th1. The activation of T cells involves the Th1 with a production of IFN-γ, IL-12 and the Tumor Necrosis Factor (TNF) (Abrahamsohn and Coffman, 1995). The activation is related to the anti-parasite inflammatory process as well as leukocyte infiltration of different parasite target tissues. These responses activate also the natural killer, which helps with its cytotoxic activity and the capacity to produce IFN-γ. IFN-γ activate macrophages M1 with high iNOS levels, inhibiting the replication of the parasites through the production of NO and cyclooxygenase 2 (COX-2) involved in the production of prostaglandins. NO reaction with the oxygen free radicals causing the destruction of the parasite (Arantes *et al.*, 2004). On the other hand, NO participate in the production of chemokines by the cardiomyocytes (Machado *et al.*, 2008). Also, the CD8+ cytotoxic T lymphocytes are responsible for the elimination of infected cells trough the perforin/granzyme system, for the activation of macrophages and to promotion of Th1 response (Gavrilescu and Denkers, 2003). The increment of COX-1 and COX-2 has been demonstrated in mice heart tissues infected with *T. cruzi* during the acute phase (Guerrero *et al.*, 2015).

The Th2 response involves the production of IL-4, IL-5, IL-10, IL-13 and the TGF-β by B cells, mastocytes and macrophages (Gutierrez *et al.*, 2009). The secretion of IL-10 plays an important immunoregulatory role in the infection by *T. cruzi*. It has been demonstrated that this cytokine can balance the pro-inflammatory response conducted by the TNF (Dutra *et al.*, 2014). Some authors suggest that the Th2 also contributes to the activation of M2 macrophages. M2 activation promotes the survival of the parasite into the host cells (Martinez and Gordon, 2014). M2 macrophages in the heart inflammatory infiltration present high levels of Arg-1 and the myeloid-derived suppressor cells (MDSCs), which express iNOS and Arg-1, are involved in the suppressing T cell proliferation. IL-4 helps IL-10 in the negative regulation of TNF production in the spleen (Cuervo *et al.*, 2008).

T. cruzi has two important characteristics: the ability to invade multiple cell types and the capacity to evade the cytotoxic systems intracellular, escaping from the parasitophorous vacuole to the cytoplasm to multiply. Also, the parasite alters a great number of signaling pathways as well antigenic presentation (Tarleton *et al.*, 1996).

1.6 *TRYPANOSOMA CRUZI* HOST CELL INTERACTION

The invasion of *T. cruzi* in the host cells involves recognition of many molecules in the surface of the parasite and the host cells (Figure 5). The genetic variability and the different forms of the parasite play an important role in the adhesion, expressing different molecules in the surface.

Parasite Molecules: PAMPs

Mucins are the major glycoproteins in the surface of the parasite. Their sugar residues interact with the mammals cells and also can act as ligands (De Souza *et al.*, 2010). In macrophages **Gp90** is anti-phagocytic being necessary for the parasite internalization. They are only presented in the mammal stages of *T. cruzi* (De Souza *et al.*, 2010).

Transialidases including Tc85 constitute a glycoprotein super family composed by gp85, gp82 and TSA-1. The members of this group are expressed on the parasite surface and their amount varies depending on the stages. Tc85 family is able to bind with different host receptor molecules, like the host cell cytokeratin 18, fibronectin and laminin (Giordano *et al.*, 1999). Tc85 is an 85kDa glycoprotein that has been identified as a ligand for fibronectin in different cells (Monocytes, neutrophils and fibroblast). Is abundant in trypomastigotes (De Souza *et al.*, 2010). **Gp82** and **gp35/50**, proteins are expressed in the metacyclic trypomastigotes and are highly immunogenic (Teixeira and Yoshida, 1986). Gp82 is only presented in metacyclic trypomastigotes and is highly expressed in the G strain compared with the CL Brener. Gp35/50 is abundant in the surface, is resistant to protease digestion and protects the metacyclic trypomastigotes from destruction in the oral route. **Gp83** is a ligand used by *T. cruzi* to attach and enter into the cells, present in all DTUs and only expressed in trypomastigotes.

Some *T.cruzi* **proteases** have been implicated in the host infection like **Cruzipain, Oligopeptidase B and Tc80. Cruzipain** is a lysosomal cysteine proteinase. It is located in the endosomal-lysosomal (reservosome) system of epimastigote and is expressed in the surface of epimastigotes and the transition form of amastigote-trypomastigote. It is secreted in the flagellar pocket and cleaves

kininogen to generate short lived kinins which stimulate IP3- mediated Ca^{2+} release. **Oligopeptidase B** is secreted by trypomastigotes and induces indirectly Ca^{+} mobilization during *T. cruzi* invasion. **Tc80** is an oligopeptidase, important for the parasite transit through the extracellular matrix.

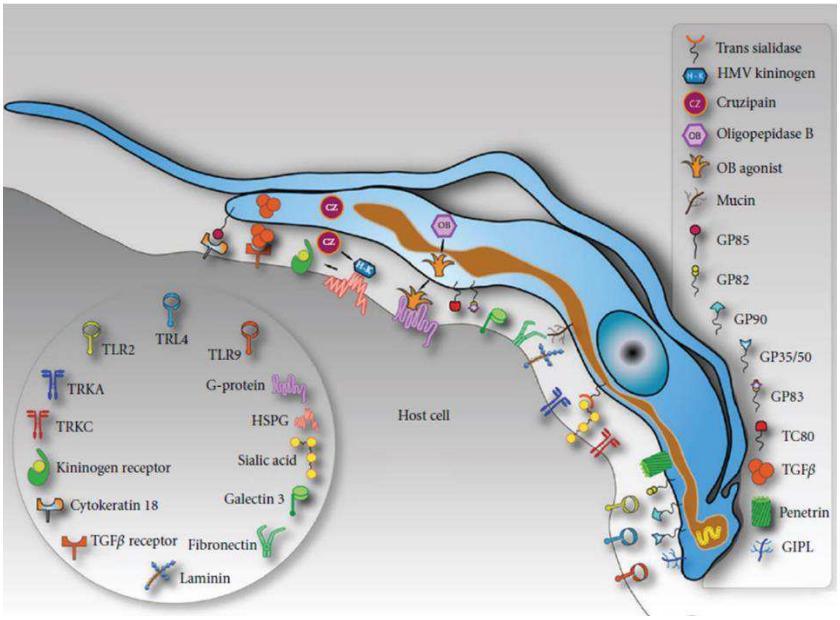

Figure 5. Model of molecules involved in parasite host-interactions. *Image taken from (Piacenza et al. 2013).*

The entry of *T. cruzi* involves a great amount of molecules in the surface of the host cell and these molecules can vary depending on the cells involved. **Integrins** are involved in the invasion process. This receptor mediates the attachment between two cells or cell and extracellular matrix. **Cytokeratine 18** is the most abundant structural proteins of epithelial cells, organized as heterodimers and form a network of 10–12 nm wide intermediate filaments. **Galectins,** a family of galactose binding lectins can bind with *T.cruzi* (Pineda *et al.*, 2015). **Galectin-3** mediates the attachment and entry in dendritic cells and in smooth muscle cells. **Fibronectin and laminin** can activate the PI-3Kinase signaling pathway. **Transforming growth factor beta (TGF-β) receptor** facilitates *T. cruzi* entry in epithelial cells. **Tyrosine kinase (Trk)** is present in neuronal, glial and dendritic cells. Trk A leads *T. cruzi* invasion through tran-sialidase bindings in the trypomastigotes. TrK C helps the host-*T. cruzi* equilibrium in the nervous system, promoting the survival of neuronal and glial cells after the infection.

The **Pattern-recognition receptors (PRRs)** are the first line of immune defense against pathogens (Piacenza *et al.*, 2012). The PRRs are expressed in the cell surface and are responsible of the recognition of the parasite. These molecules are more present in the surface myeloid of antigen-presenting cells, as macrophages and dendritic cells. Among those, the best studied are **Toll Like Receptors (TLRs)** *T. cruzi* is recognized by some TLRs; TLR-2, TLR-4 and TLR-9. TLR-2 induces phagocytosis of trypomastigotes by the activation of Ras-related protein 5 (Rab5) (Maganto-Garcia *et al.*, 2008). **Signaling Lymphocytic Activation Receptor F1 (SLAMF1)** or CD150, present inly on the surface of hematopoietic cells, is required for *T. cruzi* replication in the macrophages and dendritic cells (Calderón *et al.*, 2012).

1.7 *T. CRUZI* INVASION

Host-parasite interaction involves a great deal of parasite molecules and host receptors. Three mechanisms of *T. cruzi* entry into the host cells have been identified (Figure 6).

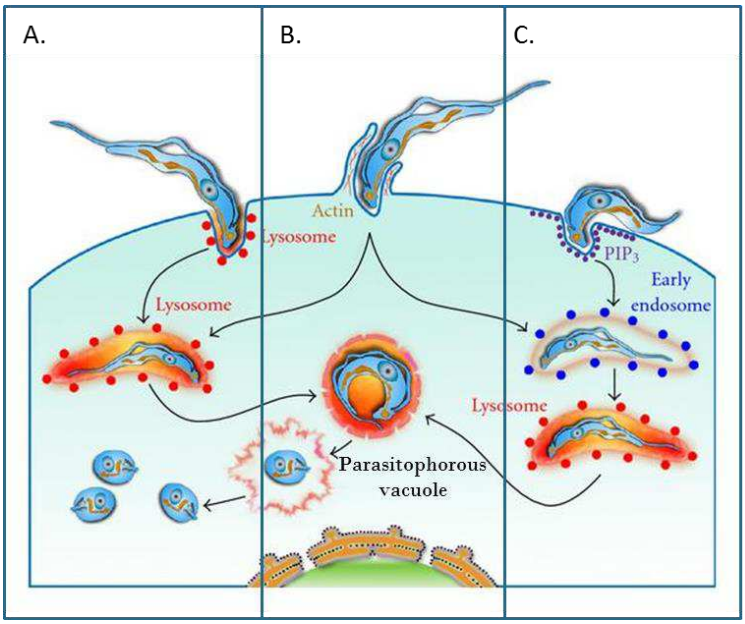

Figure 6. Model of T. cruzi invasion. *Different mechanism in the entry of T. cruzi:* ***A.*** *Lysosome dependent,* ***B.*** *Actin dependent and* ***C.*** *Lysosome independent. Image modified from (Piacenza et al. 2013).*

The lysosome dependent pathway involves lysosome and Ca^{2+} dependent fusion of lysosome with vacuole to form the parasitophorous vacuole, which begins when the host plasma membrane and the parasite enter in contact (Figure 6 A). The actin dependent pathway is a mechanism of invasion in professional phagocytic cells. In this phagocytic process, trypomastigotes penetrate into the

host cells through an expansion of the plasma membrane and can either localized in early endosomes or lysosomes culminating the formation of the parasitophorous vacuole (Figure 6 B), and finally in the lysosome independent pathway, the initial entry into the plasma membrane takes place by an invagination that recruits Phosphatidylinositol (3,4,5)-trisphosphate (PIP_3). The internalization of the parasite involves an early endosome mediated by Early endosome antigen 1 (EEA1) and Rab5 to finally fusion in a lysosome (Figure 6 C) (Caradonna and Burleigh, 2011; Maganto-Garcia *et al.*, 2008).

To establish the infection in phagocytic cells as macrophages, *T. cruzi* must endure in an oxidant environment. To survive this environment the parasite uses antioxidant enzymes, like peroxidases, to protect it against the macrophage-released reactive oxygen and nitrogen species (Piacenza *et al.*, 2012). Trypomastigotes trigger in macrophages the activation of Nicotinamide Adenine Dinucleotide Phosphate (NADPH) oxidase. As a result there is a continued production of super radical anions ($O^{\cdot -}_2$). Proinflammatory cytokines (IFN-γ and TNF), also triggered by the infection of the parasite stimulate infected macrophages to produce large amounts of (·NO) via iNOS, which oxidizes the L-arginine and transfer electrons to NADPH. The ·NO affects the parasite survival into the macrophages (Munoz-Fernandez *et al.*, 1992; Piacenza *et al.*, 2012).

Once *T. cruzi* is in the lysosomal compartment in the host cell, the disruption of the parasitophorous vacuole takes place, an important step for the intracellular infection. To initiate this disruption, trypomastigotes and amastigotes secrete a hemolysin, named TC-TOX which increases the acidification (pH 5.5) into the parasitophorous vacuole for the lysis of it. In addition, the surface neuraminidase/transialidase in the trypomastigotes facilitates the process. After the disruption of the parasitophorous vacuole, the trypomastigotes located, now in the cytoplasm of the host cells, transform into amastigotes and after several replications and transformations amastigote-trypomastigote, the motile forms of the parasite cause the rupture of the host membrane and the bloodstream infective trypomastigote can infect neighboring cells or disseminate the infection through in bloodstream (Cardoso *et al.*, 2016; Li *et al.*, 2016).

Myeloid cells are not only a major infection-susceptible cells but also play an important role in the dissemination of the parasite in new tissues acting as a “Trojan horse” (Calderón *et al.*, 2012). This hypothesis is also supported by to the lack of parasites in blood in mice infected with some strains of *T. cruzi* but presenting focal and spatiotemporally dynamic amastigote nests in tissues (Lewis *et al.*, 2014; Messenger *et al.*, 2015).

1.8 TOLL LIKE RECEPTOR

Toll like receptors (TLRs) are a protein family which plays an important role in innate immunity response in front different pathogens. It is a large family with at least 13 members, denominated from TLR-1 to TLR-13. TLR1 to TLR9 are conserved between mouse and humans. TLR-10 is expressed only in humans and TLR-11 to 13 only in mouse (Akira and Takeda, 2004).

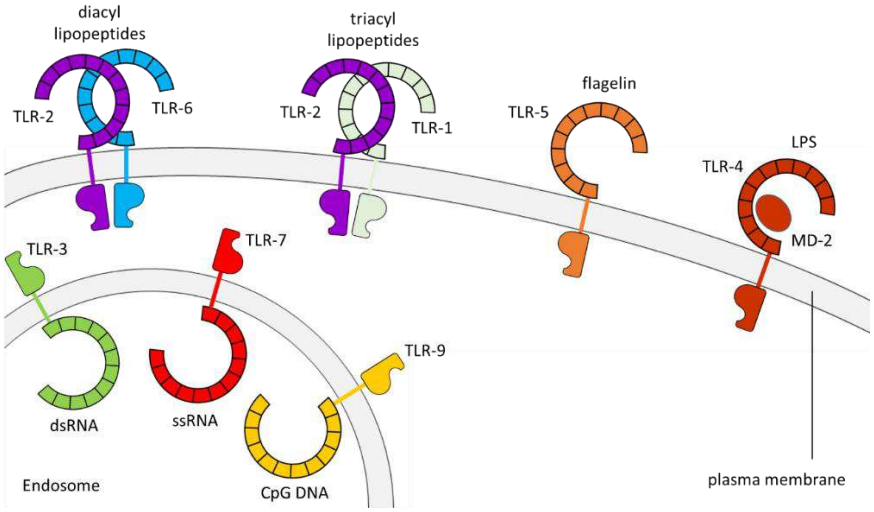

Figure 7. Cellular localization of Toll Like Receptor. *Imagen modified from* (*Charles A. Janeway Jr, Paul travers, 2011)*

TLR-1, TLR-2 and TLR-4 are expressed in the surface of the cells. In contrast, TLR-3, TLR-7, TLR-8 and TLR-9 are anchored to endosomal plasma membrane. There are several signal transduction pathways triggered by TLR engagement, but most of them use MyD88 as an adapter molecule (Takeda and Akira, 2005). Table 1 shows the details on TLR cellular localization, TLRs microorganisms ligands and origin including *T. cruzi,* that stimulates TLR2 by mucins and their related glycoinositophospholipid (GIPL) anchors (Campos *et al.*, 2001) (Campos et al. 2001).

TLRs activation by *T. cruzi* leads to the production of pro-inflammatory cytokines and chemokines necessary for the recruitment of phagocytic cells into the affected area or tissues. In Chagas disease this receptors have a crucial role, increasing the susceptibility in the MyD88-deficient mice have an increased susceptibility to infection associated with a decreased production of IL-12 and IFN-γ. *Tlr4*$^{-/-}$ infected mice present higher parasitemia an in consequence lower production of the pro-inflammatory cytokines (IFN-γ and TNF), and NO compared with the WT mice (C57BL/6) (Oliveira *et al.*, 2010).

T. cruzi also promotes host cell activation via TLR9 and TLR7 stimulating the cytokine production from macrophages and dendritic cells, respectively. *In vivo* experiments with *Tlr9*$^{-/-}$ and *Tlr7*$^{-/-}$, showed that knockout mice were more susceptible to the infection with the parasite (Bartholomeu *et al.*, 2008; Caetano *et al.*, 2011).

Table 1. TLRs. *Table modified from (Akira and Takeda, 2004). * TLRs only expressed in mice.*

Receptor	Localization	Ligand	Origin Ligand
TLR-1	Plasma membrane	Triacyl lipopeptides	Bacteria and mycobacteria
		Soluble Factors	*Neisseria meningitidis*
TLR-2	Plasma membrane	Lipoprotein/lipopetides	Various pathogens
		Peptidoglycan	Gram-positive bacteria
		Lipoteichoic acid	Gram-positive bacteria
		Lipoarabinomannan	Mycobateria
		Phenol-soluble modulin	*Staphylococcus epidermis*
		Glycoinositolphopholipids	*Trypanosoma cruzi*
		Glycolipids	*Treponema maltophilum*
		Porins	*Neisseria*
		Atypical lipopolysaccharide	*Leptospira interrogans*
		Atypical lipopolysaccharide	*Porphyromonas gingivalis*
		Zymosan	Fungi
		Heat-shock protein 70°	Host
TLR-3	Endolysosome	Double-stranded RNA	Viruses
TLR-4	Plasma membrane	Lipopolysaccharide	Gram-negative bacteria
		Taxol	Respiratory syncytial virus
		Fusion Protein	Mouse mammary-tumor virus
		Evelope protein	*Chlamydia pneumoniae*
		Heat-shock protein 60°	Host
		Heat-shock protein 70°	Host
		Type III repeat extra domain A of fibronectin	Host
		Oligosaccharides of hyaluronic acid	Host
		Polysaccharide fragments of heparan sulphate	Host
		Fibrinogen	Host
TLR-5	Plasma membrane	Flagelin	Bacteria
TLR-6	Endolysosome	Diacyl lipopeptides	*Mycoplasma*
		Lipoteichoic acid	Gram-positive bacteria
		Zymosan	Fungi
TLR-7	Endolysosome	Imidazoquinoline	Synthetic compounds
		Loxoribine	Synthetic compounds
		Bropirimine	Synthetic compounds
		Single-stranded RNA	Viruses
TLR-8	Endolysosome	Imidazoquinoline	Synthetic compounds
		Single-stranded RNA	Viruses
TLR-9	Endolysosome	CpG-conyaining DNA	Bacteria and viruses
TLR-10	Endolysosome	Not Determined	Not Determined
TLR-11*	Plasma membrane	Not Determined	Uropathogenic bacteria
TLR-12*	Endolysosome	Profilin	*Toxoplasma gondii*
TLR-13*	Endolysosome	23S ribosomal RNA	Bacteria

1.8.1 TLR-2

Glycosylphosphatidylinositol (GPI) anchors of *T.* cruzi from mucin like glycoproteins (tGPI-mucin) plays an important role triggering activation in macrophages (Campos et al. 2001). The structure of

these GIPLs is variable, for example in the strains Y, G and Tulahuén contain ceramide, while CL Brener strain contain a mixture of dihydroceramide and alkylacylglycerol species, and also vary in epimastigotes and trypomastigotes in the same strain. These GIPLs variability determines their recognition by TLR2 (alkylacylglycerol) or TLR4 (dihydroceramide), that is important to determine the activation of the immune response in the host (Ropert *et al.*, 2002).

The TLR-2 activation by the tGPI-mucin initiates IL-12, TNF and NO production, that protect the host during the early stage of the infection (Campos *et al.*, 2001). The interaction of *T. cruzi* with TLR-2 induces a Rab5 endosome dependent mechanism necessary for the invasion of the parasite in macrophages (Maganto-Garcia *et al.*, 2008).

1.9 SLAM RECEPTOR FAMILY

The signaling lymphocytic activation receptor or SLAM is a family of cell surface receptors. These receptors are type I transmembrane glycoproteins, which are expressed on most hematopoietic cells as B cells, T cells, macrophages, dendritic cells and natural killers..

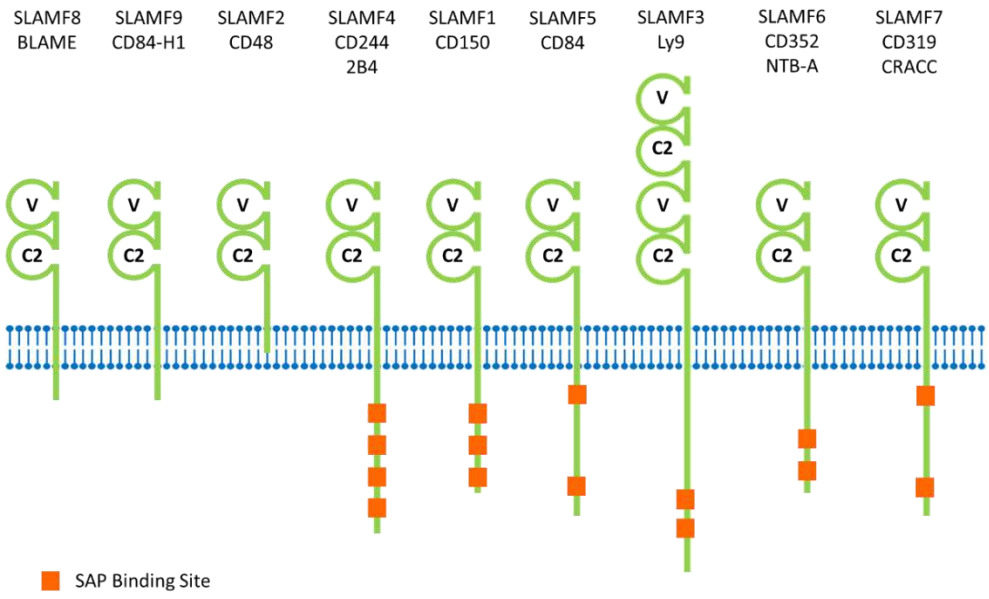

Figure 8. SLAM family of cell surface receptors. *Modified from (C. S. Ma and Deenick, 2011).*

The SLAM family has 9 members, encoded by SLAMF1-SLAMF9 in mouse and named: SLAMF1(CD150), SLAMF2 (CD48), SLAMF3 (LY9), SLAMF4 (CD244 or 2B4), SLAMF5 (CD84), SLAMF6 (CD352 or NTB-A), SLAMF7 (CD319 or CRACC), SLAMF8 (CD353 or BLAME) and SLAMFF9 (CD84-H1)

(Sintes and Engel 2010). The consensus structure of SLAM family consists of an extracellular membrane distal IgV-like domain linked to an IgC2-like proximal domain, a transmembrane region, and an intracellular domain that contains signaling tyrosine-based switch motifs in many cases (Figure 8). Seven of the nine members are self-ligand receptors, and SLAMF2 and SLAMF4 interact with each other (Van Driel *et al.*, 2016).

Six of the SLAMF receptors contain one or more copies of a unique intracellular immune receptor that contains tyrosine-based switch motif, which serves as docking site for adapter molecules and enzymes bearing Src homology 2 (SH2) domains. The adapter molecules SLAM-associated protein (SAP), EWS/FLI activated transcript-2 (EAT-2) and EAT-2-related transducer (ERT) all have high affinity for this unique motif (C. S. Ma and Deenick, 2011).

Table 2. SLAMF. *Table modified from* (Van Driel *et al.*, 2016)

Receptor	Expression	Deficiency: Resistant	Deficiency: Susceptible	SLAMF ligand	Microbial Ligand
SLAMF1	Act T, act B, mono, MΦ, DC, plat, HSC	*T. cruzi*	Gram- , *L. majo* r	Slamf1	Measles virus, *E.coli* (OmpC/F+), *S. typhimurium*
SLAMF2	Pan-Lymphocyte	*S. aureus*	$FimH^+$	Slamf4 CD2	*E. coli* ($FimH^+$)
SLAMF3	T,B,iCD8, NKT, mono, MΦ, HSC		MCMV	Slamf3	
SLAMF4	NK, NKT, T, CD8, DC, mast, mono, eo		LCMV, γHV-68	Slamf2	
SLAMF5	Pan-lymphocyte, plat, mast, eo			Slamf5	
SLAMF6	NK, NKT, T, B, MΦ, pDC	*L. mexicana, C. rodentium*	*S. typhimurium*	Slamf6	*E.coli, C. rodentium*
SLAMF7	T, B, mono, DC, NK			Slamf7	
SLAMF8	iCD8, mono, DC, MΦ, Neu, endo, FRC			Slamf8	
SLAMF9	mono, DC			Unknown	

T, T cels; B, B cells; act, activated; MΦ, macrophage; DC, dendritic cell; plat, platelet; HSC, hematopoietic stem cell; mono, monocyte; NKT, natural killerT cell; eo, eosinophil; mast, mast cell; endo, endothelial cell; FRC, fibroblastic reticular cell; LCMV, lymphocytic choriomeningitis virus; Omp, outer membrane porin; FimH, bacterial lectine; MCMV murine, murine gamma-herpes virus cytomegalovirus; γHV-68, murine gamma-herpes virus 68.

1.9.1 SLAMF1 (CD150)

SLAMF1 is expressed in the surface of T cells, B cells, macrophages and dendritic cells. In the adaptive and innate response SLAMF1 has four principal functions (Figure 9).

SLAMF1 is a co-signaling cell-surface receptor. Costimulatory signals derived from SLAM–SLAM engagements lead to an increase in IL-4 secretion in an SAP-dependent manner following TCR activation of CD4+ T cells (Figure 9 A). SLAM/SAP-mediated signaling is responsible for the development of NKT cells resulting from the SLAM–SLAM interactions between DP thymocytes (Figure 9 B). SLAMF1 is the measles receptor for activated T cells and dendritic cells (Figure 9 C). In addition is a sensor of Gram-negative bacteria; SLAM internalizes into the macrophage phagosome, where it governs key processes for bacterial removal. The interaction SLAMF1 with Ompc/F^{+} from *E.coli* results in a more effective phagocytosis in macrophages, regulating positivity the formation and activation of NADPH oxidase (NOX2) complex (Figure 9 D) *(Sintes and Engel, 2011)* .

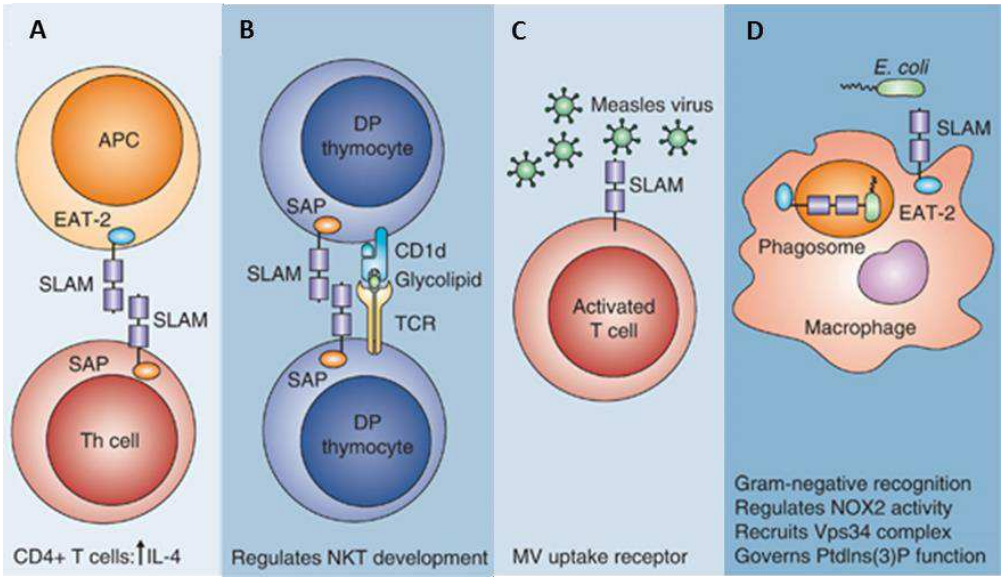

Figure 9. Role of SLAMF1 receptor. A. *Self-ligand receptor* ***B.*** *Lineage commitment* ***C.*** *Measles virus receptor* ***D.*** *Bacterial Sensor. Image modified from* (Sintes and Engel, 2011).

Also, SLAMF1 is able to act as co receptor with TLR4 in the response to LPS necessary to eliminate *Leishmania major,* increasing the production on NO and the macrophage microbicide activity (Van Driel *et al.*, 2016).

SLAMF1 is also required for the replication of *T. cruzi* in macrophages and dendritic cells. Thus, it has been reported that *Slamf1*$^{-/-}$ mice are much less susceptible to the infection with the strain Y compared with control BALB/c mice. Likely, SLAMF1 deficiency alerts macrophage entry and those cells may function as “Trojan horse” disseminating the parasite throughout the body (Calderón *et al.*, 2012).

1.10 MOUSE GENETIC BACKGROUND

One of the problems with the studies using mouse models, not only in Chagas disease is the pathogen resistance associated with the mouse genetic background. In the case of the intracellular parasite *Leishmania* it is clear that the mouse genetic background influences the infection outcome where C57BL/6 mice will not die of visceral leishmaniasis whereas BALB/c will do (Loeuillet *et al.*, 2016). In the case of Chagas disease is very important understand the association *T. cruzi*-mouse strains because may have an effect protective or pathogenic.

In this regard, there are several apparent opposing results related to the importance of immune response in experimental mice infection. Those differences may be due to the use of mouse models with different genetic background, the different strains of *T. cruzi* used but also the amount of parasite injected in the mice. Thus, infections in BALB/c and C57BL/6 mice with 2000 parasites of the strain Y showed high parasitemias that co-related with low survival where the most susceptible mice were the BALB/c and Swiss and the least are C57BL/6. A higher heart parasite load was found in BALB/c mice compared with C57BL/6. Furthermore, an efficient clearance of heart parasite load observed in C57BL/6 at 17 days post-infection (d.p.i.) but not in BALB/c, indicating that C57BL/6 mice are able to control the parasite replication in the heart and for this reason have a better chance to survive to the disease, in agreement with higher inflammation levels in C57BL/6 than BALB/c mice (Cuervo *et al.*, 2008; Sanoja *et al.*, 2013). In contrast, C57BL/6 and BALB/c mice infected with the Tulahuén strain of *T. cruzi* revealed an acute disease accompanied by thymocyte depletion, with C57BL/6 mice showing progressive and lethal disease and BALB/c mice exhibiting partial recovery (Carrera-Silva *et al.*, 2008; Roggero *et al.*, 2002).

1.11 IMMUNOPATHOLOGY OF CHAGAS DISEASE

Chagas disease presents a complex immunopathology and the mechanism is still unclear. Figure 10 summarizes the key immunopathogenic molecules expressed in myeloid cells studied in our work. Macrophages are the first responders in the infection with *T. cruzi,* where parasite surface molecules are recognized by TLRs and other receptors as SLAMF1, implicated in NADPH oxidase 2 (NOX2) activation (Dhiman and Garg, 2014). NOX2 is a multi-subunit complex that utilizes NADPH as an electron donor to reduce O_2 to superoxide ($O_2^{\cdot-}$) and Reactive Oxygen Species (ROS) production referred to as “respiratory burst” that serves as the first line of host defense against

microbes, killing them by oxidative damage of DNA, proteins and lipids (Machado *et al.*, 2012). In phagocytes, NOX2 consists of the membrane-bound catalytic sub-units $p22^{phox}$ and $gp91^{phox}$, forming the flavocytochrome b558 and the cytoplasmic regulatory sub-unities $P40^{phox}$, $P47^{phox}$, $P67^{phox}$ and the small Rho GTPase. *In vivo* experiments using $p47^{phox-/-}$ mice demonstrated that the NOX2 deficiency increased the parasite load, tissue pathogenesis and mortality and suggested to play an important role in the control of *T.cruzi* (Dhiman and Garg, 2014).

COX-2 is a key enzyme in prostaglandin production and is induced by several factors, including infection by *T. cruzi*. The role of COX-2 in mice infected with *T. cruzi* is contradictory, some authors described that COX inhibitors cause an increase in mortality and parasitemia (Mukherjee *et al.*, 2011). On the other hand, other studies associate COX-2 pharmacological inhibition with decreased parasitemia (Hideko Tatakihara *et al.*, 2008). Previous studies in our laboratory demonstrated an important role of COX-2 in the myocarditis produced by the infection by *T.cruzi,* where COX-2 is associated with leukocyte infiltration in the heart, in particular higher presence of MDSCs expressing COX-2 but also for Arg-1 and iNOS, although no significant changes in parasite burden were observed (Guerrero *et al.*, 2015).

In macrophages Arg-1 is a M2 marker, induce TGF-β and cytokines such as IL-4, IL-10 and IL-13. Arg-1 catalyzes the hydrolysis of L-arginine to ornithine and urea, which is required for polyamine synthesis, essential for the growth of cells and *T. cruzi.* Arg-1 is expressed most abundantly in the liver but is not exclusive for this organ. During the infection by *T. cruzi* has been demonstrated that its expression increases mouse susceptibility (Cuervo *et al.*, 2008; Gonzalez, 2014).

Recently, the Immune-response gene 1 (Irg-1) has been described as a novel M1 macrophage marker (Michelucci *et al.*, 2013). Irg-1 is an enzyme that produces itaconic acid or methylenesuccinic acid, that inhibits isocitrate lyase, the key enzyme of the glyoxylate shunt, a pathway necessary for microorganism to survive on limited carbon conditions (Tallam *et al.*, 2016). The antimicrobial activity of itaconic acid has been demonstrated for *Mycobacterium tuberculosis* and *Salmonella enterica*, where the growth of *M. tuberculosis in vitro* was completely inhibited at 25–50 mM, whereas for *S. enterica* 50-100 mM (Michelucci *et al.*, 2013). In the case of Chagas disease, previous metabolomics study using BALB/c mice infected with Y strain presented high levels of *Irg1* gene (Gironès *et al.*, 2014).

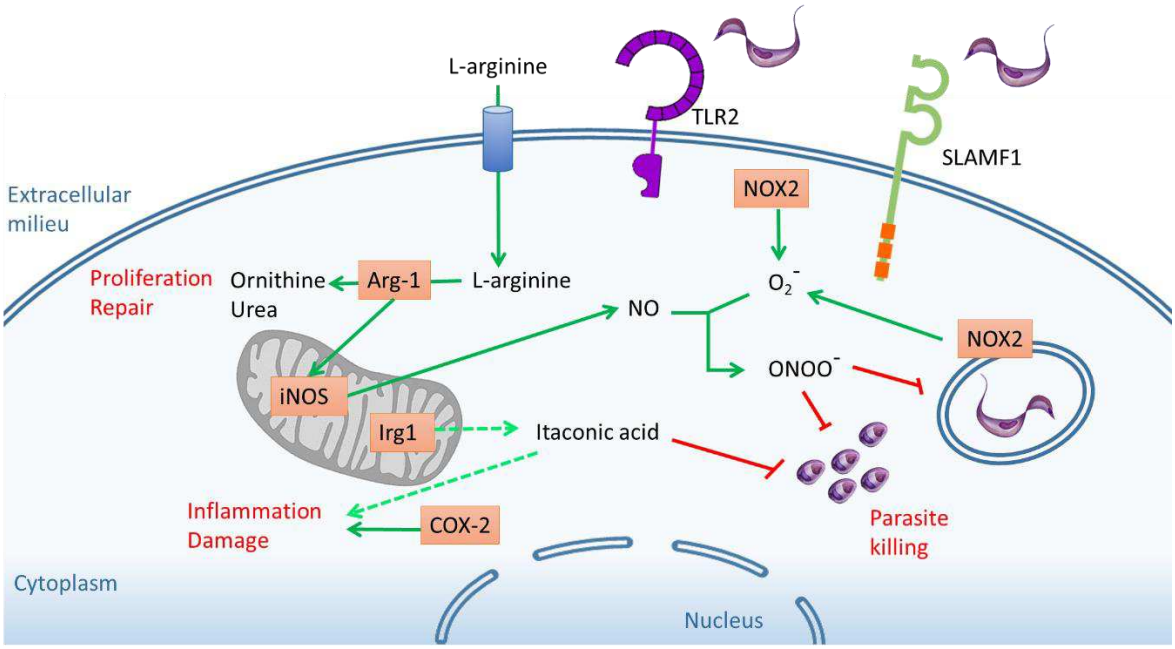

Figure 10. Model of immune regulatory genes in Chagas Disease. *Upon T. cruzi infection, activated macrophages triggering the expression of iNOS and COX-2. The NO synthesized by iNOS is involved in killing of the intracellular parasite.*

OBJECTIVES

2 OBJECTIVES

The general objective of this study was to investigate the role of *T. cruzi* and mouse genetic variability in the course of infection using a macrophage model *in vitro* and the experimental mice infection *in vivo.* For this we proposed the following specific objectives:

1. To identify the relationship between of *T. cruzi* and mouse genetic variability with parasite load in macrophages *in vitro*.
2. To determine the role of *Tlr2* and *Slamf1* in *T. cruzi* infection and its relationship with parasite load in macrophages *in vitro*.
3. To evaluate the relationship between *Slamf1* and *T. cruzi* susceptibility in the experimental mouse model *in vivo*.
4. To determine the parasiticidal activity of Itaconic acid in epimastigote cultures.

METHODS AND MATERIALS

3 METHODS AND MATERIALS

3.1 MATERIALS

3.1.1 Parasites

All *T. cruzi* strains except the Y strain were obtained from Dr. M. Miles (London School of Hygiene and Tropical Medicine, London, UK) through the European program ChagasEpiNet (Table 3). Y strain was obtained from Harvard Medical School, Boston, Massachusetts, USA. This strain was isolated originally from human patient in Brazil (Zingales *et al.*, 2009).

Table 3. T. cruzi strains

DTU	Ref. Strain	Origin	Host/vector
TcI	Dm28c	Carabobo, Venezuela	*Didelphis marsupialis*
TcI	Sylvio X10 cl1	Para, Brazil	*Homo sapiens*
TcI	C8	La Paz, Bolivia	*Triatoma infestans*
TcII	Y	São Paulo, Brazil	*Homo sapiens*
TcII	Esmeraldo cl3	Bahia, Brazil	*Homo sapiens*
TcII	Tul8 cl1	Tupiza, Bolivia	*Triatoma infestans*
TcIII	M6421 cl6	Belem, Brazil	*Homo sapiens*
TcIII	CM17	Meta, Colombia	*Dasypus sp.*
TcIV	10R26	Santa cruz, Bolivia	*Aotus sp*
TcV	Bug2148 cl1	Rio Grande so Sul, Brazil	*Triatoma infestans*
TcV	Sc43 cl1	Santa Cruz, Bolivia	*Triatoma infestans*
TcVI	VFRA cl1	Francia, Chile	*Triatoma infestans*
TcVI	Cl brener	Rio Grande so Sul, Brazil	*Triatoma infestans*
TcVI	Tulahuén cl2	Tulahuén, Chile	*Homo sapiens*
TcVI	Tulahuén	Tulahuén, Chile	*Homo sapiens*

3.1.2 Mice

Female mice *Slamf1*$^{-/-}$ (Obtained from Dr. Cox Terhost, USA), *Tlr2*$^{-/-}$ (Obtained from Dr. Shizuo Akira) and BALB/c and C57BL/6 mice (Obtained from Charles River Laboratories), mice where maintained under pathogen-free conditions at Centro de Biologia Molecular Severo Ochoa (CSIC-UAM) animal facility.

3.1.3 Ethic Statement

This study was carried out in strict accordance with the European Commission legislation for the protection of animal used purposes (2010/63/EU). The protocol for the treatment of the animals

was approved by the "Comite de Etica de Investigacion de la Comunidad de Madrid", Spain (permits PROEX 21/14 and PROEX 148/15). Animals had unlimited access to food and water. They were euthanized in a CO_2 chamber and all efforts were made to minimize their suffering.

3.2 METHODS

3.2.1 Parasite culture

- ***In vitro T. cruzi*** **trypomastigotes** Dm28c, Y, M6421 cl6, 10R26, Bug2148 cl1 and VFRA cl1 were cultured in Vero cells (ATCC number CCI-81) in RPMI with 5% FBS (RPMI complete medium containing 5% FCS, 2 mM L-glutamine, 100 U/ml penicillin, 100 μg/ml streptomycin and 0.1 mM non-essential amino acids) at 37°C in the biosafety level 3 cell cultured laboratory at Centro de Biologia Molecular Severo Ochoa (CSIC-UAM). 2-3 days after co-culture, the *T. cruzi* trypomastigotes released into the supernatants of the infected Vero cells were collected, pelleted by centrifugation (720 g, 10 min., and room temperature), 1 ml of fresh complete RPMI was restored and new plates with Vero were cells infected with 500 μl of *T. cruzi* trypomastigotes.
- **Blood *T. cruzi* trypomastigotes** from Y strain were maintained by weekly intraperitoneal inoculation in BALB/c mice.
- **Blood *T. cruzi* trypomastigotes** from the other strains Dm28c, Y, M6421 cl6, 10R26, Bug2148 cl1 and VFRA cl1 strain were maintained by intraperitoneal inoculation in BALB/c mice. These mice were immunosuppressed following the protocol of Calabrese *et al.,* were at 5 d.p.i. the mice were injected intraperitoneally with a single dose of cyclophosphamide (Sigma) (200 mg/kg of body weight) (Calabrese *et al.*, 1996).
- **Epimastigotes** 15 different strains of *T.cruzi* classified by DTU from TcI to TcVI. TcI (Dm28c, Sylvio X10 cl1 and C8), TcII (Y, esmeraldo cl3 and Tul8 cl1), TcIII (CM17 and M6421 cl6), TcVI (10R26), TcV (Bug2148 cl1 and SC43 cl1) and TcVI (Cl Brener, VFRA cl1, Tulahuén cl2 and Tulahuén) were cultured in flask of 25ml with 5ml of LIT medium (35 g of Liver Infusion,5 g of Tryptose, 4 g of NaCl, 0.4 g of KCl, 8 g of (Na_2HPO_4) $12H_2O$, 2 g of Glucose, 4 ml of Hemin in a liter of double-distilled water) supplement with 10% FBS at 28°C, in the biosafety level 3 cell cultured laboratory at Centro de Biologia Molecular Severo Ochoa (CSIC-UAM). 2/3 days after check the parasites in the microscopy and add 5ml of LIT medium.

3.2.2 Thioglycollate-elicited peritoneal macrophages

Female mice *Slamf1*$^{-/-}$, *Tlr2*$^{-/-}$, BALB/c and BL6/c57 mice between 8-12 weeks old were injected intraperitoneally with 10% thioglycollate (Gibco, Grand Island, NY) (1 ml per mouse). After 4 days, mice were euthanized by CO_2 inhalation. Peritoneal cell were collected with 10 ml of cold PBS. Peritoneal cells were pelleted by centrifugation (260 g, 10 min, 4°C) and seeded in 6-well plates (10^6 cells/well) in RPMI medium supplement with 5% FBS overnight at 37°C. Non-adherent cells were removed by gently washing three times with warm PBS. At this time, more than 90% cells correspond to macrophages.

3.2.3 *In vitro* infection

Peritoneal macrophages were co-cultured with metacyclic trypomastigotes of the *T. cruzi* strains Dm28c, Y, M6421 cl6, 10R26, Bug2148 cl1 and VFRA cl1 in a rate of 5parasites:1cell; and analyzed at 1h (Interaction), 6h (Internalization) and 24h (Intracellular proliferation). Afterwards, the cells were washed with PBS three times to remove unbound parasite.

3.2.4 *In vivo* infection

Experiments were performed in the biosafety laboratory 3 in the animal facility at Centro de Biologia Molecular Severo Ochoa (CSIC-UAM), employing groups of 5 mice BALB/c and *Slamf1*$^{-/-}$. They were infected intraperitoneally with 2000 parasites/mice with the strains Dm28c, Y and VFRA cl1. The mice were sacrificed at 14 and 21 d.p.i. , with the respective control non-infected, by CO_2 inhalation. Samples of heart, spleen and liver were analyzed by Western Blot for protein expression and quantitative real time PCR (for parasite quantification and host's mRNA gene expression).

3.2.5 DNA extraction

Parasite DNA was isolated with the High Pure Template preparation kit (Roche) from different samples:

- Infected macrophages with the different *T. cruzi* strains Dm28c, Y, M6421 cl6, 10R26, Bug2148 cl1 and VFRA cl1 at 1 h, 6 h, 24 h and their respective no infected controls. Macrophages were scrapped from the p-6 cell with 200 μl of Binding buffer and transfer to 1.5 ml tubes (Eppendorf).

- 25-35 mg of infected tissues (Heart, spleen and liver) from BALB/c and *Slamf1*$^{-/-}$ mice and the respective controls. 200 µl of tissue lysis buffer, 40 µl of proteinase K and the tissue were mixed and incubated overnight at 55°C.

For all samples 200 µl of Binding buffer and 40µl Proteinase K (except for the tissues) were added and incubated for 10 min at 70°C. After that 100 µl of isopropanol was added, mixed and applied in the filter tube were centrifuged for 1 min at 8000 g. 500 µl of Inhibitor Removal Buffer was added to the filter tube and centrifuged for 1 min at 8000 g. Two washes with 500 µl of Wash buffer was performed with a centrifugation for 1 min at 8000 g. Extra centrifuge for 10 second to remove the excess of liquid was performed and finally 50 µl of elution buffer was added followed by a centrifugation for 1 min at 8000g. The purified DNA obtained was quantified in the Nano drop (Thermo Scientific) and kept at -70°C.

3.2.6 Parasite load

For *T. cruzi* detection, qPCR reactions were conducted with 20ng of the DNA from blood and macrophages and 100 ng tissues. *T. cruzi* DNA detection was performed following Piron *et al.,* 2007(Piron et al. 2007). The parasite load were performed by triplicate amplifying the intergenic region of the non-transcribed mini-exon gene using primer Cruzi 1 (5`ASTCGGCTGATCGTTTTCGA3`) Cruzi 2 (5`AATTCCTCCAAGCAGCGGATA3`) and the genomic mouse TNF primers TNF-antisense (5`CAGCAAGCATCTATGCACTTAGACCCC3`) TNF Sense (5`TCCCTCTCATCAGTTCTATGGCCCA3` on an ABI PRISM 7900 HT instrument (Applied Biosystem). The quantity of *T. cruzi* mouse DNA in the samples was calculated from the comparative threshold cycle (C_T) values obtained from *T. cruzi* primers and normalized with the respect mouse TNF primer. The regression equation resulting from plotting the C_T values obtained from standard curve from 1000 pg to 0.001 pg of parasite DNA, and then used to extrapolate the quantity of parasite DNA in the samples. Results were expressed as pg of *T. cruzi* DNA per ng of total DNA.

3.2.7 RNA extraction

RNA extraction was performed with TRIzol reagent (Invitrogen) following their protocol. We used different samples:

- Infected macrophages with the different *T. cruzi* strains Dm28c, Y, M6421 cl6, 10R26, Bug2148 cl1 and VFRA cl1 at 1h, 6h, 24 h and their respective no infected controls.

Macrophages were scrapped from the p-6 cell with 500 μl of TRIzol reagent and transfer to 1.5 ml tubes (Eppendorf).

- 25-35 mg of infected tissues (Heart, spleen and liver) from BALB/c and *Slamf1*$^{-/-}$ mice and the respective controls. The tissues were homogenized with a PT1300D (Kinematica Polytron, Fisher Scientific) in 1 ml of TRIzol reagent.

To the homogenized samples (macrophages and tissues) 200 μl of chloroform were added and mixed vigorously. The samples were centrifuged for 15 min at 12000 g, 4°C. The aqueous upper phase was removed into a new tube and 500 μl was added to precipitated the RNA, an incubation of 20 min was performed a -20°C. Then, the samples were centrifuged for 15 min at 12000 g, 4°C. The pellet was washed with 1 ml of 75% ethanol and centrifuged for 5 min at 7500 g, 4°C. The 75% ethanol was discarded and finally after an air dry the pellet was resuspended in 30 μl of DEPC water. The purified RNA obtained was quantified in the Nano drop (Thermo Scientific) and kept at -70°C.

3.2.8 Quantitative real time PCR (qPCR) and Reverse –transcription qPCR (RT-qPCR)

Total RNA were extracted by TRIzol reagent from:

- Infected macrophages with the different *T. cruzi* strains Dm28c, Y, M6421 cl6, 10R26, Bug2148 cl1 and VFRA cl1 at 1h, 6h, 24 h and their respective no infected controls.
- 25-35 mg of infected tissues (Heart, spleen and liver) from BALB/c and *Slamf1*$^{-/-}$ mice and the respective controls.

For quantitative RT-PCR analysis, reverse transcription of total RNA was performed using the High Capacity cDNA Archive Kit (Applied Biosystems) and the amplification of different enzymes and cytokines genes was performed using gene specific oligonucleotide (Table 4) in triplicate reactions with GoTaq® qPCR Master Mix (Promega) on an ABI PRISM 7900 HT instrument (Applied Biosystem, Life Sciences). The relative quantity of each gene expression was calculated by the by the comparative threshold cycle (C_T) method following the protocol instructions. All quantifications were normalized to the ribosomal 18S gene to account for the variability in the initial concentration of RNA and in the conversion efficiency of the reverse transcription (ΔC_T). Finally, all data from samples taken from infected macrophages or infected mice were normalized with the respect to the values obtained from non-infected macrophages or non-infected mice ($\Delta\Delta C_T$). The relative quantity (RQ) was calculated as, $RQ=2^{-\Delta\Delta Ct}$.

Table 4. qPCR Primers.

Primer Name	Gene	Sequence (5`-3`)
18s Right	*18s*	CCATCCAATCGGTAGTAGCG
18s Left	*18s*	AACCCGTTGAACCCCATT
Arg-1 Right	*Arg1*	TTTTTCCAGCAGACCAGCTT
Arg-1 Left	*Arg1*	AGAGATTATCGGAGCGCCTT
Cybb Right	*p47phox*	TGCAGTGCTATCATCCAAGC
Cybb Left	*p47phox*	CTTTCTCAGGGGTTCCAGTG
Il-10 Right	*Il10*	TGTCAAATTCATTCATGGCCT
Il-10 Left	*Il10*	ATCGATTTCTCCCCTGTGAA
Il-1b Right	*Il1b*	GGTCAAAGGTTTGGAAGCAG
Il-1b Left	*Il1b*	TGTGAAATGCCACCTTTTGA
Il-6 Right	*Il6*	ACCAGAGGAAATTTTCAATAGGC
Il-6 Left	*Il6*	TGATGCACTTGCAGAAAACA
Irg-1 Right	*Irg1*	CGTGTCGAAGCTTGGCGGGT
Irg-1 Left	*Irg1*	CCTGTGCCTCGCTGCTCGAC
Slamf1 Right	*Slamf1*	TTATTGCCGTGAAAACCAGC
Slamf1 Left	*Slamf1*	TCAACCTATCATCGCAAGCA
TNF Right	*Tnf*	AGGGTCTGGGCCATAGAACT
TNF Left	*Tnf*	CCACCACGCTCTTCTGTCTAC
TLR2 Right	*Tlr2*	GCTGGAGGACTCCTAGGCT
TLR2 Left	*Tlr2*	GTCAGAAGGAAACAGTCCGC

Genes evaluated in all infected samples were divided in enzymes (3 genes) and cytokine (4 genes):

Enzymes:

- NADPH Oxidase-2 (*NOX2*): NADPH oxidase is a multisubunit enzyme comprising membrane and cytosolic components, which actively communicate during the host responses to a wide variety of stimuli (Panday et al. 2015). NOX2 mediate ROS production which have an important role in the elimination of invading microorganisms in macrophages and neutrophils. In Gram- bacteria SLAMF1 receptor regulates positively the production of NOX2 (C. S. Ma and Deenick, 2011).
- Arginase-1 (*Arg1*): is expressed most abundantly, but not exclusively, in the liver. Catalyzes the hydrolysis of L-arginine to ornithine and urea. In macrophages is a M2 marker, induce TGF-β and cytokines such as IL-4, IL-10 and IL-13 (Cuervo *et al.*, 2008). During the infection by *T. cruzi* has been demonstrated that increases susceptibility.

- Immune-response gene 1 (*Irg1*): is highly expressed in mammalian macrophages, coding for an enzyme producing itaconic acid, which have an antimicrobial effect in macrophages, inhibiting isocitrate lyase, the key enzyme of the glyoxylate shunt (Michelucci *et al.*, 2013).

Cytokines:

- Pro-inflammatory: Interleukin 1b (*Il1b*), Interleukin 6 (*Il6*) and Tumor Necrosis Factor (*Tnf*).
- Anti-inflammatory: Interleukin 10 (*Il10*).

3.2.9 Protein extraction and western blotting

Different samples for the protein extraction were used:

- 25-35 mg of infected tissues (Heart, spleen and liver) from BALB/c and *Slamf1*$^{-/-}$ mice and the respective controls. The tissues were homogenized with a PT1300D (Kinematica Polytron, Fisher Scientific) in 1 ml of RIPA (50mM Tris-HCl (pH 8), 50 mM NaCl, 1 mM EDTA, Complete Mini Protease inhibitor Cocktail tablets (Roche), 0.1% SDS, 1% Triton-X100, 0.5% sodium deoxycholate in distilled water).

The samples were lysed in RIPA for 30 min at 4ºC and supernatants were collected after centrifugation. Protein concentration was determined by the bicinchonic acid method (BCA, Pierce) using Bovine Serum Albumin for standard curve. 30 μg of heart, 30 μg of liver or 40 μg of spleen protein extracts were separated by SDS-PAGE (10-15% Poliacrylamide) and subjected to Western Blot with appropriate antibodies (Table 5) overnight. Nitrocellulose membrane Hybond-ECL (Amersham Bioscience) was also incubated with secondary antibody coupled to peroxidase and revealed by Clarity Westen ECL Substrate (Bio-Rad) and protein detected by ImageQuant™ LAS 4000 mini (GE).

Table 5. Western blot Antibodies

Antigen	Reference	Provided	Dilution	Positive control
iNOS	sc-650	Santa Cruz Biotecnology	1:1000	Raw cells +LPS
Arg-1	sc-18354	Santa Cruz Biotecnology	1:1000	Raw cells +LPS
Actin	sc-1616	Santa Cruz Biotecnology	1:1000	Raw cells +LPS
COX-2	BD-610203	BD Bioscience	1:1000	Raw cells +LPS
NOX2	sc-130543	Santa Cruz Biotecnology	1:1000	Raw cells +LPS
YAP1	14074	Cell Signalling	1:1000	

3.2.10 Reactive Oxygen Species Assay

Peritoneal macrophages BALB/c and *Slamf1*$^{-/-}$were co-cultured with metacyclic trypomastigotes of the *T. cruzi* strains Dm28c, Y, M6421 cl6, 10R26, Bug2148 cl1 and VFRA cl1 in a rate of 5parasites:1cell; at 6 h.p.i. Afterwards, the cells were washed with PBS 1X three times to remove unbound parasite. The macrophages were seed with RPMI without Red phenol. Following the CELLROX green reagent (Life Technologies) protocol, Macrophages were scrapped from the 6-well plate cell with 1 ml of RPMI without red phenol reagent and transferred to cytometry tubes. 2 µl of CellROX Green Reagent were added to the samples for a final concentration of 250 µM and incubated for 30 min at 37°C. The medium was discarded and the samples were collected, pelleted by centrifugation (720 g, 10 min. 37°C) and washed three times with PBS 1X following by centrifugation (720 g, 10 min. 37°C). The samples were fixed with paraformaldehyde 1% in PBS 20 min at 4°C protected from light. Finally, the samples were analyzed by flow cytometry in the FACSCanto II (BD Biosciences) and the data was analyzed with the program FlowJo (TriStar, Ashland, OR, USA).

3.2.11 Construction of the networks

We used data of the expression levels of the 9 genes (3 enzymes, 4 cytokines and 2 receptors) and the parasite load (*T. cruzi*) of macrophage and organ samples using qRT-PCR values to calculate the Spearman's correlation ρ(rho) between the 10 parameters with the GraphPad Prism version 5.0 for Windows (GraphPad Software, San Diego California USA). The statistically significant correlation data was introduced in text format into the Cytoscape program (http://www.cytoscape.org), a software platform for network visualization and analyses. The correlation data is detailed in the in the Appendix (Tables S2 to S16). The networks picture each strain of *T. cruzi* as a central node: Dm28c (Blue ellipse), Y (Red ellipse), M6421 cl6 (Green ellipse), 10R26 (Orange ellipse), Bug2148 cl1 (Purple ellipse) and VFRA (Pink ellipse). Pairs of data (secondary nodes) with significant correlation (Figure SX) are indicated in boxes connected to the nodes by lines (edges). For positive correlations, when data increase (+ +) or decrease (- -), continuous or dashed red lines were drawn, respectively. For negative correlations, when the first data in the pair increases and the second decreases (+ -) a continuous green line was drawn, and when the first data decreases and the second increases (- +) a dashed green line was drawn. Secondary nodes in the periphery of the central nodes indicate the associations of a particular strain and the association between principal nodes indicates common associations between different parasite strains.

3.2.12 Itaconic acid levels

Itaconic acid levels were determined in mouse heart tissues extracts from non-infected and 21 d.p.i. by Metabolon Inc. Heart tissue was defrosted at room temperature and cut approximately 80 mg. The sample was heat-inactivated at 50°C for 30 min. Follow by that 1600 µl of methanol solvent A (containing standard resuspended in 80% HPLC grade Methanol; Sigma Aldrich) were added to the heart. After incubation for 24 h at room temperature, samples were stored at -80°C until shipment in dry ice. The extracted samples were split into equal parts for analysis on the gas chromatography (GC)/mass spectrometry (MS) and liquid chromatography (LC)/MS platforms. Values were normalized in terms of raw area counts (OrigScale). For a single day run, this is equivalent to the raw data. Each biochemical in OrigScale is rescaled to set the median equal to 1 and expressed as imputed normalized counts for each biochemical (ScaledImpData) (Gironès *et al.*, 2014).

3.2.13 Inhibition Assay of Itaconate

Epimastigote TcI (Dm28c, Sylvio X10 cl1 and C8), TcII (Y, Esmeraldo cl3 and Tul8 cl1), TcIII (CM17 and M6421 cl6), TcVI (10R26), TcV (Bug2148 cl1 and SC43 cl1) and TcVI (Cl Brener, VFRA cl1, Tulahuén cl2 and Tulahuén) were cultivate in 96-well plates (10^6 parasite/well) in LIT medium supplement with 10% FBS at 28°C. We analyzed 7 different treatment conditions (0, 0.3, 1, 3, 10, 30, 100 mM of Itaconate) and control cultures were maintained without drug, for 4 days at 28°C. Each one of the 15 *T.cruzi* strains and treatment concentration was evaluated by triplicate. After 4 days of treatment parasite inhibition were determined by 3-(4,5-Dimethylthiazol-2-yl)-2,5-diphenyltetrazolium bromide assay (MTT assay), where the parasites were collected by centrifugation (720 g, 10 min, 28°C), the supernatant were removed and the pellet was resuspended in 50 µl of 5 mg/ml of MTT and incubated by 3 hours. Afterward, the pellet were collected by centrifugation (720 g, 10 min, 28°C) and resuspended in 100 µl of MTT solvent (1:1 Isopropanol : DMSO) and the absorbance read at 590 nm. The half maximal inhibitory concentration (IC_{50}) were calculated to evaluate the treatment with the GraphPad Prism version 5.0 for Windows (GraphPad Software, San Diego California USA).

3.2.14 Statistical Analysis

For *in vivo* experiments data reported is mean ± Standard deviation (SD) from groups of five mice (n=5). Results shown from *in vitro* experiments are representative of at least two experiments.

Significance was evaluated by student´s two-tailed *t*-test (95% confidence interval) with the GraphPad Prism version 5.0 for Windows (GraphPad Software, San Diego California USA).

Discriminant Analysis of Principal Components (DAPC) was performed, to assess the association between the gene expressions of enzymes, cytokines and the parasite load in BALB/c and *Slamf1*$^{-/-}$ macrophages or organs infected with the different strains of *T. cruzi* with the Statistical Package for the Social Sciences 17, SPSS.

RESULTS

4 RESULTS

4.1 MOUSE GENETIC BACKGROUND

The mouse genetic background is beginning to be considered an important factor in biomedical research since it determines disease outcome. Susceptibility and resistance to parasite infections in mice are determined by unknown genetic determinants, but there are two strains considered to be the extremes BALB/c and C57BL/6. In the case of Chagas disease BALB/c genetic background has been reported as susceptible while C57BL/6 has been reported as resistant to *in vivo* infection with the strain Y (Cuervo *et al.*, 2008). However, other strains as Tulahuén behaved differently (Carrera-Silva *et al.*, 2008). In this study we used 6 different reference strains of *T. cruzi*, classified from TcI to TcVI, with the aim to understand the role of the genetic variability of the parasite in BALB/c and C57BL/6 peritoneal macrophage model. We evaluated the three phases of the infection: The interaction (1 h.p.i.), the internalization (6 h.p.i) and the intracellular proliferation (24 h.p.i.). those times were selected based on previous evidence (Maganto-Garcia *et al.*, 2008; Zhao *et al.*, 2013).

4.1.1 Kinetics of BALB/c and C57BL/6 Peritoneal Macrophage Infection with Different Strains of *T. cruzi.*

First, we evaluated the level of infection between BALB/c and C57BL/6 peritoneal macrophages infected with the *T. cruzi* strains, measuring the parasite load in the three phases. Figure 11 shows the kinetics of the parasite load in peritoneal macrophages.

All the parasite strains showed higher intracellular proliferation (24 h.p.i.) in BALB/c macrophages than C57BL/6 macrophages, in agreement with previous *in vivo* results with the Y strain (Cuervo *et al.*, 2008; Sanoja *et al.*, 2013). Despite this, no significant differences were observed in the interaction (1 h.p.i.) among both mouse strains. Dm28c showed significantly higher replication than the rest in BALB/c but the opposite in C57BL/6 macrophages.

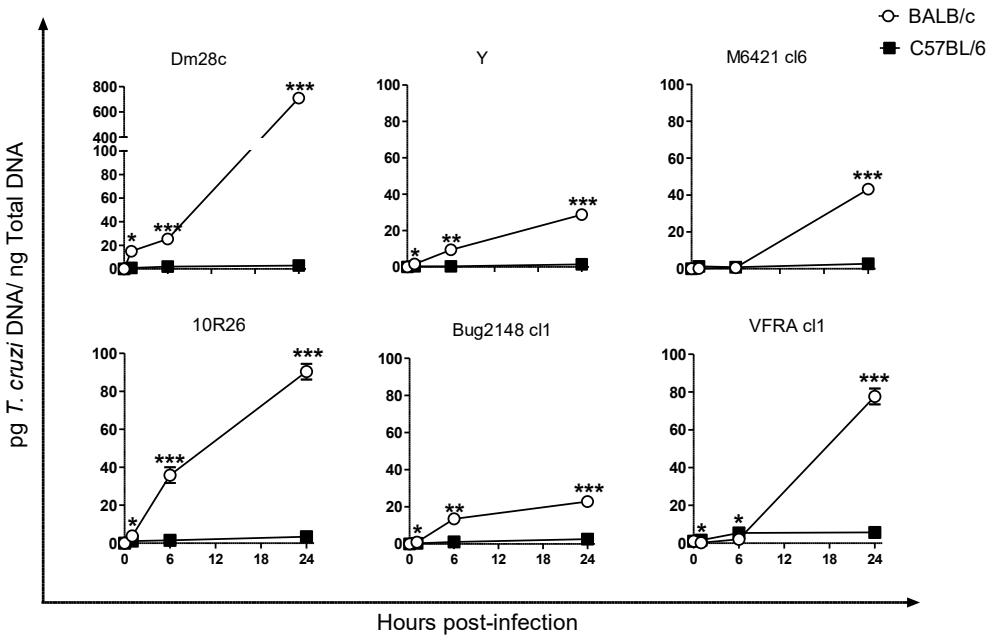

Figure 11. Parasite load in infected macrophages. *Kinetic analysis of parasite load of BALB/c and C57BL6 peritoneal macrophages at 1 h, 6 h and 24 h after infection with parasite strains of different DTUs, parasite load was quantified by qPCR. Mean and Standard error of the mean ± (SEM) of two independent experiments are represented. The asterisks indicate the statistical significance, t-student (*p<0.05, **p<0.005 and ***p<0.001), between BALB/c and C57BL/6 macrophages.*

4.1.2 Expression of Immunoregulatory Genes in C57BL/6 and BALB/c Macrophages Infected with Different Strains of *T. cruzi.*

Next, we studied the macrophage activation by analyzing the kinetics of gene expression of a panel of relevant molecules. We measured the gene expression of 3 enzymes (*Nox2, Arg1* and *Irg1)* defining macrophage M1, M2 and inflammation status, 3 pro-inflammatory cytokines (*Il1b, Il6* and *Tnf)* and the anti-inflammatory cytokine *Il10.* In addition, we also quantified gene expression of *Slamf1* and *Tlr2* receptors, known to be important for infectivity, as well as the parasite load. Table 6 summarizes the results in BALB/c and C57BL/6 macrophages infected with different parasite strains. We observed high variability in gene expression and parasite load depending on the strain. In general, we found an enhanced enzyme and cytokine gene expression in C57BL/6 macrophages infected with all the strains of *T. cruzi* compared with the infection of same strains in BALB/c macrophages. Thus the high C57BL/6 macrophage activation together with low parasite load indicated a more efficient control of infection in this strain of mice. Contrarily, BALB/c macrophages only presented higher expression of *Tnf, Slamf1* and *Tlr2* and higher parasite load compared with the C57BL/6 macrophages, indicating a less efficient control of parasite infection.

Table 6. Summary of expression of immunoregulatory genes and parasite load in BALB/c and C57BL/6 peritoneal macrophages infected with different strains of T. cruzi. *Gene expression was determined by RT-qPCR and RQ value were obtained after normalizing value from infected respect to no-infected macrophages. For each gene and parasite load a color code was given from high (Red) to low (Green). The real values obtained and the statistically significant differences between mouse strains are shown in Figure S 3 (Enzymes), Figure S 4 (Cytokines) and Figure S 5 (Receptors). Parasite load (T.cruzi) corresponds to values from Figure 11.*

		Interaction (1 h)										Internalization (6 h)										Intracellular proliferation (24 h)									
		Arg1	*Irg1*	*Cybb*	*Il1b*	*Il6*	*Il10*	*Tnf*	*Slamf1*	*Tlr2*	*T.cruzi*	*Arg1*	*Irg1*	*Cybb*	*Il1b*	*Il6*	*Il10*	*Tnf*	*Slamf1*	*Tlr2*	*T.cruzi*	*Arg1*	*Irg1*	*Cybb*	*Il1b*	*Il6*	*Il10*	*Tnf*	*Slamf1*	*Tlr2*	*T.cruzi*
BALB/c	Dm28c																														
	Y																														
	M6421 cl6																														
	10R26																														
	Bug2148 cl1																														
	VFRA c1																														
C57BL/6	Dm28c																														
	Y																														
	M6421 cl6																														
	10R26																														
	Bug2148 cl1																														
	VFRA c1																														

High Low

Despite this general tendency, we observed differences in gene expression and parasite load depending on the infecting *T.cruzi* strain. To further analyze the data, we performed Discriminant Analysis of Principal Components (DAPC) with the gene expression and parasite load data, to find associations between activation state of the macrophages, mice and *T. cruzi* strains. The analysis was performed with the gene expression of the 3 enzymes, 4 cytokines and the parasite load in the three different phases of the *in vitro* infection evaluated.

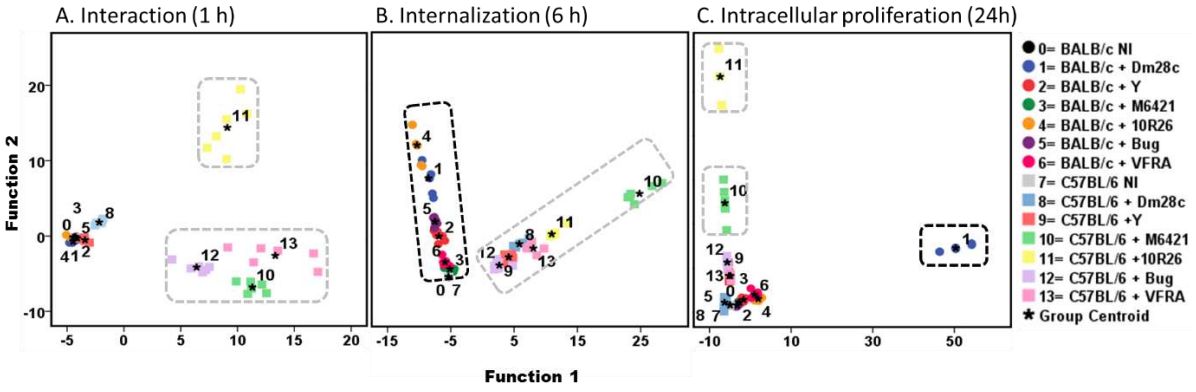

Figure 12. Discriminant Analysis of Principal Components (DAPC). *These scatterplots show the first two principal components of the DAPC of gene expression and parasite load data according to the three different phases of macrophage infection with the different T. cruzi strains.* ***A.*** *Interaction at 1 h.p.i.* ***B.*** *Internalization at 6 h.p.i.* ***C.*** *Intracellular proliferation at 24 h.p.i. The diagrams show clustering of BALB/c peritoneal macrophages infected with the different strains of T. cruzi (Black dashed line) and C57BL/6 (Gray dashed line).*

The discriminant analysis of principal components at 1 h.p.i. (Figure ***12*** A), was able to discriminate 76.7%, where 52% and 24.7% are explained in first (x-axis) and second (y-axis) principal components, respectively. Three different clusters were found, the first was the infection in C57BL/6 macrophages with the strains M6421 cl6, Bug2148 cl1 and VFRA cl1; the second was the infection

with 10R26 in C57BL/6 macrophages and in the third one the rest of the infections including Dm28c and Y in C57BL/6 macrophages and all the strains in BALB/c macrophages.

Table 7. Discriminant frequencies in the interaction phase in BALB/c and C57BL/6 peritoneal macrophages infected with different strains of T. cruzi

1 h			Theoretical Group													
			BALB/c							C57BL/6						
			NI %(N)	Dm28c %(N)	Y %(N)	M6421 %(N)	10R26 %(N)	Bug2148 %(N)	VRFA %(N)	NI %(N)	Dm28c %(N)	Y %(N)	M6421 %(N)	10R26 %(N)	Bug2148 %(N)	VRFA %(N)
Real Group	BALB/c	NI	100 (6)													
		Dm28c		100 (6)												
		Y			100 (6)											
		M6421				67 (4)		17 (1)	17 (1)							
		10R26			33 (2)		67 (4)									
		Bug2148						83 (5)	17 (1)							
		VFRA				17 (1)		17 (1)	67 (4)							
	C57BL/6	NI								100 (6)						
		Dm28c									100 (6)					
		Y			17 (1)							83 (5)				
		M6421											100 (6)			
		10R26												100 (6)		
		Bug2148													100 (6)	
		VFRA														100 (6)

Table 7 shows that the theoretical groups predicted by the DAPC analysis matched in a high percent with the real groups. We found that all the infections with the different strains of T. cruzi discriminated between BALB/c and C57BL/6 mouse genetic background, except infection in C57BL/6 with the Y that was grouped as a BALB/c infection.

Table 8. Discriminant frequencies in the internalization phase in BALB/c and C57BL/6 peritoneal macrophages infected with different strains of T. cruzi

6 h			Theoretical Group													
			BALB/c							C57BL/6						
			NI %(N)	Dm28c %(N)	Y %(N)	M6421 %(N)	10R26 %(N)	Bug2148 %(N)	VRFA %(N)	NI %(N)	Dm28c %(N)	Y %(N)	M6421 %(N)	10R26 %(N)	Bug2148 %(N)	VRFA %(N)
Real Group	BALB/c	NI	100 (6)													
		Dm28c		83 (5)			17 (1)									
		Y			83 (5)			17 (1)								
		M6421				67 (4)			33 (2)							
		10R26		17 (1)			83 (5)									
		Bug2148						100 (6)								
		VFRA				17 (1)			83 (5)							
	C57BL/6	NI								100 (6)						
		Dm28c									100 (6)					
		Y										100 (6)				
		M6421											100 (6)			
		10R26												100 (6)		
		Bug2148													100 (6)	
		VFRA														100 (6)

DAPC analysis at 6 h.p.i. discriminated 78.9 % this phase, which 61.5% and 17.4 % are explained in first (x-axis) and second (y-axis) principal components, respectively. Two different clusters were found, one for all infected in C57BL/6 and the other all infection in BALB/c and the non-infected controls BALB/c and C57BL/6 (Figure ***12*** B). The percent of the discrimination shown in Table 8 demonstrated that in this phase with the components evaluated, the infections in C57BL/6

macrophages with the different strains of *T. cruzi* were able to discriminate each group in a 100%. In contrast, the infection in BALB/c macrophages with the *T. cruzi* strains could discriminate one in 100%, four in 83% and the last one 67%.

The DAPC analysis at 24 h.p.i was only able to discriminate 88.2% our model, which 71.7% and 16.5% are explained in first (x-axis) and second (y-axis) principal components, respectively. At this time, more heterogeneity was found as should be expected as longer time passed. Thus, only BALB/c macrophages infected with Dm28c and M6421 cl6 and 10R26 in C57BL/6 macrophages were discriminated (Figure ***12*** C). The percent of the discrimination is shown in Table 9 and again we found a clear discrimination between the infections in BALB/c and C57BL/6 macrophages with all strains and better discrimination in the C57BL/6 infections.

Thus, mouse gene expression and parasite load data DAPC was able to correctly discriminate between groups in a high percent indicating a high heterogeneity in the activation of macrophages depending on mouse and parasite strains, being this effect more evident as the intracellular infection progress.

However, the mouse genetic background seems more important than the parasite strain in the process of macrophage activation and it is influence in parasite load at different times, especially at 1 h.p.i. and 6 h.p.i. At 24 h.p.i. only 3 combination of mouse and parasite load grouped separated from the rest.

Table 9. Discriminant frequencies in the intracellular proliferation phase in BALB/c and C57BL/6 peritoneal macrophages infected with different strains of T. cruzi.

24 h			Theoretical Group													
			BALB/c							C57BL/6						
			NI %(N)	Dm28c %(N)	Y %(N)	M6421 %(N)	10R26 %(N)	Bug2148 %(N)	VRFA %(N)	NI %(N)	Dm28c %(N)	Y %(N)	M6421 %(N)	10R26 %(N)	Bug2148 %(N)	VRFA %(N)
Real Group	BALB/c	NI	100 (6)													
		Dm28c		100 (6)												
		Y			100 (6)											
		M6421				100 (6)										
		10R26					83 (5)		17 (1)							
		Bug2148			17 (1)			83 (5)								
		VFRA							100 (6)							
	C57BL/6	NI								100 (6)						
		Dm28c									100 (6)					
		Y										100 (6)				
		M6421											83 (5)		17 (1)	
		10R26												100 (6)		
		Bug2148													100 (6)	
		VFRA														100 (6)

4.1.3 Correlation Networks

Finally, correlation analysis were performed for determine the direction and strength of a relationship between our variables.

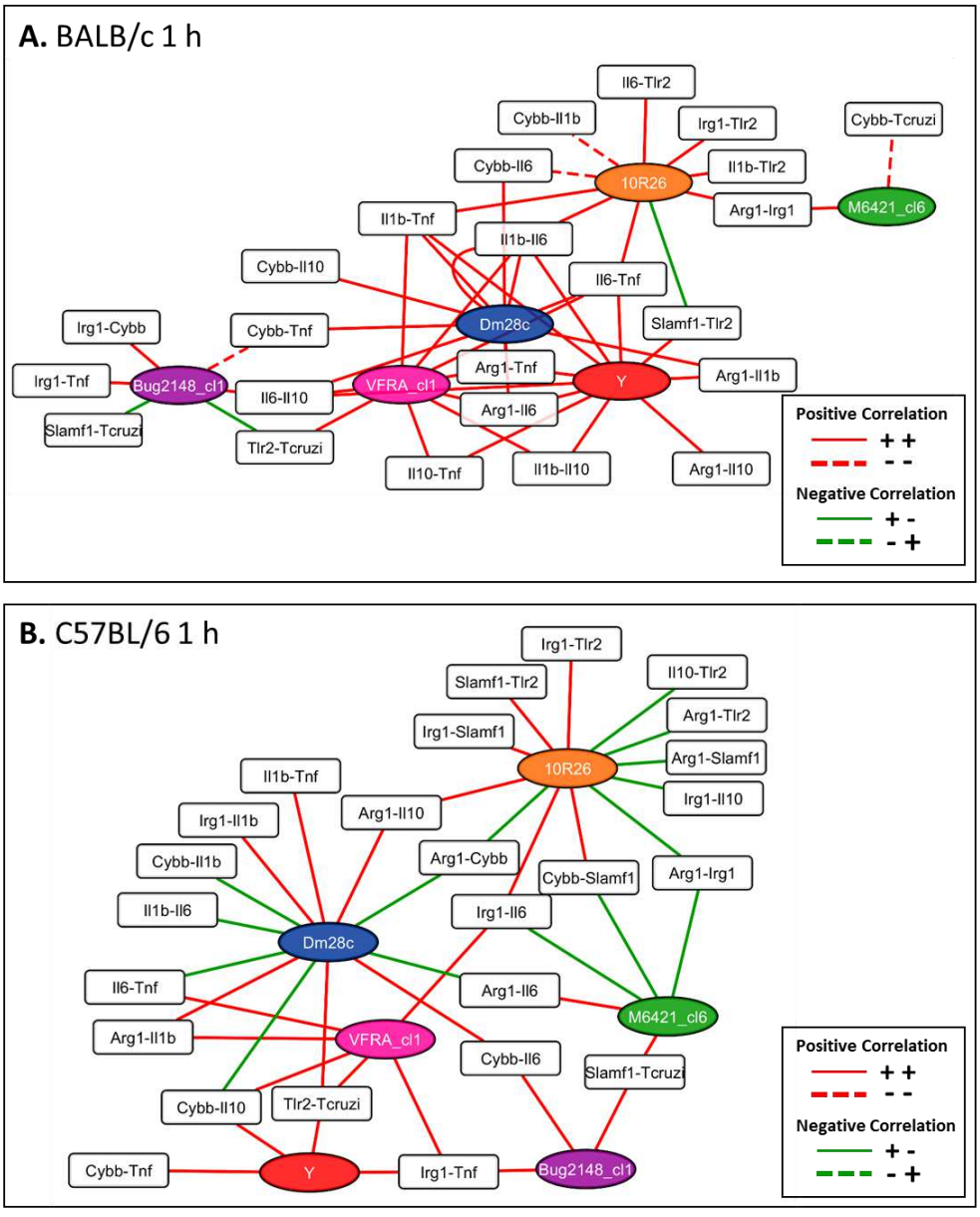

Figure 13. Networks of the macrophage activation during the interaction phase with the different strains of T. cruzi. A. *BALB/c macrophages.* ***B.*** *C57BL/6 macrophages. Networks were generated and represented as indicated in the Methods section.*

We included gene expression of the immunoregulatory genes, as well as the receptor expression (*Slamf1* and *Tlr2)* and the parasite load in the analysis. As in the summary of the genes we found

different patterns of positive or negative correlations (during interaction in Table S 2, internalization in Table S 3 and intracellular proliferation in Table S 4) depending not only on the mouse genetic background of the infected macrophages but also between the different strains of *T. cruzi.* In order to easily visualize the correlation we used the Cytoscape software to draw correlation network.

We used the different strains of *T.cruzi* as central nodes. During the interaction in BALB/c macrophages the resulting network was composed of 24 secondary nodes and 49 edges (Figure 13 A) and C57BL/6 was composed of 25 secondary nodes and 42 edges (Figure 13 B), with 6 as the maximum degree of connectivity of a node and 1 as the minimum.

We found an aggrupation between the Dm28c, Y and VFRA cl1 strains by positive correlations during the interaction of BALB/c macrophages. In contrast, for C57BL/6 many of the correlations for Dm28c were negative, therefore changing the shape of the network and drawing it apart, indicating that this strain has a different behavior in macrophages depending on the mouse genetic background. In the case of the Y strain in C57BL/6 the loss and appearance of new correlations in of correlations compared to BALB/c separated it from Dm28c and VFRA cl1. In the case of 10R26 and Bug2148 cl1 infections in BALB/c macrophages there were few negative correlations, while in C57BL/6 macrophages Dm28c, 10R26 and M6421 cl6 present more negative than positive correlation. The increment of negative correlation in C57BL/6 mouse genetic background associated with the low parasite load, which could indicate a substantial interaction and early signal transduction after binding of *T.cruzi* to macrophages. Interestingly, a positive correlation between the parasite load and *Tlr2* was found in the infection in C57BL/6 macrophages with the strain Dm28c, Y and VFRA cl1; and positive correlation between the parasite load and *Slamf1* with the strains M6421 cl6 and Bug218 cl6 with the same of mouse macrophages, in agreement with gene expression show in Table S 2, Table 6 and parasite load (Figure 11). Interestingly, in BALB/c macrophages high expression of *Tlr2* and *Slamf1* correlated with low parasite load of Bug2148_cl1. However, in C57BL/6 high expression of *Tlr2* correlated with high parasite load of Y and Dm28c, and *Slamf1* with M6421_cl1 and Bug2148_cl1.

The resulting networks during the internalization phase in BALB/c macrophages was composed of 18 secondary nodes and 28 edges (Figure 14 A) and C57BL/6 was composed of 8 secondary nodes and 14 edges (Figure 14 B), with 6 as the maximum degree of connectivity of a node and 1 as the minimum. In both cases a reduction compared with interaction phase was found in secondary nodes and edges. In C57BL/6 internalization no significant positive or negative correlations associated with

the strain VFRA cl1 were found. In BALB/c and C57BL/6 macrophages infected with the 10R26 there were less correlations during the internalization compared to the interaction, this and the increment in the parasite load indicated the lack of control of the infection during this phase. In both cases the strain showing more association with the others strains was Dm28c, in BALB/c with Y, M6421 cl6 Bug2148 cl1 and VFRA cl1 and in C57BL/6 with M6421 cl6, 10R26 and Bug2148 cl1. Association in C57BL/6 macrophages was found between the down regulation of both, parasite load and gene expression of *Slamf1* and *Tlr2* receptors.

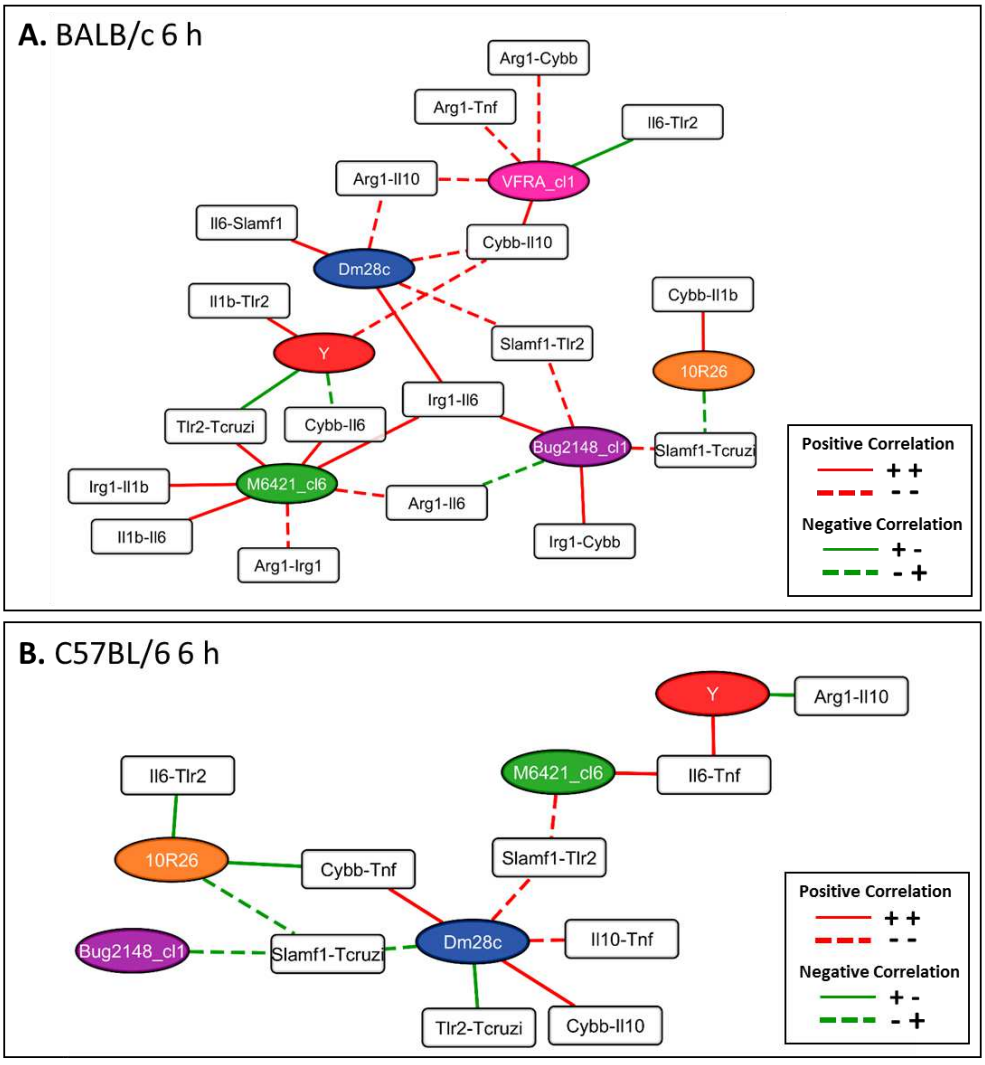

Figure 14. Networks of the macrophage activation during the internalization phase with the different strains of T. cruzi. A. *BALB/c macrophages.* ***B.*** *C57BL/6 macrophages. Networks were generated and represented as indicated in the Methods section.*

In the phase of intracellular proliferation the resulting network for BALB/c macrophages was composed of 14 secondary nodes and 20 edges (Figure 15 A) and for C57BL/6 macrophages it was

composed of 15 secondary nodes and 20 edges (Figure 15 B), with 6 as the maximum degree of connectivity of a node and 1 as the minimum. No significant correlations were found in the intracellular proliferation of Dm28c in BALB/c macrophages and the internalization of VFRA cl1 in C57BL6 macrophages, were in both cases high parasite load was found respect to other parasite strain (Figure 11), likes because the high level of infection with Dm28c reduced the macrophage control of infection or even at this phase the macrophage killed and released new parasites. Again, higher numbers of positive correlations where found in all infections in BALB/c macrophages compared to C57BL/6 macrophages.

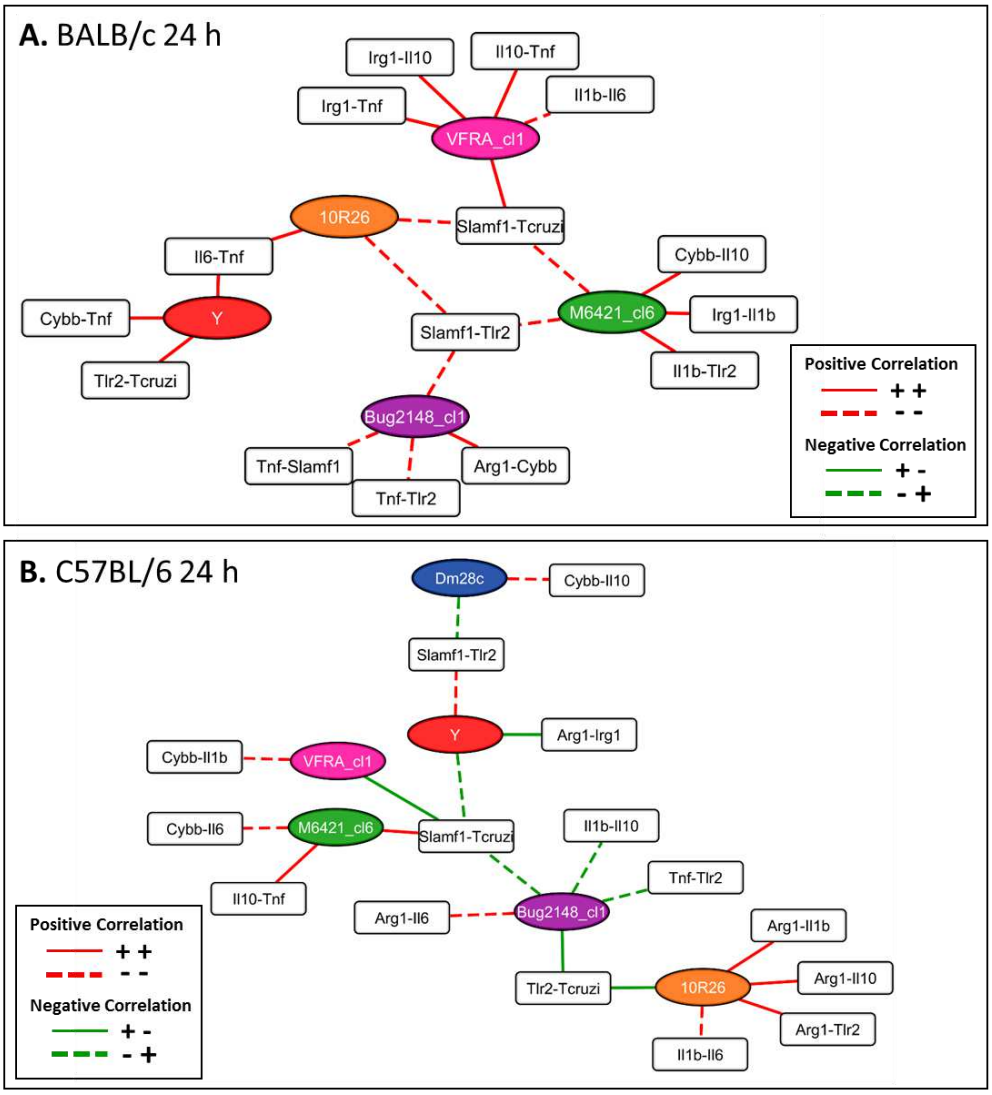

Figure 15. Networks of the macrophage activation during the intracellular proliferation phase with the different strains of T. cruzi. A. *BALB/c macrophages.* ***B.*** *C57BL/6 macrophages. Networks were generated and represented as indicated in the Methods section.*

4.2 TLR2 IN MACROPHAGES

TLR receptors play an important role in the entry of diverse pathogens, previous studies using the Y strain demonstrated that TLR2 is required for the entry of *T. cruzi* and in the previous section we show that TLR2 expression positively correlates with the parasite load especially during the interaction at 1 h, for many parasite strains. On the other hand, the variability of the structure of the GIPLs in the parasite, which is different depending on the parasite strain, determines the recognition by TLR2 or TLR4 (Campos *et al.*, 2001). For this reason we study the role of TLR2 in macrophage activation and the pathogen recognition with different *T. cruzi* strains.

4.2.1 Kinetics of C57BL/6 and *Tlr2*$^{-/-}$ Peritoneal Macrophage Infection with Different Strains of *T.cruzi.*

To determine the role of TLR2 receptor, we analyzed the kinetic of parasite load inside *Tlr2*$^{-/-}$ peritoneal macrophages to evaluate their susceptibility. The *Tlr2*$^{-/-}$ mouse strain used has a C57BL/6 background, for this reason we compared the rate of infection between *Tlr2*$^{-/-}$ and C57BL/6 peritoneal macrophages infected with the *T. cruzi* strains.

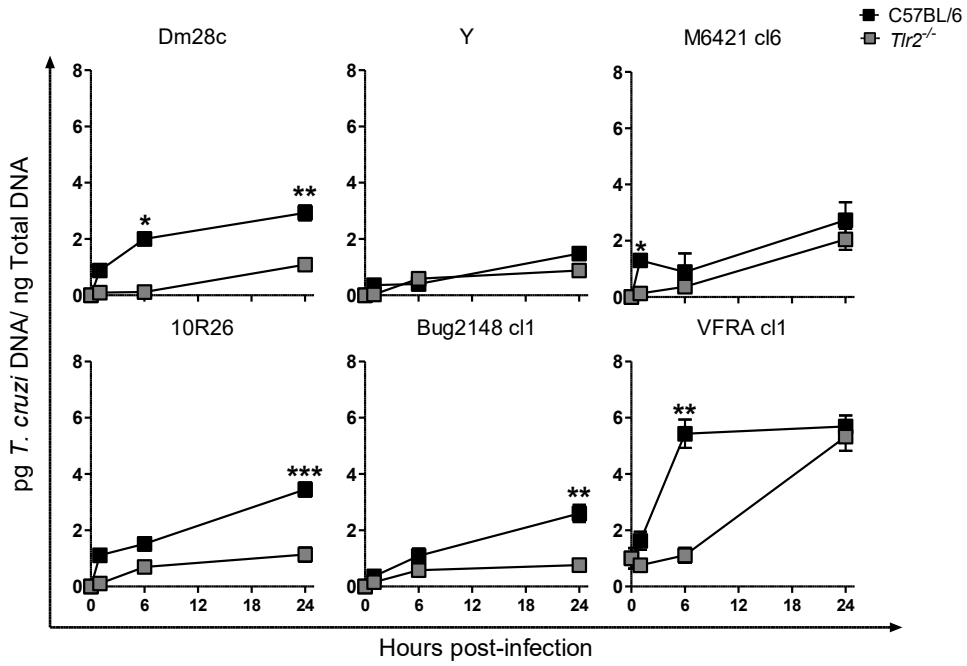

Figure 16. Kinetic of parasite load in C57BL/6 and Tlr2$^{-/-}$ peritoneal macrophages*. Kinetic analysis of parasite load of C57BL6 and Tlr2$^{-/-}$ peritoneal macrophages at 1 h, 6 h and 24 h after infection with parasite strains of different DTUs, parasite load was quantified by qPCR. Mean and Standard error of the mean ± (SEM) two independent experiments are represented. The asterisks indicate the statistical significance, t-student (*p<0.05, **p<0.005 and ***p<0.001), between Tlr2$^{-/-}$ and C57BL/6 macrophages.*

Figure 16 shows parasite loads in peritoneal macrophages at different times. We found that *Tlr2*$^{-/-}$ macrophages presented lower parasite load compared with C57BL/6 macrophages. These were significant at 1 h.p.i. for M6421 cl6, at 6 h.p.i. for Dm28c and VFRA cl 1 and at 24 h.p.i. for Dm28c and 10R26. However, in other conditions parasite load was also lower in *Tlr2*$^{-/-}$ macrophages in comparison with C57BL/6, indicating the importance of *Tlr2* for *T. cruzi* entry at all times points.

4.2.2 Role of TLR2 Receptor in the Phases of Peritoneal Macrophages Infected with Different Strains of *T. cruzi*

To evaluate the effect of TLR2 receptor efficiency in the different phases, we first normalized parasite load of *Tlr2*$^{-/-}$peritoneal infected macrophages in different phases by dividing *Tlr2*$^{-/-}$ parasite load by C57BL/6 parasite load. Secondly, we took the value of parasite load at 1 h.p.i, Figure 17 A shows normalized parasite load at 1 h.p.i. Parasite load in the internalization phase at 6 h.p.i. was normalized respect normalized levels at interaction phase (Figure 17 B). Finally, intracellular proliferation at 24 h.p.i. was normalized respect normalized levels at internalization phase (Figure 17 C). We found that *Tlr2* receptor is required for the interaction, internalization and the intracellular proliferation for all strains, except for the internalization of Y.

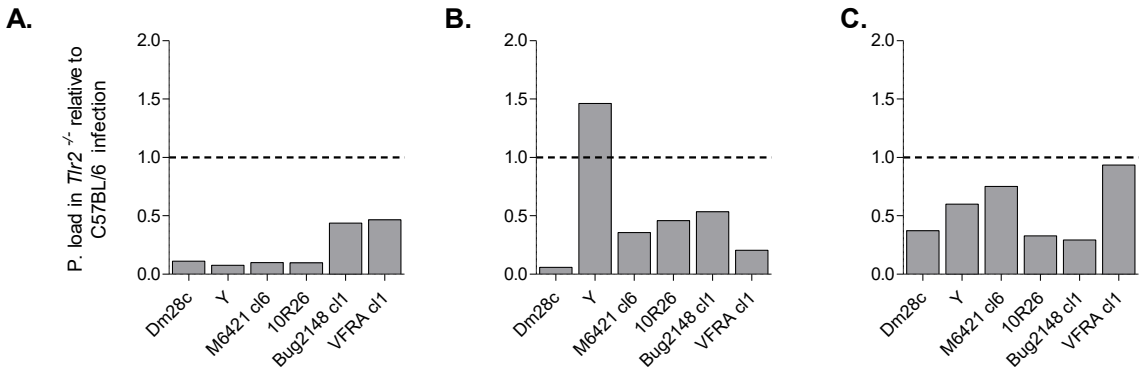

Figure 17. Effect of TLR2 deficiency on parasite load of peritoneal macrophages respect C57BL/6. *Dashed lines correspond to normalized C57BL/6 parasite load (equal to 1 for all parasite strains). Gray boxes correspond to normalized values of Tlr2*$^{-/-}$ *macrophages at each stage of infection.* ***A.*** *Interaction at 1 h.p.i.* ***B.*** *Internalization at 6 h.p.i.* ***C.*** *Replication at 24 h.p.i.*

4.2.3 Expression of Immunoregulatory Genes in C57BL/6 and *Tlr2*$^{-/-}$ Macrophages Infected with Different Strains of *T. cruzi.*

Table 10 summarizes the gene expression of the 3 enzymes, 4 cytokines, 2 receptors and the parasite load of *Tlr2*$^{-/-}$ and C57BL/6 macrophages infected with the different strains of *T. cruzi*

(Figure S 6, Figure S 7 and Figure S 8). A stronger activation was found in C57BL/6 than *Tlr2*$^{-/-}$ macrophages, as it would be expected if *T. cruzi* binds to TLR2. However, there was high parasite load in *Tlr2*$^{-/-}$ macrophages infected with VFRA cl1 compared with the rest of parasite strains, which was similar to the values that we found in the C57BL/6 macrophage infections, at 24 h.p.i nonetheless this is not resulting in higher activation of macrophages with that strain.

Table 10. Summary of expression of immunoregulatory genes and parasite load in C57BL/6 and Tlr2*$^{-/-}$ *peritoneal macrophages infected with different strains of T. cruzi. *Gene expression was determined by RT-qPCR and RQ value were obtained after normalizing value from infected respect to no-infected macrophages. Results are shown in Figure S 5 (Enzymes), Figure S 6 (Cytokines) and Figure S 7(Receptors). Parasite load (T.cruzi) correspond to value from Figure 16. For each gene and parasite load a color code was given from high (Red) to low (Green).*

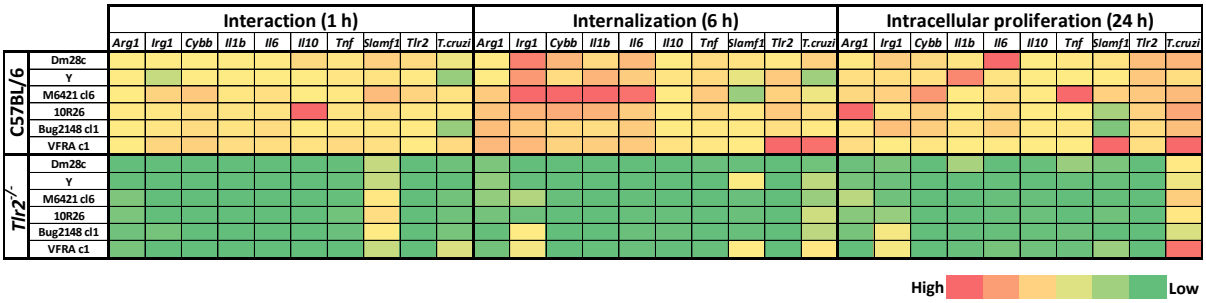

The discriminant analysis of principal components was performed with the gene expression of the 3 enzymes, 4 cytokines and the parasite load in the three different phases evaluated (Figure 18) to further determine the role of *Tlr2* in the activation of macrophages infected with different strains of *T. cruzi.*

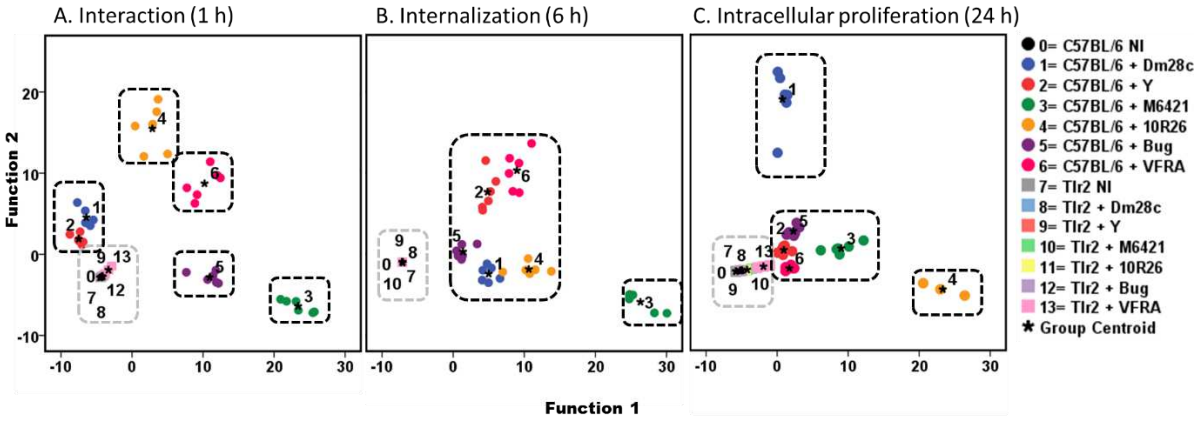

Figure 18. Discriminant Analysis of Principal Components (DAPC). *These scatterplots show the first two principal components of the DAPC of gene expression and parasite load data according to the three different phases of the macrophage infection with the different T. cruzi strains.* ***A.*** *Interaction at 1h* ***B.*** *Internalization at 6h* ***C.*** *Intracellular proliferation at 24h. The diagrams show clusters of C57BL/6 peritoneal macrophages infected with the different strains of T. cruzi (Black dashed line) and Tlr2* $^{-/-}$ *(Gray dashed line).*

The DAPC analysis was able to discriminate 84% in our model, in which 58.4% and 25.6% are explained in first (x-axis) and second (y-axis) principal components, respectively. We observed that the data allowed discrimination of M6421 cl 6 to VFRA cl 1 infecting parasite strains in C57BL/6 macrophages but not for Dm28c and Y that grouped together (Figure 18 A, Black dashed line boxes from 1 to 6). More importantly, *Tlr2*$^{-/-}$ infected macrophages and non-infected controls grouped together (Figure 18 A, gray dashed line boxes), likely indicating the low positive binding and poor activation of *Tlr2*$^{-/-}$ macrophages by all *T.cruzi* strains.

Table 11. Discriminant frequencies in the interaction in Tlr2$^{-/-}$ and C57BL/6 peritoneal macrophages infected with different strains of T. cruzi.

1 h		Theoretical Group													
		C57BL/6							*Tlr2*$^{-/-}$						
		NI %(N)	Dm28c %(N)	Y %(N)	M6421 %(N)	10R26 %(N)	Bug2148 %(N)	VRFA %(N)	NI %(N)	Dm28c %(N)	Y %(N)	M6421 %(N)	10R26 %(N)	Bug2148 %(N)	VRFA %(N)
Real Group C57BL/6	NI	100 (6)													
	Dm28c		100 (6)												
	Y			100 (6)											
	M6421				100 (6)										
	10R26					100 (6)									
	Bug2148						100 (6)								
	VFRA							100 (6)							
Real Group *Tlr2*$^{-/-}$	NI								100 (6)						
	Dm28c								33 (2)	33 (2)				33 (2)	
	Y	17 (1)								33 (2)	50 (3)	17 (1)			
	M6421									17 (1)		33 (2)	33 (2)	17 (1)	
	10R26										17 (1)		50 (3)	33 (2)	
	Bug2148										33 (2)	17 (1)		50 (3)	
	VFRA													33 (2)	67 (4)

The percent of the discrimination is shown in Table 11, a 100% of discrimination was found for all the infections with different *T. cruzi* strains in C57BL/6 macrophages. The discrimination for *Tlr2*$^{-/-}$ was worse than in the infections in C57BL/6 macrophages with values of only a 33% in some cases, these low frequencies are likely associated with the lower parasite load found.

Table 12. Gene expression and parasite load discriminant frequencies in the internalization Tlr2$^{-/-}$ and C57BL/6 peritoneal macrophages infected with different strains of T. cruzi.

6 h		Theoretical Group													
		C57BL/6							*Tlr2*$^{-/-}$						
		NI %(N)	Dm28c %(N)	Y %(N)	M6421 %(N)	10R26 %(N)	Bug2148 %(N)	VRFA %(N)	NI %(N)	Dm28c %(N)	Y %(N)	M6421 %(N)	10R26 %(N)	Bug2148 %(N)	VRFA %(N)
Real Group C57BL/6	NI	100 (6)													
	Dm28c		100 (6)												
	Y			100 (6)											
	M6421				100 (6)										
	10R26					100 (6)									
	Bug2148						100 (6)								
	VFRA							100 (6)							
Real Group *Tlr2*$^{-/-}$	NI								100 (6)						
	Dm28c									100 (6)					
	Y									33 (2)	33 (2)				33 (2)
	M6421									33 (2)	33 (2)	33 (2)			
	10R26												33 (2)	33 (2)	33 (2)
	Bug2148									33 (2)				33 (2)	33 (2)
	VFRA											33 (2)			67 (4)

The DAPC analysis at 6 h.p.i. was able to discriminate 86.6% in our model, which 74.12% and 12% are explained in first (x-axis) and second (y-axis) principal components, respectively. We found 3

clusters: one for infection in *Tlr2* $^{-/-}$ with al strains of *T. cruzi* together with NI, another for the infection of C57BL/6 macrophages with all the strains of *T. cruzi* except M6421 cl6 and the last one with the infection in C57BL/6 macrophages with M6421 cl6.

Table 12, shows again a clear discrimination in the infection in the C57BL/6 macrophages but even worst discrimination compared with the interaction in the all cases of the infection in the *Tlr2* $^{-/-}$ macrophages.

Table 13. Gene expression and parasite load discriminant frequencies in the internalization Tlr2 $^{-/-}$ ***and C57BL/6 peritoneal macrophages infected with different strains of T. cruzi.***

24 h			Theoretical Group														
			C57BL/6							*Tlr2* $^{-/-}$							
			NI %(N)	Dm28c %(N)	Y %(N)	M6421 %(N)	10R26 %(N)	Bug2148 %(N)	VRFA %(N)	NI %(N)	Dm28c %(N)	Y %(N)	M6421 %(N)	10R26 %(N)	Bug2148 %(N)	VRFA %(N)
Real Group	C57BL/6	NI	100 (6)														
		Dm28c		100 (6)													
		Y			100 (6)												
		M6421				100 (6)											
		10R26					100 (6)										
		Bug2148						100 (6)									
		VFRA							100 (6)								
	Tlr2 $^{-/-}$	NI								100 (6)							
		Dm28c									33 (2)		33 (2)		33 (2)		
		Y										33 (2)		33 (2)	33 (2)		
		M6421											67 (4)	33 (2)			
		10R26											33 (2)	33 (2)	33 (2)		
		Bug2148												33 (2)	67 (4)		
		VFRA														100 (6)	

The DAPC analysis at 24 h.p.i. was able to discriminate 77.2% in our model, which 50.9% and 26.3% are explained in first (x-axis) and second (y-axis) principal components, respectively. We found 4 clusters: one for infection in *Tlr2* $^{-/-}$ with al strains of *T. cruzi* and NI, another for the infection of C57BL/6 macrophages with all the strains of *T. cruzi* except Dm28c and VFRA cl1 and the others two with the infections in C57BL/6 macrophages with Dm28c and VFRA cl1. The percent of the discrimination is on Table 13.

4.2.4 Correlation Networks

We performed network correlation analysis, including gene expression of the immunoregulatory genes, as well as the receptor expression (*Slamf1* and *Tlr2)* and the parasite load. As in the summary of the genes we found different patterns of positive or negative correlations depending of the macrophage infection with the different strains of *T. cruzi* using Cytoscape. Specific changes, appearance and disappearance in the correlations between the C57BL/6 and *Tlr2* $^{-/-}$ on each infection phase evaluated will indicate the role of TLR2 receptor in the infection with the different strains of *T. cruzi.* Correlations are shown in the appendix section 8 (Interaction in Table S 5, Internalization in

Table S 6 and Intracellular replication in Table S 7). We used the different strains of *T. cruzi* as central nodes.

During the interaction C57BL/6 resulting network was composed of 25 secondary nodes and 42 edges (Figure 19 A) and *Tlr2*$^{-/-}$ was composed of 19 secondary nodes and 32 edges (Figure 19 B), with 6 as the maximum degree of connectivity of a node and 1 as the minimum.

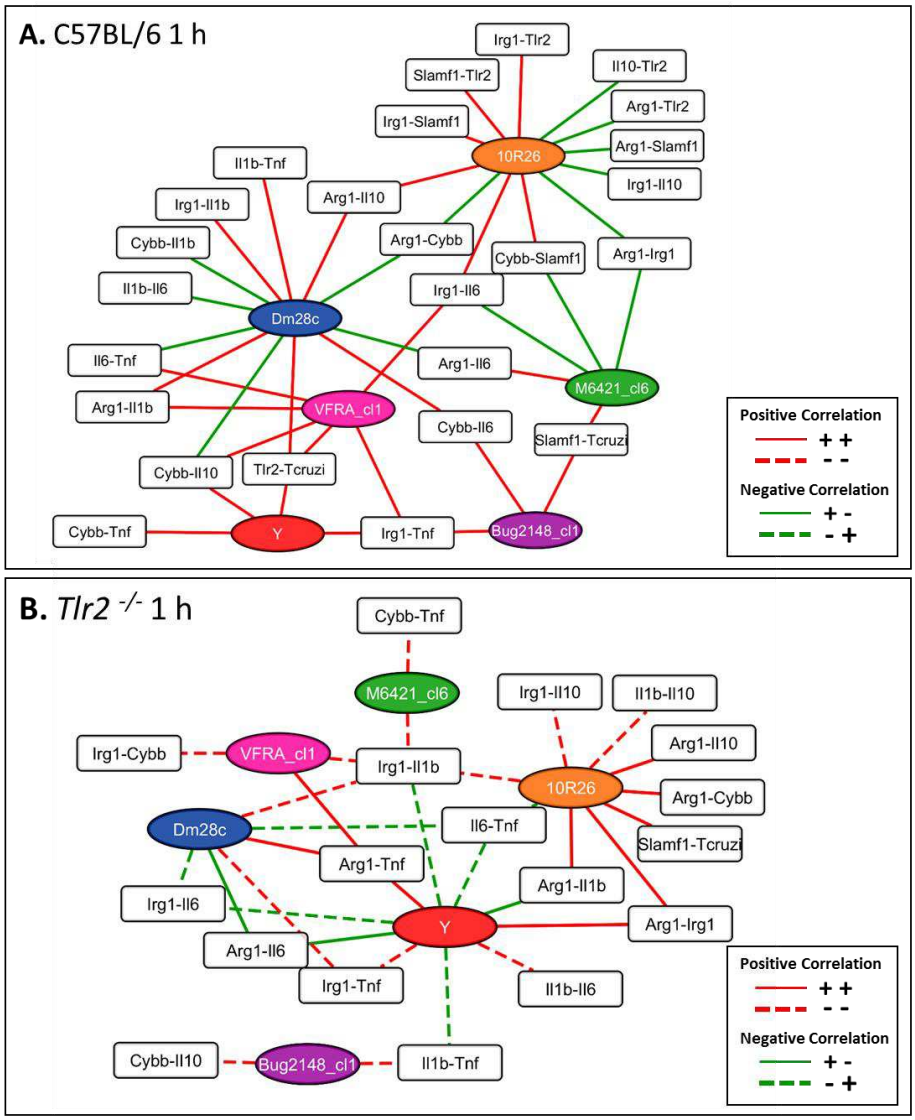

Figure 19. Networks of the macrophage activation during the interaction phase with the different strains of T.cruzi. A. *C57BL/6 macrophages.* ***B.*** *Tlr2*$^{-/-}$ *macrophages. Networks were generated and represented as indicated in the Methods section.*

We found an aggrupation based in the correlation of the infected macrophage with the different strains in *Tlr2*$^{-/-}$ between Y strain as a central node and all other strains showing as the common strain in this phase. Interestingly, a huge change from positive correlation to negative was found in

C57BL/6 to *Tlr2*$^{-/-}$ infected with the Y strain, respectively. In *Tlr2*$^{-/-}$ macrophages there is no correlation with the parasite load, except for the Bug2148 cl1 and M6421 cl6 in which there is a positive correlation between parasite load and *Slamf1* gene expression. As mentioned for C57BL/6 macrophages we found positive and negative correlation between many genes, but for TLR2 deficiency seems to reverse this tendency depending on the infecting strain. Besides, the overall number of negative correlations was lower than for C57BL/6 indicating a certain dysregulation in *Tlr2*$^{-/-}$ macrophages.

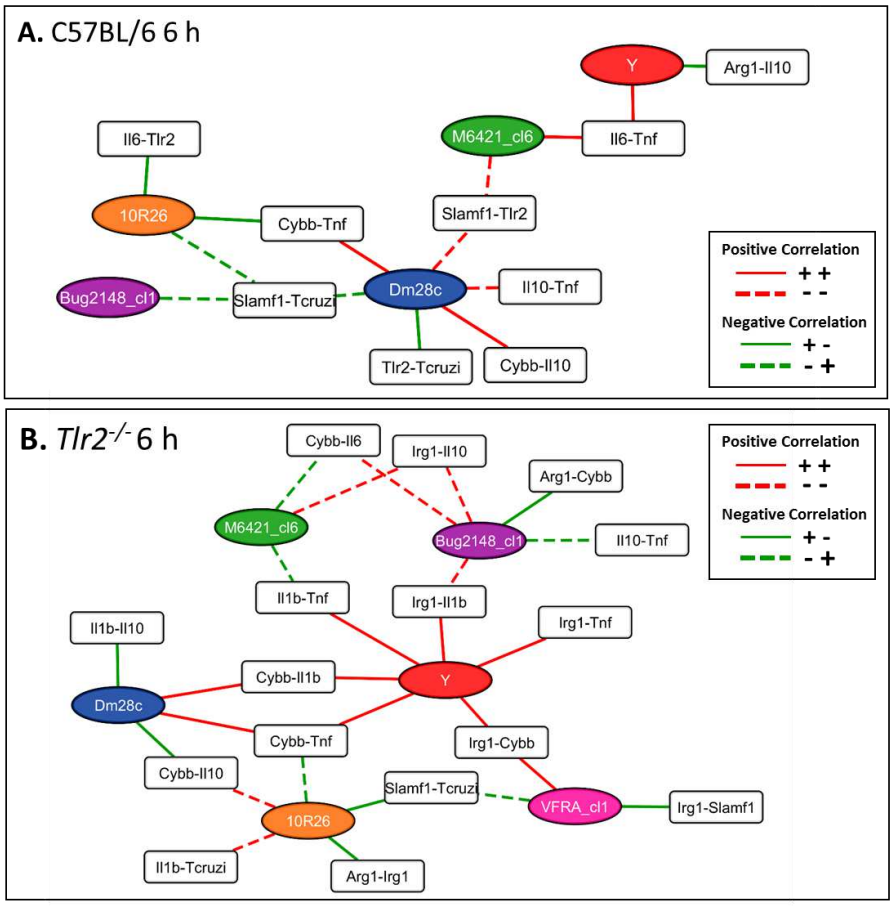

Figure 20. Networks of the macrophage activation during the internalization phase with the different strains of T.cruzi. A. *C57BL/6 macrophages.* ***B.*** *Tlr2*$^{-/-}$ *macrophages. Networks were generated and represented as indicated in the Methods section.*

The resulting networks during the internalization in C57BL/6 macrophages were composed of 8 secondary nodes and 14 edges (Figure 20 A) and *Tlr2*$^{-/-}$was composed of 16 secondary node and 26 edges (Figure 20 B), with 6 as the maximum degree of connectivity of a node and 1 as the minimum. While in C57BL/6 the central axis in the network is Dm28c with negative correlations, in the *Tlr2*$^{-/-}$ it changed as in the interaction phase to the Y strain, but in this case with only positive correlations.

The strain VFRA cl1 which did not present correlations in C57BL/6 macrophages, did present them in *Tlr2*$^{-/-}$, with a negative correlation associated with the *Slamf1* suggesting as increment in the parasite load at this phase where the SLAMF1 receptor is down-regulated and the parasite can be better internalized in the absence of this receptor (Figure 23).

At 6 h.p.i there are few correlations in C57BL/6 infected macrophages, but in *Tlr2*$^{-/-}$ macrophages we observed both positive and negative gene expression correlations, which could indicate even more regulated macrophage activation after infection. The negative correlations observed for C57BL/6 macrophages infected with Dm28c and Bug2148 cl1 between the *Slamf1* and the parasite load are lost in the absence of *Tlr2* indicating a possible relation between the two receptors with this strain.

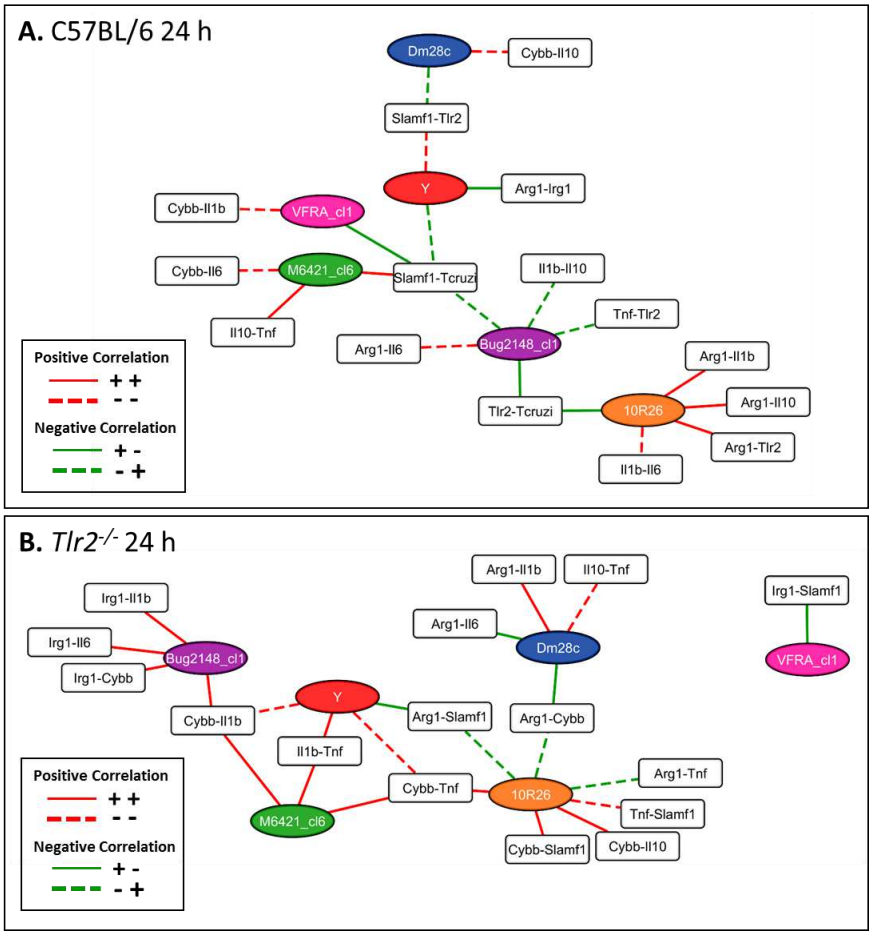

Figure 21. Networks of the macrophage activation during the intracellular phase proliferation with the different strains of T.cruzi. A. *C57BL/6 macrophages.* ***B.*** *Tlr2*$^{-/-}$ *macrophages. Networks were generated and represented as indicated in the Methods section.*

In the intracellular proliferation phase C57BL/6 resulting network was composed of 15 secondary nodes and 20 edges (Figure 21 A) and *Tlr2*$^{-/-}$ was composed of 15 secondary node and 20 edges (Figure 21 B), with 6 as the maximum degree of connectivity of a node and 1 as the minimum. In

Tlr2$^{-/-}$ macrophages infected with the VFRA cl1 appear as separate group and only with one negative correlation, probably because is the only strain which at this phase has similar parasite load as in C57BL/6 macrophages. *Tlr2*$^{-/-}$ macrophages infected with the strain Y, M6421 cl6 and 10R26 present more significant correlations associated with the gene expression of *Tnf*, *Cybb, Il1b* and *Il10.* In *Tlr2*$^{-/-}$ infected with Y a positive correlation between the receptors (*Slamf1-Tlr2)* and the negative correlation between the parasite load and *Slamf1,* indicate a down-regulation of this receptor by TLR2.

4.3 SLAMF1 IN MACROPHAGES

SLAMF1 receptor has been considered as a molecule detrimental for the host in some infection because it helps the entry of pathogens as measles virus, *Leishmania* major and also in the case of *T. cruzi*. *In vitro* infections with the Y strain in *Slamf1*$^{-/-}$ dendritic cells and macrophages demonstrated to be more resistant than the wild type cells (BALB/c) (Calderón *et al.*, 2012). We addressed the role of SLAMF1 receptor in the infection with the different strains of *T. cruzi,* using first the macrophage model. In this case we used as controls BALB/c peritoneal macrophages because the SLAMF1 deficiency is in this mouse genetic background.

4.3.1 Kinetics of BALB/c and *Slamf1*$^{-/-}$ Peritoneal Macrophage Infection with Different Strains of *T. cruzi.*

We first determined the parasite load of infection in *Slamf1*$^{-/-}$ and BALB/c peritoneal macrophages. We compared the rate of infection between *Slamf1*$^{-/-}$ and BALB/c peritoneal macrophages infected with the *T. cruzi* strains, measuring the parasite load in the three phases, as described before.

Figure 22 shows the kinetic of the parasite load in peritoneal macrophages. In general, we found that *Slamf1*$^{-/-}$ macrophages presented lower parasite load than BALB/c macrophages for all the strains, except for VFRA cl1, that showed the opposite values and higher parasite load. In addition, we found higher parasite load in both strains compared with C57BL/6 mice (Figure 11).

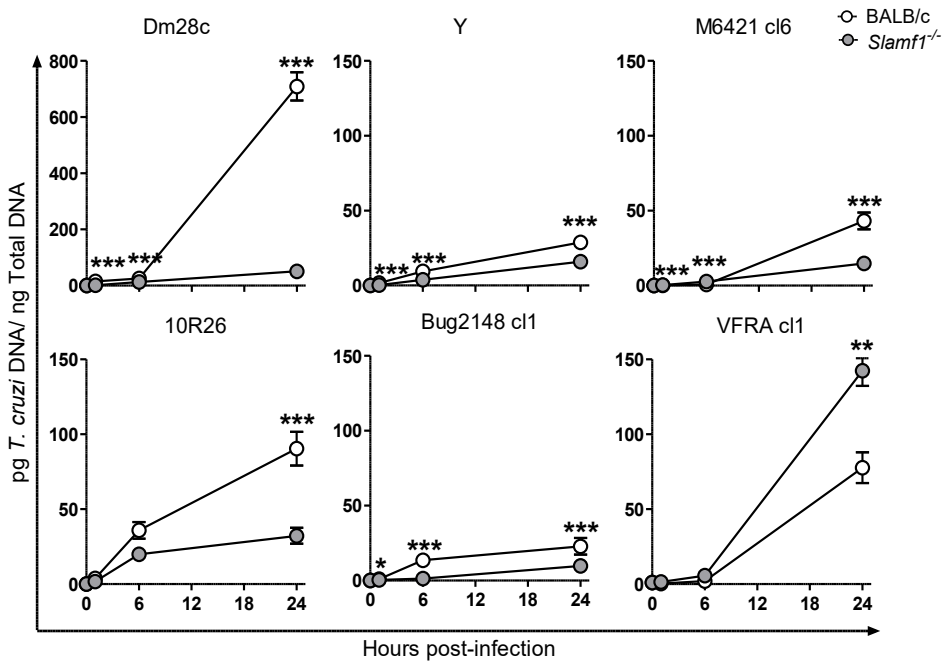

Figure 22. Kinetics of parasite load in Slamf1$^{-/-}$ and BALB/c - peritoneal macrophages. *Kinetic analysis of parasite load of BALB/c and Slamf1$^{-/-}$ peritoneal macrophages at 1 h, 6 h and 24 h after infection with parasite strains of different DTUs. Parasite load was quantified by qPCR. Mean and Standard error of the mean ± (SEM) in two independent experiments are represented. The asterisks indicate the statistical significance, t-student (*p<0.05, **p<0.005 and ***p<0.001), between BALB/c and Slamf1$^{-/-}$ macrophages.*

4.3.2 Role of SLAMF1 Receptor in the different Phases of Macrophage Infection with Different Strains of *T. cruzi.*

To further evaluate the effect of SLAMF1 receptor in *T. cruzi* strain infectivity, we first normalized parasite load of *Slamf1$^{-/-}$* infected peritoneal macrophages in different phases by dividing *Slamf1$^{-/-}$* parasite load by BALB/c parasite load. Figure 21 A shows normalized parasite load at 1 h.p.i. Parasite load during the internalization phase at 6 h.p.i. was normalized respect normalized level at the interaction phase (Figure 21 B). Finally, intracellular proliferation at 24 h.p.i. was normalized respect the internalization phase normalized level (Figure 21 C). We found that *Slamf1* receptor is required for the interaction and internalization. Thus Slamf1 facilitates Dm28c, Y, 10R26 and Bug2148 cl1 strains entry, but might be blocking it in the case of M6421 cl6 and VFRA cl1 strains. The intracellular proliferation was lower for all strains in *Slamf1$^{-/-}$* macrophages compared to BALB/c, except for VFRA cl1, suggesting an inhibitory role of Slamf1 in all phases of the infection with those strains.

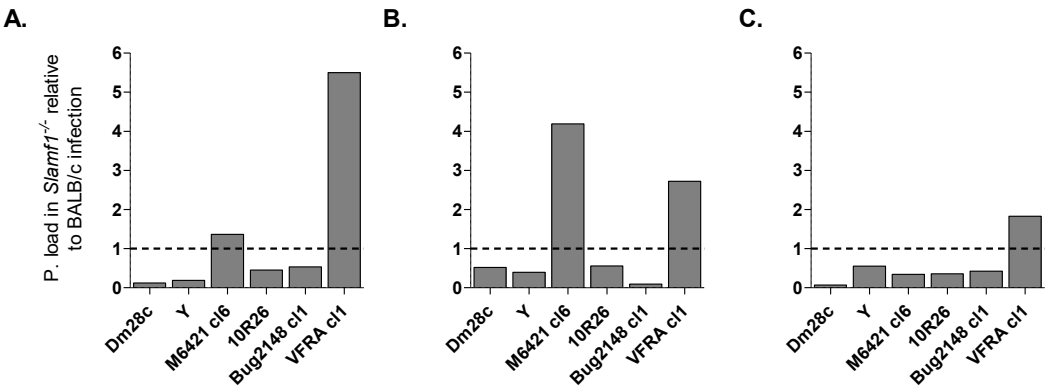

Figure 23. Effect of SLAMF1 deficiency on parasite load of peritoneal macrophages respect BALB/c. *Dashed lines correspond to normalized BALB/c parasite load (equal to 1 for all parasite strains). Gray boxes correspond to normalized values of Slamf1$^{-/-}$ macrophages at each stage of infection.* ***A.*** *Interaction at 1 h.p.i.* ***B.*** *Internalization at 6 h.p.i.* ***C.*** *Replication at 24 h.p.i.*

4.3.3 Expression of Immunoregulatory Genes in BALB/c and *Slamf1*$^{-/-}$ Macrophages Infected with Different Strains of *T. cruzi.*

Table 14 is a summary of the gene expression of the 3 enzymes, 4 cytokines, 2 receptor and the parasite load of *Slamf1*$^{-/-}$ and BALB/c macrophages infected with the different strains of *T. cruzi*. We could not find a defined pattern in this case.

Table 14. Summary of expression of immunoregulatory genes and parasite load in BALB/c and Slamf1$^{-/-}$ peritoneal macrophages infected with different strains of T. cruzi. *Gene expression was determined by RT-qPCR and RQ value were obtained after normalizing value from infected respect to no-infected macrophages. Results are shown in Figure S 9 (Enzymes), Figure S 10 (Cytokines) and Figure S 11 (Receptors). Parasite load (T.cruzi) correspond to value from Figure 22. For each gene and parasite load a color code was given from high (Red) to low (Green).*

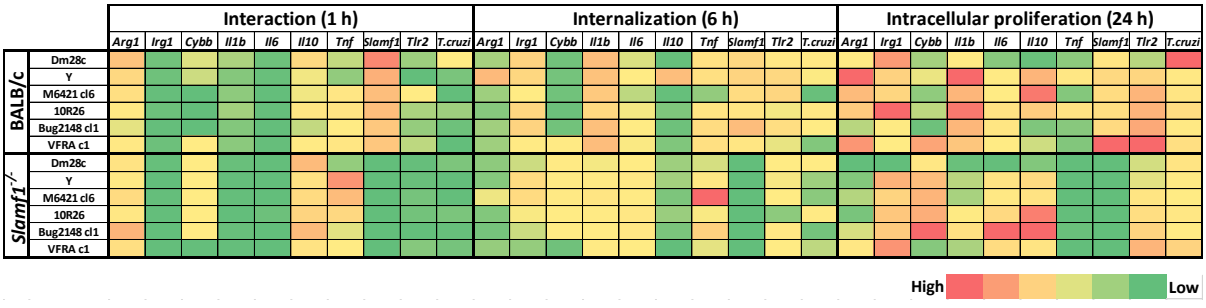

We performed a discriminant analysis of principal components to further determine the role of SLAMF1 in the activation of macrophages infected with different strains of *T. cruzi.* The analysis was performed with the panel of gene expression of the 3 enzymes, 4 cytokines and the parasite load in

the model of infection in peritoneal macrophages with *T. cruzi* in the three different phases evaluated.

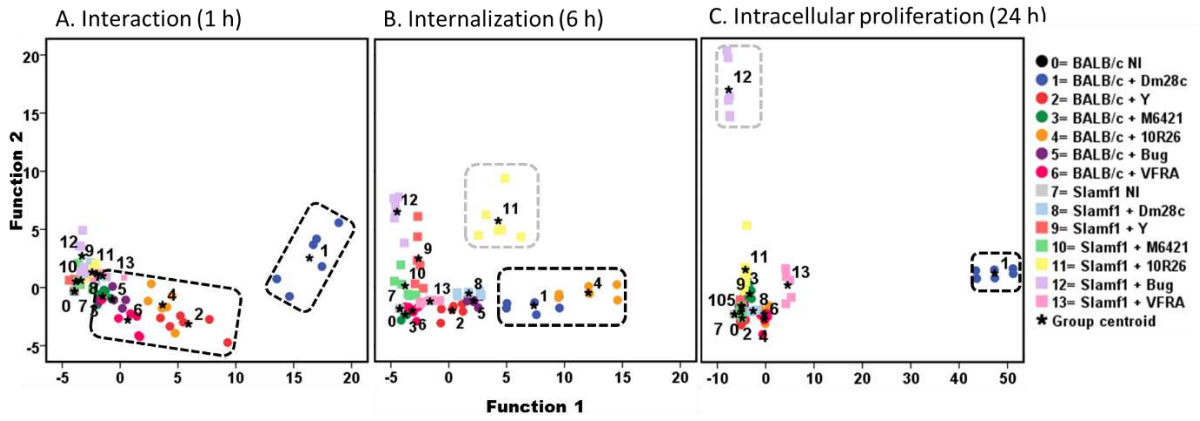

Figure 24. Discriminant Analysis of Principal Components (DAPC). *These scatterplots show the first two principal components of the DAPC of gene expression and parasite load data according to the three different phases of the macrophage infection with the different T. cruzi strains.* ***A.*** *Interaction at 1h* ***B.*** *Internalization at 6h* ***C.*** *Intracellular proliferation at 24h. The diagrams show clusters of BALB/c peritoneal macrophages infected with the different strains of T. cruzi (Black dashed line) and Slamf1 $^{-/-}$(Gray dashed line).*

In this study BALB/c and *Slamf1*$^{-/-}$ macrophages presented lower discrimination between groups than in C57BL6 and *Tlr2*$^{-/-}$(Figure 18). The DAPC at 1 h.p.i. analysis was able to discriminate 85.3% in our model, which 77.5% and 7.8% are explained in first (x-axis) and second (y-axis) principal components, respectively. We found 3 clusters: one for infection in *Slamf1*$^{-/-}$ with al strains of *T. cruzi* and NI, another for the BALB/c infection with Dm28c and another one for the infection of BALB/c macrophages with the rest strains (Figure 24 A). The percent of the discrimination is on Table 15. This likely reflects the influence of SLAMF1 in the attachment of the parasites of different strains as well as the higher interaction of DM28c with BALB/c already mentioned.

Table 15. Discriminant frequencies in the interaction in Slamf1$^{-/-}$ and BALB/c peritoneal macrophages infected with different strains of T. cruzi.

1 h		Theoretical Group													
		BALB/c							*Slamf1* $^{-/-}$						
		NI %(N)	Dm28c %(N)	Y %(N)	M6421 %(N)	10R26 %(N)	Bug2148 %(N)	VRFA %(N)	NI %(N)	Dm28c %(N)	Y %(N)	M6421 %(N)	10R26 %(N)	Bug2148 %(N)	VRFA %(N)
Real Group	BALB/c														
	NI	100 (6)													
	Dm28c		100 (6)												
	Y			100 (6)											
	M6421				83 (5)		17 (1)								
	10R26					100 (6)									
	Bug2148						100 (6)								
	VFRA							83 (5)		17 (1)					
	Slamf1$^{-/-}$														
	NI								100 (6)						
	Dm28c									83 (5)			17 (1)		
	Y										83 (5)		17 (1)		
	M6421										17 (1)	67 (4)	17 (1)		
	10R26												100 (6)		
	Bug2148									17 (1)		17 (1)		67 (4)	
	VFRA														100 (6)

The DAPC analysis at 6 h.p.i. was able to discriminate 87.5% in our model, which 66% and 21.6% are explained in first (x-axis) and second (y-axis) principal components, respectively (Figure 24 B). We found 3 clusters, one for the infection of *Slamf1*$^{-/-}$ macrophages with 10R26, another for the BALB/c macrophages infected with Dm28c and 10R26 and finally the last one for the other infected and non-infected. The percent of the discrimination is shown in Table 16.

Table 16. Discriminant frequencies in the internalization in Slamf1$^{-/-}$ and BALB/c peritoneal macrophages infected with different strains of T. cruzi.

6 h		Theoretical Group													
		BALB/c							*Slamf1* $^{-/-}$						
		NI %(N)	Dm28c %(N)	Y %(N)	M6421 %(N)	10R26 %(N)	Bug2148 %(N)	VRFA %(N)	NI %(N)	Dm28c %(N)	Y %(N)	M6421 %(N)	10R26 %(N)	Bug2148 %(N)	VRFA %(N)
Real Group	BALB/c														
	NI	100 (6)													
	Dm28c		83 (5)			17 (1)									
	Y			83 (5)			17 (1)								
	M6421				100 (6)										
	10R26					100 (6)									
	Bug2148						100 (6)								
	VFRA				50 (3)			33 (2)	17 (1)						
	Slamf1$^{-/-}$														
	NI								100 (6)						
	Dm28c									100 (6)					
	Y				17 (1)			17 (1)			67 (4)				
	M6421				17 (1)							83 (5)			
	10R26												100 (6)		
	Bug2148													100 (6)	
	VFRA														100 (6)

The DAPC analysis at 24 h.p.i. was able to discriminate 95% in our model, which 83.9% and 11.1% are explained in first (x-axis) and second (y-axis) principal components, respectively (Figure 24 C). Three different clusters were found, one for the BALB/c macrophages infected with Dm28c, other for the infection of *Slamf1*$^{-/-}$ macrophages with VFRA and one for the rest of the infected and non-infected. The percent of the discrimination is shown in Table 17.

Table 17. Discriminant frequencies in the intracellular proliferation in Slamf1$^{-/-}$ and BALB/c peritoneal macrophages infected with different strains of T. cruzi.

24 h		Theoretical Group													
		BALB/c							*Slamf1* $^{-/-}$						
		NI %(N)	Dm28c %(N)	Y %(N)	M6421 %(N)	10R26 %(N)	Bug2148 %(N)	VRFA %(N)	NI %(N)	Dm28c %(N)	Y %(N)	M6421 %(N)	10R26 %(N)	Bug2148 %(N)	VRFA %(N)
Real Group BALB/c	NI	100 (6)													
	Dm28c		100 (6)												
	Y			67 (4)			33 (2)								
	M6421				83 (5)					17 (1)					
	10R26					100 (6)									
	Bug2148	17 (1)					83 (5)								
	VFRA							100 (6)							
Real Group *Slamf1*$^{-/-}$	NI								100 (6)						
	Dm28c									100 (6)					
	Y										100 (6)				
	M6421											100 (6)			
	10R26												100 (6)		
	Bug2148													100 (6)	
	VFRA														100 (6)

4.3.4 Correlation Networks

We performed a network correlation analysis, where we included gene expression of the immunoregulatory genes, as well as the receptor expression (*Slamf1* and *Tlr2)* and the parasite load. As in the summary of gene expression we found different patterns of positive or negative correlations depending of the macrophage infection with the different strains of *T. cruzi* using Cytoscape. Changes, appearance and disappearance in the correlations between BALB/c and *Slamf1*$^{-/-}$ on each phase evaluated indicate the role of SLAMF1 receptor in the infection with the different strains of *T. cruzi* are detailed in the appendix section 8 (Interaction in Table S 8, Internalization in Table S 9 and Intracellular proliferation in Table S 10).

As mentioned before, using the different strains of *T.cruzi* as central nodes, during the interaction phase BALB/c the resulting network was composed of 24 secondary nodes and 49 edges (Figure 25 A). On the other hand, *Slamf1*$^{-/-}$ was composed of 27 secondary nodes and 50 edges (Figure 25 B), with 6 as the maximum degree of connectivity of a node and 1 as the minimum. At 1 h.p.i BALB/c macrophage network showed an aggrupation between the Dm28c, Y and VFRA cl1, while in *Slamf1*$^{-/-}$ macrophages the cluster was between the strains Y, M6421 cl6 and 10R26. The strain VFRA cl1 in the network of *Slamf1*$^{-/-}$ was apart from the other strains, likely associated to the very different pattern of this strain where the deficiency of SLAMF1 incremented the parasite load in macrophages. The negative correlation in the *Slamf1*$^{-/-}$ infected with the strain Y could be associated with the resistant profile in the *in vivo* experiments, efficiently activating macrophages for the control of the infection.

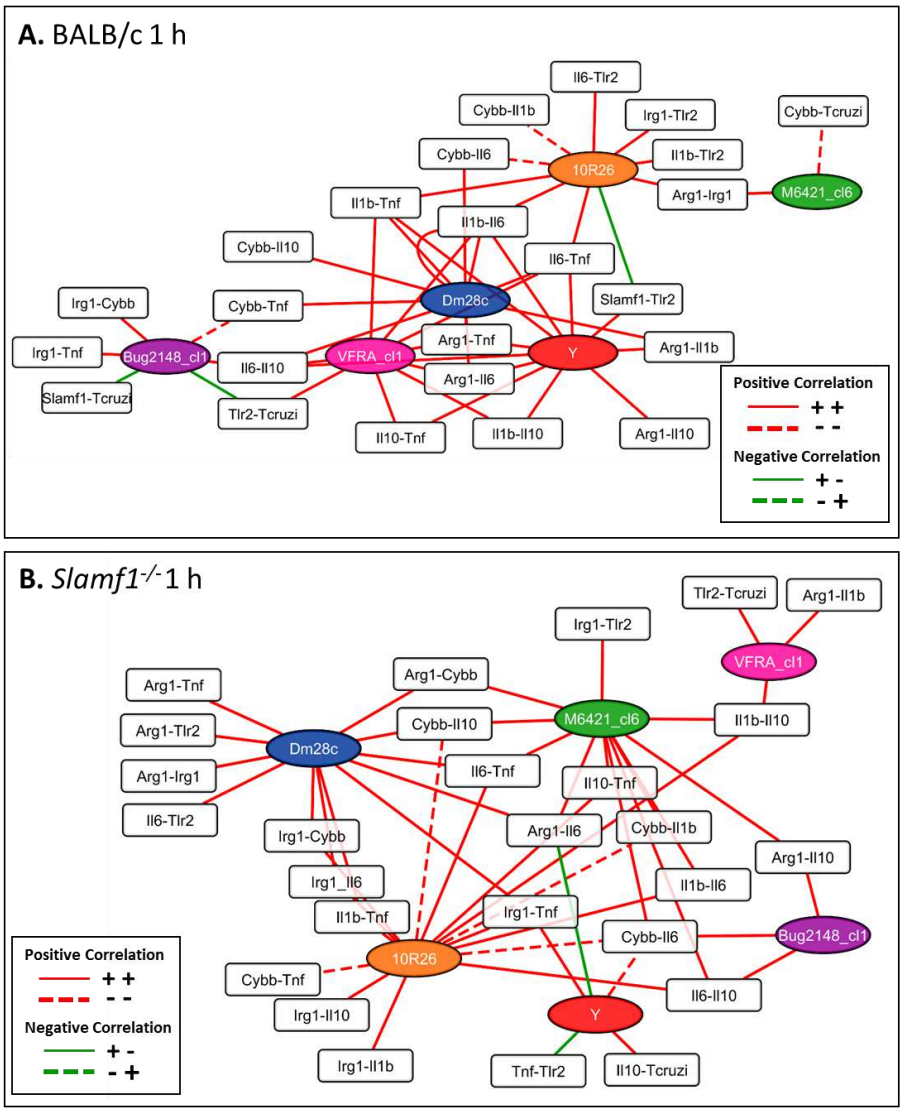

Figure 25. Networks of the macrophage activation during the interaction phase with the different strains of T.cruzi. A. *BALB/c macrophages.* ***B.*** *Slamf1$^{-/-}$ macrophages. Networks were generated and represented as indicated in the Methods section.*

The resulting networks during the internalization in BALB/c macrophages was composed of 18 secondary nodes and 28 edges (Figure 26 A) whereas *Slamf1$^{-/-}$* was composed of 16 secondary nodes and 22 edges (Figure 26 B), with 6 as the maximum degree of connectivity of a node and 1 as the minimum. Interestingly, the pattern of the node was very different depending of SLAMF1 deficiency. Thus, *Slamf1$^{-/-}$* macrophages infected with the strain Y present many more edges than the rest. On the other hand, the strain 10R26 is separated in the network. Interestingly, at this phase was when this strain presented higher amount of ROS, as can be observed in Figure 29.

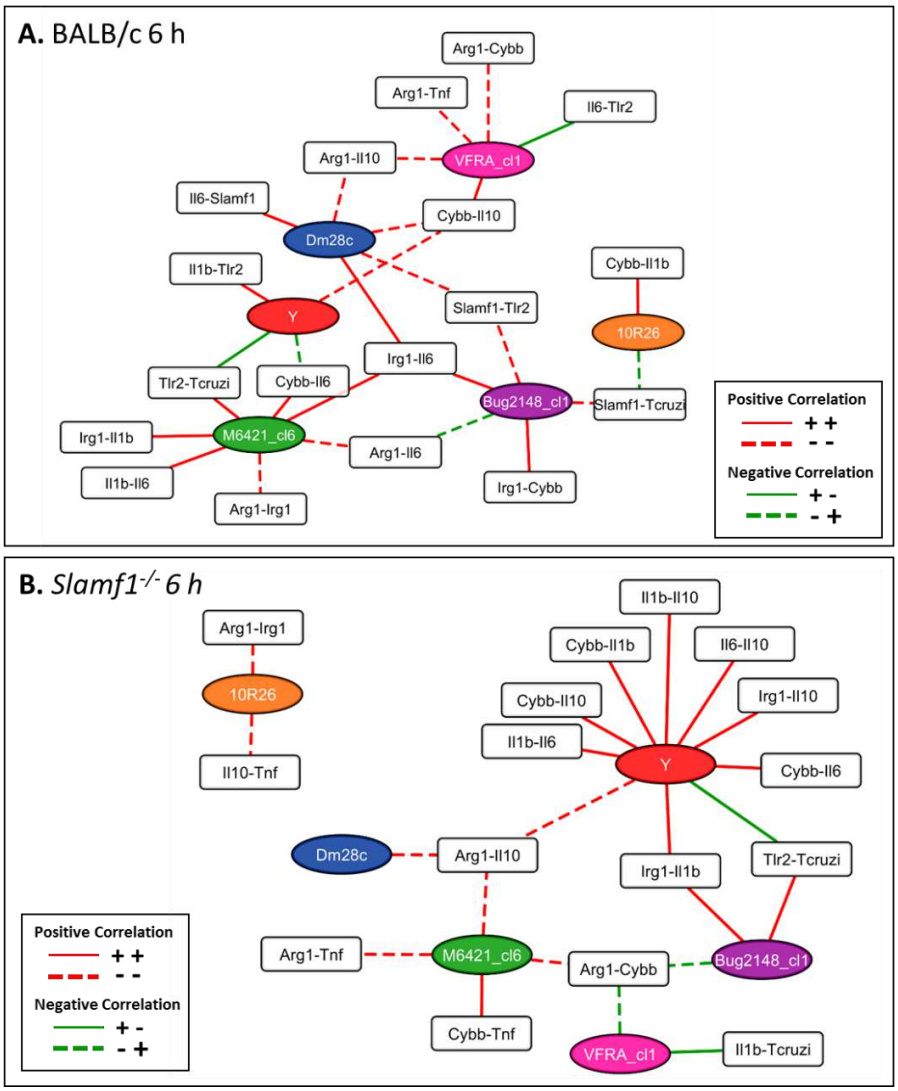

Figure 26. Networks of the macrophage activation during the internalization phase with the different strains of T.cruzi. A. *BALB/c macrophages.* ***B.*** *Slamf1$^{-/-}$ macrophages. Networks were generated and represented as indicated in the Methods section.*

Finally, in the intracellular proliferation BALB/c resulting network was composed of 14 secondary nodes and 20 edges (Figure 27 A) whereas *Slamf1$^{-/-}$* was again different and composed of 14 secondary node and 18 edges (Figure 27 B), with 6 as the maximum degree of connectivity of a node and 1 as the minimum. The network in *Slamf1$^{-/-}$* shows the Dm28c and M6421 cl6 separated from the other strains, and few common correlations between the strains, indicating a highly variable effort of SLAMF1 deficiency in *T. cruzi* intracellular proliferation depending on the infecting strain, as also indicated in Table 14.

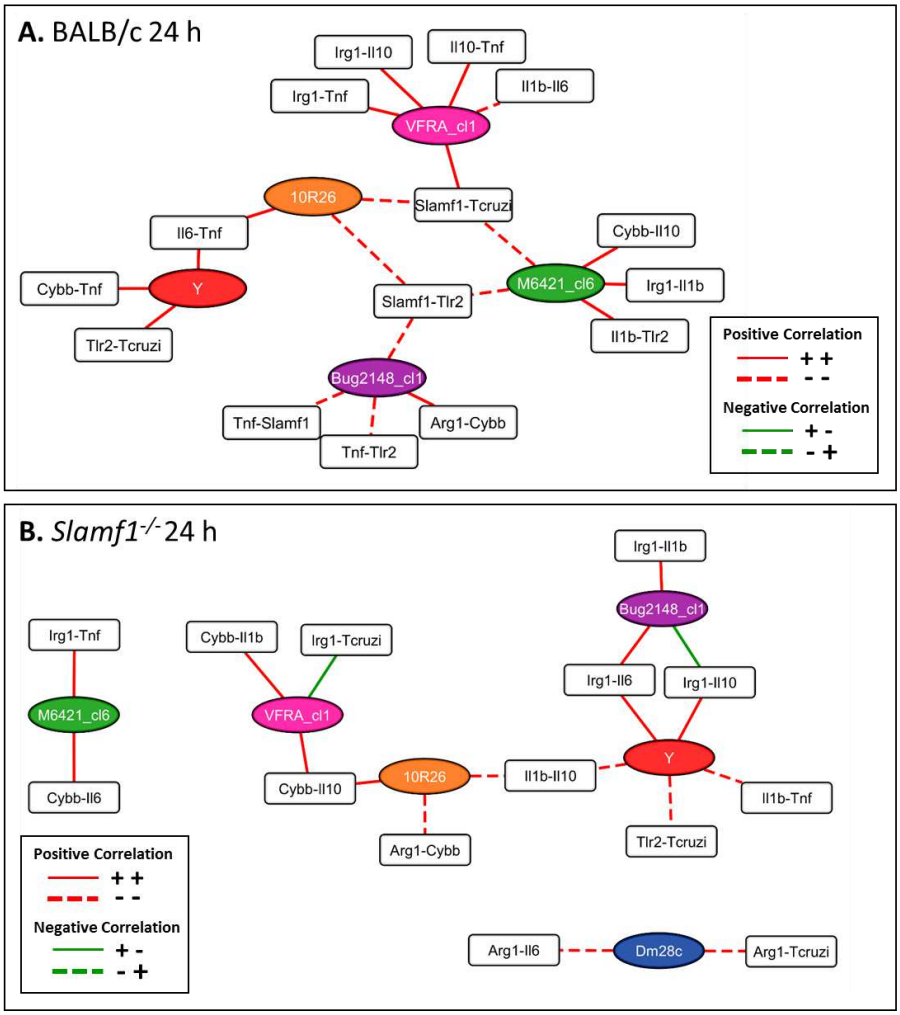

Figure 27. Networks of the macrophage activation during the intracellular proliferation phase with the different strains of T.cruzi. A. *BALB/c macrophages.* ***B.*** *Slamf1$^{-/-}$ macrophages. Networks were generated and represented as indicated in the Methods section.*

4.3.5 SLAMF1 regulates NOX and ROS

SLAMF1 induces production of PI3P, which positively regulates the activity of the NOX2 enzyme and phagolysosomal maturation. Higher mounts of ROS and NOX2 could explain why the *Slamf1$^{-/-}$* macrophages are less susceptible to the infection by *T. cruzi.* So, next we analyzed NOX2 expression at 6 h.p.i., taken as the end-point of internalization, and compared it with ROS production.

As already shown, *NOX2* gene expression was higher in *Slamf1$^{-/-}$*macrophages with all strains of *T. cruzi* except for VFRA cl1 which present the opposite results (Figure 28). Next, we evaluated the amounts of ROS in the cells by a cytofluorometry assay (Figure 29).

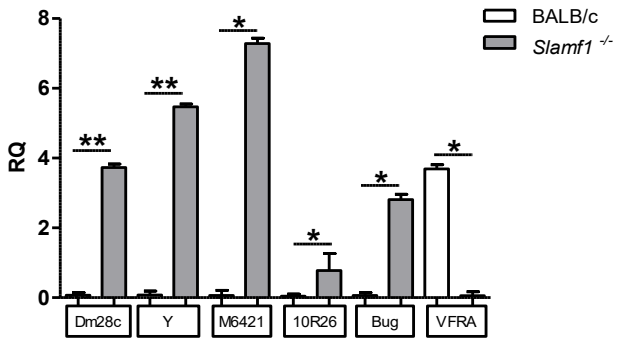

Figure 28. Gene expression of NOX2 in Slamf1$^{-/-}$ and BALB/c peritoneal macrophages infected of different parasite strains at 6 h.p.i. *Standard error of the mean ± (SEM) are represented. The asterisks indicate the statistical significance, t-student (*p<0.05 and **p<0.005), between BALB/c and Slamf1$^{-/-}$ macrophages.*

In agreement with *NOX2* gene expression, we found the lowest ROS production in the *Slamf1*$^{-/-}$ macrophages infected with VFRA cl1, suggesting an association between parasite load, and the production of ROS and *NOX2* gene expression. Higher production of ROS and *NOX2* gene expression is associated with lower parasite loads, which indicates that ROS and NOX2 production help to the elimination of the parasite in macrophages.

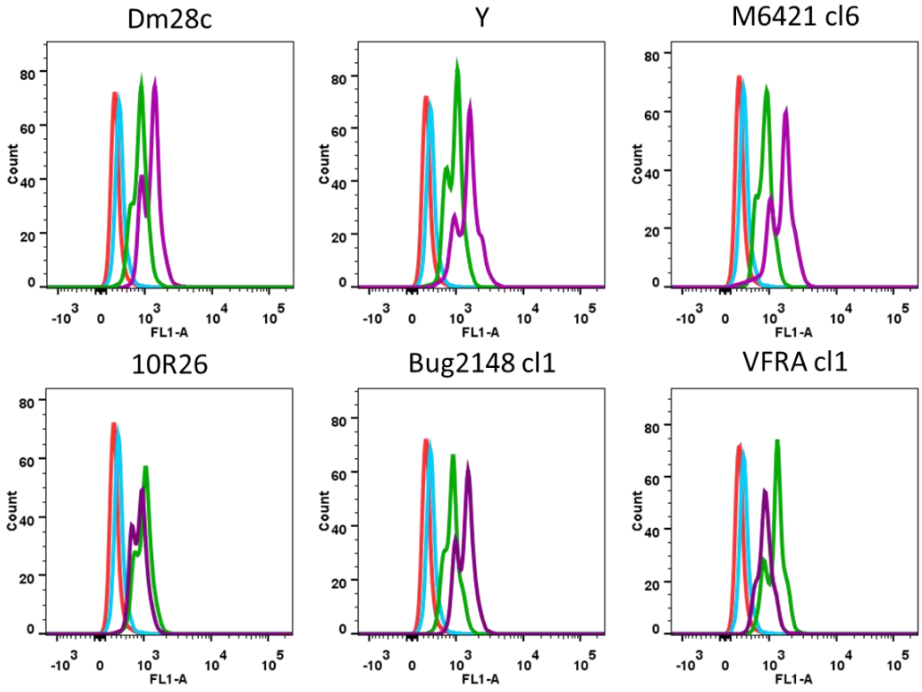

Figure 29. Reactive Oxygen Species in Slamf1$^{-/-}$ and BALB/c peritoneal macrophages infected of different parasite strains at 6 h.p.i. *The diagrams show Non-infected BALB/c macrophages (Red line), Non-infected Slamf1$^{-/-}$(Blue line), BALB/c infected with the different strains of T. cruzi (Green line) and Slamf1$^{-/-}$(Purple line).*

4.4 *IN VIVO INFECTION*

BALB/c and *Slamf1*$^{-/-}$ mice were infected with three of the six different strains of *T. cruzi* that showed the most divergent effects *in vitro* in infecting macrophages, detailed below.

The Dm28c strain had been previously described not causing parasitemia in infected BALB/c and C57BL/6 mice (de Melo Medeiros *et al.*, 2010), but it caused the highest parasite load in BALB/c peritoneal macrophages in our *in vitro* experiments.

The Y strain that caused a peak of parasitemia between the 7-11 d.p.i and multiple experiments in BALB/c mice infected that demonstrated it is highly lethal in this model where just 30-40% of the mice survive the first 21 d.p.i. with high (2000 parasite/mouse) and low (50 parasite/mouse) inoculums of *T. cruzi* (Sanoja *et al.*, 2013) . In addition, previous studies in our lab demonstrated that *Slamf1*$^{-/-}$ mice infected with this strain are resistant to the infection (Calderón *et al.*, 2012).

The VFRA cl1 strain presents a late peak of parasitemia compared with the Y and had been demonstrated to produce a mild infection, where all the BALB/c mice survive to the infection but presenting cardiac pathology (Rodriguez *et al.*, 2014). Also, *in vitro* VFRA cl 1 presented higher parasite load in the absence of SLAMF1 at all infection phases (1, 6 and 24 h.p.i.), suggesting that the receptor is somehow detrimental for parasite infection.

4.4.1 Parasitemias.

As previously described, 30% of BALB/c mice succumbed to infection with the Y strain, while Slamf1$^{-/-}$ mice showed 100% survival. Infection with Dm28c and VFRA cl1 strains did not cause mortality in BALB/c neither *Slamf1*$^{-/-}$ mice (data not shown). BALB/c and *Slamf1*$^{-/-}$ infected with the Y strain presented a first peak of parasitemia at 9 d.p.i, but the parasitemia was lower in the *Slamf1*$^{-/-}$ (Figure 30A). We did not find any detectable parasitemia of Dm28c in BALB/c and neither in *Slamf1*$^{-/-}$ mice. Finally, the BALB/c and *Slamf1*$^{-/-}$ infected with the VFRA cl1 strain presented similar amounts of parasites in blood and a late peak of parasitemia at 14-16 d.p.i compared with the infection with the Y strain (Figure 30 B).

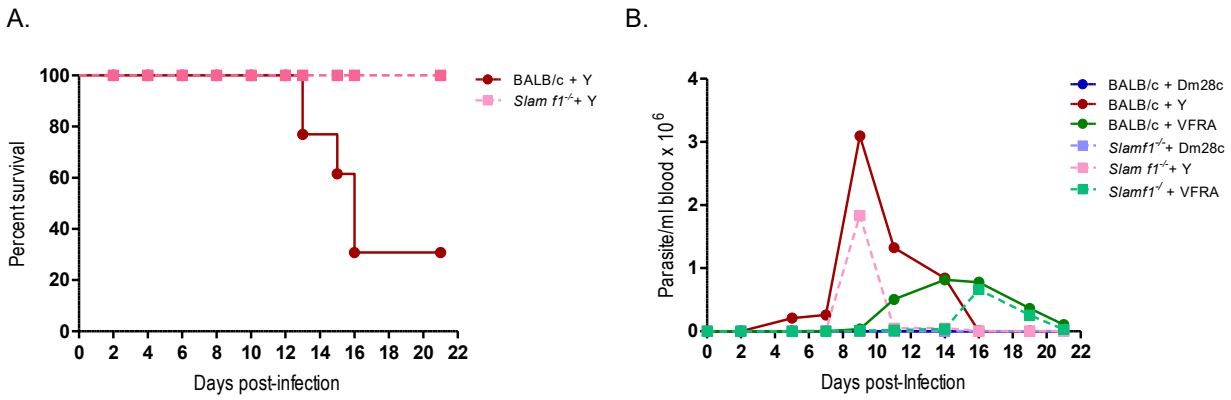

Figure 30. Time course of T. cruzi infection in Slamf1$^{-/-}$ mice and BALB/c. A. *Survival was monitored from 0 to 21 d.p.i. Only the Y strain caused the death of BALB/c mice.* ***B.*** *Parasitemia was monitored every 2 or 3 days from 0 to 21 d.p.i.; Mean parasitemias of 5 mice per group infected with Dm28c, Y and VFRA cl1 strains is shown.*

4.4.2 SPLEEN

Next, we analyzed the effect of *T. cruzi* infection in several of the most important organs spleen, heart and liver to better understand the outcome of the infection. *T. cruzi* infection promotes splenomegaly in mice and humans. Splenocytes are important cells involved in the host immune response since splenectomy prior to infection increases susceptibility to infection, as ascertained by the numbers of circulating parasites (de Meis *et al.*, 2009). In addition, splenomegaly is related to increased formation of granulocytes (Goni *et al.*, 2002) and MDSCs (Gonzalez, 2014), with suppressor activities and also able to produce NO to fight the infection.

4.4.2.1 Splenomegaly and Parasite Load

In order to evaluate the splenomegaly we weigh sacrificed mice (g) and spleens (mg) and calculated the spleen weight/body weight ratio at 14 and 21 d.p.i. We found significantly higher splenomegaly indexes in BALB/c and *Slamf1*$^{-/-}$ mice infected with all the strains evaluated at 14 d.p.i. compared with their respective non-infected controls (NI) (Figure 31 A). Interestingly, in BALB/c mice splenomegaly was significantly higher than in *Slamf1*$^{-/-}$ mice infected with all strains, except for the infection with Y at 21 d.p.i. (Figure 31 A and B). Spleen parasite load was lower, for Dm28c and Y although did not reach significant difference in *Slamf1*$^{-/-}$ spleen than in BALB/c infected spleens, strains and both times of infection (Figure 31 C and D). In contrast, in VFRA cl1 infection parasite levels in spleen were either identical or slightly higher, but again did not reach statistical

significance. Interestingly, we found an overall Spearman correlation of 0.6572 with a significance of P< 0.0001 between the splenomegaly and parasite load.

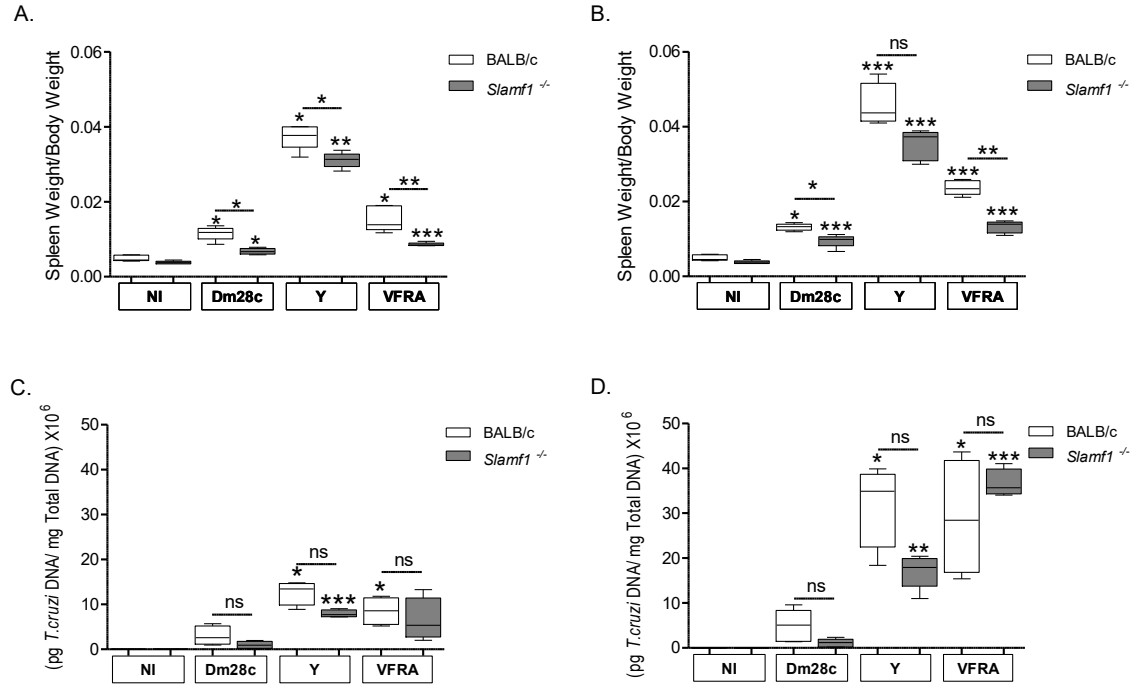

Figure 31. Splenomegaly and parasite load in spleen of BALB/c and Slamf1$^{-/-}$ mice infected with the different strains. A. *Splenomegaly at 14 d.p.i.* ***B.*** *Splenomegaly at 21 d.p.i.* ***C.*** *Parasite load at 14 d.p.i.* ***D.*** *Parasite load at 21 d.p.i. Means and Standard errors of the means ± (SEM) of 5 mice per group are represented. The asterisks indicate the statistical significance, t-student (*p<0.05, **p<0.005 and ***p<0.001), when comparing BALB/c and Slamf1$^{-/-}$ infected mice.*

4.4.2.2 Spleen Gene expression

We next analyzed the same immunoregulatory enzymes and cytokines genes evaluated in the macrophage model. Table 18 summarizes the gene expression of *Irg1, Cybb, Il1b, Il6, Il10* and *Tnf*.

Table 18 shows the great diversity in the gene expression in the infected BALB/c mice. Thus, in spleens from Dm28c infected mice gene expression was higher at 14 d.p.i., being infection reduced at 21 d.p.i. In contrast, in Y and VFRA cl1 infections gene expression increased at 14 d.p.i. that was maintained at 21 d.p.i. For VFRA cl1 in BALB/c mice at 14 d.p.i., there was higher levels *Irg1*, *Il6* and *Il10* than in infections with the other parasite strains. However, *Slamf1*$^{-/-}$mice showed increased expression of *Irg1*, *Cybb, Il6* and *Tnf* respect to BALB/c mice infected with Dm28c, and also, but lower, with the Y strain.

Table 18. Summary of expression by of immunoregulatory genes and parasite load in spleen of BALB/c and Slamf1$^{-/-}$ mice infected with different strains of T. cruzi. *Gene expression was determined by RT-qPCR and RQ value were obtained after normalizing value from infected respect to no-infected spleens. Results are shown in Figure S 12 (Enzymes) and Figure S 13(Cytokines). Parasite loads (T. cruzi) correspond to values from Figure 31. For each gene and parasite load a color code was given from high (Red) to low (Green).*

		14 d.p.i.							21 d.p.i.						
		Irg1	*Cybb*	*Il1b*	*Il6*	*Il10*	*Tnf*	*T.cruzi*	*Irg1*	*Cybb*	*Il1b*	*Il6*	*Il10*	*Tnf*	*T.cruzi*
BALB/c	Dm28c														
	Y														
	VFRA cl1														
Slamf1$^{-/-}$	Dm28c														
	Y														
	VFRA cl1														

High **Low**

The analysis of discriminant of principal components was performed with the gene expression of the 2 enzymes, 4 cytokines and the parasite load at 14 and 21 d.p.i. The DAPC analysis of spleen at 14 d.p.i. was able to discriminate 99.7% in our model, which 81.7% and 17.9% are explained in first (x-axis) and second (y-axis) principal components, respectively. We found at 14 d.p.i. that infections with Dm28c in BALB/c and *Slamf1*$^{-/-}$ mice are more separated in the DAPC from the other infections (Y and VFRA cl1) and the non-infected controls. This is because of the earlier peak of the gene expression observed with this strain.

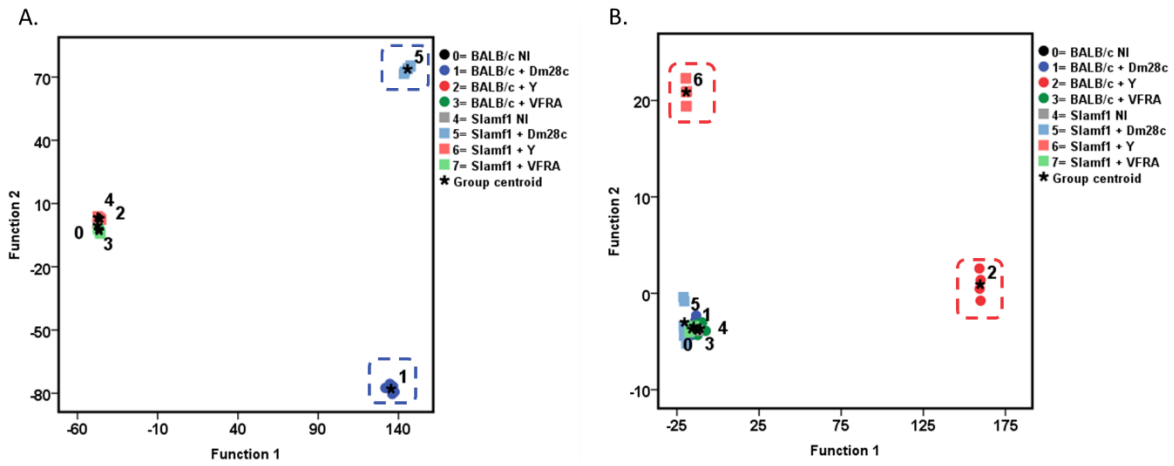

Figure 32. Discriminant Analysis of Principal Components (DAPC). *These scatterplots show the first two principal components of the DAPC of data according to the spleens infected with the different T. cruzi strains.* ***A.*** *14d.p.i.* ***B.*** *21 d.p.i. The diagrams show clusters of with the different strains of T. cruzi Dm28c (Blue dashed line) and Y (Red dashed line).*

Table 19 shows 100% discrimination in all the cases except for BALB/c infected with VFRA cl1 strain.

Table 19. Discriminant frequencies in spleens of Slamf1$^{-/-}$ and BALB/c mice infected with different strains of T. cruzi at 14 d.p.i.

14 d.p.i.			Theoretical Group							
			BALB/c				*Slamf1* $^{-/-}$			
			NI %(N)	Dm28c %(N)	Y %(N)	VFRA cl1 %(N)	NI %(N)	Dm28c %(N)	Y %(N)	VFRA cl1 %(N)
Real Group	BALB/c	NI	100 (6)							
		Dm28c		100 (6)						
		Y			83 (5)	17 (1)				
		VFRA cl1				100 (6)				
	Slamf1$^{-/-}$	NI					100 (6)			
		Dm28c						100 (6)		
		Y							100 (6)	
		VFRA cl1								100 (6)

The DAPC analysis of spleen at 21 d.p.i. was able to discriminate 99.8% in our model, in which 97.1% and 2.7% are explained in first (x-axis) and second (y-axis) principal components, respectively. We found that infections with Y in BALB/c and *Slamf1*$^{-/-}$ mice are more separated in the DAPC compared with the other infections and the controls associated with the very high gene expression observed with this strain at this time point. The percent of discrimination in Table 20, shows again 100% discrimination in all cases except for BALB/c spleens infected with VFRA cl1.

Table 20. Discriminant frequencies in spleens of Slamf1$^{-/-}$ and BALB/c mice infected with different strains of T. cruzi at 21 d.p.i.

21 d.p.i.			Theoretical Group							
			BALB/c				*Slamf1* $^{-/-}$			
			NI %(N)	Dm28c %(N)	Y %(N)	VFRA cl1 %(N)	NI %(N)	Dm28c %(N)	Y %(N)	VFRA cl1 %(N)
Real Group	BALB/c	NI	100 (6)							
		Dm28c		100 (6)						
		Y			100 (6)					
		VFRA cl1		17 (1)		67 (4)	17 (1)			
	Slamf1$^{-/-}$	NI					100 (6)			
		Dm28c						100 (6)		
		Y							100 (6)	
		VFRA cl1								100 (6)

4.4.2.3 Spleen Correlation Networks

We identified different networks with the correlations between gene expression of the immunoregulatory genes and the parasite load in the analysis of the BALB/c and *Slamf1*$^{-/-}$spleens at 14 and 21dp.i. Using the Cytoscape software, we visualized the correlations between the strains shown in the appendix section 8 (Table S 11 and Table S 12) and compared the obtained networks between the BALB/c and the *Slamf1*$^{-/-}$. Appearance and disappearance of the correlations between BALB/c and *Slamf1*$^{-/-}$ spleen at the different days of sacrifice indicate the differential role of SLAMF1 receptor in the infection with the different strains of *T. cruzi*. Statistical significance of the correlations are shown in the appendix section 8 (Table S 13 and Table S 14).

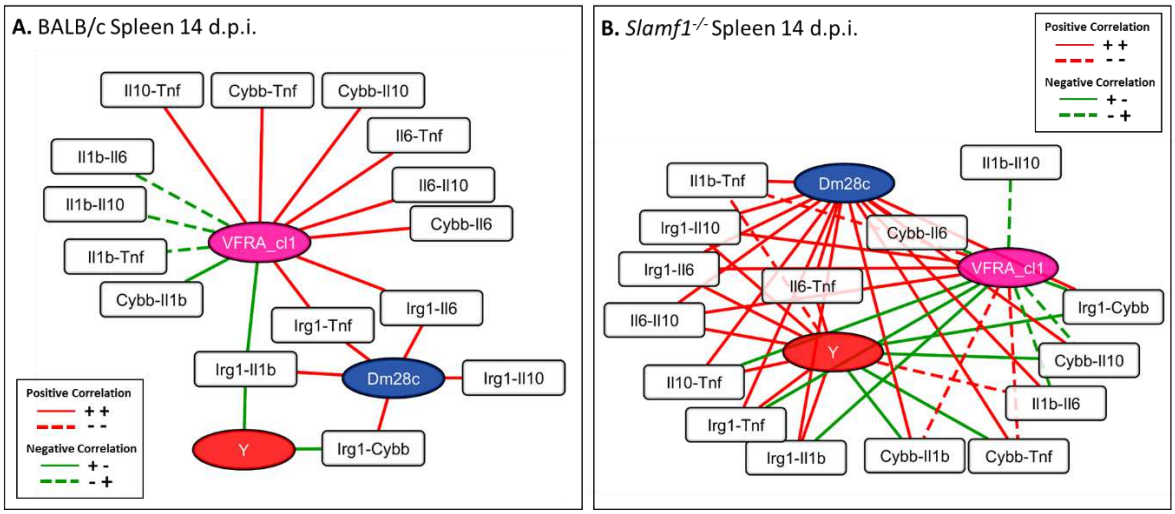

Figure 33. Networks of the spleen of BALB/c and Slamf1$^{-/-}$ mice. A. *BALB/c spleen at 14 d.p.i.* ***B.*** *Slamf1$^{-/-}$ spleen at 14 d.p.i. Networks were generated and represented as indicated in the Methods section.*

Using the different strains of *T. cruzi* as central nodes, in the spleens of BALB/c mice infected with the different strains the resulting network was composed of 15 secondary nodes and 20 edges (Figure 33 A) whereas *Slamf1*$^{-/-}$ infection network was composed of 15 secondary nodes and 41 edges (Figure 33 B), with 3 as the maximum degree of connectivity of a node and 1 as the minimum.

We found more correlations in BALB/c spleen of mice infected with the VFRA cl1 strain than with Dm28c and Y, and several of those correlations were exclusive of VFRA cl1 strain. Interestingly, the interactions shared between the strains always contain the *Irg1* gene, Y strain contains only negative correlations while Dm28c had only positive correlation indicating a different immune response in the spleen for each strain. In contrast, almost all correlations in the *Slamf1*$^{-/-}$ were shared between all the strains evaluated, and only the correlation between *Il1b-Il10* was exclusive for the infection with VFRA cl1 where and two other correlations were shared for only two of the strains evaluated. This could be indicative of the importance of SLAMF1 receptor in generating variability in BALB/c mice immune response upon infection with different strains. As in BALB/c network Dm28c presented only positive correlations while the strains Y and VFRA cl1 presented positive and negative correlations.

At 21 d.p.i the network was composed of 15 secondary nodes and 30 edges (Figure 34 A) and *Slamf1*$^{-/-}$ was composed of 15 secondary nodes and 42 edges (Figure 34 B), with 3 as the maximum degree of connectivity of a node and 1 as the minimum.

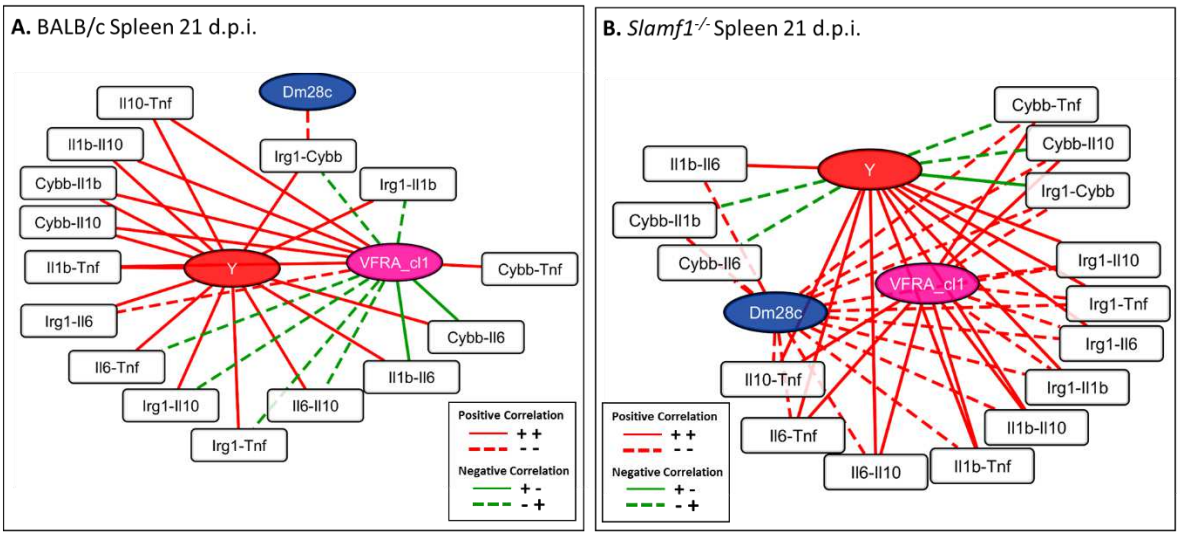

Figure 34. Networks of the spleen of BALB/c and Slamf1$^{-/-}$ mice. A. *BALB/c spleen at 21 d.p.i.* ***B.*** *Slamf1$^{-/-}$ spleen at 21 d.p.i. Networks were generated and represented as indicated in the Methods section.*

We found at 21 d.p.i. more correlations between Y and VFRA cl1 than at 14 d.p.i, in which several correlations that were exclusive of VFRA cl1 shows are now common with the strain Y. Only one correlation was VFRA cl1 strain exclusive, moreover, was the only strain at this day with negative correlations. The infection with the Dm28c shared just one positive correlation with the other strains. However, in *Slamf1$^{-/-}$* spleens the correlations were common in almost all cases among the three different strains and only three correlations were shared by two strains (Dm28c and Y). In contrast, the Y strains presented some negative correlations in comparison with the infection with BALB/c infection where the correlations were only positive.

4.4.2.4 Spleen Protein expression

The proteins COX-2, NOX2, iNOS and Arg-1 play an important role in parasite elimination after the infection. We evaluated the expression of these proteins in the samples of BALB/c and *Slamf1$^{-/-}$ T. cruzi* spleens infected with the Dm28c, Y and VFRA cl1 at 14 and 21 d.p.i. and the NI controls (Figure 35).

Surprisingly, iNOS protein in the spleen was not detected in any case. Only BALB/c mice infected with Y expressed Arg-1 at 14 d.p.i. indicating that *Slamf1$^{-/-}$* receptor is implicated on the detection of this enzyme in the spleen. COX-2 levels were higher at 14 d.p.i. being higher in the mice infected with Y than the others 2 strains and more expressed in *Slamf1$^{-/-}$* mice. NOX2 was induced at 14 d.p.i. in all conditions being higher in *Slamf1$^{-/-}$* spleens of mice infected with VFRA cl1. At 21 higher

expression of NOX2 was observed in all conditions except for BALB/c and *Slamf1*$^{-/-}$ mice infected with the Y strain, in which slights decreased compared to 14 d.p.i.

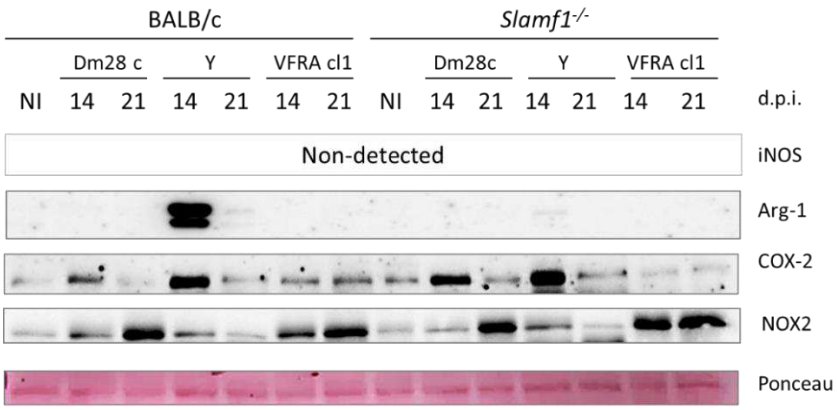

Figure 35. Protein Expression level in Spleen of BALB/c and Slamf1*$^{-/-}$ *mice infected with Different Strains of T. cruzi. *Expression levels of iNOS, Arg-1, COX-2 and NOX2 at 14 and 21 d.p.i. and their respective controls. Ponceau staining is shown as a loading control.*

4.4.3 HEART

4.4.3.1 Heart Hypertrophy and Parasite Load

The heart is one of the most important organs affected by *T. cruzi* infection in humans. We evaluated the hypertrophy in the heart, by weighting the heart of the sacrificed animals (mg) at 14 and 21 d.p.i. and dividing it by the body weight (g) to calculate the heart weight/body weight ratio (Figure 36 A and B).

We observed a higher hypertrophy, although not significant, in Y and VFRA cl1 infected BALB/c mice. In contrast, we observed significant increment of heart weight/body weight ratio in *Slamf1*$^{-/-}$ mice infected with Dm28c and VFRA cl1 at 14 d.p.i. and with Y and VFRA at 21 d.p.i. compared to NI infected *Slamf1*$^{-/-}$. Regarding parasite load, the Y strain was the most infective, followed by VFRA cl1 and finally Dm28c (Figure 36 A and B). *Slamf1*$^{-/-}$ mice showed lower parasite load than the wild type in the cases of Dm28c and Y, but not for VFRA cl1 where the parasite load was higher in the knockout than the wild type. This result is in concordance with what we found *in vitro*, where *Slamf1*$^{-/-}$ deficient macrophages showed less parasite load than BALB/c in Dm28c and Y but not in VFRA cl1. In addition we found that heart hypertrophy seems to be associated with the actual parasite load, where the higher parasite load resulted in an overall higher heart weight/body weight ratio with a Spearman correlation of 0.6793 and a significance of $p<0.001$.

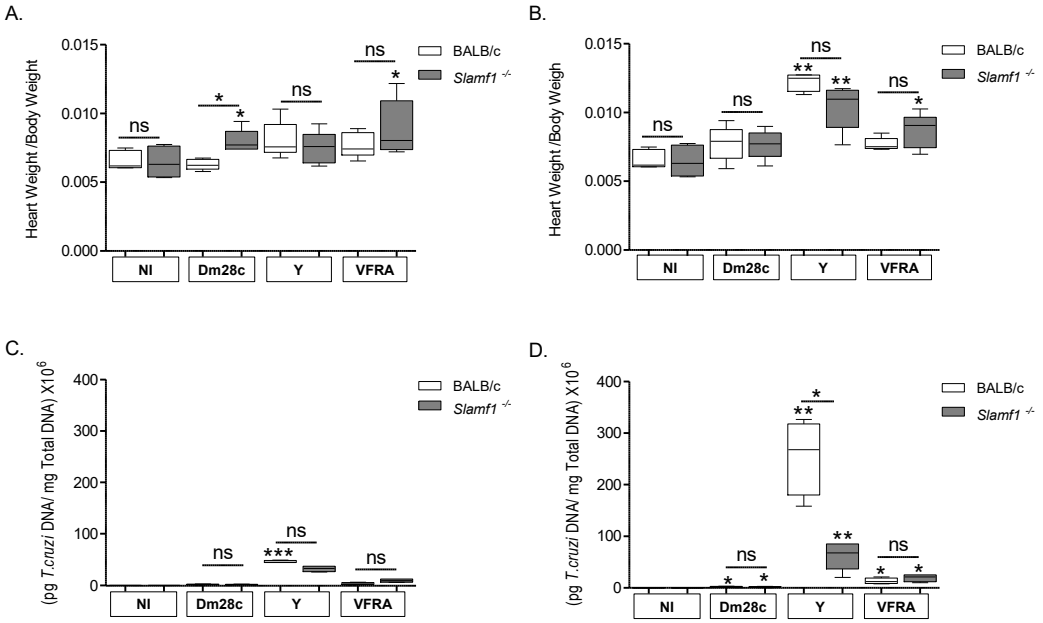

Figure 36. Heart hypertrophy and parasite load in BALB/c and Slamf1$^{-/-}$ mice infected with the different strains of T. cruzi at 14 and 21 d.p.i. A. *Hypertrophy at 14 d.p.i* ***B.*** *Hypertrophy at 21 d.p.i.* ***C.*** *Parasite load at 14 d.p.i. and* ***D.*** *Parasite load at 21d.p.i. Means and Standard errors of the means ± (SEM) of 5 mice per group are represented. The asterisks indicate the statistical significance, t-student (*p<0.05, **p<0.005 and ***p<0.001), when comparing the infected BALB/c and Slamf1$^{-/-}$ mice.*

4.4.3.2 Heart Gene Expression

Table 21 presents a summary of the gene expression of the enzyme and cytokines evaluated. We found a peak of activation at 14 d.pi. in BALB/c and *Slamf1*$^{-/-}$ mice infected with the Y indicating that this strain would cause, more cardiac damage compared to the Dm28c and VFRA cl1. This activation is also associated with the higher hypertrophy and higher parasite loads found in the hearts of the mice infected with this strain.

Table 21. Summary of expression of immunoregulatory genes and parasite load in heart of BALB/c and Slamf1$^{-/-}$ mice infected with different strains of T. cruzi. *Gene expression was determined by RT-qPCR and RQ value were obtained after normalizing value from infected respect to no-infected hearts. Results are shown in Figure S 14 (Enzymes) and Figure S 15 (cytokines). Parasite load (T.cruzi) corresponds to value from Figure 35. For each gene and parasite load a color code was given from high (Red) to low (Green).*

		14 d.p.i.								21 d.p.i.							
		Arg1	*Irg1*	*Cybb*	*Il1b*	*Il6*	*Il10*	*Tnf*	*T.cruzi*	*Arg1*	*Irg1*	*Cybb*	*Il1b*	*Il6*	*Il10*	*Tnf*	*T.cruzi*
BALB/c	Dm28c																
	Y																
	VFRA cl1																
Slamf1$^{-/-}$	Dm28c																
	Y																
	VFRA cl1																

High — Low

The analysis of discriminant of principal components was performed with the gene expression of the 3 enzymes, 4 cytokines and the parasite load at 14 and 21 d.p.i.

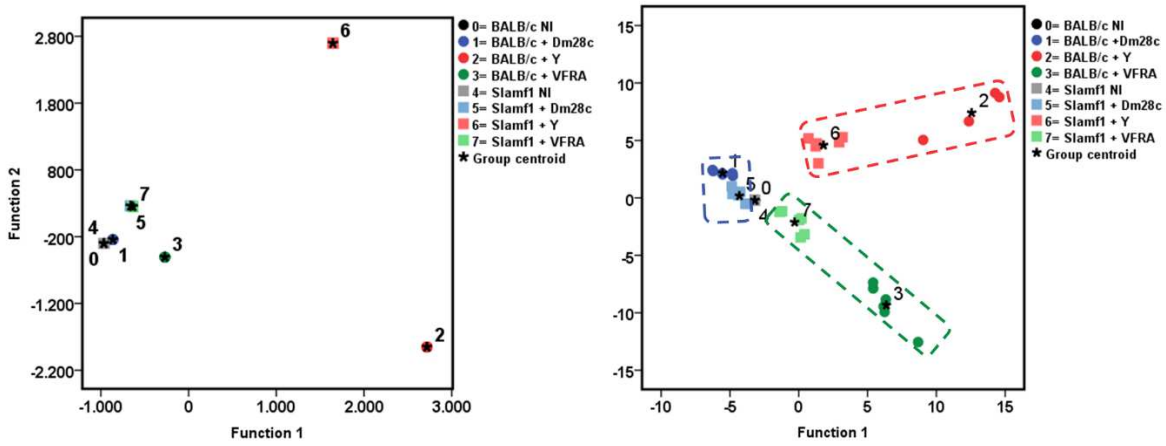

Figure 37. Discriminant Analisis of Principal Components (DAPC). These scatterplots show the first two principal components of the DAPC of data according to the hearts infected with the different T. cruzi strains. ***A.*** *14 d.p.i.* ***B.*** *21 d.p.i. The diagrams show clusters of with the different strains of T. cruzi Dm28c (Blue dashed line), Y (Red dashed line) and VFRA (Green dashed line).*

The DAPC analysis in Heart at 14 d.p.i. was able to discriminate 99.2% in our model, which 54.2% and 45% are explained in first (x-axis) and second (y-axis) principal components, respectively. We found at 14 d.p.i. that infections with Y in BALB/c and *Slamf1*$^{-/-}$ mice are more separated in the DAPC compared with the other infections and the controls, that is because of the high gene expression and the higher parasitemia found in the heart with the Y strain. Table 22 shows that discrimination was 100% in all cases.

Table 22. Discriminant frequencies in hearts of Slamf1$^{-/-}$ and BALB/c mice infected with different strains of T. cruzi at 14 d.p.i.

14 d.p.i.			Theoretical Group							
			BALB/c				*Slamf1* $^{-/-}$			
			NI %(N)	Dm28c %(N)	Y %(N)	VFRA cl1 %(N)	NI %(N)	Dm28c %(N)	Y %(N)	VFRA cl1 %(N)
Real Group	BALB/c	NI	100 (6)							
		Dm28c		100 (6)						
		Y			100 (6)					
		VFRA cl1				100 (6)				
	Slamf1 $^{-/-}$	NI					100 (6)			
		Dm28c						100 (6)		
		Y							100 (6)	
		VFRA cl1								100 (6)

The DAPC analysis in the hearts at 21 d.p.i. was able to discriminate 91.7% in our model, which 53.8% and 37.9% are explained in first (x-axis) and second (y-axis) principal components,

respectively. We found three different clusters associated with the strains of *T. cruzi.* Table 23 shows that discrimination was 100% for all strain, except for BALB/c heart infected with Y strain.

Table 23. Discriminant frequencies in hearts of Slamf1$^{-/-}$ and BALB/c mice infected with different strains of T. cruzi at 21 d.p.i.

21 d.p.i.			Theoretical Group							
			BALB/c				*Slamf1* $^{-/-}$			
			NI %(N)	Dm28c %(N)	Y %(N)	VFRA cl1 %(N)	NI %(N)	Dm28c %(N)	Y %(N)	VFRA cl1 %(N)
Real Group	BALB/c	NI	100 (6)							
		Dm28c		67 (4)			17 (1)	17 (1)		
		Y			100 (6)					
		VFRA cl1				100 (6)				
	Slamf1 $^{-/-}$	NI					100 (6)			
		Dm28c						100 (6)		
		Y							100 (6)	
		VFRA cl1								100 (6)

4.4.3.3 Heart Correlation Networks

We draw a network with the correlations of the gene expression of the immunoregulatory genes and the parasite loads in hearts of BALB/c and *Slamf1*$^{-/-}$infected with the different strains of *T. cruzi.* All the correlations found at 14 d.p.i. were positive and with a significance of $p<0.001$. Using the Cytoscape software we visualized the correlation between the strains and compared the resulting BALB/c and the *Slamf1*$^{-/-}$ networks. Appearance and disappearance in the correlations between BALB/c and *Slamf1*$^{-/-}$ at the different days post-infection indicate the role of Slamf1 receptor in the infection with the different strains of *T. cruzi.* Statistical significance of the correlations are shown in the appendix section 8 (Table S 13 and Table S 14).

The resulting network at 14 d.p.i. was composed of 21 secondary nodes and 56 edges (Figure 38 A) and *Slamf1*$^{-/-}$ was composed of 21 secondary nodes and 52 edges (Figure 38 B), with 3 as the maximum degree of connectivity of a node and 1 as the minimum and the different strains of *T. cruzi* were used as central nodes.

We found several correlations between the three parasite strains in BALB/c hearts of mice at 14 d.p.i., being the rest of the correlations only common between the Dm28c and VFRA cl1 strains. In the *Slamf1*$^{-/-}$ hearts of mice also several correlations were common between the three strains but correlation between Dm28c and Y, and Y with VFRA cl1 were found. In the *Slamf1*$^{-/-}$ hearts of mice infected with the Dm28c and VFRA cl 1 strains we found exclusive correlations.

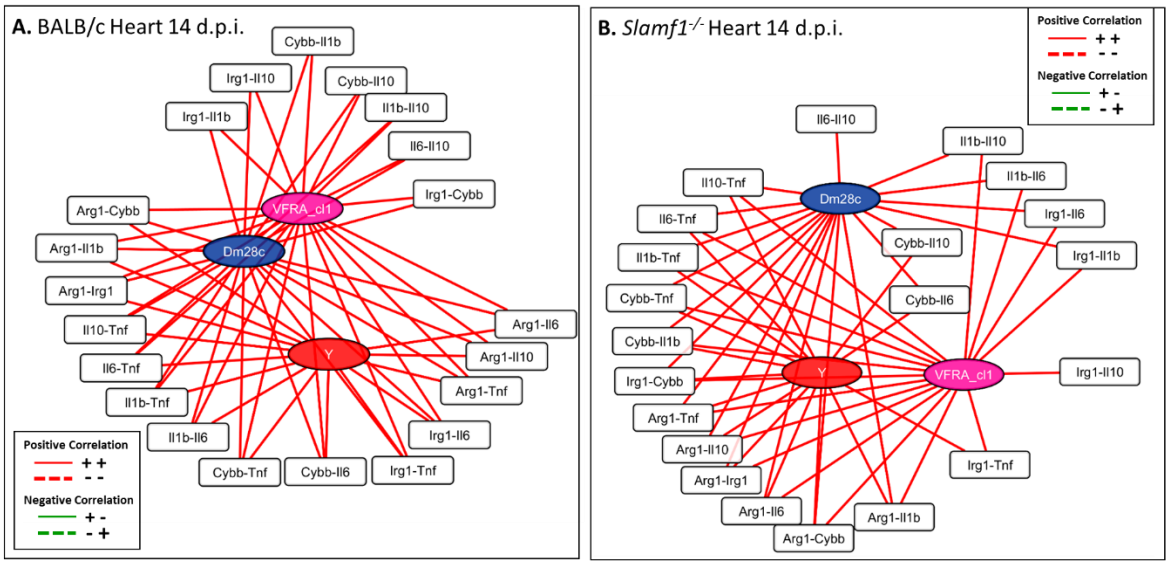

Figure 38. Networks of the hearts of BALB/c and Slamf1$^{-/-}$ mice. A. *BALB/c hearts at 14 d.p.i.* ***B.*** *Slamf1$^{-/-}$ mice at 14 d.p.i. Networks were generated and represented as indicated in the Methods section.*

At 21 d.p.i., the hearts of BALB/c mice infected with the different strains of *T. cruzi* presented a network composed of 21 secondary nodes and 58 edges (Figure 39 A) whereas in *Slamf1$^{-/-}$* it was composed of 21 secondary nodes and 42 edges (Figure 39 B).

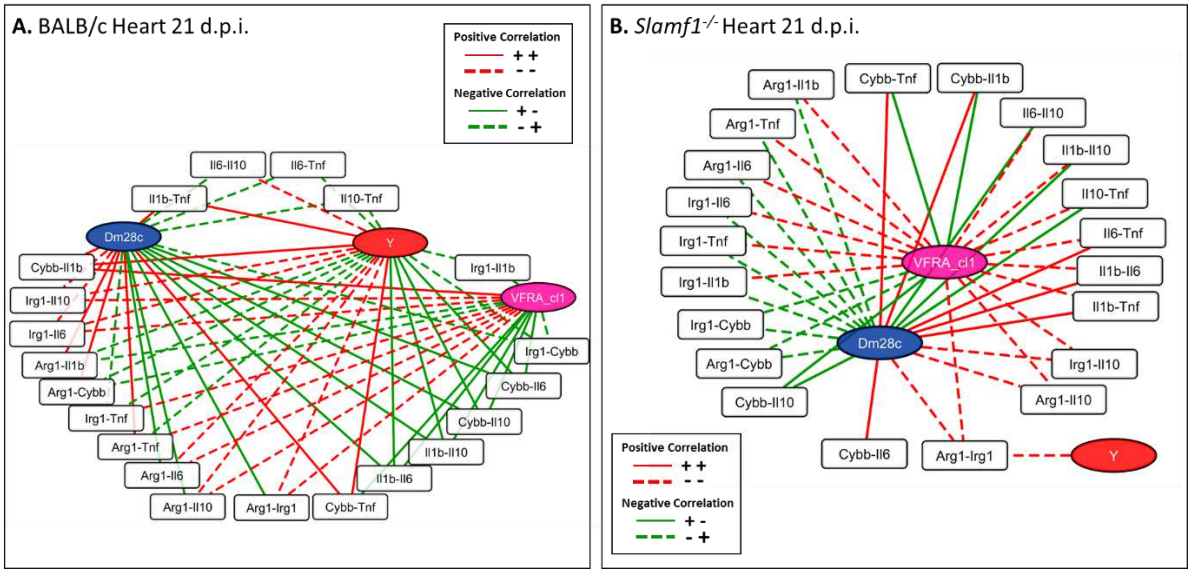

Figure 39. Networks of the hearts of BALB/c and Slamf1$^{-/-}$ mice. A. *BALB/c hearts at 21 d.p.i.* ***B.*** *Slamf1$^{-/-}$ mice at 21 d.p.i. Networks were generated and represented as indicated in the Methods section.*

Correlations in BALB/c hearts of mice infected with the different parasite strains were mostly common between the three strains. In this case several common correlations between the strains Y and Dm28c were also found, two negatives for both strains, one positive for both also and one positive for Y but no for Dm28c. In contrast in *Slamf1$^{-/-}$* hearts of mice the common correlation were

mostly between Dm28c and VFRA cl1, and only one positive correlation between *Arg1-Irg1* where found in the infection with Y strain that was common with the others strains. Besides, a strain exclusive positive correlation was found in the case of Dm28c.

4.4.3.4 Heart Protein Expression

We evaluated the same proteins as in the spleen (iNOS, NOX2, COX-2 and Arg-1) in the heart and in addition YAP-1, an indicator of cardiomyocyte proliferation (Figure 40). iNOS expression was higher in the heart of mice infected with Y, and in the absence of SLAMF1 there was a decrease in their expression at 21 d.p.i. compared with BALB/c. Similar results on iNOS expression were observed when infected with VFRA cl1 although the expression was much lower. Finally, there was slight increase in iNOS expression with the Dm28c that was similar in both BALB/c and *Slamf1*$^{-/-}$mice. Interestingly, in hearts of mice infected with Y strain there were higher levels of iNOS, Arg-1 and COX-2 than in the ones infected with Dm28c and VFRA cl1, also indicative of a more aggressive infection. Moreover SLAMF1 deficiency lowered iNOS levels while it further increased Arg-1 and COX-2 in Y strain infected hearts.

The NOX2 expression was much higher at 14 d.p.i. in the hearts of mice infected with Y strain compared with Dm28c and VFRA cl1, where the increment were at 21 d.p.i.

YAP-1 expression was higher in hearths of BALB/c mice infected with Y strain, follow by VFRA cl1 and the lowest in Dm28c correlating with the hypertrophy values. Interesting, SLAMF1 deficiency resulted in a diminished expression.

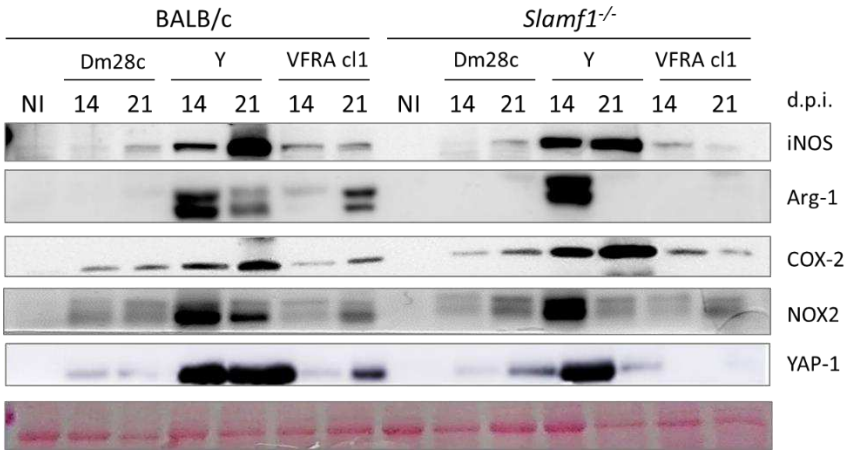

Figure 40. Protein Expression level in heart of BALB/c and Slamf1$^{-/-}$ mice infected with Different Strains of T. cruzi. *Expression levels of iNOS, Arg-1, COX-2, NOX2 and YAP-1 at 14 and 21 d.p.i. and their respective controls.*

4.4.4 LIVER

4.4.4.1 Hepatomegaly and Parasite Load

In the case of the liver we evaluated the hepatomegaly generated by *T. cruzi.* We weighted the liver of the sacrificed animals to evaluate the hepatomegaly at 14 and 21 d.p.i. and dividing the liver weight (mg) by the body weight (g) to calculate the liver weight/body weight ratio.

Hepatomegaly was induced by infection with the 3 strains in a similar fashion (Figure 41 A and B). We found higher hepatomegaly in BALB/c compared with *Slamf1*$^{-/-}$ mice for all strains. As in the spleen, but in contrast to heart hypertrophy, we didn't find a correlation between the parasite load (Figure 41 C and D) and hepatomegaly, with Spearman correlation of 0.3165 and significance of $p<0.005$. Dm28c and Y in BALB/c mice present similar hepatomegaly but the parasite load is lower in Dm28c compared with Y or VFRA cl1. Interestingly, livers infected with VFRA cl1 presented higher parasite load in the *Slamf1*$^{-/-}$ than BALB/c mice, indicating that SLAMF1 may help to control the infection in the liver.

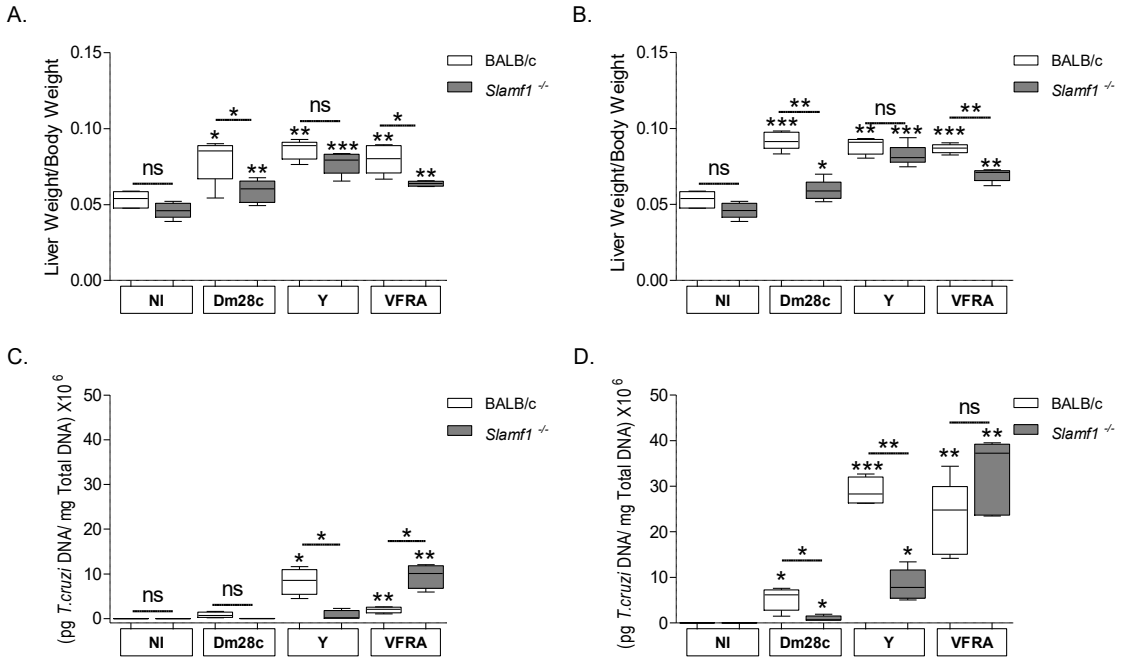

Figure 41. Hepatomegaly and parasite load of BALB/c and Slamf1$^{-/-}$ mice infected with the different strains of T. cruzi at 14 and 21 d.p.i. A. *Hepatomegaly at 14d.p.i* ***B.*** *Hepatomegaly at 21d.p.i.* ***C.*** *Parasite load at 14 d.p.i and* ***D.*** *Parasite load at 21d.p.i. Means and Standard errors of the means ± (SEM) of 5 mice per group are represented. The asterisks indicate the statistical significance, t-student (*p<0.05, **p<0.005 and ***p<0.001), when comparing the infected BALB/c and Slamf1$^{-/-}$ mice.*

4.4.4.2 Liver Gene Expression

The summary of the gene expression of the enzymes, cytokines and parasite load is presented in Table 24. We found an overexpression for almost all genes evaluated at 14 d.p.i. that decreased at 21 d.p.i. in BALB/c. A similar global pattern was found in Slamf1$^{-/-}$ livers of infected mice despite there was lower parasite load. However, some genes as *Il6* had higher expression in *Slamf1*$^{-/-}$ at 14 d.p.i., except for Dm28c.

Table 24. Summary of expression of immunoregulatory genes and parasite load in liver of BALB/c and Slamf1*$^{-/-}$ *mice infected with different strains of T. cruzi. *Gene expression was determined by RT-qPCR and RQ value were obtained after normalizing value from infected respect to no-infected livers. Results are shown in Figure S 16 (Enzymes) and Figure S 17 (Cytokines). Parasite loads (T.cruzi) correspond to value from Figure 41. For each gene and parasite load a color code was given from high (Red) to low (Green).*

		14 d.p.i.							21 d.p.i.						
		Irg1	*Cybb*	*Il1b*	*Il6*	*Il10*	*Tnf*	*T.cruzi*	*Irg1*	*Cybb*	*Il1b*	*Il6*	*Il10*	*Tnf*	*T.cruzi*
BALB/c	Dm28c														
	Y														
	VFRA cl1														
Slamf1$^{-/-}$	Dm28c														
	Y														
	VFRA cl1														

High **Low**

The analysis of discriminant of principal components was performed with the gene expression of the 2 enzymes, 4 cytokines and the parasite load at 14 and 21 d.p.i.

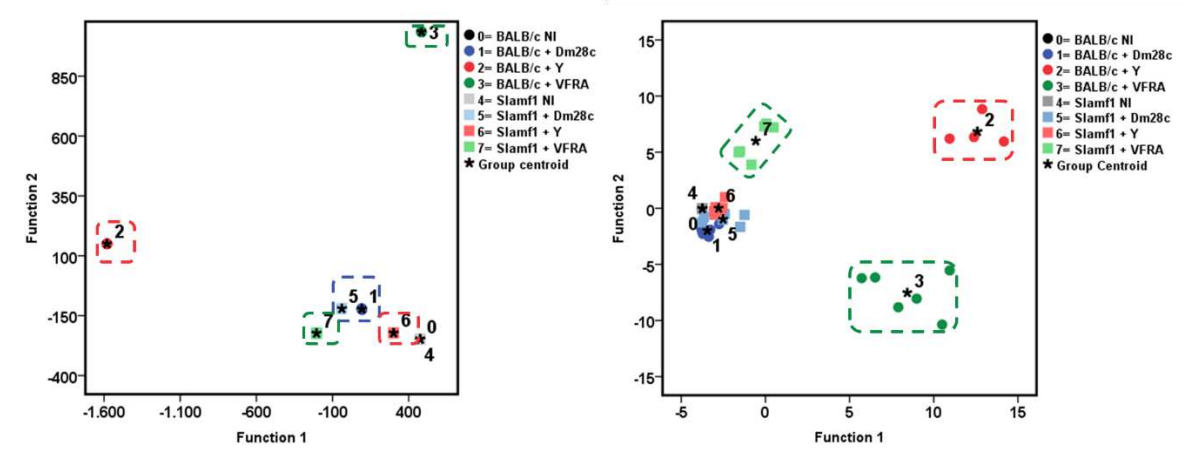

Figure 42. Discriminant Analyze of Principal Components (DAPC). *These scatterplots show the first two principal components of the DAPC of data according to the livers infected with the different T. cruzi strains.* ***A.*** *14d.p.i.* ***B.*** *21 d.p.i. The diagrams show clusters of with the different strains of T. cruzi Dm28c (Blue dashed line), Y (Red dashed line) and VFRA (Green dashed line).*

The DAPC analysis in the livers at 14 d.p.i. was able to discriminate 99.7% in our model, which 71% and 28.7% are explained in first (x-axis) and second (y-axis) principal components. We found 5

different clusters: One for the infection with the Dm28c in BALB/c and *Slamf1*$^{-/-}$ mice indicative of similar response in both groups, other two clusters for the infections with Y one for infection in BALB/c and the other in *Slamf1*$^{-/-}$ mice, and the last two cluster with the infections of the VFRA cl1, one for infection in BALB/c and the other *Slamf1*$^{-/-}$ mice. This suspect that SLAMF1 deficiency affect liver response more in Y and VFRA cl1 than in Dm28c. The percent of discrimination is on Table 25 shows that discrimination was 100% in all cases.

Table 25. Discriminant frequencies in livers of Slamf1$^{-/-}$ and BALB/c mice infected with different strains of T. cruzi at 14 d.p.i.

14 d.p.i.			Theoretical Group							
			BALB/c				*Slamf1*$^{-/-}$			
			NI %(N)	Dm28c %(N)	Y %(N)	VFRA cl1 %(N)	NI %(N)	Dm28c %(N)	Y %(N)	VFRA cl1 %(N)
Real Group	BALB/c	NI	100 (6)							
		Dm28c		100 (6)						
		Y			100 (6)					
		VFRA cl1				100 (6)				
	Slamf1$^{-/-}$	NI					100 (6)			
		Dm28c						100 (6)		
		Y							100 (6)	
		VFRA cl1								100 (6)

The DAPC analysis in the livers at 21 d.p.i. was able to discriminate 84.8% in our model, which 54.5% and 30.3% are explained in first (x-axis) and second (y-axis) principal components. We found 4 different clusters in this case. One for BALB/c and *Slamf1*$^{-/-}$ mice with Dm28c, the *Slamf1*$^{-/-}$ mice infected with the Y and the NI mice; the second one is the cluster infected with Y in BALB/c mice, and the last two clusters include the infections with the VFRA cl1, one for infection in BALB/c and the other in *Slamf1*$^{-/-}$ mice. The percent of discrimination is on Table 26 shows that discrimination was 100% in all cases, except for the infections in *Slamf1*$^{-/-}$ infected with Dm28c and Y strains.

Table 26. Discriminant frequencies in livers of Slamf1$^{-/-}$ and BALB/c mice infected with different strains of T. cruzi at 14 d.p.i.

21 d.p.i.			Theoretical Group							
			BALB/c				*Slamf1*$^{-/-}$			
			NI %(N)	Dm28c %(N)	Y %(N)	VFRA cl1 %(N)	NI %(N)	Dm28c %(N)	Y %(N)	VFRA cl1 %(N)
Real Group	BALB/c	NI	100 (6)							
		Dm28c		67 (4)				33 (2)		
		Y			100 (6)					
		VFRA cl1				100 (6)				
	Slamf1$^{-/-}$	NI					100 (6)			
		Dm28c	17 (1)				17 (1)	67 (4)		
		Y						33 (2)	67 (4)	
		VFRA cl1								100 (6)

4.4.4.3 Liver Correlations Network

As in the other organs evaluated, we generated a network with the correlations of the gene expression of the immunoregulatory genes and the parasite load in the livers of BALB/c and *Slamf1*$^{-/-}$ infected with the different strains of *T. cruzi.* All the correlations found at 14 d.p.i. were positive and with a significance of $p<0.001$. Using the software Cytoscape we visualized the correlations between the strains and compared the networks of BALB/c and the *Slamf1*$^{-/-}$. Appearance and disappearance in the correlations between BALB/c and *Slamf1*$^{-/-}$ livers at the different days of sacrificed indicate the role of SLAMF1 receptor in the infection with the different strains of *T. cruzi* are explained in the appendix section 8 (Table S 15 and Table S 16).

We found in the livers of BALB/c mice infected with the different strains of *T. cruzi* and sacrificed at 14 d.p.i. that the resulting network was composed of 15 secondary nodes and 29 edges (A) and *Slamf1*$^{-/-}$ was composed of 13 secondary nodes and 16 edges (B), with 3 as the maximum degree of connectivity of a node and 1 as the minimum and the different strains of *T. cruzi* were used as central nodes. We found three correlations in common between the three strains in the liver of BALB/c mice, two between Dm28c and Y, and six between Y and VFRA cl1 which had also some strain exclusive correlations. In contrast, fewer correlations were found in the liver of *Slamf1*$^{-/-}$ at 14 d.p.i. not a single correlation with the Y strain, two correlations in common between Dm28c and VFRA cl1 and the rest were strain exclusive correlations.

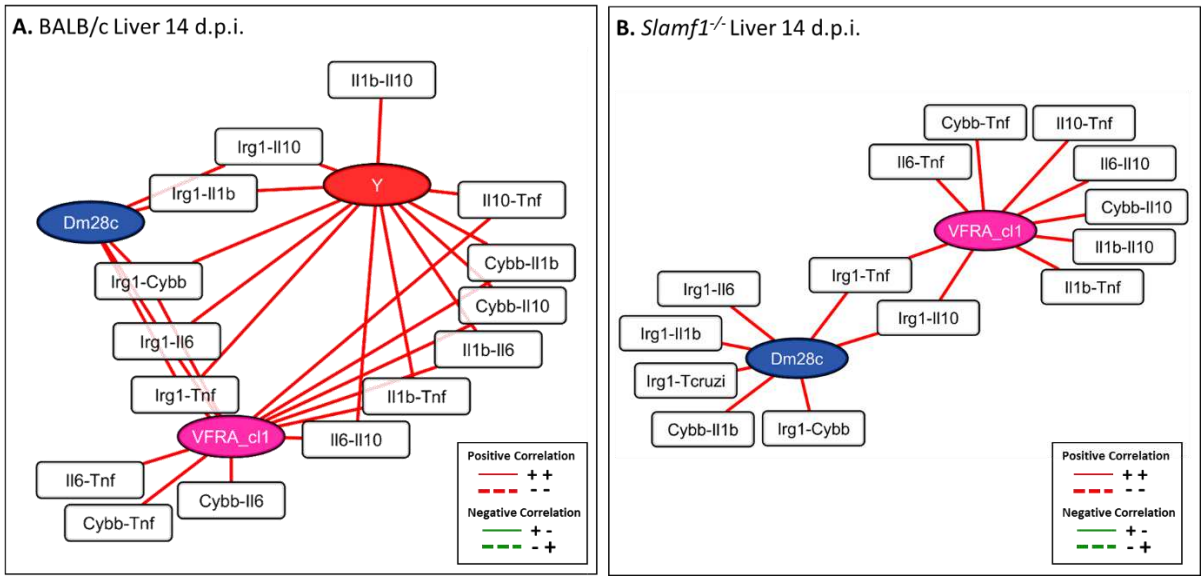

Figure 43. Networks of the livers of BALB/c and Slamf1*$^{-/-}$*mice. A. *BALB/c liver at 14 d.p.i.* ***B.*** *Slamf1*$^{-/-}$ *liver at 14 d.p.i. Networks were generated and represented as indicated in the Methods section.*

At 21 d.p.i. we found in the livers of BALB/c mice infected with the different strains of *T. cruzi* that the resulting network was composed of 15 secondary nodes and 45 edges (A) whereas *Slamf1*$^{-/-}$ was composed of 15 secondary nodes and 44 edges (B).

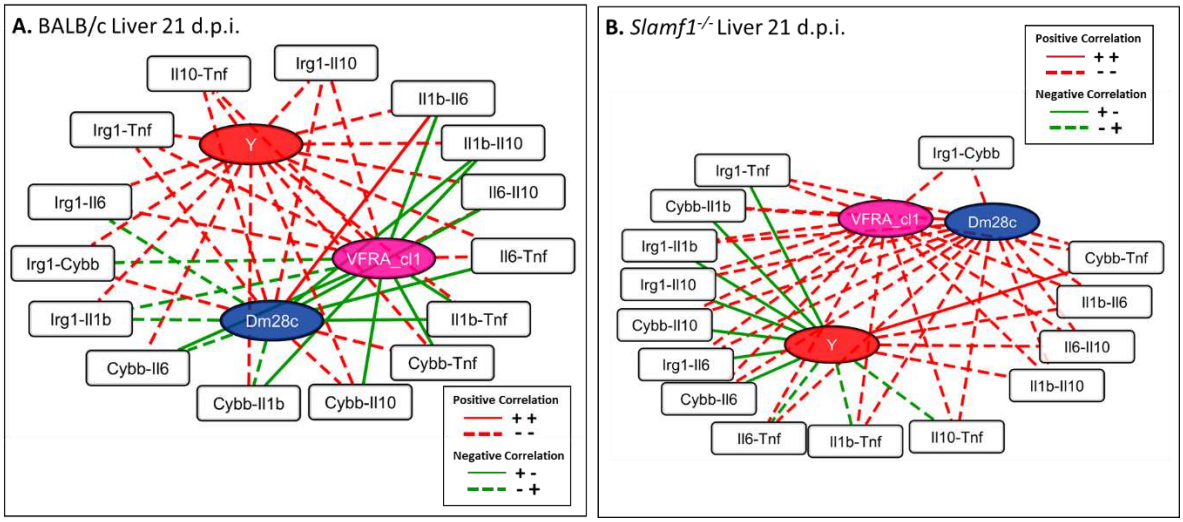

Figure 44. Networks of the livers of BALB/c and Slamf1*$^{-/-}$*mice. A. *BALB/c liver at 21 d.p.i.* ***B.*** *Slamf1*$^{-/-}$ *liver at 21 d.p.i. Networks were generated and represented as indicated in the Methods section.*

The liver of BALB/c mice correlation network involves only common correlations between the three strains evaluated, but while Y presents just positive correlations Dm28c and VFRA cl1 present both negative and positive, indicating a rather similar immune response at this point in the liver for both strains. Similarly, in the liver of *Slamf1*$^{-/-}$ mice almost all the correlations where shared by the three strains evaluated except one between Dm28c and VFRA cl1. Interestingly, in contrast to BALB/c, only Y strain presented negative correlations in *Slamf1*$^{-/-}$ mice. This indicates an important effect of SLAMF1 deficiency in the immune response in the liver for Y strain.

4.4.4.4 Liver Protein expression

Finally, as in the spleen and heart the expression of iNOS, NOX2, COX-2 and Arg-1 were evaluated. The level of iNOS was higher at 21 d.p.i., in BALB/c mice infected with all strains. In the case of *Slamf1*$^{-/-}$ infected mice, higher levels of iNOS were found for the Dm28c strain but not for the Y and VFRA cl1 strains at 21 d.p.i. COX-2 was higher in the infections with Dm28c and Y in BALB/c and *Slamf1*$^{-/-}$mice at 21 d.p.i. Again the higher expression in the infection with VFRA cl1 was at 14 d.p.i. No greater differences were observed in *Slamf1*$^{-/-}$ infection with COX-2 as compared to BALB/c. The expression of NOX2 was higher in BALB/c mice at 21 d.p.i. for Dm28c, as for Y infection where again

higher as at 14 for VFRA cl1. SLAMF1 deficiency results in lower levels of NOX2 as compared to infection in BALB/c mice. High expression of Arg-1 was found in the liver as it was expected, because of the expression of this enzyme in the liver.

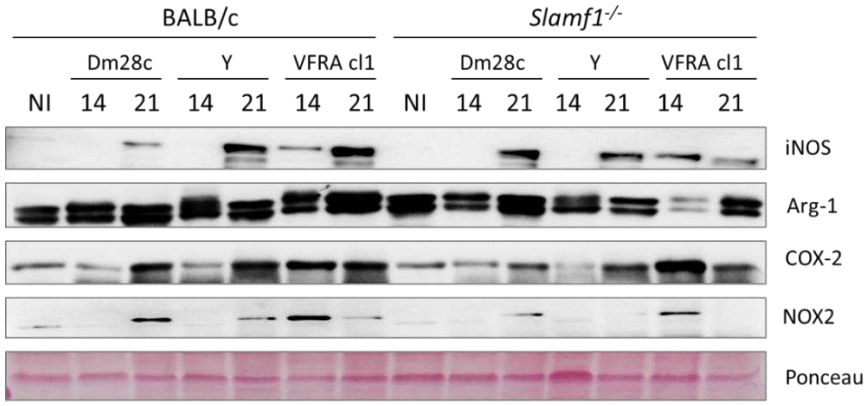

Figure 45. Protein Expression level in liver of BALB/c and Slamf1$^{-/-}$ mice infected with Different Strains of T. cruzi. *Expression levels of iNOS, NOX2, COX-2 and Arg-1 at 14 and 21 d.p.i. and their respective controls.*

4.5 THE EFFECT OF ITACONIC ACID ON PARASITE REPLICATION

Irg1 is coding for an enzyme producing itaconic acid, which is an organic compound that inhibits isocitrate lyase, the key enzyme of the glyoxylate shunt, a pathway essential for microorganism growth under specific conditions, as parasites (Michelucci *et al.*, 2013). The *Irg1* gene showed the highest level of expression in heart tissue of BALB/c mice infected with the Y strain, and it is expression is related to SLAMF1, since there was increased *Irg1* expression in *Slamf1*$^{-/-}$ compared to BALB/c at 14 d.p.i. (Figure 46 A). Thus, since infection and immune response in the heart mainly determine the outcome of the disease we looked for this metabolite in the hearts of BALB/c mice in previous metabolomic study (Gironès *et al.*, 2014). Figure 46 B show that itaconate was undetectable in NI hearts but progressively incremented in infected hearts.

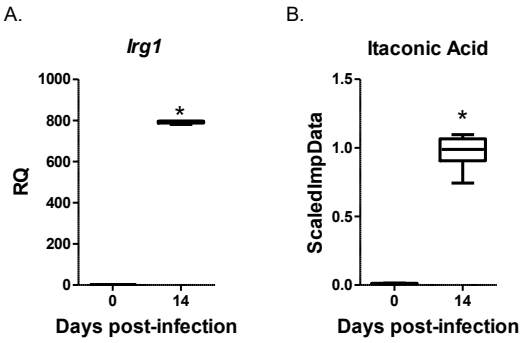

Figure 46. Irg1 expression and Itaconic acid production in heart of BALB/c heart infected with Y strain. A. *Irg1 gene expression by RT-qPCR.* ***B.*** *Itaconic acid relative levels (ScaledImpData) determined by Metabolomics.*

Since *Irg1* expression has been also associated to antimicrobial effects (Michelucci *et al.*, 2013) we performed a preliminary study of its effect on parasite replication using epimastigotes, the replicative form of the parasite in the vector of the disease, of 15 different strains of *T. cruzi* and grouped them by strain type or DTUs since previous studies have found correlation of drug susceptibility with strains DTUs (Aquilino *et al.*, 2012; Pineda *et al.*, 2015). All *T. cruzi* strains were sensible to itaconate (Figure 47). Reference strains showed considerable variation in treatment sensitivity, TcI were the more resistant (IC_{50}:48.51mM) and TcV were the more susceptible (IC_{50}:16.30mM). The results were reproducible in two independent experiments, and indicate the potential of stronger derivatives of this metabolite with higher affinity for the Isocitrate lyase for the treatment of *T. cruzi* infection (Cordes *et al.*, 2015).

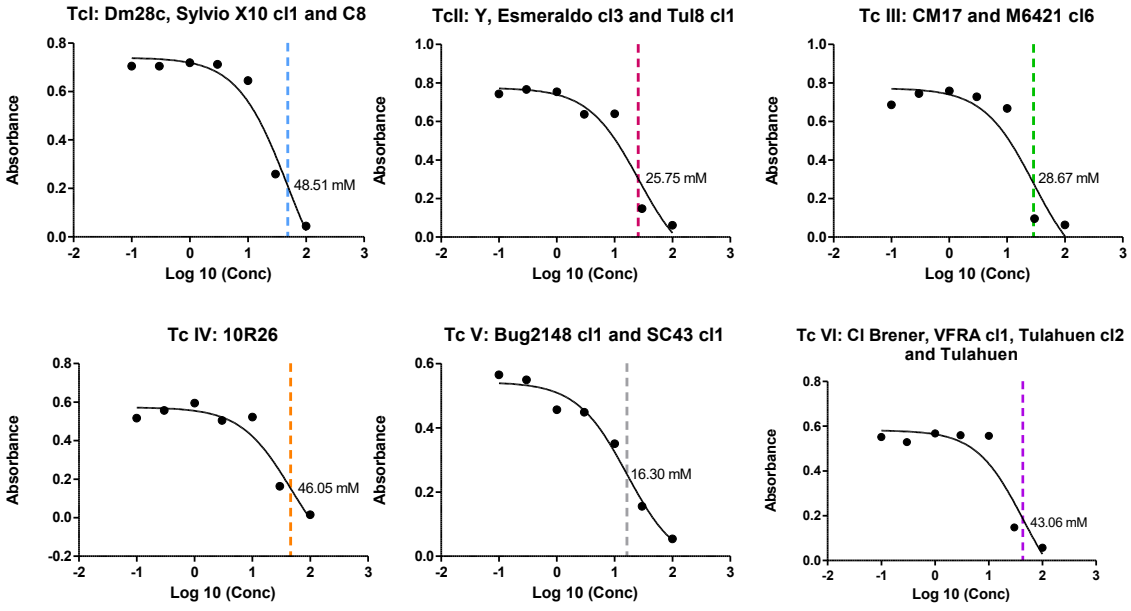

Figure 47. In vitro activity of Itaconic Acid against epimastigotes of T. cruzi.

DISCUSSION

5 DISCUSSION

Chagas disease is a highly heterogeneous and complex (several clinical manifestations and phase, many way of transmission) disease. Moreover, the influence of host genetics, especially in experimental infection, is becoming to be recognized. If this were not enough, recently a great genetic heterogeneity has been described for the parasite. However, most of the reported publications in the field have been performed with only one strain of parasite, one strain of mice combination. This has led to many apparently contradictory results.

The role of the genetic background of the host and the high genetic variability by *T. cruzi* are crucial to understand Chagas disease. The high genetic variability of *T cruzi* is a new problem to be solved in Chagas disease. The parasite has been classified in 6 different DTUs, but the lack of clear associations between the DTUs and the clinical manifestations plus the drug resistance associated with the DTUs, are an obstacle for understanding the mechanism of infection by *T. cruzi* to address those problems. We use two mouse strains with different genetic background and 6 different strains of *T. cruzi,* representing each of the 6 DTUs, to understand the host-parasite interaction in macrophages, since this cell type is also considered key in the elimination or dissemination of the parasite.

We arbitrarily divided macrophage infection in 3 phases based in previous evidence (Maganto-Garcia *et al.*, 2008; Zhao *et al.*, 2013). From 0 to 1 h.p.i. where most of the binding of the parasite takes place (Interaction). From 1 to 6 h.p.i., where all parasites bound are internalized by endocytic mechanism (Internalization) and later they escape to the cytoplasm where they proliferate (6 to 24 h.p.i.). We did choose longer times to avoid macrophage lysis by the parasite, which seriously confound the data. Nevertheless, proliferation usually expand from 48 to 72 h.p.i.

We found a clear effect of mouse genetic background in the *T. cruzi* infection, where BALB/c peritoneal macrophages were more susceptible to the infection of *T. cruzi* than C57BL/6, no matter the strains of *T. cruzi* or the phase of the intracellular infection. It is worth mentioning that BALB/c and C57BL/6 basal gene expression in NI macrophages was similar except for *Arg1* with higher ΔCT (Figure S 1) in BALB/c macrophages, which means higher basal gene expression than in C57BL/6 macrophages. Arg-1 is a M2 marker and it is greater basal level in BALB/c macrophages could be

guiding an ant-inflammatory response after *T. cruzi* infection. In addition, *Cybb* and *Tnf* showed higher basal expression in *Tlr2*$^{-/-}$ and *Slamf1*$^{-/-}$ macrophages respect to C57BL/6 and BALB/c, respectively, being the last ones very similar. Thus these small variations should be taken into account in the subsequent analysis that illustrates changes from basal levels of non-infected macrophages. These would be in agreement with the lower induction of pro-inflammatory genes, as *Tnf* in BALB/c macrophages. The induction of *Slamf1* gene expression was similar in different mouse and parasite strains at 1h, but decreased thereafter, with great variations between parasite strains.

The lower parasite load in all phases analyzed in C57BL/6 macrophages was associated with an in general higher gene expression of macrophage activation genes which indicate a better defense mechanism in C57BL/6 macrophages compared with the BALB/c macrophages. This difference between BALB/c and C57BL/6 have been already documented in other intracellular parasites as *Leishmania* (Rabhi *et al.*, 2013).

In particular, major differences were observed in the interaction phase, where enzymes and cytokines expression were lower in BALB/c than C57BL/6 macrophages. This indicates faster triggering of activation in C57BL/6 that may be is a key to control infection. However, *Tnf* and *Slamf1* gene expression was similar. At the internalization phase, *Irg1* and *Il1b* presented higher levels in C57BL/6 than BALB/c macrophages, and *Tlr2* expression incremented in several conditions. As expected, the greatest variability was observed at the intracellular proliferation phase since the intracellular parasite may affect many signals transduction pathways, where Dm28c infected macrophages showed the highest parasite load in BALB/c and the lowest in C57BL/6. However, there were some exceptions. Thus, we found in BALB/c macrophages infected with *T. cruzi* strains higher gene expression of *Tnf* and *Slamf1* during the interaction and *Il1b* and *Tlr2* during the internalization. Also, we found the *Irg1* overexpressed during the internalization in BALB/c macrophages, Irg1 was also previously shown to be expressed in mouse macrophages under different TLR ligand stimulations and contributes to immune responses through the production of ROS (Tallam *et al.*, 2016).

Interestingly, it has been described that the infection by *T. cruzi* induces high levels of iNOS and large amounts of NO in cultured macrophages with secretion of *Tnf*, *Il6* and *Il1b* (Zanluqui, 2015). The higher expression of the *Slamf1,* and especially *Tlr2* receptors in BALB/c macrophages, compared with C57BL/6, since TLR-2 is required for the attachment/entry of all strains could

indicate that this receptor conduces by a positive feedback mechanism to higher replication in BALB/c macrophages.

The DAPC analysis showed a clear grouping between the BALB/c and C57BL/6 peritoneal macrophages, for all strains showing again how different is the response to the *T. cruzi* infection depending on the mouse genetic background. Internalization phase showed the best separation between the different backgrounds, likely because in this phase we found bigger differences between an activation in the BALB/c and C57BL/6 infections. The higher levels of *Tnf* associated with the high parasite load may play a crucial role in the susceptibility of the BALB/c macrophages, despite being considered as early replicative cytokine (Munoz-Fernandez *et al.*, 1992) and suggest that parasite load is directly triggering of TNF.

Curiously, the analysis of correlations in the three phases showed much more negative correlations associated with the C57BL/6 than BALB/c macrophages. An explanation to these could be that a lack of down-regulation between the cytokines and enzymes in the BALB/c macrophages leads to higher parasite load. Our results showed that BALB/c macrophages were more susceptible to the infection with all the strains of *T. cruzi,* but this could be different in other type of cells as dendritic cells, natural killer, cardiomyocytes, etc...

We have previously described some correlation between cytokines and DTUs in patients, but this was only done in TcI and TcII and mixed infections. Thus any correlation with our *in vitro* data in macrophages is not guaranteed. Presumably, strain-specific recognition by other components of the immune system (Antibodies, B cells, or T cells), could lead to the differential responses observed in patients (Poveda *et al.*, 2014). Our studies in macrophages involving all the possible different strain of *T. cruzi* supports the convenience of further studies in patients to get relevant conclusions.

5.1 TLR2 PLAYS A CRUCIAL ROLE IN THE ENTRY OF ALL STRAINS OF *T. CRUZI* IN MACROPHAGES.

TLR2 plays a role both in controlling the entry of several pathogens as well as to determine the activation of the immune response in the host. In the case of T. cruzi it has been described that TLR2 is necessary for the endocytosis of Y strain parasites in macrophages (Maganto-Garcia et al., 2008).

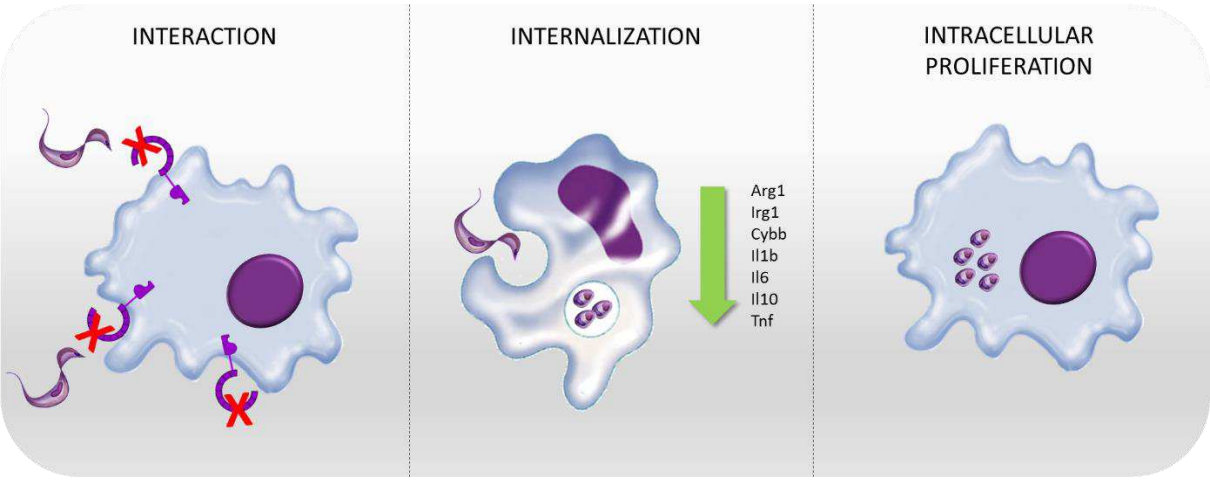

Figure 48. Effect of TLR2 deficiency in the macrophage model of infection with T. cruzi. *The figure shows that all strains of T. cruzi behaved similarly in Tlr2$^{-/-}$ macrophages: there was less parasite contact with macrophages during* ***interaction*** *phase, lower activation of the immunoregulatory genes during the* ***internalization*** *phase, and lower parasite loads at the* ***intracellular proliferation*** *phase compared to C57BL/6 macrophages.*

Our results, confirm the crucial role of this receptor in the entry of all different *T. cruzi* strains studied. A model of infection in *Tlr2*$^{-/-}$ macrophages was drawn according with our results. Figure 48, shows the putative role of TLR2 receptor during the different phases of *T. cruzi* infection in peritoneal macrophages. We found that the deficiency of *Tlr2*$^{-/-}$ in peritoneal macrophages inhibited the interaction of the different strains of *T. cruzi*. During the internalization a lower induction of the immunoregulatory genes associated with low parasite loads was found in the *Tlr2*$^{-/-}$macrophages comparing with the infected C57BL/6 macrophages. Finally, as a result of the low amounts of parasite able to infect the macrophages we found a lower parasite load in the intracellular proliferation phase.

The DAPC analysis demonstrated the clustering of the infections in *Tlr2*$^{-/-}$ macrophages with all strains of *T. cruzi* and with the respective non-infected controls (C57BL/6 and *Tlr2*$^{-/-}$) clustered together. Contrarily, infections in C57BL/6 macrophages grouped a part from the rest. This clearly corroborated the crucial role of TLR2 in the infection determined by their involvement in recognition.

However, once the binding an entry has taken place, the influence of TLR2 deficiency was variable among strains. Thus, despite 90% reduction in binding at 1 h.p.i. for Y and M6421 cl6 and 50% for VFRA cl1, the efficiency in the internalization for Y or the intracellular proliferation of VFRA cl1, results in similar parasite output in *Tlr2*$^{-/-}$ macrophages as compared to C57BL/6.

This indicates that differences in the amount of the expression of GILPs or other surface proteins of the parasite associated with TLRs or other receptors, may also contribute to binding to the host in later times. Thus, it has been reported that G, Y and Tulahuén strains contain ceramide, while CL Brener strain contains a mixture of alkylacylglycerol and dihydropceramide species in their surface, recognized by TLR2 and TLR4, respectively (Ropert *et al.*, 2002).

5.2 SLAMF1 ACTS AS A STRAIN-DEPENDENT SENSOR IN *T. CRUZI* INFECTION MEDIATED BY NOX2.

SLAMF1 is an important receptor in myeloid cells, controlling the entry and replication of different pathogens as measles virus and gram negative bacteria. Previously, our group described that SLAMF1 incremented susceptibility to infections with the Y strain both in vitro and in vivo (Calderón et al., 2012). We extended this study to different strains and found that the SLAMF1 receptor is important to control the T. cruzi infection in peritoneal macrophages, where the deficiency of this receptor resulted in lower parasite load in comparison with the BALB/c macrophages, as in the case of the Y strain, only for 5 out of 6 strains of T. cruzi, but not for VFRA cl1 strain.

According to our results we propose a model (Figure 49), where parasite load at the interaction phase in the Slamf1-/- macrophages was reduced compared to BALB/c macrophages which indicates that SLAMF1 is required for the entry of T. cruzi for Dm28c, Y, M6421 cl6 and Bug2148 cl1 strains of T. cruzi evaluated, but not for the VFRA cl1. At the internalization phase, the SLAMF1 receptor regulates the production of NOX and ROS in the phagosome that eliminate pathogens in the parasitophorous vacuole (C. Ma et al., 2012). We found higher levels of NOX2 gene and ROS in Slamf1-/- macrophages and lower parasite load infected with all strains, except for VFRA cl1, that showed the opposite, lower NOX2 and ROS levels and higher parasite load, demonstrating the effectiveness of NOX2 and ROS for parasite control.

This enhancement of ROS and NOX2 in the absence of SLAMF1 is somehow surprising since in bacterial infection SLAMF1 deficiency results in decreased NOX2 activity and ROS production (Berger et al., 2010; C. Ma et al., 2012).

It has been described that the SLAMF1 receptor plays the role of bacterial sensor, where SLAMF1 induces production of PI3P, which positively regulates the activity of the NOX2 enzyme and phagolysosomal maturation for the elimination of Gram negative, but no Gram positive, bacteria (Ma et al. 2012). In contrast, we found that the deficiency of SLAMF1 increased the amounts of

NOX2 and ROS expression in the parasitophorous vacuole the role of these molecules is controversial, some authors propose ROS as necessary for parasite replication while the others suggest an microbicidal role (Goes et al., 2016).We found an association between the parasite load and the expression of NOX2 and ROS, where the higher the parasite load the lower amounts of NOX2 and ROS. Thus, in our model SLAMF1 acts as a strain-dependent sensor in T. cruzi infection mediated by NOX2. The deficiency of SLAMF1 reduced parasite load in infections with Dm28c to Bug2148 cl1 strains, but increased with VFRA cl1 strain.

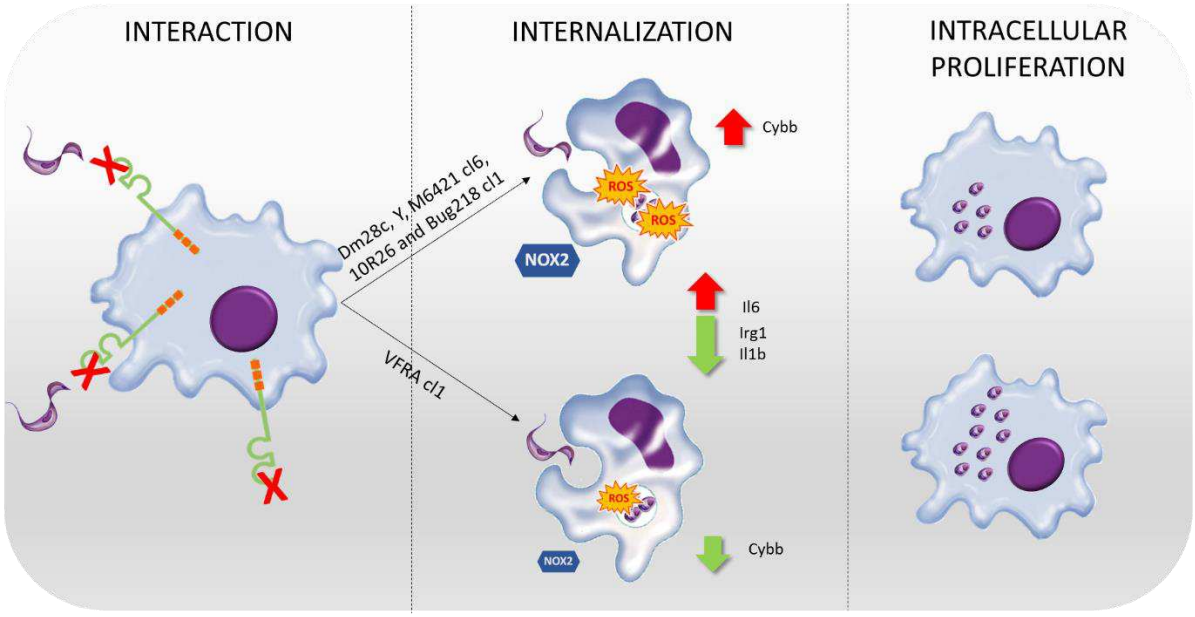

Figure 49. Effect of SLAMF1 deficiency in the macrophage model of infection with T. cruzi. *The figure shows that T. cruzi strains caused similar and different effects in Tlr2$^{-/-}$ compared to C57BL/6 macrophages. There was less parasite contact with macrophages during* ***interaction*** *phase in infections with all the strains. During the* ***internalization phase*** *there was higher expression of Il6 and lower expression of Il1b and Irg1 for all the strains; VFRA cl1 showed lower expression of Il10, Cybb (NOX2) and lower ROS production than other strains; Y strain showed lower expression of Arg1 and Il10 than other strains; and M6421 cl6 showed lower expression of Tnf than other strains. Finally, at the* ***intracellular proliferation phase*** *all the strains showed less parasite load compared to C57BL/6 macrophages, except VFRA cl1 strain.*

Preliminary studies from our laboratory suggest that the T. cruzi trans-sialidases are possible ligands of the SLAMF1 receptor. The importance of this molecule lies in that T. cruzi is unable to synthesize sialic acids de novo and needs to take from the host. Trans-sialidases are expressed in great amounts on the surface membrane of trypomastigotes and during the invasion in host cells and are necessary for successful infection (Frasch, 2000). Those trans-sialidase properties will confer to trans-sialidase-SLAMF1 interaction a prominent role in T.cruzi infection in myeloid cells since them all also expressed high levels of SLAMF1 on the surface (C. Ma et al., 2012). The relationship

between DTUs and trans-sialidases is still unclear, but evolutionary events did show differences in transialidase expression in different strains. The expression of this complex family of virulent surface molecules may be a key to better understand the mechanism of infection and its relationship with T. cruzi evolution. In our case it could explain why SLAMF1 receptor is acting as a pathogen sensor.

5.3 SLAMF1 ROLE *IN VIVO* INFECTION

The experimental mouse model of *T.cruzi* infection is thought to be very similar to human Chagas disease, at cellular, molecular and disease outcome level. However, reports show apparent contradictions depending on the mouse strains and *T.cruzi* used. We studied the susceptible BALB/c mouse with three different *T. cruzi* strains having different levels of infection and severity, trying to simulate the diverse possible outcomes or pathologies in humans. Our results show high mortality with the Y strain during the acute phase. For the other two strains Dm28c and VFRA cl1 the infection was less aggressive. However, we found relatively high parasitemia in BALB/c mice infected with the VFRA cl1 despite none of them died. Thus, we did not find clear association between the parasitemia and the severity of the disease, despite the previous report (Tarleton *et al.*, 1996). This relationship is likely true for the same strain (higher parasitemia-higher disease) but clearly not when comparing different strains.

In humans TcI presents a broad geographical distribution and has been associated with chronic cardiomyopathy. Even though we used mice with susceptible background (BALB/c) and the strain Dm28c a TcI presented the highest parasite load in peritoneal macrophage infections, the infection was the less virulent. In agreement with precious reports a 100% of the mice survived to the acute infection and we did not find parasites in blood, probably because of the use of a lower inoculum (2000 parasites/mouse) than the previously described where BALB/c mice infected with ≤ 5000 parasite/mouse which presented some parasite in blood (de Melo Medeiros *et al.*, 2010).
Previous results in the laboratory indicated that during *in vivo* infection with the Y strain, alterations in myeloid populations are progressively observed in bone marrow, then spleen and finally infiltrating cardiac tissue (Gonzalez, 2014). Thus, one could think that a good control of parasite replication in the spleen would lead to lower parasite loads in the other organs as we observed.

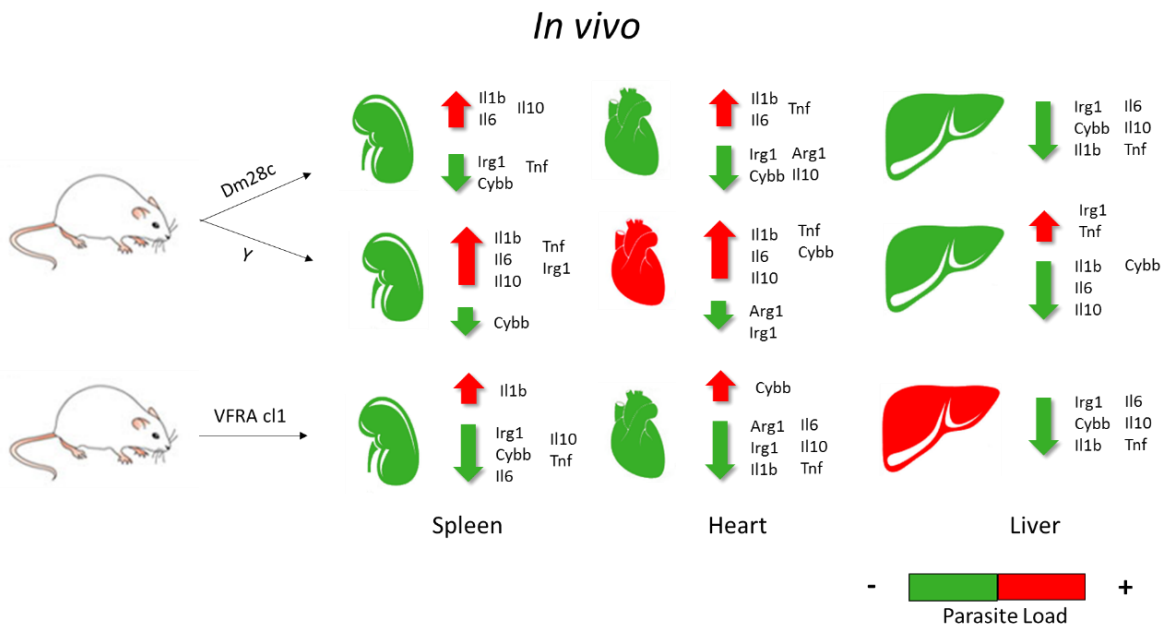

Figure 50. Effect of SLAMF1 deficiency in mice infection. *The figure shows a summary of gene expression of the immunoregulatory genes in spleen, heart and liver during acute phase (21 d.p.i.) in Slamf1$^{-/-}$ mice infected with the different strains of T. cruzi compared with BALB/c mice. Infections with the Dm28c and Y strains presented lower parasite load compared to BALB/c mice, in contrast the infection in Slamf1$^{-/-}$ infected with the VFRA cl1 presented higher parasite load compared with BALB/c.*

The lack of parasites in blood and the great ability of Dm28c to infect macrophages *in vitro*, plus the presence of low parasite load in the spleen and the liver, and even less in heart, suggests that *in vivo* others immune cells may control the infection. These possibility will be in agreement with the "Trojan horse" hypothesis (Calderón *et al.*, 2012; Messenger *et al.*, 2015). Alternatively, it is possible that Dm28c infects others cell types like cardiomyocytes and SLAMF1 deficiency in those cells may impair parasite replication in the heart.

Our results, in BALB/c mice infected with Dm28c strain showed a lower parasite load in Dm28c comparison with the mice infected with Y and VFRA cl1. The highest parasite load at 21 d.p.i. was found in the liver followed by the spleen and heart, with 5.25, 4.92 and 1.89 (pg *T. cruzi* DNA/ mg total DNA) X10^{6}, respectively. The higher presence in the spleen and liver, could indicate a tropism of this strain towards these organs. Previous studies with Dm28c failed to display inflammatory infiltrate and showed rare amastigote nests even after inoculating with ≤ 5000 parasite/mouse (Calvet *et al.*, 2004; de Melo Medeiros *et al.*, 2010), this is consistent with our results where we found very low parasite load in the heart. In the *Slamf1*$^{-/-}$ mice the parasite load was even lower than in the BALB/c mice having a reduction of 80.38% in the liver, 78.45% in the spleen and 17.98%

in the heart. The reduction of the parasite load in the *Slamf1*$^{-/-}$ mice suggest the importance of this receptor in the entry of the Dm28c in the host cells as shown in macrophages.

In fact, the spleen of mice infected with Dm28c strain showed higher expression of macrophage activation genes at 14 d.p.i. than with the other 2 strains, indicating that an early control of the infection results in a more efficient elimination of the parasite. This points out to an efficient immune response to Dm28c for control the infection in contrast to Y infection. The absence of SLAMF1 expression even increased gene expression indicating of better activation and further decreased parasite load, indicating a detrimental role of this receptor. We also found higher gene expression at 21 d.p.i. in *Slamf1*$^{-/-}$ than in BALB/c mice, although it was lower than at 14 d.p.i.

The lack of changes in the heart indicates that Dm28c strain has preferential tropism for spleen and liver tissues in this mouse model. The liver and the spleen play an important role in the elimination of the parasite or other pathogens. We conclude in base to our results that the more affected organ to the infection with the strain Dm28c during acute phase was the liver.

The increment of iNOS in spleen cells of the mice infected with the Y strain has been associated with damage in this organ due to toxicity of NO (Abrahamsohn and Coffman, 1995). The increment of the iNOS and higher levels in the expression of Th1 cytokines has been detected also in the liver of mice infected with the same strain (Novaes *et al.*, 2015). However, we could no detect iNOS protein in the spleen samples for any strain. However, higher amounts of NOX2 were found at 21 d.p.i. in both BALB/c and *Slamf1*$^{-/-}$, indicating a fast parasite elimination by the host. The amount of iNOS in the heart infected with Dm28c were similar for BALB/c and *Slamf1*$^{-/-}$ with low expression compared with the Y strain. Taking into account all the above, we suggest that, host elimination in liver and spleen is very likely the reason why Dm28c parasites do not get to infect the heart, rather than the differential tissue tropism hypothesized before.

Finally, the results obtained with the Dm28c strain illustrate the importance of preserving infection of heart tissue for a better outcome of the disease.

TcII strains are the most associated with cardiomyopathy in Latin America, where most of the human cases have been reported infected with this DTU. The Y strain is a TcII has been used in several immunological studies and is lethal in BALB/c mouse model even with low (50 parasites/mouse) doses (Sanoja *et al.*, 2013). Previous studies in infected *Slamf1*$^{-/-}$ with the Y strain demonstrated a complete resistance of them to the parasite in comparison with infected BALB/c

mice (Calderón *et al.*, 2012). In agreement with those, our results show a survival of a 30% and 100% in BALB/c and *Slamf1*$^{-/-}$ mice, respectively.

We found that BALB/c mice infected with Y strain at 21 d.p.i. presented higher parasite load in the heart (255.24 (pg *T. cruzi* DNA/ mg total DNA) X10^6), followed by the spleen (32.02 (pg *T. cruzi* DNA/ mg total DNA) X10^6) and liver (28.89 (pg *T. cruzi* DNA/ mg total DNA) X10^6). The *Slamf1*$^{-/-}$ mice infected with the strain Y presented also a reduction of the parasite load in all the organs. In the heart the parasite load was reduced in a 75.5%, in the spleen 46.78% and in the liver 70.7%. This indicates a high heart tropism of the Y strain.

Cardiac damage has been associated with the infection with the Y strain (Calderón *et al.*, 2012) which showed here the highest parasite load in comparison with the Dm28c and VFRA cl1 strains in this organ. An early induction (14 d.p.i.) of the immune response genes was observed in BALB/c that decreased in *Slamf1*$^{-/-}$ hearts of infected mice, except for *Irg1*, which presented higher levels in *Slamf1*$^{-/-}$. These results illustrate the importance of this gene not previously studied in the context of *T. cruzi* infection. Irg1 produces itaconic acid which was recently described as a marker of M1 macrophages with anti-mycobacterial activity (Jha *et al.*, 2016; Michelucci *et al.*, 2013). We found that itaconic acid has an inhibitory activity against all strains of *T. cruzi* with different IC_{50} according to their DTU classification, as it has been described for many other inhibitors (Aquilino *et al.*, 2012).

The high expression of iNOS and high parasite load in the hearts of BALB/c mice infected with Y strain may cause more damage and eventually the death of the animals by cardiac dysfunction. We found lower amounts of *Arg1* in the hearts of BALB/c than in *Slamf1*$^{-/-}$ mice, an enzyme that has been associated with mouse susceptibility to *T. cruzi* infection (Cuervo *et al.*, 2008). Higher amounts of this protein were found in the spleen of the BALB/c mice at 21 d.p.i. only when infected with the lethal Y strain. This confirms the presence of MDSC in Y strain and also could indicate that the highest levels of MDSC during *T. cruzi* infection are related to heart disease, since Dm28c or VFRA cl1 express Arg-1 in very low or undetectable levels. As in the macrophages higher levels of NOX2 in *Slamf1*$^{-/-}$ mice were associated with lower parasite load.

The differences observed with the Y strain in in vitro and in vivo models, which change from poorly infected macrophages to lethal infections in mice, demonstrates the use of different host cells in the dissemination of the parasite and a strain/DTU-specific recognition by the immune system (Poveda et al. 2014).

We have described previously that the Y strain is characterized by the presence of high numbers of MDSCs expressing iNOS, Arg-1 and COX-2 in heart tissue. Here we show that strains behave differently, being NOX2 at high levels as well as others enzymes characteristic of MDSC at lower levels for some strains.

As in the results obtained *In vitro* for the BALB/c and *Slamf1*$^{-/-}$ macrophages infected with the VFRA cl1 the deficiency of SLAMF1 receptor incremented the parasite load in the organs analyzed. At 21 d.p.i., the spleen of BALB/c mice presented the higher parasite load, followed by the heart and liver, with 29, 13.38 and 5.25 (pg *T. cruzi* DNA/ mg total DNA) X10^6. In contrast, the higher parasite load in *Slamf1*$^{-/-}$ was found in the spleen, followed by the liver and finally the heart. Also, we found an increment in the parasite load of the *Slamf1*$^{-/-}$ organs, 83.90% in the liver, 30.85% in the heart and 20.78% in the spleen.

The mice infected with the Y shows a similar to acute cardiomyopathy in humans, while VFRA cl1 is similar to chronic cardiomyopathy.

Taken together our results indicate an extreme variability of the immunopathological response to *T. cruzi* putting a word caution in reaching any conclusion in the mouse model based on a single mouse/parasite strain combination.

CONCLUSIONS

6 CONCLUSIONS

1. BALB/c are more susceptible to the *T. cruzi* infection than C57BL/6 macrophages with all the parasite strains studied.

2. *Trypanosoma cruzi* genetic variability greatly affected parasite replication in macrophages, being some parasite strains more infective than others.

3. TLR2 receptor is necessary for the entry of parasites of all *T. cruzi* strains studied and also affect different phases of macrophage *in vitro* infection, except for the Y strain in which intracellular proliferation was not affected by the TLR2 deficiency.

4. SLAMF1 acts as a strain-dependent sensor in *T. cruzi* macrophage *in vitro* infection, being parasite intracellular proliferation restricted by ROS production which was higher in *Slamf1*$^{-/-}$ than in BALB/c macrophages for all the strains, except after infection with the VFRA cl1 strain.

5. *In vivo,* the most infective strain in BALB/c mice was Y, followed by VFRA cl1 and finally Dm28c. Dm28c strain induced earlier activation of immune response in spleen of BALB/c mice that developed a milder infection without detectable parasitemia, presented less lower parasite load in heart tissue, and less MDSCs marker expression than mice infected with the other strains.

6. The *Slamf1*$^{-/-}$ mice showed lower parasite load than the BALB/c infected with Dm28c and Y strains in all the organs studied. In contrast, in VFRA cl1 infection the parasite load tended to be higher in *Slamf1*$^{-/-}$ than BALB/c in liver and heart. These results are in agreement with what we found *in vitro*, supporting the macrophage "Trojan Horse" model.

7. The *Slamf1*$^{-/-}$ mice are resistant to mortality induced by Y strain infection having less MDSC markers in the heart at 21 dpi.

8. There is an extreme variability in the immunopathological response depending on the mouse/parasite strain combination. Thus, conclusions based on experiments performed with single parasite/mouse strain combinations should be taken with caution.

9. Infectivity of the parasite strains *in vitro* and *in vivo* not always correlated indicating that other immune cells with different susceptibility to infection are controlling the outcome of the disease *in vivo*, which should be further studied.

10. *Irg1* expression and itaconic acid, an inhibitor of pathogen's isocitrate lyase, was detected in heart of mice infected with the Y strain. Itaconic acid inhibited the growth of several parasite strains of different DTUs *in vitro* indicating that parasite isocitrate lyase inhibitors could be useful for treatment of Chagas disease.

CONCLUSIONES

1. Los macrófagos BALB/c son más susceptibles a la infección que los C57BL/6 en todas las cepas de *T. cruzi* estudiadas

2. La variabilidad genética de *T. cruzi* afectó en gran medida la replicación del parásito, siendo unas cepas más infectivas que otras.

3. El receptor TLR2 es necesario para la entrada de parásitos de todas las cepas de *T. cruzi* estudiadas y afecta las distintas fases de la infección *in vitro* en macrófagos, a excepción de la cepa VFRA cl1 que no se vio afectada por la deficiencia en TLR2.

4. El receptor SLAMF1 se comporta como un sensor cepa-dependiente en la infección de macrófagos *in vitro*, estando la replicación intracelular restringida por la producción de ROS, que fue mayor en macrófagos *Slamf1*$^{-/-}$ que en BALB/c para todas las cepas de parásito, a excepción de la cepa VFRA cl1.

5. *In vivo*, la cepa Y fue la más infectiva, seguida de la cepa VFRA y finalmente la Dm28c. Ésta última indujo una activación de la respuesta inmunológica temprana en el bazo de ratones BALB/c, que desarrollaron una infección más leve sin parasitemia detectable, más baja carga parasitaria y menos presencia de MDSCs en corazón que las demás cepas estudiadas.

6. Los ratones *Slamf1*$^{-/-}$ mostraron menor carga parasitaria que los BALB/c infectados con las cepas DM28c e Y en todos los órganos estudiados. Por el contrario, con la cepa VFRA cl1 la carga parasitaria tendió a ser mayor en hígado y corazón de ratones *Slamf1*$^{-/-}$ que en BALB/c, apoyando el modelo del macrófago como “Caballo de Troya”.

7. Los ratones *Slamf1*$^{-/-}$ son resistentes a la mortalidad inducida por la infección con la cepa Y presentando una expresión de marcadores de MDSCs menor en corazón a 21 d.p.i.

8. Existe una gran variabilidad en la respuesta inmunopatogenica dependiendo de la combinación parasito/ratón utilizada. Por lo tanto, las conclusiones basadas en estudios utilizando combinaciones únicas de parasito/ratón deben tomarse con cautela.

9. La infectividad de las cepas *in vitro* e *in vivo* no siempre correlacionó indicando que otras células inmunes con distinta susceptibilidad a la infección están controlando el desarrollo de la enfermedad *in vivo*, aspecto que merece estudiarse en el futuro.

10. La expresión de *Irg1* y el ácido itacónico, un inhibidor de la isocitrato liasa de patógenos, fueron detectados en el corazón de ratones BALB/c infectados con la cepa Y. El ácido itacónico inhibió el crecimiento de muchas cepas de distintas DTUs *in vitro*, indicando que inhibidores de la isocitrato liasa podrían ser útiles para el tratamiento de la enfermedad de Chagas.

REFERENCES

7 REFERENCE

Abrahamsohn, I. A. and Coffman, R. L. (1995), 'Cytokine and nitric oxide regulation of the immunosuppression in Trypanosoma cruzi infection.', *Journal of immunology (Baltimore, Md. : 1950)*. Journal Article, Research Support, Non-U.S. Gov't. United States, **155**(8): 3955–3963.

Akira, S. and Takeda, K. (2004), 'Toll-like receptor signalling', *Nature Reviews Immunology*, **4**(7): 499–511. http://www.nature.com/doifinder/10.1038/nri1391.

Aquilino, C., Gonzalez Rubio, M. L., Seco, E. M., Escudero, L., Corvo, L., Soto, M., Fresno, M., Malpartida, F. and Bonay, P. (2012), 'Differential Trypanocidal Activity of Novel Macrolide Antibiotics; Correlation to Genetic Lineage', *PLOS ONE*. JOUR. Public Library of Science, **7**(7): e40901. http://dx.doi.org/10.1371%2Fjournal.pone.0040901.

Arantes, R. M. E., Marche, H. H. F., Bahia, M. T., Cunha, F. Q., Rossi, M. a and Silva, J. S. (2004), 'Interferon-gamma-induced nitric oxide causes intrinsic intestinal denervation in Trypanosoma cruzi-infected mice.', *The American journal of pathology*, **164**(4): 1361–1368.

Bartholomeu, D. C., Ropert, C., Melo, M. B., Parroche, P., Junqueira, C. F., Teixeira, S. M. R., *et al.* (2008), 'Recruitment and endo-lysosomal activation of TLR9 in dendritic cells infected with Trypanosoma cruzi.', *The Journal of Immunology*, **181**(2): 1333–1344. http://eutils.ncbi.nlm.nih.gov/entrez/eutils/elink.fcgi?dbfrom=pubmed&id=18606688&retmode=ref&cmd=prlinks\npapers2://publication/uuid/37166399-D5D1-4D61-9ADF-04678C06A2A1.

Berger, S. B., Romero, X., Ma, C., Wang, G., Faubion, W. A., Liao, G., *et al.* (2010), 'SLAM is a microbial sensor that regulates bacterial phagosome functions in macrophages', *Nature Immunology*. JOUR. , **11**(10): 920–927. http://www.ncbi.nlm.nih.gov/pmc/articles/PMC3338319/.

Brener, Z. (1971), 'Life cycle of Trypanosoma cruzi.', *Revista do Instituto de Medicina Tropical de Sao Paulo*. Journal Article. BRAZIL, **13**(3): 171–178.

Brener, Z. (1972), 'A new aspect of Trypanosoma cruzi life-cycle in the invertebrate host.', *The Journal of protozoology*. Journal Article. United States, **19**(1): 23–27.

Burgos, J. M., Altcheh, J., Bisio, M., Duffy, T., Valadares, H. M. S., Seidenstein, M. E., *et al.* (2007), 'Direct molecular profiling of minicircle signatures and lineages of Trypanosoma cruzi bloodstream populations causing congenital Chagas disease', *International Journal for Parasitology*. JOUR. , **37**(12): 1319–1327. http://www.sciencedirect.com/science/article/pii/S0020751907001385.

Caetano, B. C., Carmo, B. B., Melo, M. B., Cerny, A., dos Santos, S. L., Bartholomeu, D. C., Golenbock, D. T. and Gazzinelli, R. T. (2011), 'Requirement of UNC93B1 reveals a critical role for TLR7 in host resistance to primary infection with Trypanosoma cruzi.', *Journal of immunology (Baltimore, Md. : 1950)*, **187**(4): 1903–11. http://www.pubmedcentral.nih.gov/articlerender.fcgi?artid=3150366&tool=pmcentrez&rendertype=abstract.

Calabrese, K., Lagrange, P. H. and da Costa, S. C. (1996), 'Chagas' disease: enhancement of systemic inflammatory reaction in cyclophosphamide treated mice.', *International journal of immunopharmacology*. Comparative Study, Journal Article, Research Support, Non-U.S. Gov't. ENGLAND, **18**(8–9): 505–514.

Calderón, J., Maganto-Garcia, E., Punzón, C., Carrión, J., Terhorst, C. and Fresno, M. (2012), 'The receptor Slamf1 on the surface of myeloid lineage cells controls susceptibility to infection by Trypanosoma cruzi', *PLoS Pathogens*, **8**(7): 38.

Calvet, C. M., Meuser, M., Almeida, D., Meirelles, M. N. L. and Pereira, M. C. S. (2004), 'Trypanosoma

cruzi–cardiomyocyte interaction: role of fibronectin in the recognition process and extracellular matrix expression in vitro and in vivo', *Experimental Parasitology*. JOUR. , **107**(1–2): 20–30. http://www.sciencedirect.com/science/article/pii/S0014489404000645.

Campos, M. A., Almeida, I. C., Takeuchi, O., Akira, S., Valente, E. P., Procopio, D. O., *et al.* (2001), 'Activation of Toll-like receptor-2 by glycosylphosphatidylinositol anchors from a protozoan parasite', *J Immunol*, **167**(1): 416–423. http://www.ncbi.nlm.nih.gov/entrez/query.fcgi?cmd=Retrieve&db=PubMed&dopt=Citation&list_uids=11418678\nhttp://www.jimmunol.org/cgi/reprint/167/1/416.pdf.

Caradonna, K. L. and Burleigh, B. A. (2011), *Mechanisms of host cell invasion by trypanosoma cruzi*, *Advances in Parasitology*. Elsevier Ltd. http://dx.doi.org/10.1016/B978-0-12-385895-5.00002-5.

Cardoso, M. S., Reis-Cunha, J. L. and Bartholomeu, D. C. (2016), 'Evasion of the immune response by trypanosoma cruzi during acute infection', *Frontiers in Immunology*, **6**(JAN): 1–15.

Carrera-Silva, E. A., Cano, R. C., Guinazu, N., Aoki, M. P., Pellegrini, A. and Gea, S. (2008), 'TLR2, TLR4 and TLR9 are differentially modulated in liver lethally injured from BALB/c and C57BL/6 mice during Trypanosoma cruzi acute infection.', *Molecular immunology*. Comparative Study, Journal Article, Research Support, Non-U.S. Gov't. England, **45**(13): 3580–3588.

Charles A. Janeway Jr, Paul travers, M. W. (2011), *Janeway's Immunobiology*.

Cordes, T., Michelucci, A. and Hiller, K. (2015), 'Itaconic Acid: The Surprising Role of an Industrial Compound as a Mammalian Antimicrobial Metabolite.', *Annual review of nutrition*. Journal Article, Research Support, Non-U.S. Gov't, Review. United States, **35**: 451–473.

Costales, J. and Rowland, E. C. (2007), 'a Role for Protease Activity and Host-Cell Permeability During the Process of Trypanosoma Cruzi Egress From Infected Cells a Role for Protease Activity and Host-Cell Permeability During the Process of Trypanosoma Cruzi Egress From Infected Cells', **93**(6): 1350–1359.

Coura, J. R., Junqueira, A. C. V, Fernandes, O., Valente, S. A. S. and Miles, M. A. (2002), 'Emerging Chagas disease in Amazonian Brazil', *Trends in Parasitology*, **18**(4): 171–176.

Cuervo, H., Pineda, M. A., Aoki, M. P., Gea, S., Fresno, M. and Gironès, N. (2008), 'Inducible Nitric Oxide Synthase and Arginase Expression in Heart Tissue during Acute *Trypanosoma cruzi* Infection in Mice: Arginase I Is Expressed in Infiltrating CD68 $^{+}$ Macrophages', *The Journal of Infectious Diseases*, **197**(12): 1772–1782. http://jid.oxfordjournals.org/lookup/doi/10.1086/529527.

Cunha-Neto, E., Dzau, V. J., Allen, P. D., Stamatiou, D., Benvenutti, L., Higuchi, M. L., *et al.* (2005), 'Cardiac gene expression profiling provides evidence for cytokinopathy as a molecular mechanism in Chagas' disease cardiomyopathy.', *The American journal of pathology*. American Society for Investigative Pathology, **167**(2): 305–313. http://dx.doi.org/10.1016/S0002-9440(10)62976-8.

de Meis, J., Morrot, A., Farias-de-Oliveira, D. A., Villa-Verde, D. M. S. and Savino, W. (2009), 'Differential Regional Immune Response in Chagas Disease', *PLOS Neglected Tropical Diseases*. JOUR. Public Library of Science, **3**(7): e417. http://dx.doi.org/10.1371%2Fjournal.pntd.0000417.

de Melo Medeiros, M., Araújo-Jorge, T. C., Batista, W. S., da Silva, T. M. O. A. and de Souza, A. P. (2010), 'Trypanosoma cruzi infection: do distinct populations cause intestinal motility alteration?', *Parasitology Research*. JOUR. , **107**(1): 239–242. http://dx.doi.org/10.1007/s00436-010-1871-5.

De Souza, W., De Carvalho, T. M. U. and Barrias, E. S. (2010), 'Review on Trypanosoma cruzi: Host cell interaction', *International Journal of Cell Biology*, **2010**.

Dhiman, M. and Garg, N. J. (2014), 'P47(phox−/−) Mice Are Compromised in Expansion and

Activation of CD8(+) T Cells and Susceptible to Trypanosoma cruzi Infection', *PLoS Pathogens*. JOUR. San Francisco, USA: Public Library of Science, **10**(12): e1004516. http://www.ncbi.nlm.nih.gov/pmc/articles/PMC4256457/.

Diosque, P., Barnabé, C., Padilla, A. M., Marco, J. D., Cardozo, R. M., Cimino, R. O., Nasser, J. R., Tibayrenc, M. and Basombrío, M. A. (2003), 'Multilocus enzyme electrophoresis analysis of Trypanosoma cruzi isolates from a geographically restricted endemic area for Chagas' disease in Argentina', *International Journal for Parasitology*, **33**(10): 997–1003.

Dutra, W. O., Menezes, C. A. S., Magalhães, L. M. D. and Gollob, K. J. (2014), 'Immunoregulatory networks in human Chagas disease', *Parasite immunology*. JOUR. , **36**(8): 377–387. http://www.ncbi.nlm.nih.gov/pmc/articles/PMC4143493/.

Frasch, A. C. (2000), 'Functional diversity in the trans-sialidase and mucin families in Trypanosoma cruzi.', *Parasitology today (Personal ed.)*. Journal Article, Research Support, Non-U.S. Gov't, Review. England, **16**(7): 282–286.

Gavrilescu, L. C. and Denkers, E. Y. (2003), 'Apoptosis and the Balance of Homeostatic and Pathologic Responses to Protozoan Infection', *Infection and Immunity*, **71**(11): 6109–6115.

Giordano, R., Fouts, D. L., Tewari, D., Colli, W., Manning, J. E. and Alves, M. J. (1999), 'Cloning of a surface membrane glycoprotein specific for the infective form of Trypanosoma cruzi having adhesive properties to laminin.', *The Journal of biological chemistry*. Journal Article, Research Support, Non-U.S. Gov't, Research Support, U.S. Gov't, P.H.S. UNITED STATES, **274**(6): 3461–3468.

Gironès, N., Carbajosa, S., Guerrero, N. A., Poveda, C., Chillón-Marinas, C. and Fresno, M. (2014), 'Global Metabolomic Profiling of Acute Myocarditis Caused by Trypanosoma cruzi Infection', *PLOS Neglected Tropical Diseases*. JOUR. Public Library of Science, **8**(11): e3337. http://dx.doi.org/10.1371%2Fjournal.pntd.0003337.

Goes, G. R., Rocha, P. S., Diniz, A. R. S., Aguiar, P. H. N., Machado, C. R. and Vieira, L. Q. (2016), 'Trypanosoma cruzi Needs a Signal Provided by Reactive Oxygen Species to Infect Macrophages', *PLoS Neglected Tropical Diseases*, **10**(4): 1–25.

Goni, O., Alcaide, P. and Fresno, M. (2002), 'Immunosuppression during acute Trypanosoma cruzi infection: involvement of Ly6G (Gr1(+))CD11b(+)immature myeloid suppressor cells.', *International immunology*. Journal Article, Research Support, Non-U.S. Gov't. England, **14**(10): 1125–1134.

Gonzalez, S. C. (2014), *Alteraciones en la hematopoyeis y el metabolismo de L-arginina durante la infeccion aguda experimental por Trypanosoma cruzi*.

Guerrero, N. A., Camacho, M., Vila, L., Íñiguez, M. A., Chillón-Marinas, C., Cuervo, H., Poveda, C., Fresno, M. and Gironès, N. (2015), 'Cyclooxygenase-2 and Prostaglandin E2 Signaling through Prostaglandin Receptor EP-2 Favor the Development of Myocarditis during Acute Trypanosoma cruzi Infection', *PLOS Neglected Tropical Diseases*. JOUR. Public Library of Science, **9**(8): e0004025. http://dx.doi.org/10.1371%2Fjournal.pntd.0004025.

Gұhl, F., Jaramillo, C., Vallejo, G. A., Yockteng, R., CÁRDENAS-ARROYO, F., Fornaciari, G., Arriaza, B. and Aufderheide, A. C. (1999), 'Isolation of Trypanosoma cruzi DNA in 4,000-year-old mummified human tissue from northern Chile', *American Journal of Physical Anthropology*. JOUR. Wiley Online Library, **108**(4): 401–407. http://dx.doi.org/10.1002/(SICI)1096-8644(199904)108:4<401::AID-AJPA2>3.0.CO.

Gutierrez, F. R. S., Guedes, P. M. M., Gazzinelli, R. T. and Silva, J. S. (2009), 'The role of parasite persistence in pathogenesis of Chagas heart disease.', *Parasite immunology*. Journal Article, Research Support, Non-U.S. Gov't, Review. England, **31**(11): 673–685.

Hideko Tatakihara, V. L., Cecchini, R., Borges, C. L., Malvezi, A. D., Graça-De Souza, V. K., Yamada-Ogatta, S. F., Rizzo, L. V. and Pinge-Filho, P. (2008), 'Effects of cyclooxygenase inhibitors on

parasite burden, anemia and oxidative stress in murine Trypanosoma cruzi infection', *FEMS Immunology and Medical Microbiology*, **52**(1): 47–58.

Jha, A. K., Huang, S. C.-C., Sergushichev, A., Lampropoulou, V., Ivanova, Y., Loginicheva, E., *et al.* (2016), 'Network Integration of Parallel Metabolic and Transcriptional Data Reveals Metabolic Modules that Regulate Macrophage Polarization', *Immunity*. JOUR. Elsevier, **42**(3): 419–430. http://dx.doi.org/10.1016/j.immuni.2015.02.005.

Kierszenbaum, F., de Diego, J. L., Fresno, M. and Sztein, M. B. (1999), 'Inhibitory effects of the Trypanosoma cruzi membrane glycoprotein AGC10 on the expression of IL-2 receptor chains and secretion of cytokines by subpopulations of activated human T lymphocytes.', *European journal of immunology*. Journal Article, Research Support, Non-U.S. Gov't, Research Support, U.S. Gov't, P.H.S. Germany, **29**(5): 1684–1691.

Lewis, M. D., Fortes Francisco, A., Taylor, M. C., Burrell-Saward, H., Mclatchie, A. P., Miles, M. A. and Kelly, J. M. (2014), 'Bioluminescence imaging of chronic Trypanosoma cruzi infections reveals tissue-specific parasite dynamics and heart disease in the absence of locally persistent infection', *Cellular Microbiology*, **16**(9): 1285–1300.

Li, Y., Shah-Simpson, S., Okrah, K., Belew, A. T., Choi, J., Caradonna, K. L., *et al.* (2016), 'Transcriptome Remodeling in Trypanosoma cruzi and Human Cells during Intracellular Infection', *PLoS Pathogens*, **12**(4): 1–30.

Loeuillet, C., Bañuls, A.-L. and Hide, M. (2016), 'Study of Leishmania pathogenesis in mice: experimental considerations.', *Parasites & vectors*. Parasites & Vectors, **9**(1): 144. http://parasitesandvectors.biomedcentral.com/articles/10.1186/s13071-016-1413-9.

Ma, C. S. and Deenick, E. K. (2011), 'The role of SAP and SLAM family molecules in the humoral immune response', *Annals of the New York Academy of Sciences*, **1217**(1): 32–44.

Ma, C., Wang, N., Detre, C., Wang, G., O'Keeffe, M. and Terhorst, C. (2012), 'Receptor signaling lymphocyte-activation molecule family 1 (Slamf1) regulates membrane fusion and NADPH oxidase 2 (NOX2) activity by recruiting a Beclin-1/Vps34/ultraviolet radiation resistance-associated gene (UVRAG) complex', *Journal of Biological Chemistry*, **287**(22): 18359–18365.

Machado, F. S., Dutra, W. O., Esper, L., Gollob, K., Teixeira, M. M., Factor, S. M., *et al.* (2012), 'Current Understanding of Immunity to Trypanosoma cruzi Infection and Pathogenesis of Chagas Disease', *Seminars in immunopathology*. JOUR. , **34**(6): 753–770. http://www.ncbi.nlm.nih.gov/pmc/articles/PMC3498515/.

Machado, F. S., Souto, J. T., Rossi, M. A., Esper, L., Tanowitz, H. B., Aliberti, J. and Silva, J. S. (2008), 'Nitric Oxide Synthase-2 modulates chemokine production by Trypanosoma cruzi-infected cardiac myocytes', *Microbes and infection / Institut Pasteur*. JOUR. , **10**(14–15): 1558–1566. http://www.ncbi.nlm.nih.gov/pmc/articles/PMC2643379/.

Maganto-Garcia, E., Punzon, C., Terhorst, C., Fresno, M., Israel, B. and Medical, D. (2008), 'HHS Public Access', *Traffic*, **9**(8): 1299–1315.

Marcili, A., Lima, L., Valente, V. C., Valente, S. A., Batista, J. S., Junqueira, A. C. V, *et al.* (2009), 'Comparative phylogeography of Trypanosoma cruzi TCIIc: New hosts, association with terrestrial ecotopes, and spatial clustering', *Infection, Genetics and Evolution*, **9**(6): 1265–1274.

Marin-Neto, J. A. and Rassi, A. J. (2009), 'Update on Chagas heart disease on the first centenary of its discovery.', *Revista espanola de cardiologia*. Comment, Editorial. Spain, 1211–1216.

Martinez, F. O. and Gordon, S. (2014), 'The M1 and M2 paradigm of macrophage activation: time for reassessment', *F1000Prime Reports*. JOUR. Faculty of 1000 Ltd, **6**: 13. http://www.ncbi.nlm.nih.gov/pmc/articles/PMC3944738/.

Messenger, L. a, Miles, M. a and Bern, C. (2015), 'Between a bug and a hard place: Trypanosoma cruzi genetic diversity and the clinical outcomes of Chagas disease.', *Expert review of anti-infective therapy*. Informa UK, Ltd., **13**(8): 995–1029.

http://www.pubmedcentral.nih.gov/articlerender.fcgi?artid=4784490&tool=pmcentrez&rendertype=abstract.

Michelucci, A., Cordes, T., Ghelfi, J., Pailot, A., Reiling, N., Goldmann, O., *et al.* (2013), 'Immune-responsive gene 1 protein links metabolism to immunity by catalyzing itaconic acid production.', *Proceedings of the National Academy of Sciences of the United States of America*, **110**(19): 7820–5. http://www.pubmedcentral.nih.gov/articlerender.fcgi?artid=3651434&tool=pmcentrez&rendertype=abstract\nhttp://www.ncbi.nlm.nih.gov/pubmed/23610393\nhttp://www.pubmedcentral.nih.gov/articlerender.fcgi?artid=PMC3651434.

Mukherjee, S., Machado, F. S., Huang, H., Oz, H. S., Jelicks, L. A., Prado, C. M., *et al.* (2011), 'Aspirin Treatment of Mice Infected with Trypanosoma cruzi and Implications for the Pathogenesis of Chagas Disease', *PLOS ONE*. JOUR. Public Library of Science, **6**(2): e16959. http://dx.doi.org/10.1371%2Fjournal.pone.0016959.

Munoz-Fernandez, M. A., Fernandez, M. A. and Fresno, M. (1992), 'Synergism between tumor necrosis factor-alpha and interferon-gamma on macrophage activation for the killing of intracellular Trypanosoma cruzi through a nitric oxide-dependent mechanism.', *European journal of immunology*. Journal Article, Research Support, Non-U.S. Gov't. Germany, **22**(2): 301–307.

Novaes, R. D., Santos, E. C., Cupertino, M. C., Bastos, D. S. S., Oliveira, J. M., Carvalho, T. V, Neves, M. M., Oliveira, L. L. and Talvani, A. (2015), 'Trypanosoma cruzi infection and benznidazole therapy independently stimulate oxidative status and structural pathological remodeling of the liver tissue in mice', *Parasitology Research*. JOUR. , **114**(8): 2873–2881. http://dx.doi.org/10.1007/s00436-015-4488-x.

Oliveira, A.-C., de Alencar, B. C., Tzelepis, F., Klezewsky, W., da Silva, R. N., Neves, F. S., *et al.* (2010), 'Impaired innate immunity in Tlr4(-/-) mice but preserved CD8+ T cell responses against Trypanosoma cruzi in Tlr4-, Tlr2-, Tlr9- or Myd88-deficient mice.', *PLoS pathogens*, **6**(4): e1000870. http://journals.plos.org/plospathogens/article?id=10.1371/journal.ppat.1000870.

Parker, E. R. and Sethi, A. (2011), 'Chagas Disease: Coming to a Place Near You', *Dermatologic Clinics*. JOUR. , **29**(1): 53–62. http://www.sciencedirect.com/science/article/pii/S0733863510001361.

Pérez-Ayala, A., Pérez-Molina, J. A., Norman, F., Navarro, M., Monge-Maillo, B., Díaz-Menéndez, M., *et al.* (2011), 'Chagas disease in Latin American migrants: A Spanish challenge', *Clinical Microbiology and Infection*, **17**(7): 1108–1113.

Piacenza, L., Peluffo, G., Alvarez, M. N., Martínez, A. and Radi, R. (2012), 'Antioxidant Enzymes As Virulence Factors in Chagas Disease', *Antioxidants & Redox Signaling*, **19**(7): 120521095928000.

Pineda, M. A., Corvo, L., Soto, M., Fresno, M. and Bonay, P. (2015), 'Interactions of human galectins with Trypanosoma cruzi: binding profile correlate with genetic clustering of lineages.', *Glycobiology*. Journal Article, Research Support, Non-U.S. Gov't. England, **25**(2): 197–210.

Pinto Dias, J. C. (2013), 'Human chagas disease and migration in the context of globalization: Some particular aspects', *Journal of Tropical Medicine*, **2013**.

Poveda, C., Fresno, M., Gironès, N., Martins-Filho, O. A., Ramírez, J. D., Santi-Rocca, J., *et al.* (2014), 'Cytokine profiling in chagas disease: Towards understanding the association with infecting Trypanosoma cruzi discrete typing units (A benefit trial sub-study)', *PLoS ONE*, **9**(3): 1–8.

Prata, A. (2001), 'Clinical and epidemiological aspects of Chagas disease.', *The Lancet. Infectious diseases*, **1**(2): 92–100. http://www.sciencedirect.com/science/article/pii/S1473309901000652.

Rabhi, I., Rabhi, S., Ben-Othman, R., Aniba, M. R., Trentin, B., Piquemal, D., Regnault, B. and Guizani-

Tabbane, L. (2013), 'Comparative analysis of resistant and susceptible macrophage gene expression response to Leishmania majorparasite', *BMC Genomics*. article. , **14**(1): 723. http://dx.doi.org/10.1186/1471-2164-14-723.

Ramírez, J. D., Montilla, M., Cucunubá, Z. M., Floréz, A. C., Zambrano, P. and Guhl, F. (2013), 'Molecular Epidemiology of Human Oral Chagas Disease Outbreaks in Colombia', *PLoS Neglected Tropical Diseases*, **7**(2): 1–7.

Rassi Jr., A., Rassi, A. and Marcondes de Rezende, J. (2012), 'American Trypanosomiasis (Chagas Disease)', *Infectious Disease Clinics of North America*. JOUR. , **26**(2): 275–291. http://www.sciencedirect.com/science/article/pii/S0891552012000116.

Rassi Jr, A., Rassi, A. and Marin-Neto, J. A. (2010), 'Chagas disease', *The Lancet*. JOUR. , **375**(9723): 1388–1402. http://www.sciencedirect.com/science/article/pii/S014067361060061X.

Rodriguez, H. O., Guerrero, N. A., Fortes, A., Santi-Rocca, J., Gironès, N. and Fresno, M. (2014), 'Trypanosoma cruzi strains cause different myocarditis patterns in infected mice', *Acta Tropica*. Elsevier B.V., **139**: 57–66. http://dx.doi.org/10.1016/j.actatropica.2014.07.005.

Roggero, E., Perez, A., Tamae-Kakazu, M., Piazzon, I., Nepomnaschy, I., Wietzerbin, J., Serra, E., Srevelli, S. and Obottasso, O. (2002), 'Differential susceptibility to acute Trypanosoma cruzi infection in BALB/c and C57BL/6 mice is not associated with a distinct parasite load but cytokine abnormalities', *Clinical and Experimental Immunology*, **128**(3): 421–428.

Ropert, C., Ferreira, L. R. P., Campos, M. A. S., Procópio, D. O., Travassos, L. R., Ferguson, M. A. J., *et al.* (2002), 'Macrophage signaling by glycosylphosphatidylinositol-anchored mucin-like glycoproteins derived from Trypanosoma cruzi trypomastigotes', *Microbes and Infection*, **4**(9): 1015–1025.

Sanjabi, S., Zenewicz, L. A., Kamanaka, M. and Flavell, R. A. (2009), 'Anti- and Pro-inflammatory Roles of TGF-β, IL-10, and IL-22 In Immunity and Autoimmunity', *Current opinion in pharmacology*. JOUR. , **9**(4): 447–453. http://www.ncbi.nlm.nih.gov/pmc/articles/PMC2755239/.

Sanoja, C., Carbajosa, S., Fresno, M. and Gironès, N. (2013), 'Analysis of the Dynamics of Infiltrating CD4+ T Cell Subsets in the Heart during Experimental Trypanosoma cruzi Infection', *PLoS ONE*, **8**(6).

Silva, J. S., Aliberti, J. C., Martins, G. A., Souza, M. A., Souto, J. T. and Padua, M. A. (1998), 'The role of IL-12 in experimental Trypanosoma cruzi infection.', *Brazilian journal of medical and biological research = Revista brasileira de pesquisas medicas e biologicas*. Journal Article, Research Support, Non-U.S. Gov't. Brazil, **31**(1): 111–115.

Sintes, J. and Engel, P. (2011), 'SLAM (CD150) is a multitasking immunoreceptor: from cosignalling to bacterial recognition', *Immunology and Cell Biology*. Nature Publishing Group, **89**(2): 161–163. http://dx.doi.org/10.1038/icb.2010.145\n<Go to ISI>://000287445400001.

Takeda, K. and Akira, S. (2005), 'Toll-like receptors in innate immunity', *International Immunology*, **17**(1): 1–14.

Tallam, A., Perumal, T. M., Antony, P. M., J??ger, C., Fritz, J. V., Vallar, L., Balling, R., Del Sol, A. and Michelucci, A. (2016), 'Gene Regulatory Network Inference of Immunoresponsive Gene 1 (IRG1) Identifies Interferon Regulatory Factor 1 (IRF1) as Its Transcriptional Regulator in Mammalian Macrophages', *PLoS ONE*, **11**(2): 1–28.

Tarleton, R. L., Grusby, M. J., Postan, M. and Glimcher, L. H. (1996), 'Trypanosoma cruzi infection in MHC-deficient mice: further evidence for the role of both class I- and class II-restricted T cells in immune resistance and disease.', *International immunology*. Journal Article, Research Support, Non-U.S. Gov't, Research Support, U.S. Gov't, P.H.S. ENGLAND, **8**(1): 13–22.

Teixeira, M. M. and Yoshida, N. (1986), 'Stage-specific surface antigens of metacyclic trypomastigotes of Trypanosoma cruzi identified by monoclonal antibodies.', *Molecular and biochemical parasitology*. Journal Article, Research Support, Non-U.S. Gov't. NETHERLANDS,

18(3): 271–282.
Van Driel, B. J., Liao, G., Engel, P. and Terhorst, C. (2016), 'Responses to microbial challenges by SLAMF receptors', *Frontiers in Immunology*, **7**(JAN): 1–14.
Westenberger, S. J., Cerqueira, G. C., El-Sayed, N. M., Zingales, B., Campbell, D. a and Sturm, N. R. (2006), 'Trypanosoma cruzi mitochondrial maxicircles display species- and strain-specific variation and a conserved element in the non-coding region.', *BMC genomics*, **7**: 60. http://www.pubmedcentral.nih.gov/articlerender.fcgi?artid=1559615&tool=pmcentrez&rendertype=abstract.
World Health Organization (2015), 'Chagas disease in Latin America: an epidemiological update based on 2010 estimates', *Weekly Epidemiological Record*, (6): 33–44.
Zafra, G., Mantilla, J. C., Valadares, H. M., Macedo, A. M. and González, C. I. (2008), 'Evidence of Trypanosoma cruzi II infection in Colombian chagasic patients', *Parasitology Research*. JOUR. , **103**(3): 731–734. http://dx.doi.org/10.1007/s00436-008-1034-0.
Zanluqui, N. G. (2015), 'Macrophage Polarization in Chagas Disease', *Journal of Clinical and Cellular Immunology*, **6**(2): 1–6. http://www.omicsonline.org/open-access/macrophage-polarization-in-chagas-disease-2155-9899-1000317.php?aid=51835.
Zhao, X., Kumar, P., Shah-Simpson, S., Caradonna, K. L., Galjart, N., Teygong, C., Blader, I., Wittmann, T. and Burleigh, B. A. (2013), 'Host microtubule plus-end binding protein CLASP1 influences sequential steps in the Trypanosoma cruzi infection process', *Cellular Microbiology*, **15**(4): 571–584.
Zingales, B., Andrade, S. G., Briones, M. R. S., Campbell, D. A., Chiari, E., Fernandes, O., *et al.* (2009), 'A new consensus for Trypanosoma cruzi intraspecific nomenclature: Second revision meeting recommends TcI to TcVI', *Memorias do Instituto Oswaldo Cruz*, **104**(7): 1051–1054.
Zingales, B., Miles, M. A., Campbell, D. A., Tibayrenc, M., Macedo, A. M., Teixeira, M. M. G., *et al.* (2012), 'The revised Trypanosoma cruzi subspecific nomenclature: Rationale, epidemiological relevance and research applications', *Infection, Genetics and Evolution*. Elsevier B.V., **12**(2): 240–253. http://dx.doi.org/10.1016/j.meegid.2011.12.009.

APPENDIX 1

Figures and Tables

8 APPENDIX 1

8.1 FIGURES

8.1.1 Control ΔCT Values

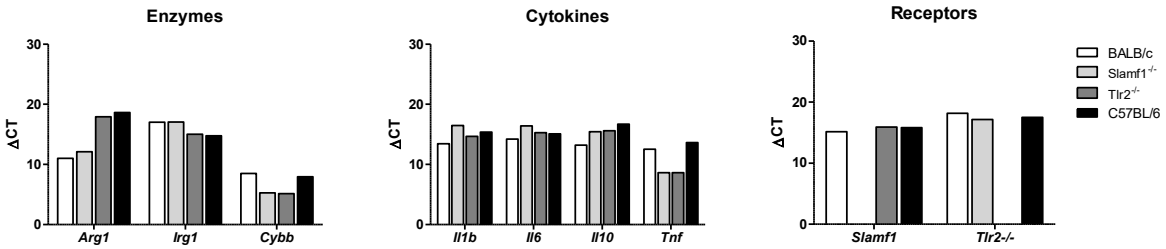

Figure S 1. Non Infected macrophages.

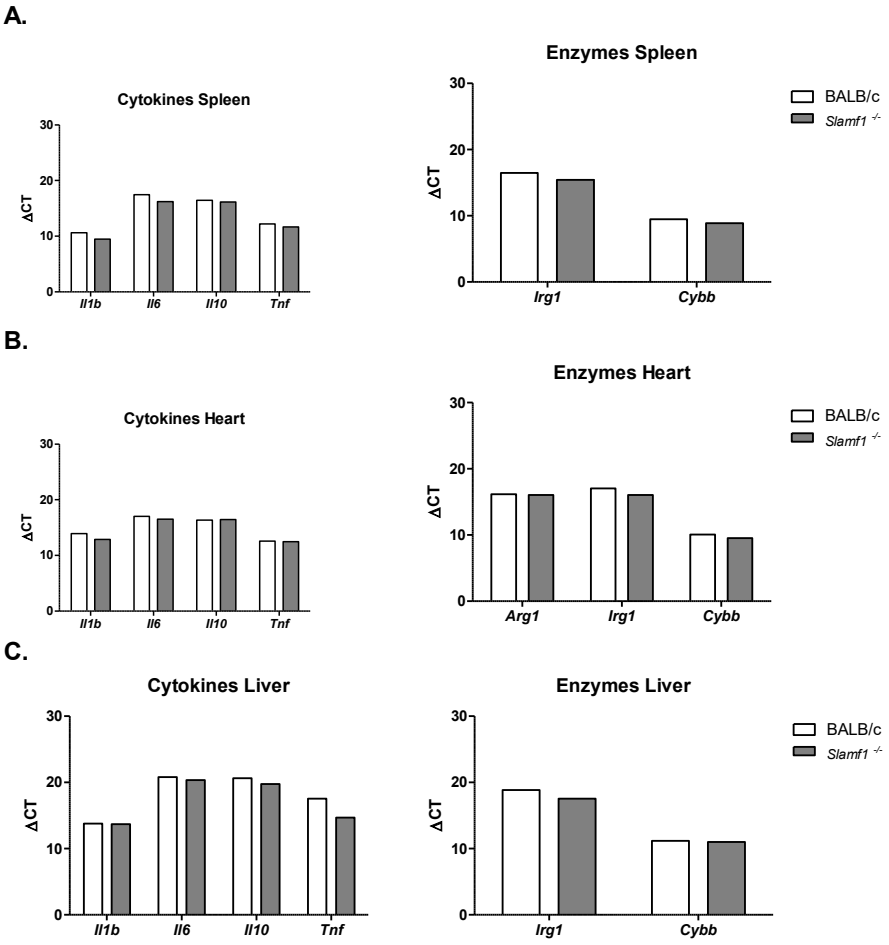

Figure S 2. Non-infected mice controls. A. *Spleen.* ***B.*** *Heart* ***C.*** *Liver.*

8.1.2 Mouse Genetic Background

A. *Arg1*

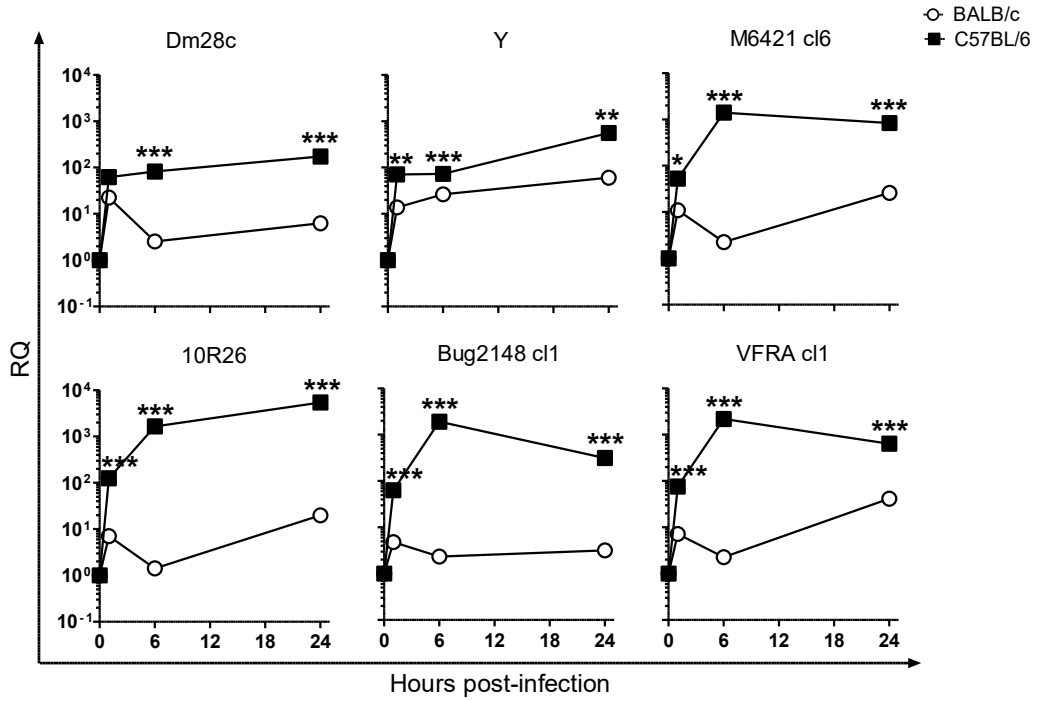

B. *Irg1*

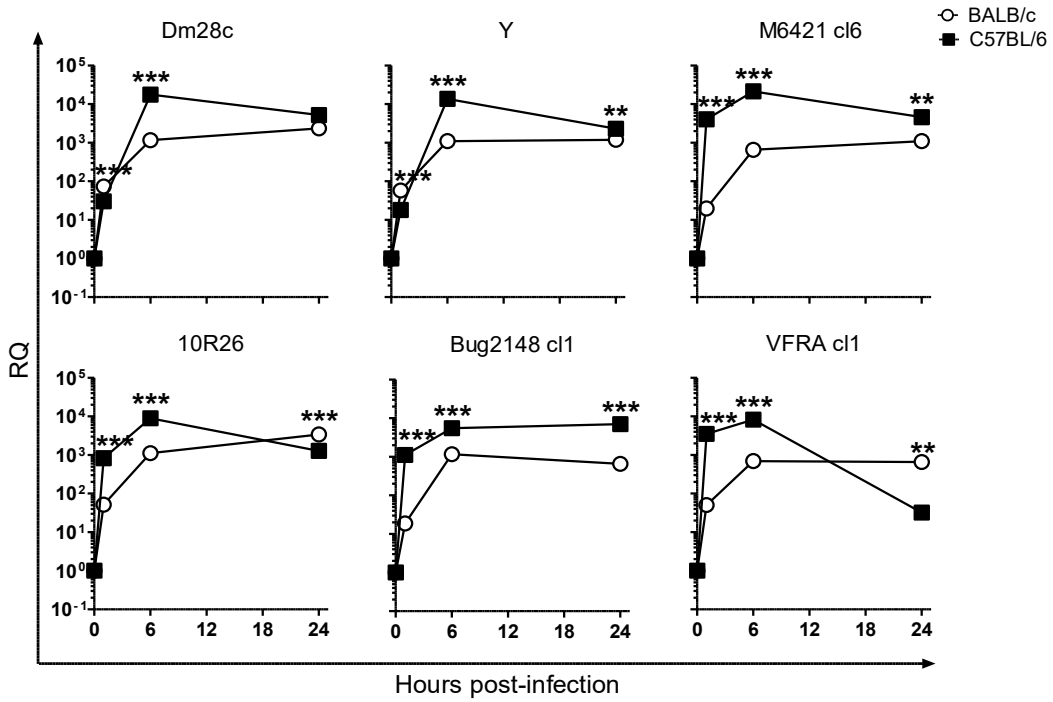

C. *Cybb*

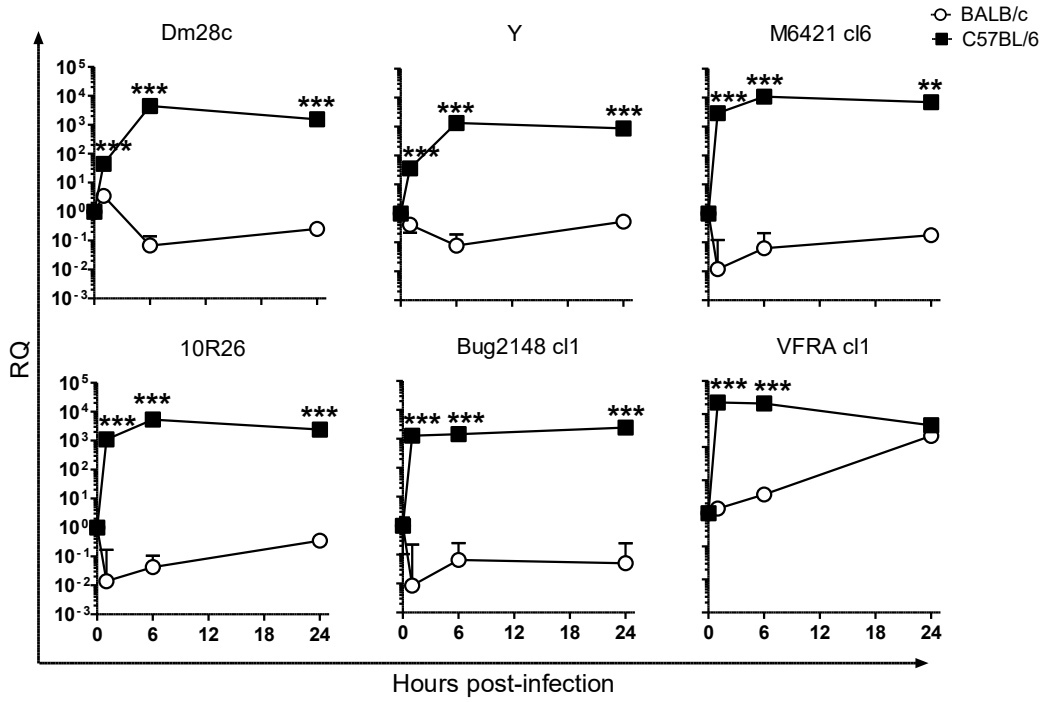

Figure S 3. Kinetics of enzymes gene expression in peritoneal macrophages of BALB/c and C57BL/6 infected with parasite of different DTU´s, in a ratio of 5 Parasites: 1 macrophages. A. *Arg1.* ***B.*** *Irg1.* ***C.*** *Cybb. Standard error of the mean ± (SEM) are represented. The asterisks indicate the statistical significance, t-student (*p<0.05, **p<0.005 and ***p<0.001), between BALB/c and C57BL/6 macrophages.*

A. *Il1b*

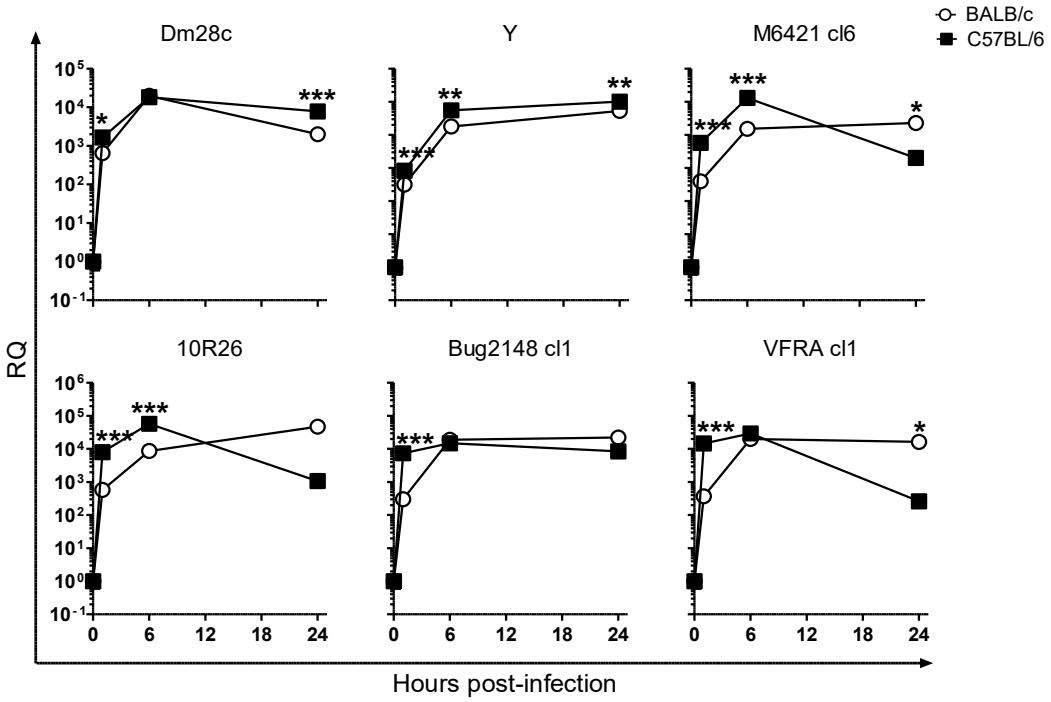
BALB/c
C57BL/6
Dm28c
Y
M6421 cl6
10R26
Bug2148 cl1
VFRA cl1
RQ
Hours post-infection

B. *Il6*

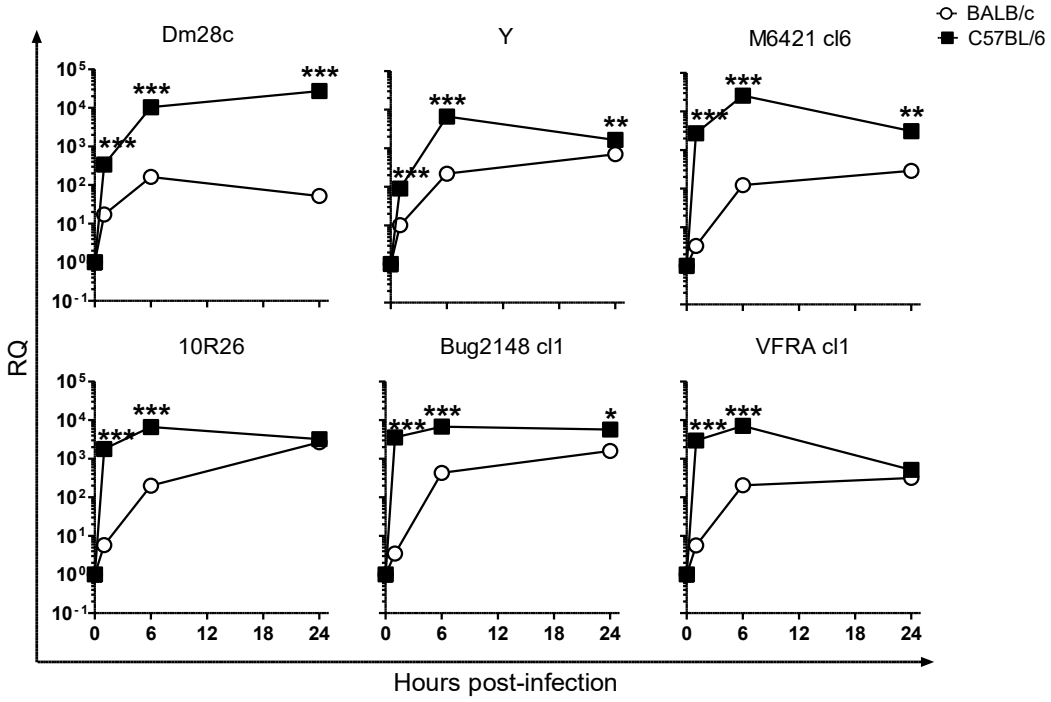
BALB/c
C57BL/6
Dm28c
Y
M6421 cl6
10R26
Bug2148 cl1
VFRA cl1
RQ
Hours post-infection

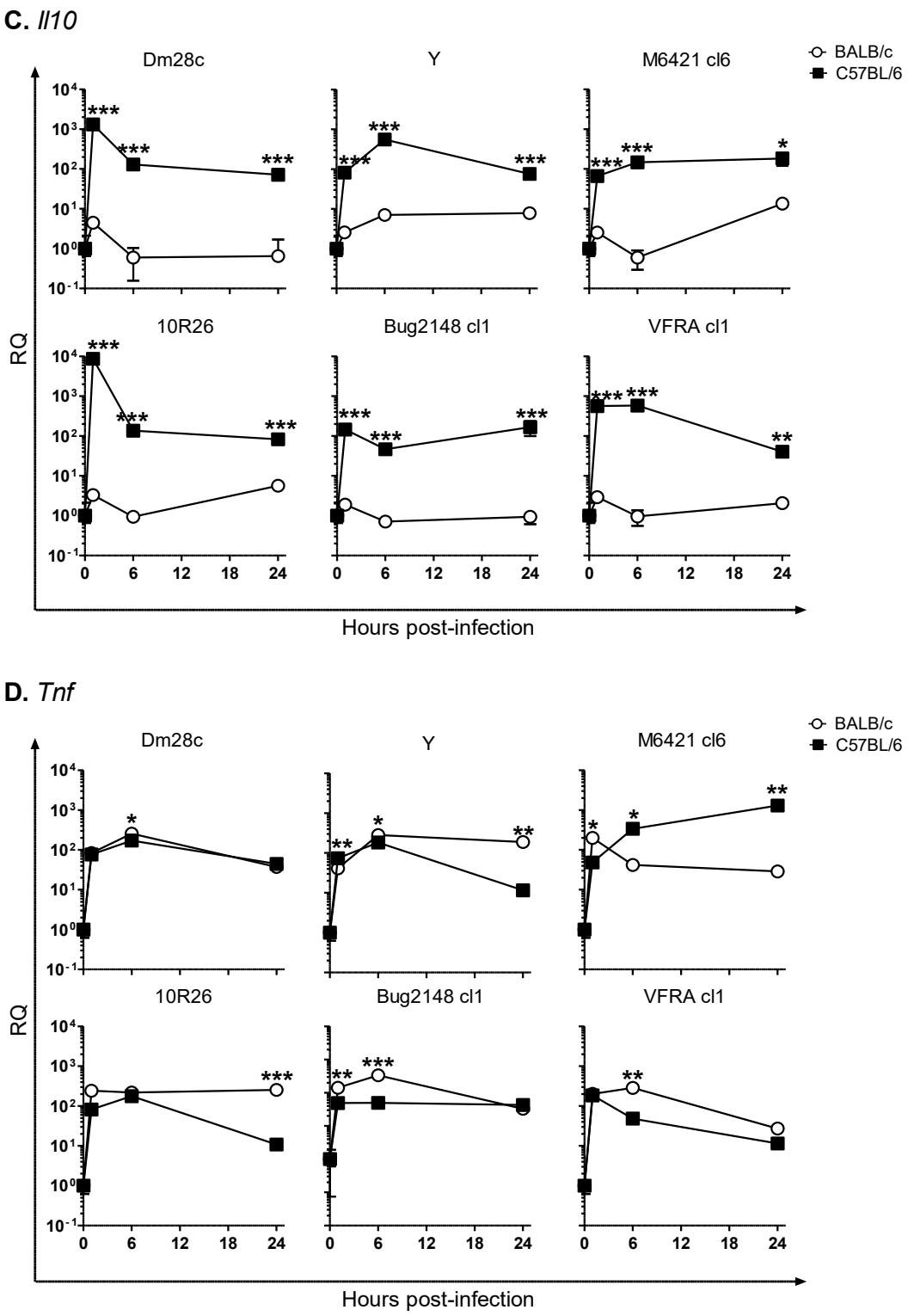

Figure S 4. Kinetic of enzymes gene expression in peritoneal macrophages of BALB/c and C57BL/6 infected with parasite of different DTU´s, in a ratio of 5:1 Parasites, macrophage. . A. *Il1b.* ***B.*** *Il6.* ***C.*** *Il10* ***D.*** *Tnf. Standard error of the mean ± (SEM) are represented. The asterisks indicate the statistical significance, t-student (*p<0.05, **p<0.005 and ***p<0.001), between BALB/c and C57BL/6 macrophages*.

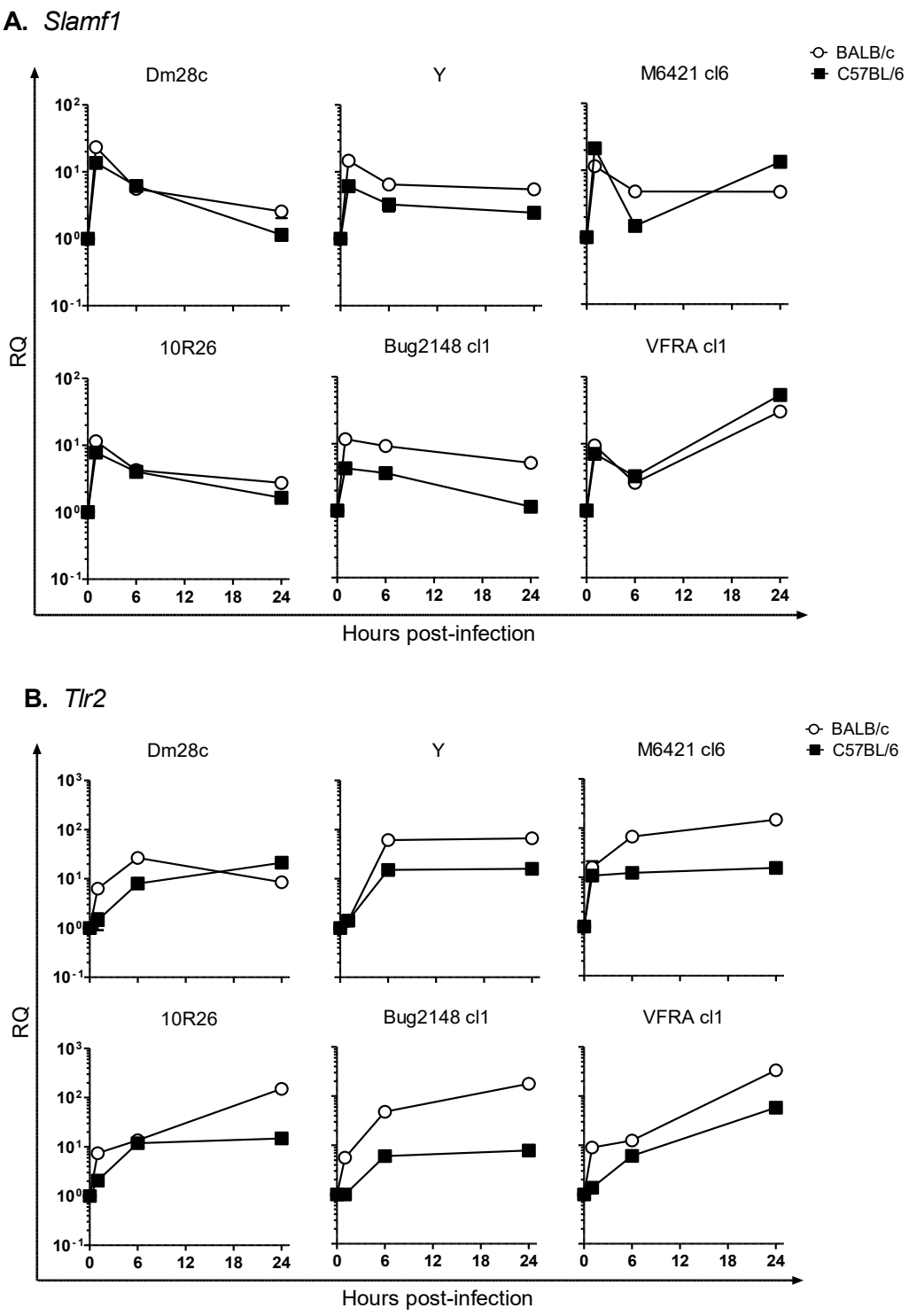

Figure S 5. Kinetic of cytokines gene expression in peritoneal macrophages of BALB/c and C57BL/6 infected with parasite of different DTU´s, in a ratio of 5:1 Parasites, macrophage. A. *Slamf1.* ***B.*** *Tlr2. Standard error of the mean ± (SEM) are represented. The asterisks indicate the statistical significance, t-student (*p<0.05, **p<0.005 and ***p<0.001), between C57BL/6 and BALB/c macrophages*

8.1.3 TLR2 in macrophages

A. *Arg1*

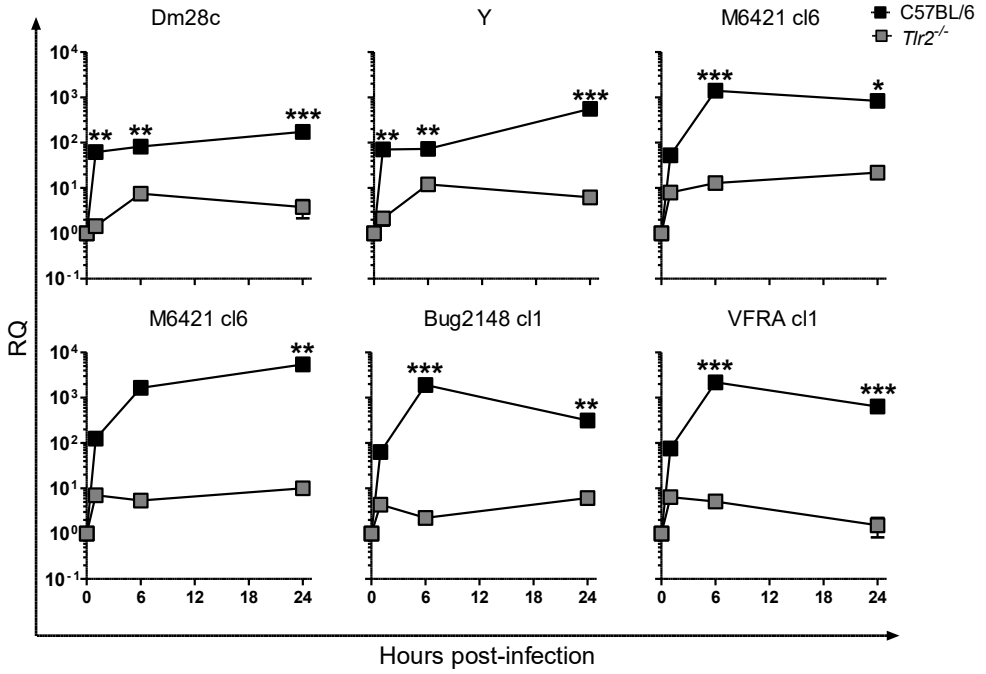

B. *Irg1*

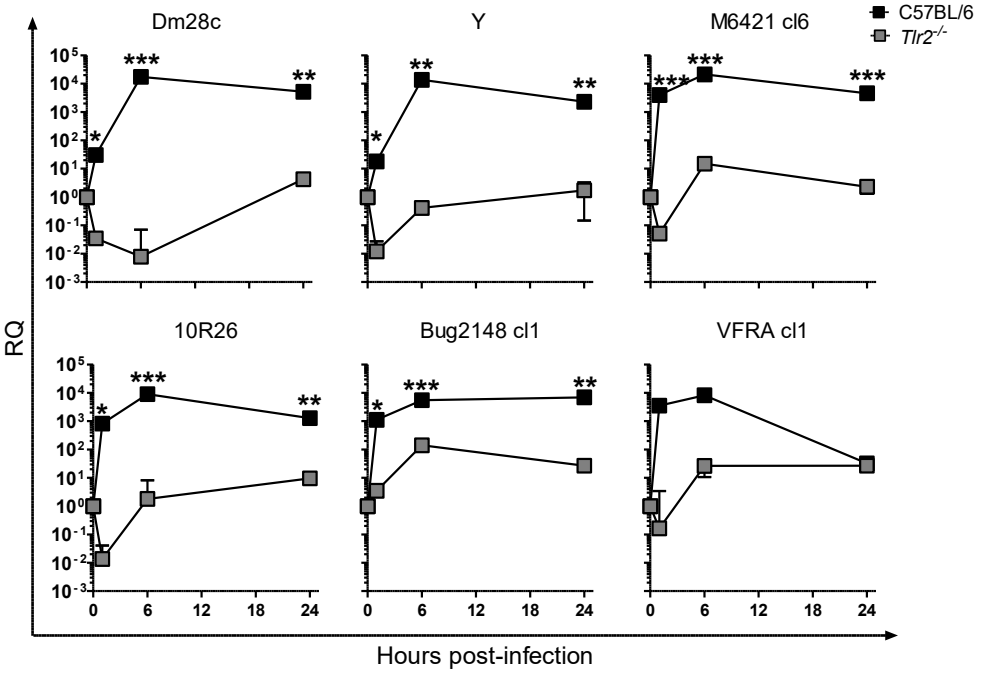

C. *Cybb*

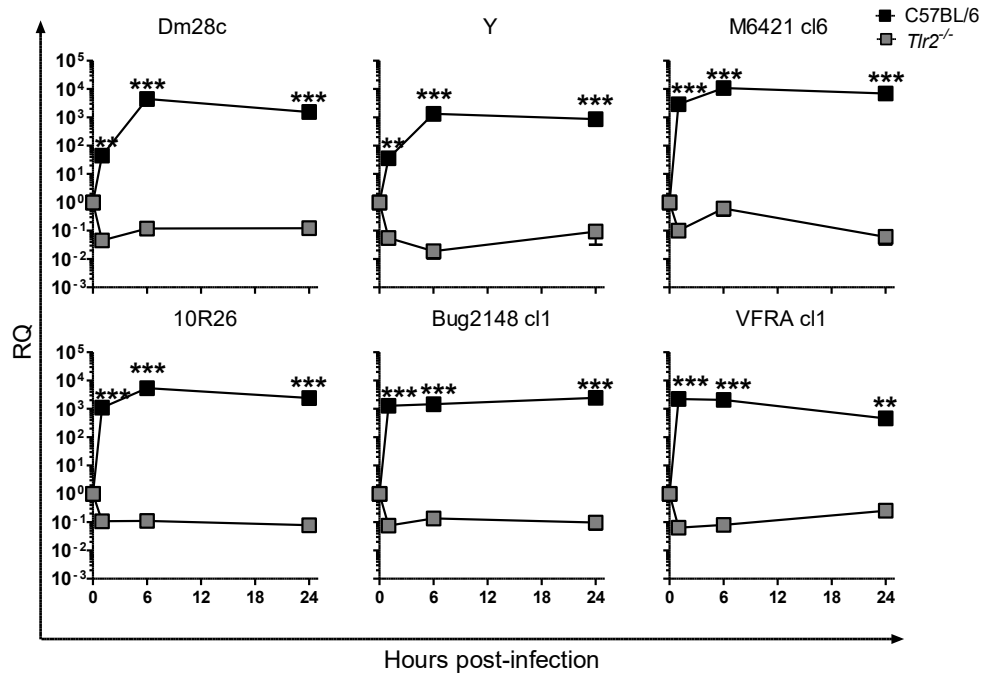

Figure S 6. Kinetic of enzymes gene expression in peritoneal macrophages of Tlr2$^{-/-}$ and C57BL/6 infected with parasite of different DTU´s, in a ratio of 5:1 Parasites, macrophage. A. *Arg1.* ***B.*** *Irg1.* ***C.*** *Cybb. Standard error of the mean ± (SEM) are represented. The asterisks indicate the statistical significance, t-student (*p<0.05, **p<0.005 and ***p<0.001), between Tlr2$^{-/-}$ and C57BL/6 macrophages.*

A. *Il1b*

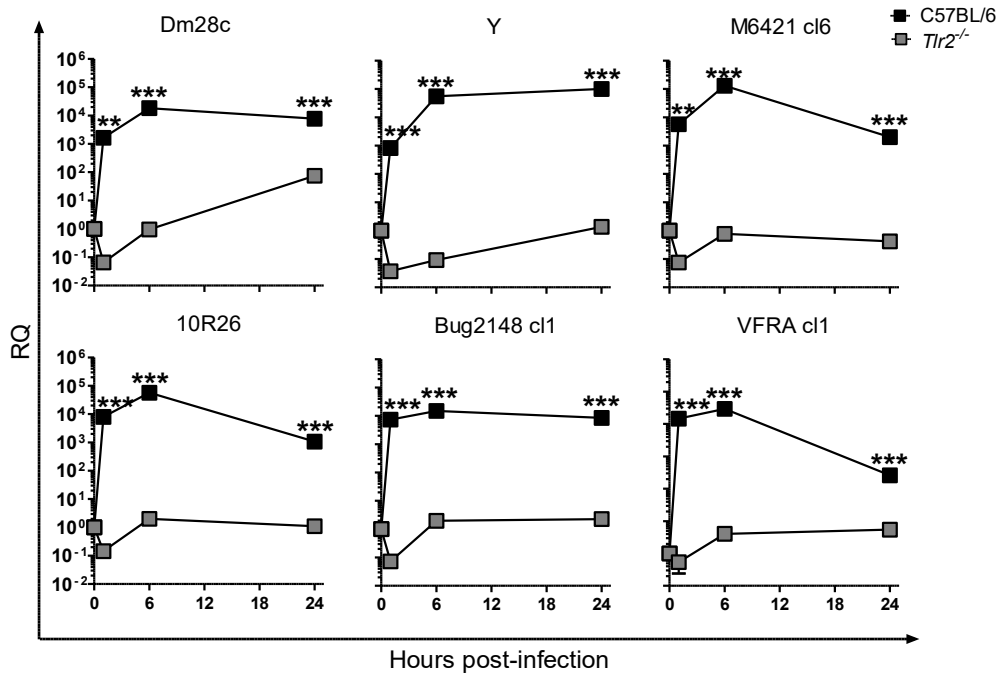
C57BL/6
Tlr2-/-
Dm28c
Y
M6421 cl6
10R26
Bug2148 cl1
VFRA cl1
RQ
Hours post-infection

B. *Il6*

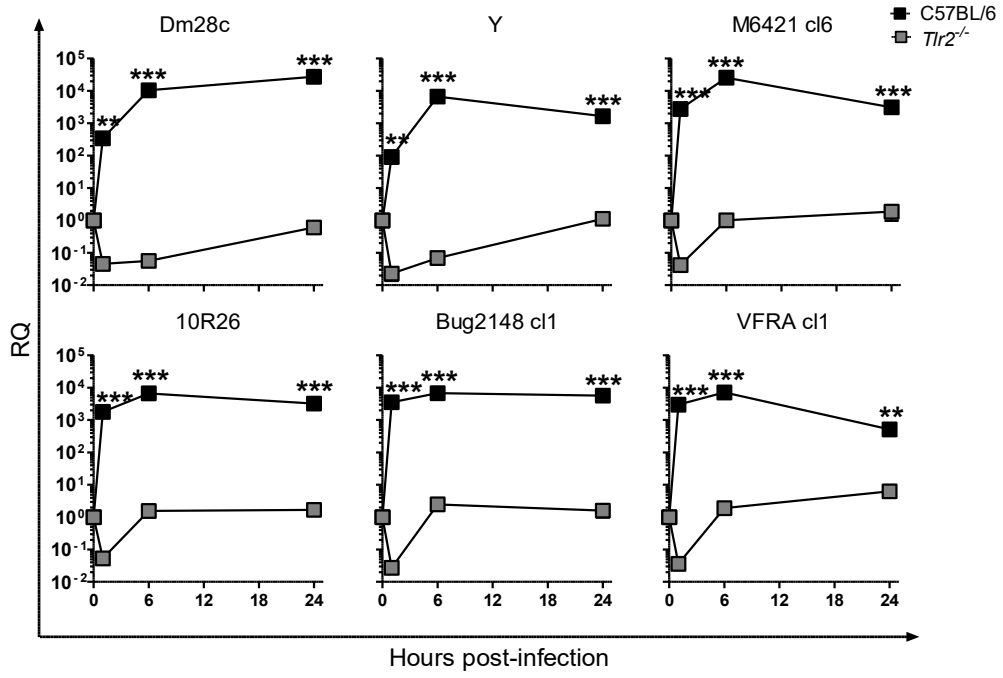
C57BL/6
Tlr2-/-
Dm28c
Y
M6421 cl6
10R26
Bug2148 cl1
VFRA cl1
RQ
Hours post-infection

C. *Il10*

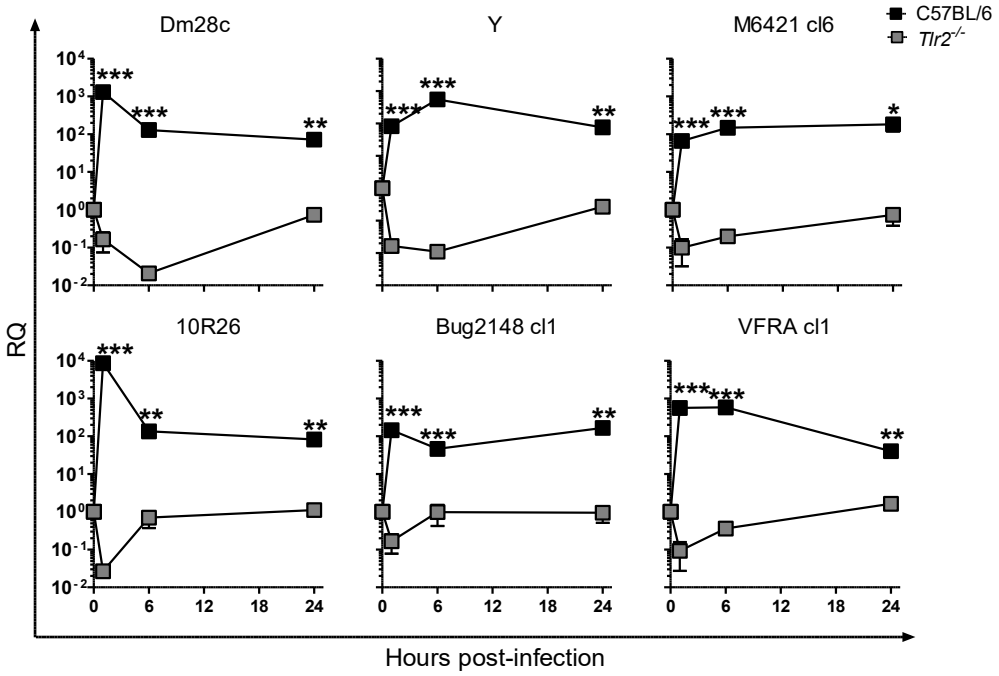

D. *Tnf*

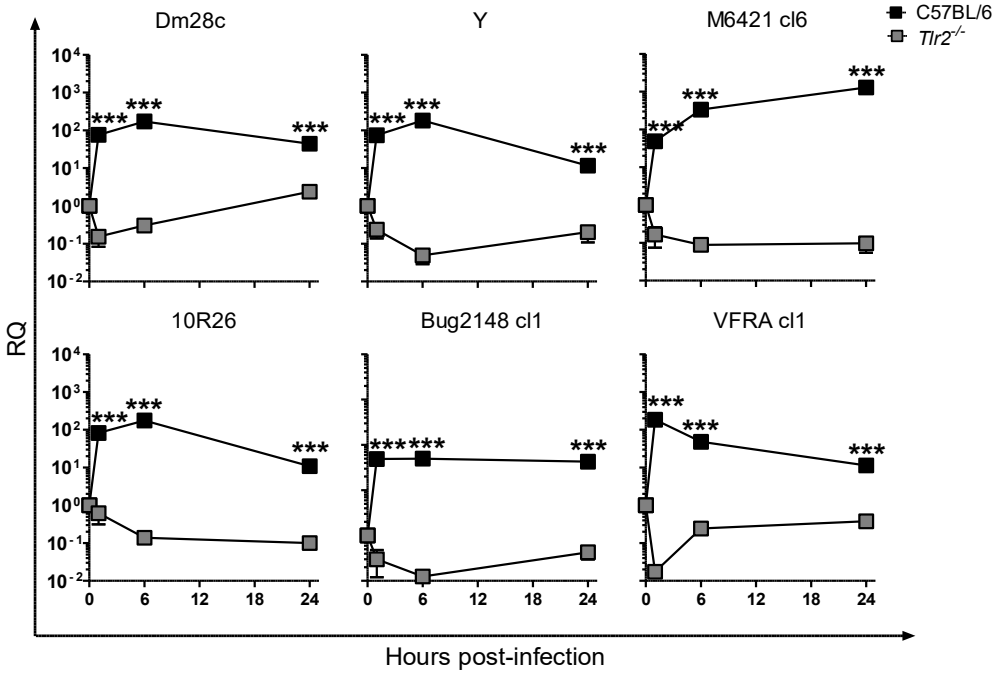

Figure S 7. Kinetic of cytokines gene expression in peritoneal macrophages of Tlr2$^{-/-}$ and C57BL/6 infected with parasite of different DTU´s, in a ratio of 5:1 Parasites, macrophage. A. *Il1b.* ***B.*** *Il6.* ***C.*** *Il10* ***D.*** *Tnf. Standard error of the mean ± (SEM) are represented. The asterisks indicate the statistical significance, t-student (*p<0.05, **p<0.005 and ***p<0.001), between Tlr2$^{-/-}$ and C57BL/6 macrophages.*

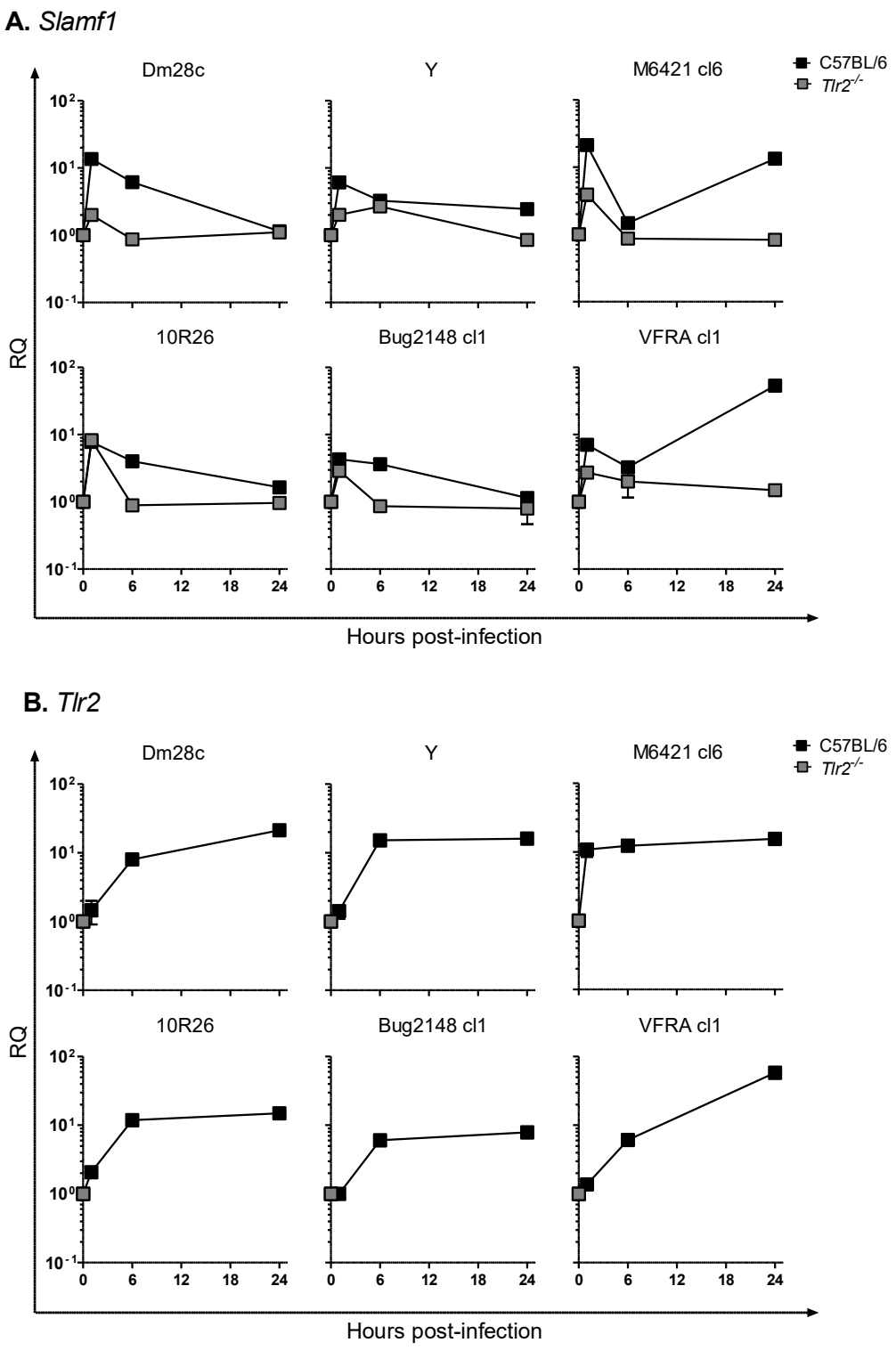

Figure S 8. Kinetic of cytokines gene expression in peritoneal macrophages of Tlr2$^{-/-}$ and C57BL/6 infected with parasite of different DTU´s, in a ratio of 5:1 Parasites, macrophage. A. *Slamf1.* ***B.*** *Tlr2. Standard error of the mean ± (SEM) are represented. The asterisks indicate the statistical significance, t-student (*p<0.05, **p<0.005 and ***p<0.001), between C57BL/6 and Tlr2$^{-/-}$ macrophages.*

8.1.4 SLAMF1 in macrophages

A. *Arg1*

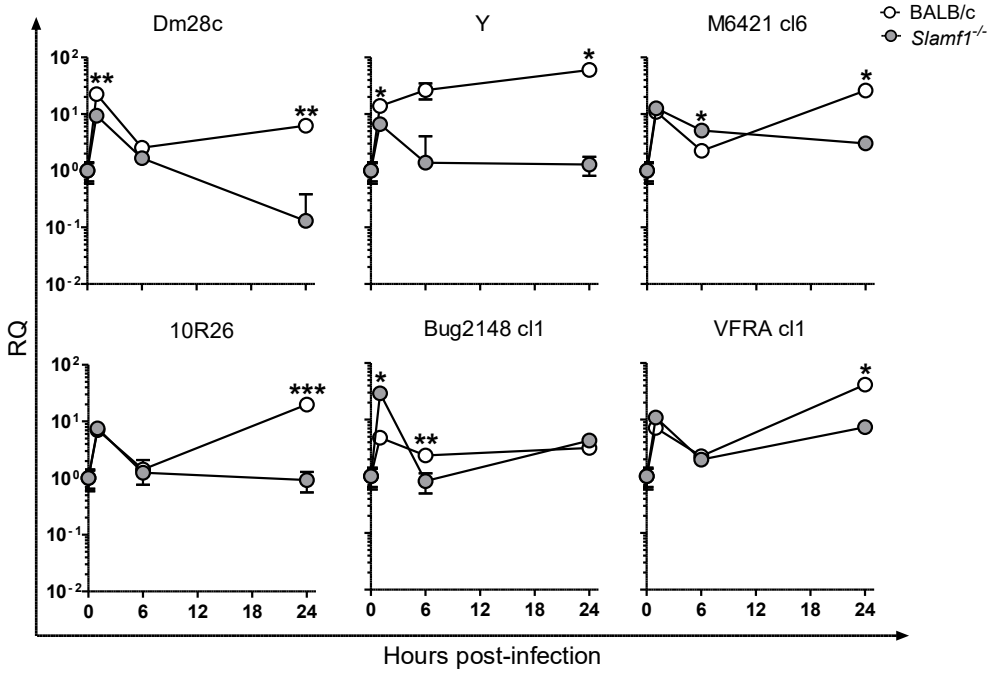

B. *Irg1*

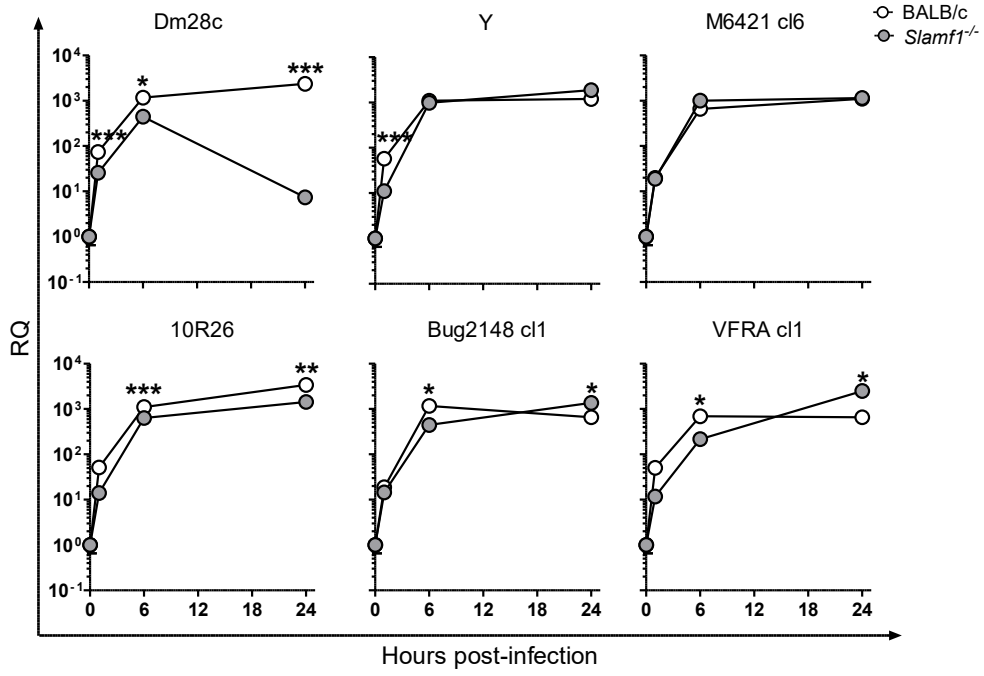

C. *Cybb*

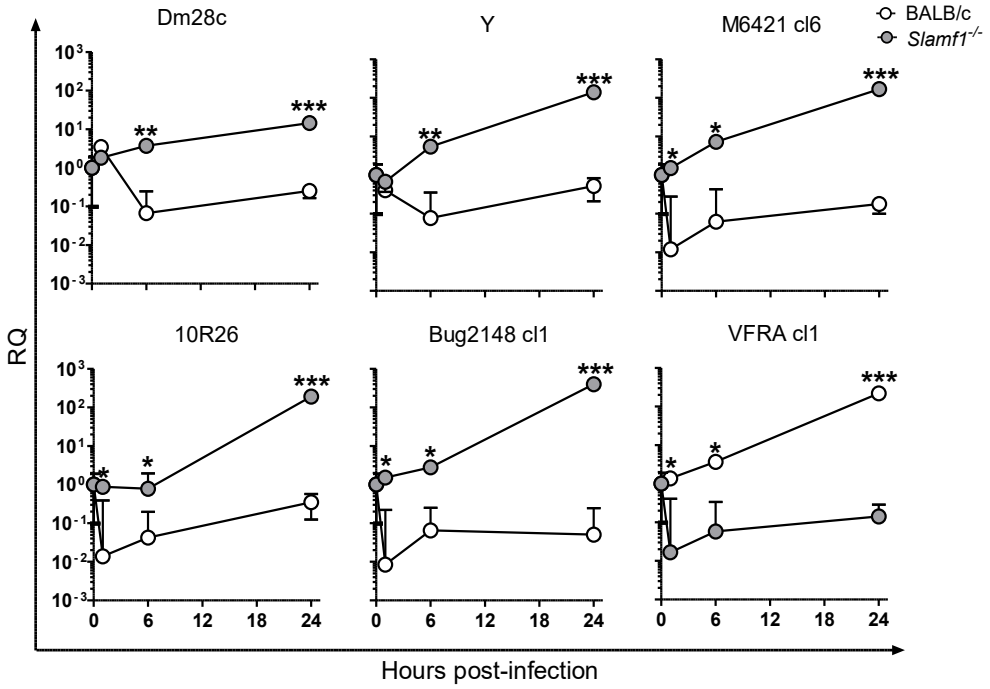

Figure S 9.Kinetic of enzymes gene expression in peritoneal macrophages of Slamf1$^{-/-}$ and BALB/c infected with parasite of different DTU´s, in a ratio of 5:1 Parasites, macrophage. A. *Arg1.* ***B.*** *Irg1.* ***C.*** *Cybb. Standard error of the mean ± (SEM) are represented. The asterisks indicate the statistical significance, t-student (*p<0.05, **p<0.005 and ***p<0.001), between BALB/c and Slamf1$^{-/-}$ macrophages.*

A. *Il1b*

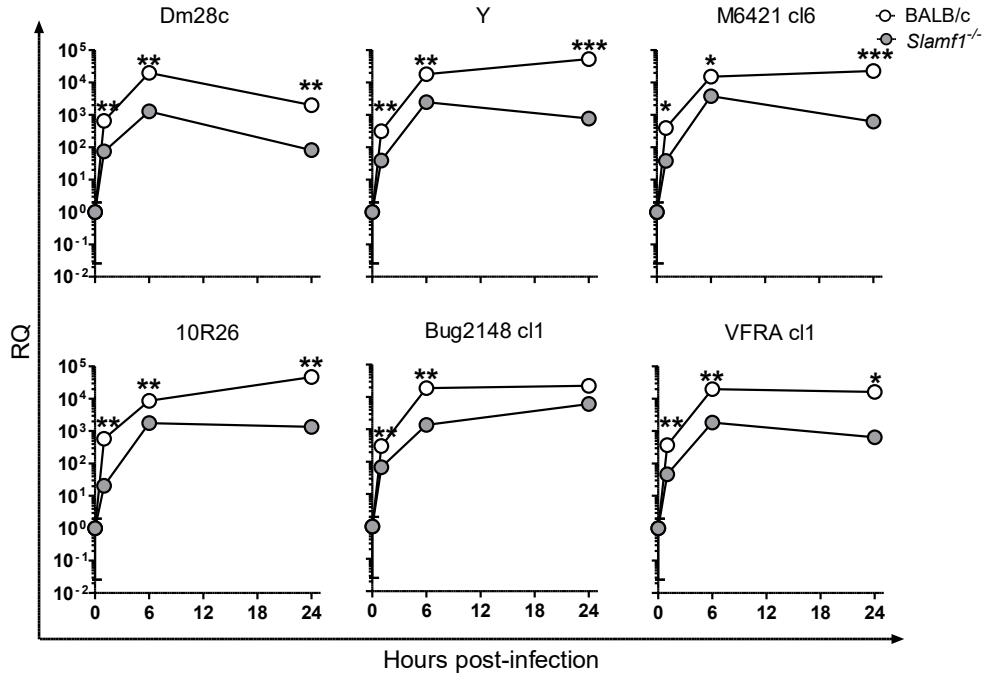
Dm28c
Y
M6421 cl6
BALB/c
Slamf1-/-
10R26
Bug2148 cl1
VFRA cl1
RQ
Hours post-infection

B. *Il6*

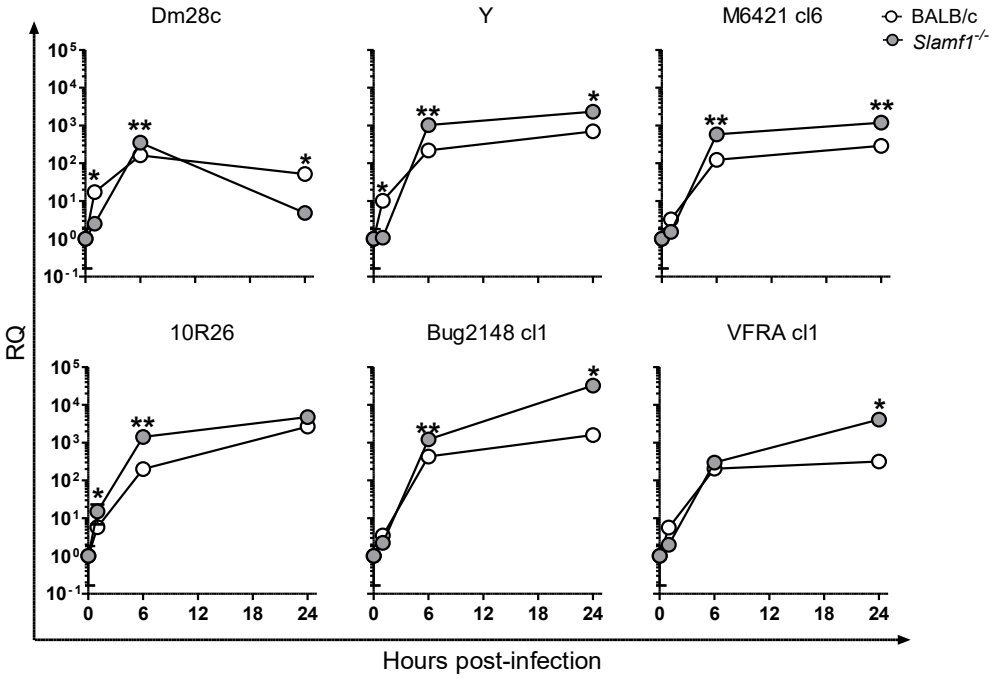
Dm28c
Y
M6421 cl6
BALB/c
Slamf1-/-
10R26
Bug2148 cl1
VFRA cl1
RQ
Hours post-infection

C. *Il10*

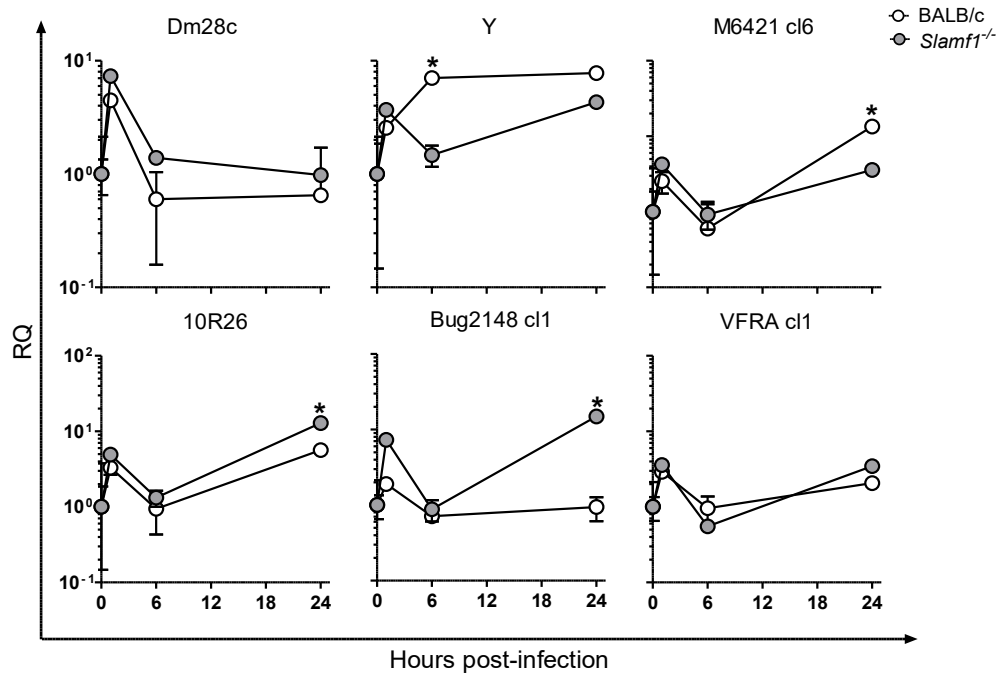

D. *Tnf*

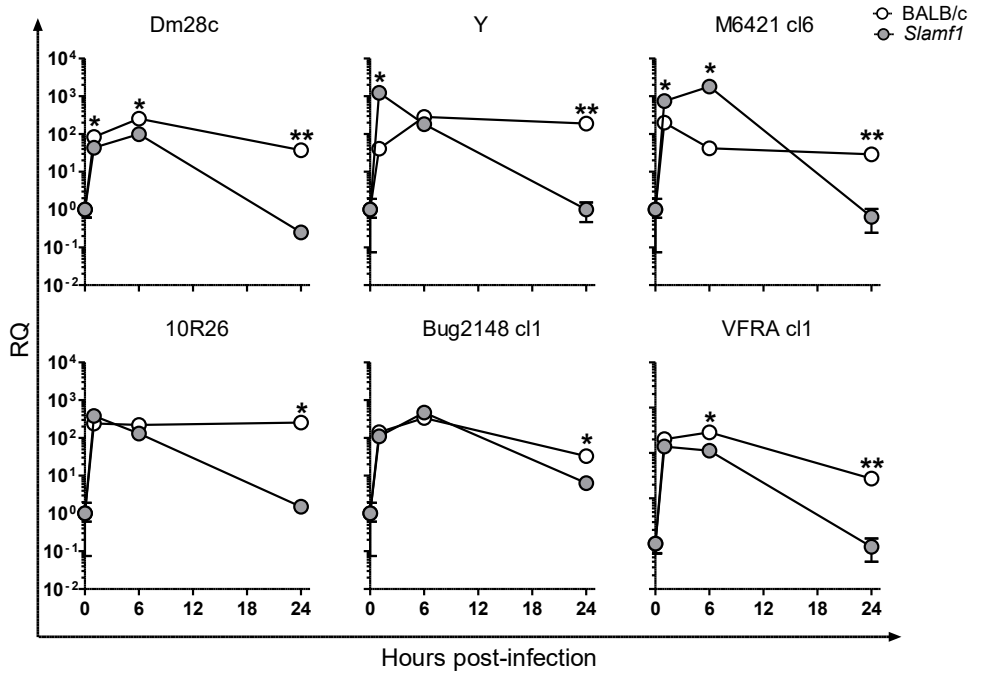

Figure S 10. Kinetic of cytokines gene expression in peritoneal macrophages of Slamf1$^{-/-}$ and BALB/c infected with parasite of different DTU´s, in a ratio of 5:1 Parasites, macrophage. A. *Il1b.* ***B.*** *Il6.* ***C.*** *Il10* ***D.*** *Tnf. Standard error of the mean ± (SEM) are represented. The asterisks indicate the statistical significance, t-student (*p<0.05, **p<0.005 and ***p<0.001), between BALB/c and Slamf1$^{-/-}$ macrophages.*

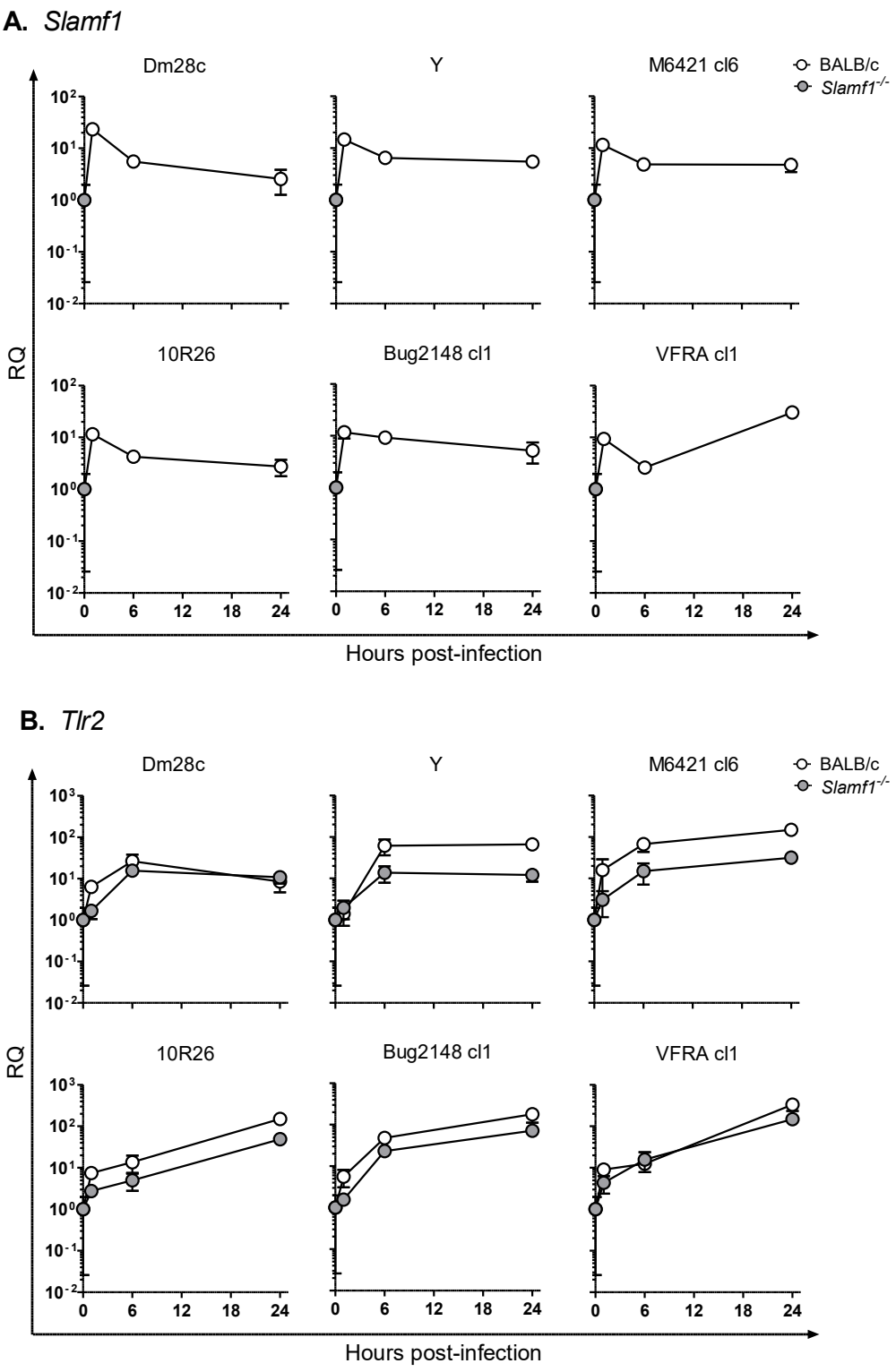

Figure S 11. Kinetic of cytokines gene expression in peritoneal macrophages of Slamf1$^{-/-}$ and BALB/c infected with parasite of different DTU´s, in a ratio of 5:1 Parasites, macrophage. A. *Slamf1.* ***B.*** *Tlr2. Standard error of the mean ± (SEM) are represented. The asterisks indicate the statistical significance, t-student (*p<0.05, **p<0.005 and ***p<0.001), between BALB/c and Slamf1$^{-/-}$ macrophages.*

8.1.5 Spleen

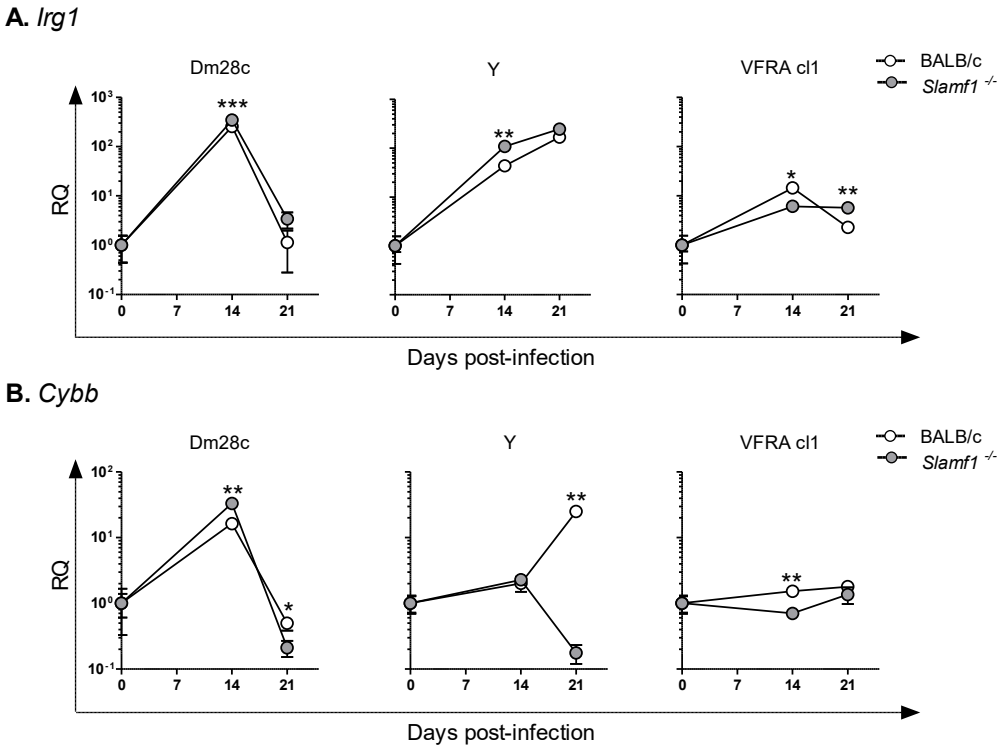

Figure S 12. Gene expression in the spleen Slamf1$^{-/-}$ and BALB/c mice infected with Dm28c, Y and VFRA cl1 the data represent the results of groups 5 mice per group, the data were normalized with respect to NI mice. ***A.*** *Irg1.* ***B.*** *Cybb. Represented the Standard error of the mean ± (SEM). The asterisk indicate the statistical significance, t-student (*p<0.05, **p<0.005 and ***p<0.001), comparing the infected BALB/c and Slamf1$^{-/-}$ mice.*

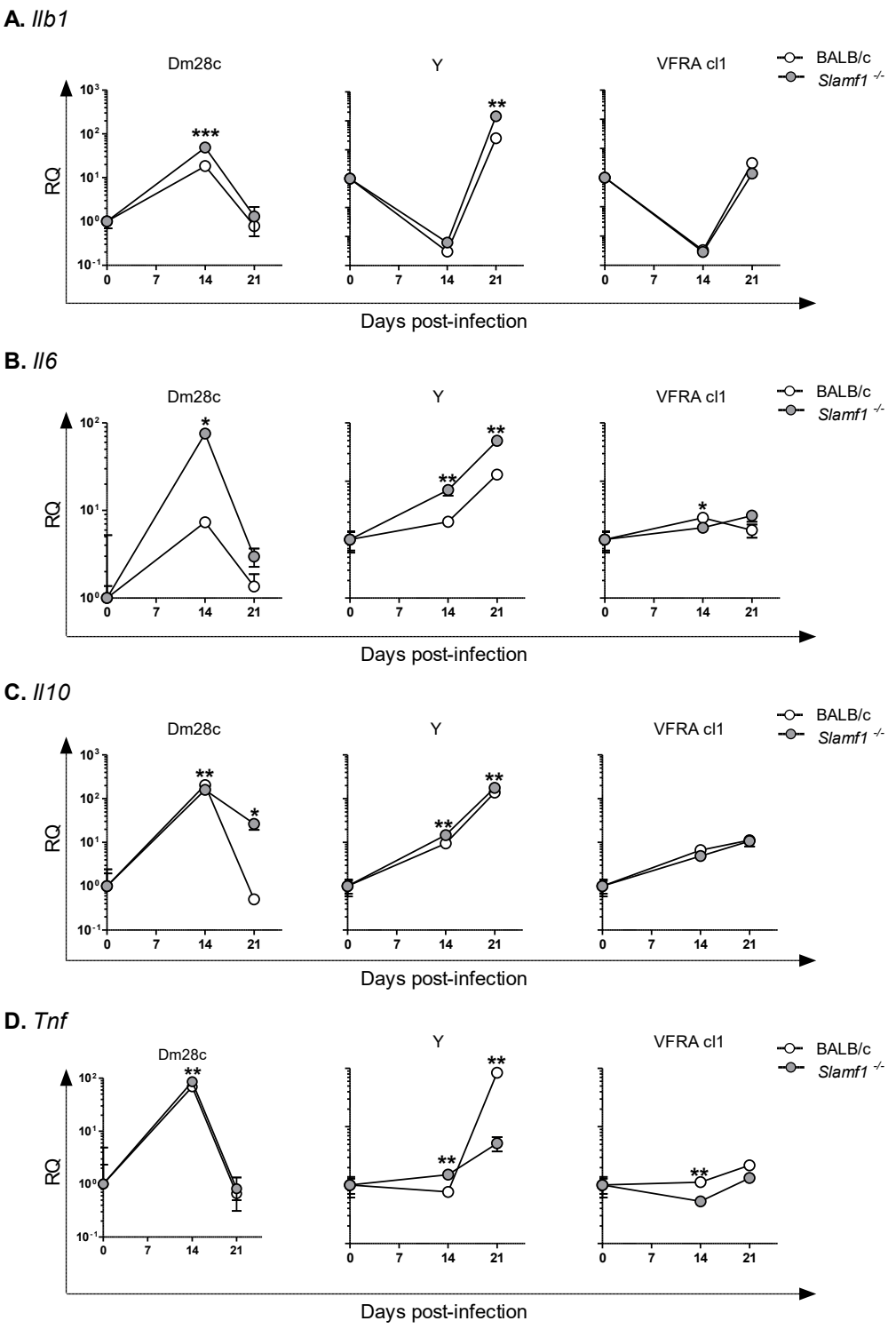

Figure S 13. Gene expression in the spleen Slamf1$^{-/-}$ and BALB/c mice infected with Dm28c, Y and VFRA cl1 the data represent the results of groups 5 mice per group, the data were normalized with respect to NI mice. ***A.*** *Il1b.* ***B.*** *Il6.* ***C.*** *Il10* ***D.*** *Tnf. Represented the Standard error of the mean ± (SEM). The asterisk indicate the statistical significance, t-student (*p<0.05, **p<0.005 and ***p<0.001), comparing the infected BALB/c and Slamf1$^{-/-}$mice.*

8.1.6 Heart

A. *Arg1*

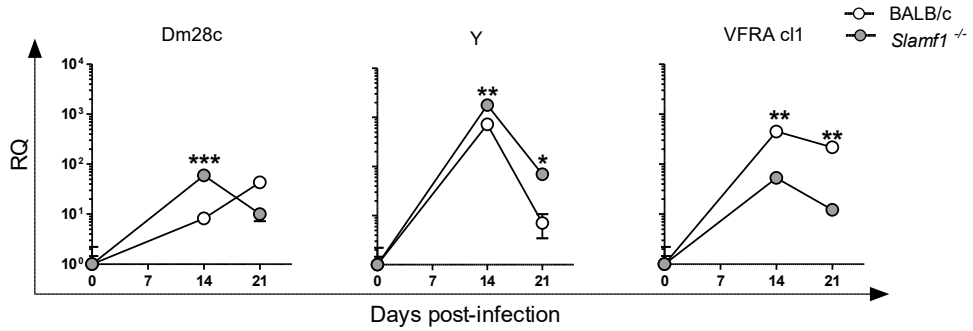

B. *Irg1*

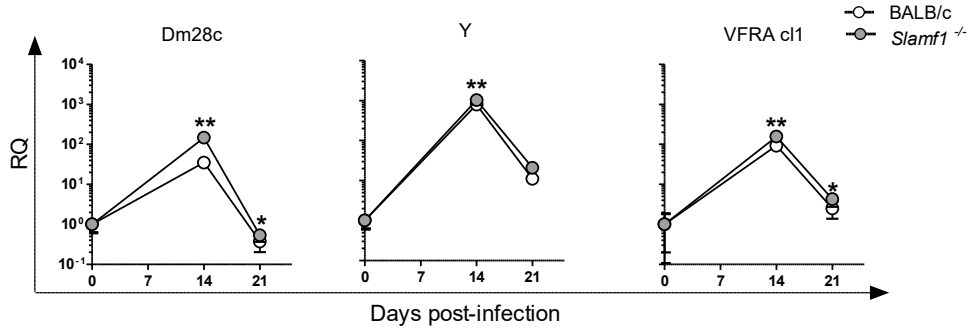

C. *Cybb*

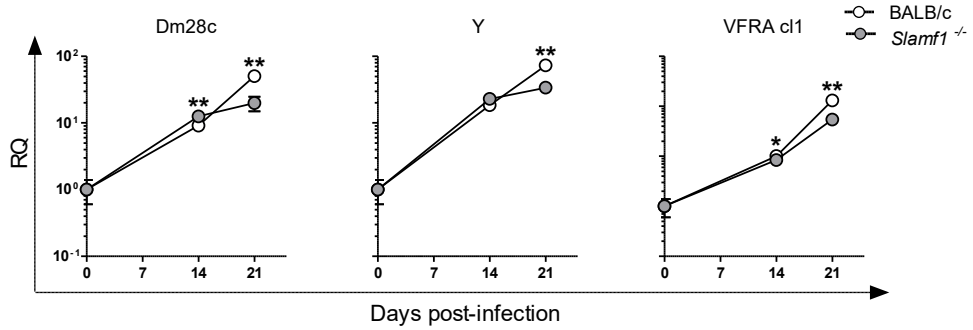

Figure S 14. Gene expression in heart of Slamf1$^{-/-}$ and BALB/c mice infected with Dm28c, Y and VFRA cl1 the data represent the results of groups 5 mice per group, the data were normalized with respect to NI mice. A. *Arg1.* ***B.*** *Irg1.* ***C.*** *Cybb. Represented the Standard error of the mean ± (SEM). The asterisk indicate the statistical significance, t-student (*p<0.05, **p<0.005 and ***p<0.001), comparing the infected BALB/c and Slamf1$^{-/-}$ mice.*

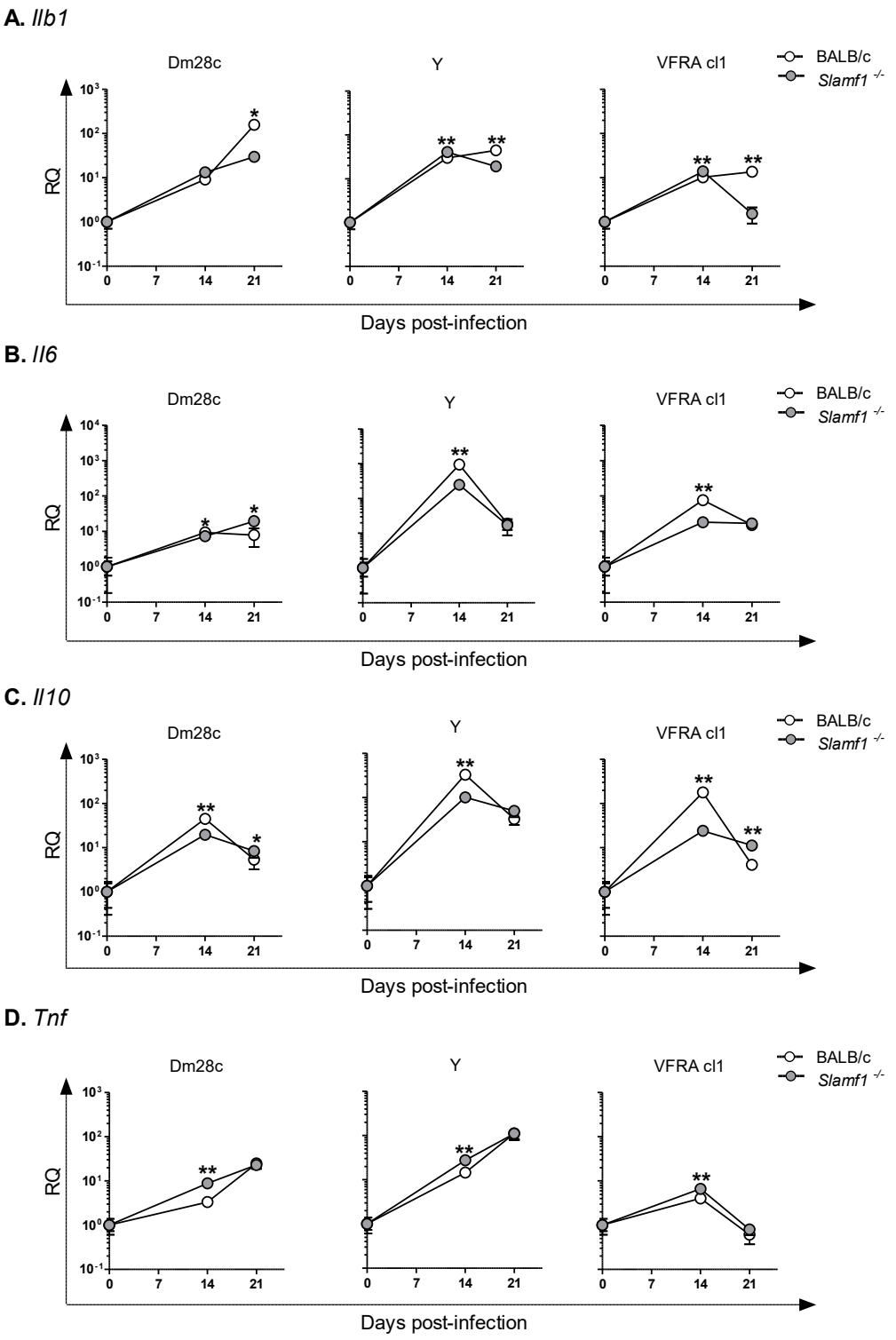

Figure S 15. Gene expression in heart Slamf1$^{-/-}$ and BALB/c mice infected Dm28c, Y and VFRA cl1 the data represent the results of groups 5 mice per group, the data were normalized with respect to NI mice. A. *Il1b.* ***B.*** *Il6.* ***C.*** *Il10* ***D.*** *Tnf. Represented the Standard error of the mean ± (SEM). The asterisk indicate the statistical significance, t-student (*p<0.05, **p<0.005 and ***p<0.001), comparing the infected BALB/c and Slamf1$^{-/-}$ mice.*

8.1.7 Liver

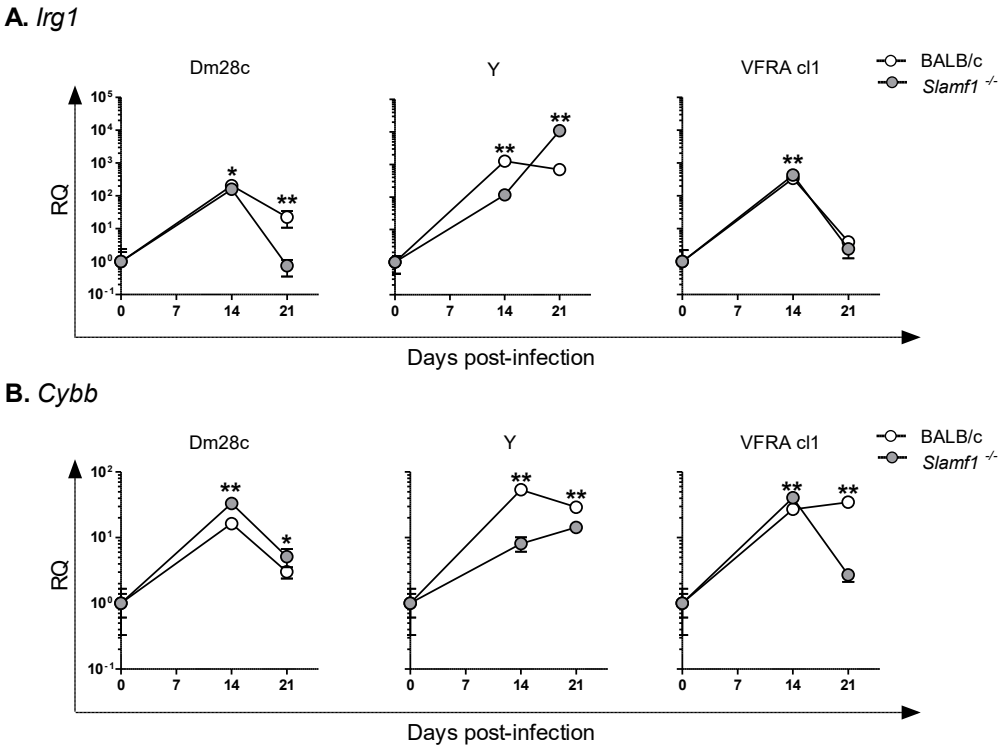

Figure S 16. Gene expression in liver of Slamf1$^{-/-}$ and BALB/c mice infected with Dm28c, Y and VFRA cl1 the data represent the results of groups 5 mice per group, the data were normalized with respect to NI mice. A. *Irg1.* ***B.*** *Cybb. Represented the Standard error of the mean ± (SEM). The asterisk indicate the statistical significance, t-student (*p<0.05, **p<0.005 and ***p<0.001), comparing the infected BALB/c and Slamf1$^{-/-}$ mice.*

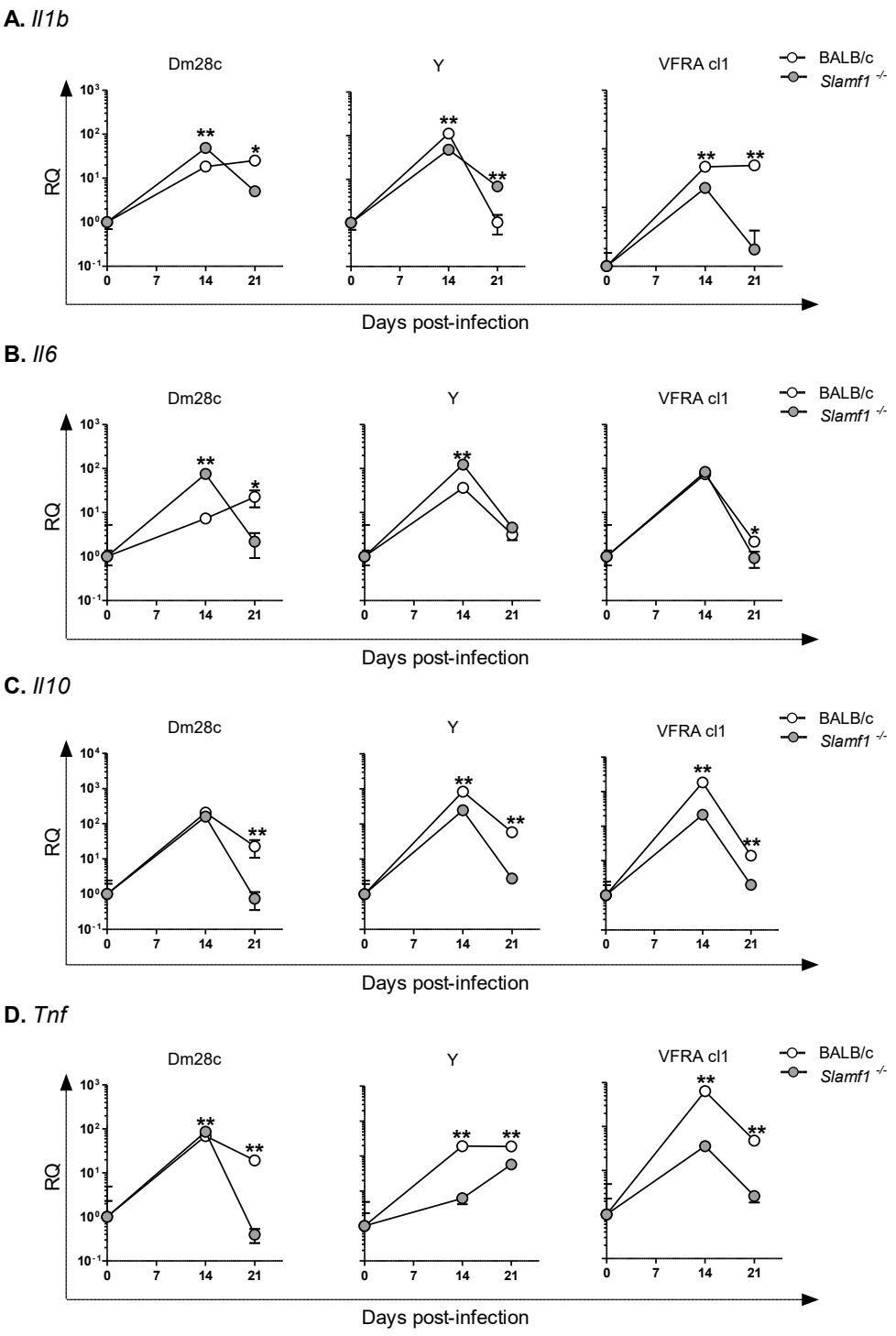

Figure S 17. Gene expression in liver Slamf1$^{-/-}$ and BALB/c mice infected with Dm28c, Y and VFRA cl1 the data represent the results of groups 5 mice per group, the data were normalized with respect to NI mice. A. *Il1b.* ***B.*** *Il6.* ***C.*** *Il10* ***D.*** *Tnf. Represented the Standard error of the mean ± (SEM). The asterisk indicate the statistical significance, t-student (*p<0.05, **p<0.005 and ***p<0.001), comparing the infected BALB/c and Slamf1$^{-/-}$mice.*

8.1.8 Histopatology Heart

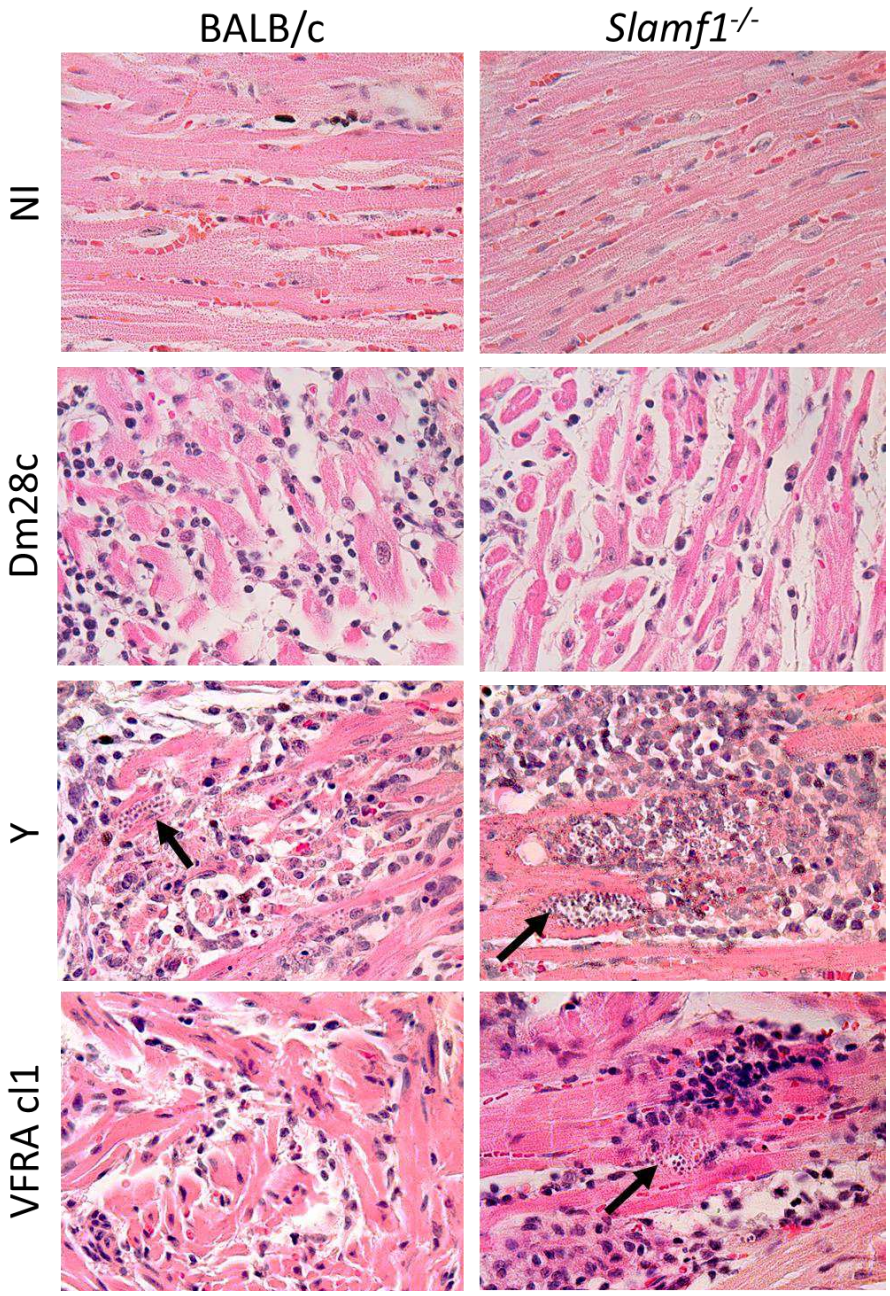

Figure S 18. Histologic of cardiac tissue of BALB/c and Slamf1$^{-/-}$heart infected with the different trains of T. cruzi at 14 d.p.i. *Arrows indicate amasigote nested.*

8.2 TABLE

8.2.1 Reference Strains

Table S 1. Reference strains and corresponding discrete typing units (DTUs).

Strain	DTUs	Country	Host/Vector
92101601P cl1	TcI	Georgia, Usa	*Didelphis marsupialis*
CA-1	TcI	Argentina	*Homo sapiens*
Colombiana	TcI	Colombia	*Homo sapiens*
Cuica cl1	TcI	Sao Paulo, Brazil	*Philander opossum*
Cutia Cl1	TcI	Espirito Santo, Brazil	*Dasprocta aguti*
Davis 9.90	TcI	Tegucigalpa, Honduras	*Triatoma dimidiata*
Dm28c	**TcI**	**Carabobo, Venezuela**	***Didelphis marsupialis***
Dm7	TcI	Casanare, Colombia	*Didelphis marsupialis*
G	TcI	Amazonas, Brazil	Opossum
Gamba cl1	TcI	Sao Paulo, Brazil	*Didelphis azarae*
JEM C	TcI	Boyaca, Colombia	*Homo sapiens*
Jose	TcI	Paraiba, Brazil	*Homo sapiens*
K-98	TcI	Argentina	*Homo sapiens*
PALC	TcI	Casanare, Colombia	*Rhodnius prolixus*
Sylvio X10 cl1	TcI	Para, Brazil	*Homo sapiens*
Td11C	TcI	Boyaca, Colombia	*Triatoma dimidiata*
X10/1	TcI	Para, Brazil	*Homo sapiens*
YuYu	TcI	Minas Gerais, Brazil	*Triatoma infestans*
12SF	TcII	Bahia, Brazil	*Homo sapiens*
21SF	TcII	Bahia, Brazil	*Homo sapiens*
Esmeraldo cl3	TcII	Bahia, Brazil	*Homo sapiens*
IVV cl4	TcII	Cuncumen, Chile	*Homo sapiens*
MAS cl1	TcII	Minas Gerais, Brazil	*Homo sapiens*
Peruvian	TcII	Peru	*Homo sapiens*
Tu18 cl1	TcII	Tupiza, Bolivia	*Triatoma dimidiata*
Y	**TcII**	**Sao Paulo, Brazil**	***Homo sapiens***
3663	TcIII	Amazonas, Brazil	*Oanstrongylus geniculatus*
3869	TcIII	Amazonas, Brazil	*Homo sapiens*
4182	TcIII	Amazonas, Brazil	*Rhodnius brethesi*
CM17	TcIII	Meta, Colombia	*Dasypus sp.*
M5631 cl5	TcIII	Para, Brazil	*Dasypus novemcinctus*
M6421 cl6	**TcIII**	**Para, Brazil**	***Homo sapiens***
X109/2	TcIII	Makthlawiya, Paraguay	*Canis familiaris*
10R26	**TcIV**	**Santa cruz, Bolivia**	***Aotus sp***
4167	TcIV	Amazonas, Brazil	*Rhodnius brethesi*
92122102R	TcIV	Georgia, Usa	*Procyon lotor*
CanIII cl1	TcIV	Para, Brazil	*Homo sapiens*
Dog Theis	TcIV	Oklahoma, USA	*Canis familiaris*
92.80 cl 2	TcV	Santa Cruz, Bolivia	*Homo sapiens*
Bug2148 cl1	**TcV**	**Rio Grande do Sul, Brazil**	***Triatoma infestans***
Bug2149 cl10	TcV	Rio Grande do Sul, Brazil	*Triatoma infestans*
MN cl 2	TcV	Region IV, Chile	*Homo sapiens*
NR cl3	TcV	Salvador, Chile	*Homo sapiens*
Sc43 cl1	TcV	Santa Cruz, Bolivia	*Triatoma infestans*
SO3 cl5	TcV	Potosi, Bolivia	*Triatoma infestans*
CL	TcVI	Rio Grande do Sul, Brazil	*Triatoma infestans*
CL Brener	TcVI	Rio Grande do Sul, Brazil	*Triatoma infestans*
P63 cl1	TcVI	Makthlawiya, Paraguay	*Triatoma infestans*
RA	TcVI	Argentina	*Homo sapiens*
Tulahuen	TcVI	Tulahuen, Chile	*Homo sapiens*
Tulahuen cl2	TcVI	Tulahuen, Chile	*Homo sapiens*
VFRA	**TcVI**	**Francia, Chile**	***Triatoma infestans***

8.2.2 Mouse Genetic Background

Table S 2. Gene Expression and parasite load correlations in BALB/c (Right) and C57BL/6(Left) peritoneal macrophages infected with different strains of T. cruzi in the interaction (1h).

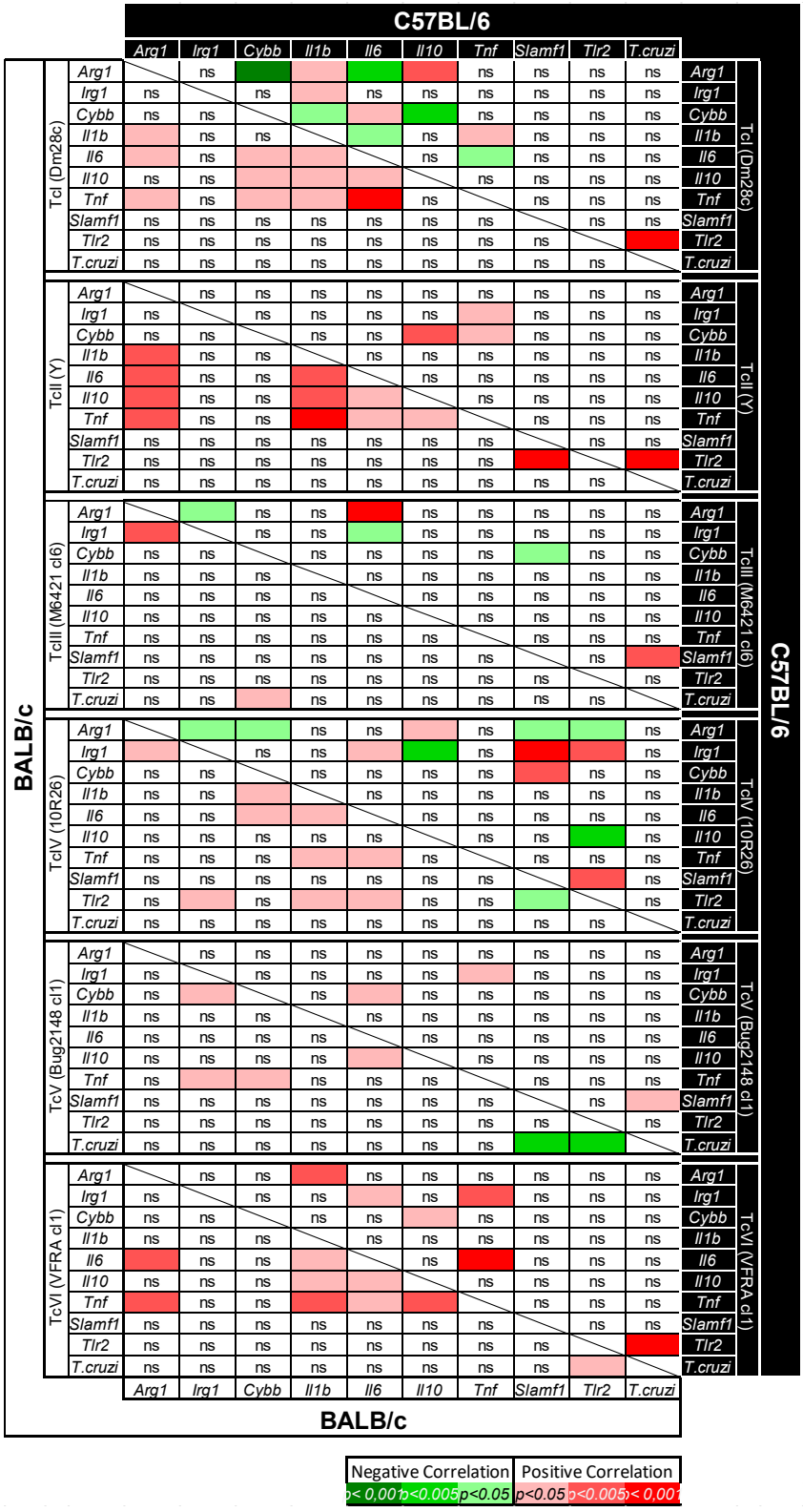

Bearing in that gene expression in most cases was higher in C57BL/6 than BALB/c macrophages, we analyzed positive and negative gene expression correlation for each mouse strain upon infection at different time.Table S 2 shows the correlation during the Interaction:

- Dm28c: BALB/c macrophages present only positive correlations between *Tnf-Cybb, Arg1-Tnf, Il1b-Il10* and *Il10-Il6*. In contrast, correlations of *Cybb-Arg1*, *Il6-Arg-1, Il10-Cybb, Il6-Il1b* and *Tnf-Il6* changes from positive in BALB/c to negative in C57BL/6 macrophages. Positive correlation between *Il10-Arg1, T. cruzi-Tlr2* and *Il1b-Irg1* and negative correlation between *Il1b-Cybb* was found for C57BL/6 macrophages.
- Y: We found only positive correlation for both mouse genetic backgrounds. In BALB/c macrophages that correlation were *Arg1-Il1b, Arg1-Il6, Arg1-10, Arg1-Tnf, Il1b-Il6, Il1b-Il10,*
- *Il1b-Tnf, Il6-Il10, Il-6Tnf, Il10-Tnf* and *Slamf1-Tnf.* Positive correlation between *Irg1-Tnf, Cybb-Tnf, T. cruzi-Tlr2* and *Cybb-Il10* was found for C57BL/6 macrophages.
- M6421 cl6: BALB/c macrophages present only positive correlations between *Cybb-T. cruzi*. In contrast, the correlation between *Arg1-Irg1* changes from positive in BALB/c to negative in C57BL/6 macrophages. Positive correlation between *Il6-Arg1* and *Slamf1-T. cruzi,* and negative correlations between *Irg1-Il6* and *Cybb-Slamf1* were found for C57BL/6 macrophages.
- 10R26: BALB/c macrophages present positive correlation between *Il1b-Cybb, Il6-Cybb, Il6-Il1b, Tnf-Il1b, Tnf-Il6, Tlr2-Il1b* and *Tlr2-Il6,* and negative correlations between *Tlr2-Slamf1*. In contrast, the correlation between *Arg1-Irg1* changes from positive in BALB/c to negative in C57BL/6 macrophages. Positive correlation between *Arg1-Il10, Irg1-Il6, Irg1-Slamf1* and *Cybb-Slamf1,* and negative correlations between *Arg1-Cybb, Arg1-Slamf1, Arg1-Tlr2, Irg1-Il10* and *Il10-Tlr2* were found for C57BL/6 macrophages.
- Bug2148 cl1: BALB/c macrophages present positive correlation between *Cybb-Irg1, Tnf-Cybb* and *Il10-Il6.* Positive correlation between *Cybb-Il6,* and negative correlations between was *T. cruzi-Tlr2* found for C57BL/6 macrophages. Correlation between *T. cruzi-Slamf1* changes from positive in BALB/c to negative in C57BL/6 macrophages.
- VFRA cl1: BALB/c macrophages present positive correlation between *Arg1-Il6, Arg1-Tnf, Il1b-Il6, Il1b-Il10, Il1b-Tnf, Il6-Il10* and *Il10-Tnf.* C57BL/6 macrophages present also positive correlations between *Arg-I1b, Irg1-Il6, Irg1-Tnf* and *Cybb-Il10.*

Table S 3. Gene Expression and parasite load correlations in BALB/c (Right) and C57BL/6(Left) peritoneal macrophages infected with different strains of T. cruzi in the internalization (6h).

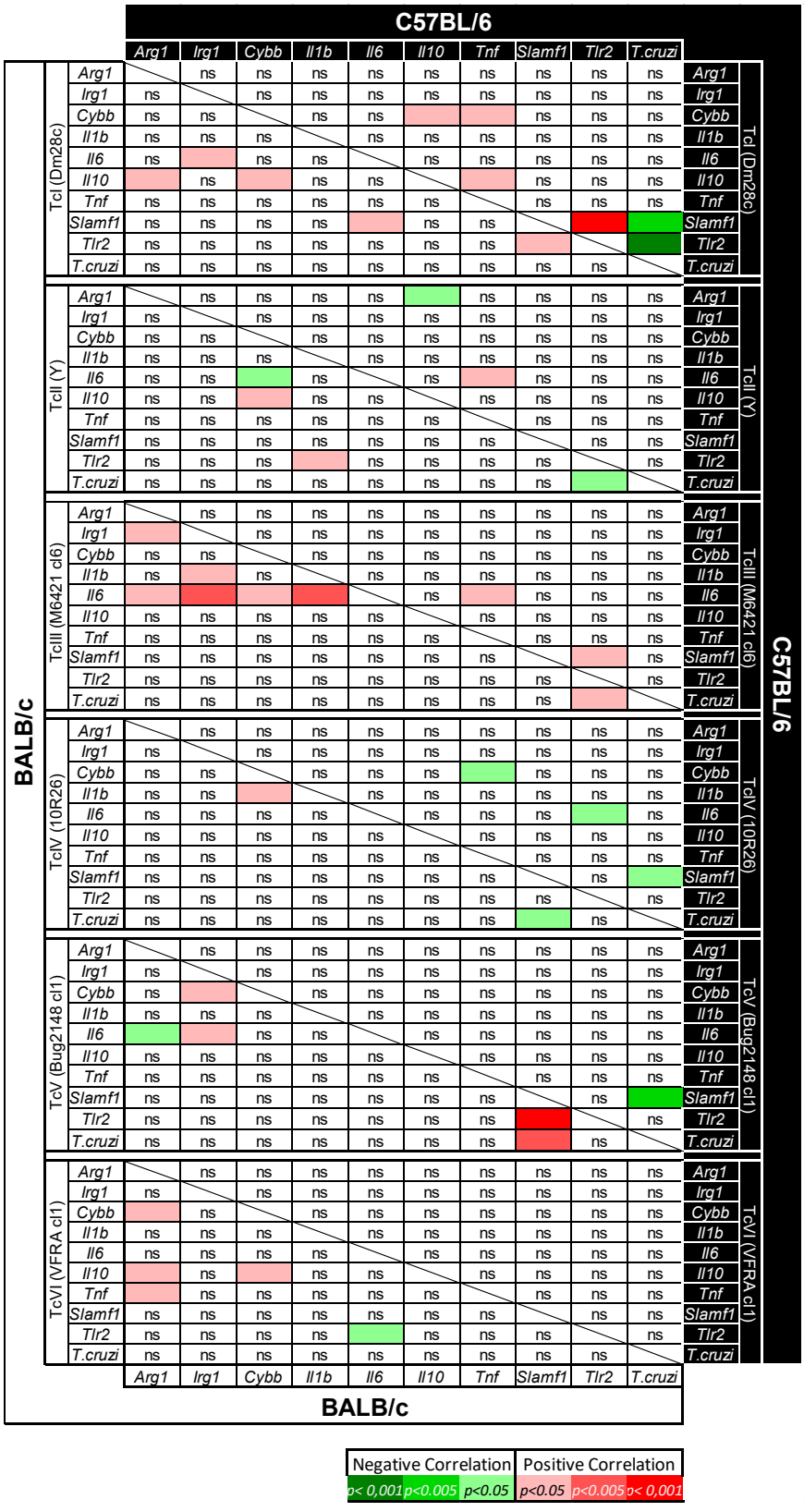

Table S 3 shows gene expression and parasite load correlations during Internalization:

- Dm28c: BALB/c macrophages present positive correlation between *Arg1-Il10, Irg1-Il6* and *Il6-Slamf1.* Positive correlation between *Cybb-Tnf* and *Il10-Tnf,* and negative correlations between *T. cruzi-Slamf1* and *T. cruzi-Tlr2* were found for C57BL/6 macrophages.
- Y: Positive correlation between Cybb-Il10 and Il1b-Tlr2, and negative correlations between Cybb-Il6 and *T. cruzi*-Tlr2 were found for BALB/c macrophages. Positive correlation between Il6-Tnf, and negative correlations between Arg1-Il10 was found for C57BL/6 macrophages.
- M6421 cl6: Only positive correlations were found in both mouse genetic background, where in BALB/c were *Arg1-Irg1, Arg1-Il6, Irg1-Il1b, Irg1-Il6, Cybb-Il6, Il1b-Il6* and *T. cruzi-Tlr2;* and in C57BL/6 were *Il6-Tnf* and *Slamf1-Tlr2.*
- 10R26: Positive correlation in BALB/c was found between *Cybb-Il1b.* Only negative correlation were found in C57BL/6 macrophages. Only negative correlation were found in C57BL/6 macrophages, *Cybb-Tnf* and *Il6-Tlr2.*
- Bug2148 cl1: The correlation between *T. cruzi-Slamf1* changes from positive in BALB/c to negative in C57BL/6 macrophages. Positive correlation between *Irg1-Cybb, Irg1-Il6* and *Slamf1-Tlr2,* and negative correlations between *Arg1-Il6* was found for BALB/c.
- VFRA cl1: We found only correlation in BALB/c macrophages where positive were *Arg1-Cybb, Arg1-Il10, Arg1-Tnf* and *Cybb-Il10,* and negative was *Il6-Tlr2.*

Finally, Table S 4 present the correlations during the intracellular proliferation.

- Dm28c: We found only correlation in C57Bl/6 macrophages where positive was *Il10-Cybb*, and the negative was *Slmaf1-Tlr2.*
- Y: BALB/c macrophages presented only positive correlation between *Cybb-Tnf, Il6-Tnf* and *Tlr2-T. cruzi*. C57BL/6 present a positive correlation between *Slamf1-Tlr2*, and negatives correlation between *Arg1-Irg1* and *Slamf1-Tlr2.*
- 10R26: Positive correlation were found in BALB/c between *Il6-Tnf, Slamf1-Tlr2* and *Slamf1-T. cruzi.*In the case of C57BL/6 the positive correlation were *Arg1-Il1b, Arg1-Il6, Arg-Tlr2* and *Il1b-Il6,* the negative correlation was *Tlr2-T. cruzi.*

Table S 4. Gene Expression and parasite load correlations in BALB/c (Right) and C57BL/6(Left) peritoneal macrophages infected with different strains of T. cruzi in the intracellular proliferation (24h).

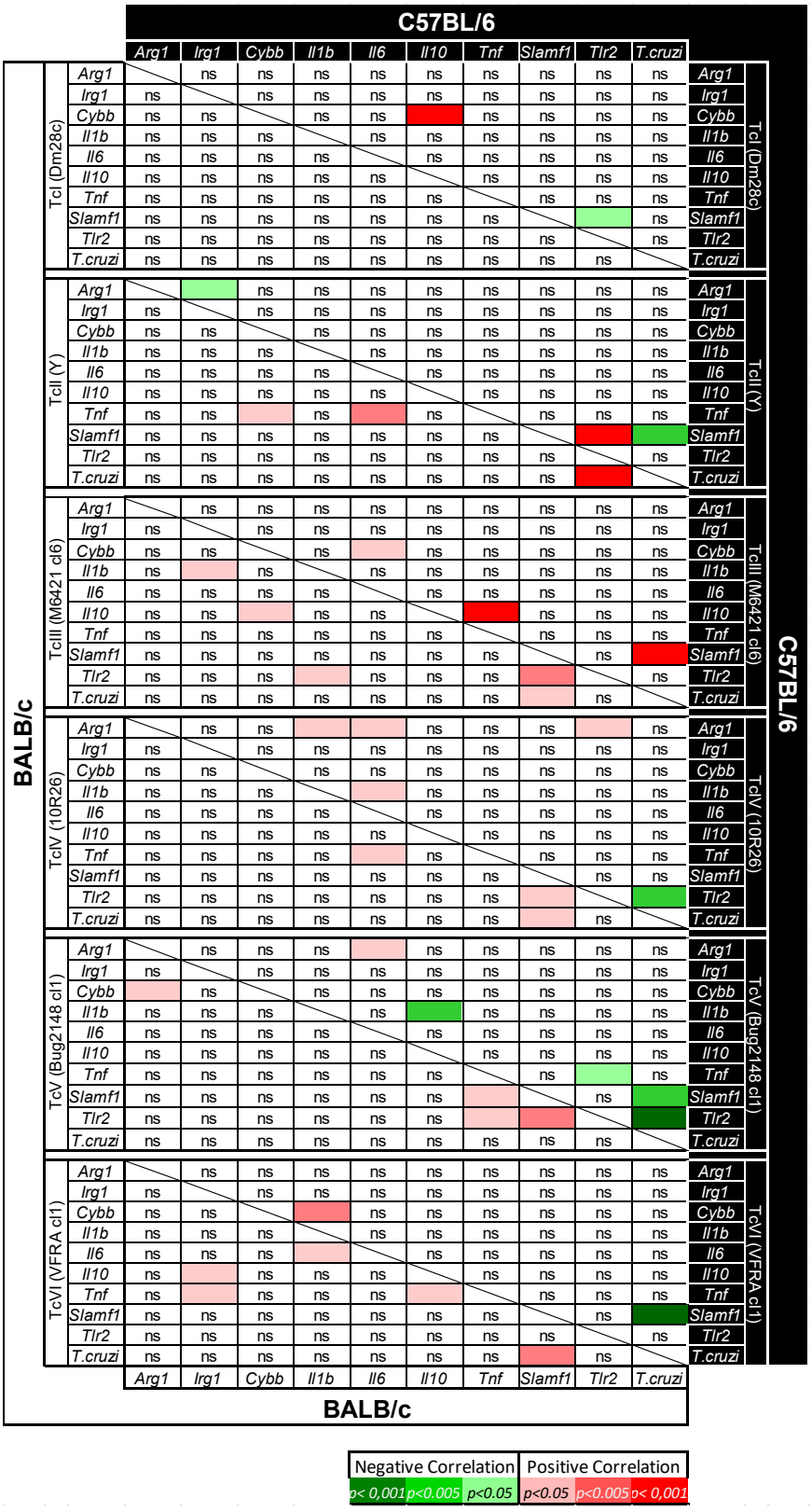

- Bug2148 cl1: Only positive correlations were found in BALB/c macrophages between *Arg1-Cybb, Tnf-Slamf1* and *Slamf1-Tlr2.* The correlation between *Tnf-Tlr2* changes from positive in BALB/c to negative in C57BL/6 macrophages. A positive correlation was found in C57BL/6 between *Arg1-Il6,* and negatives correlation between *Il1b-Il10, Slamf1-T. cruzi* and *Tlr2-T. cruzi.*
- M6421 cl6: For both background we found positive correction. BALB/c were *Irg1-Il1b, Cybb-Il10, Il1b-Tlr2* and *Slamf1-Tlr2*. C57BL/6 were *Il6-Cybb* and *Il10-Tnf.*
- VFRA cl1: Only positive correlations were found in BALB/c macrophages between *Irg1-Il10, Irg1-Tnf, Il1b-Il6* and *Il10-Tnf.* The correlation between *Slamf1-T. cruzi* changes from positive in BALB/c to negative in C57BL/6 macrophages. The positive correlation between *Cybb-Il1b* was found in C57BL/6 macrophages.

Table S 5 shows the correlation during the Interaction:

- Dm28c: Positive correlations associated with the *Tlr2* deficiency were found in *Tlr2*$^{-/-}$ macrophages between *Arg1-Tnf* and I*rg1-Tnf,* and a negative correlation between *Irg1-Il6.* The correlations that disappear from C57BL/6 to *Tlr2*$^{-/-}$ macrophages were the positive between *Arg1-Il1b, Arg1-Il10, Cybb-Il6, Il1b-Tnf* and *Tlr2-T. cruzi,* and the negatives *Arg1-Cybb, Cybb-Il1b, Cybb-Il10* and *Il10-Il6.*
- Y: Positive correlations associated with the *Tlr2* deficiency were found in *Tlr2*$^{-/-}$ macrophages between *Arg1-Irg1, Arg1-Tnf* and *Il1b-Il6,* and negative correlations were *Arg1-Il1b, Arg1-Il6, Irg1-Il1b, Irg1-Il6, Il1b-Tnf* and *Il6-Tnf.* All the correlations that disappear from C57BL/6 to *Tlr2*$^{-/-}$ macrophages were the positive between *Cybb-Il10, Cybb-Tnf* and *Tlr2-T. cruzi.*
- M6421 cl6: Only positive correlations associated with the *Tlr2* deficiency were found in *Tlr2*$^{-/-}$ macrophages between *Irg1-Il1b* and *Cybb-Tnf.* The correlations that disappear from C57BL/6 to *Tlr2*$^{-/-}$ macrophages was the positive between *Arg1-Il6,* and the negatives *Arg1-Irg1, Irg1-Il6, Cybb-Slamf1* and *Slamf1-T. cruzi.*

8.2.3 TLR2 in macrophages

Table S 5. Gene expression and parasite load correlation between C57BL/6 (Right) and Tlr2$^{-/-}$ (Left) peritoneal macrophages infected with different strains of T. cruzi in the interaction (1h).

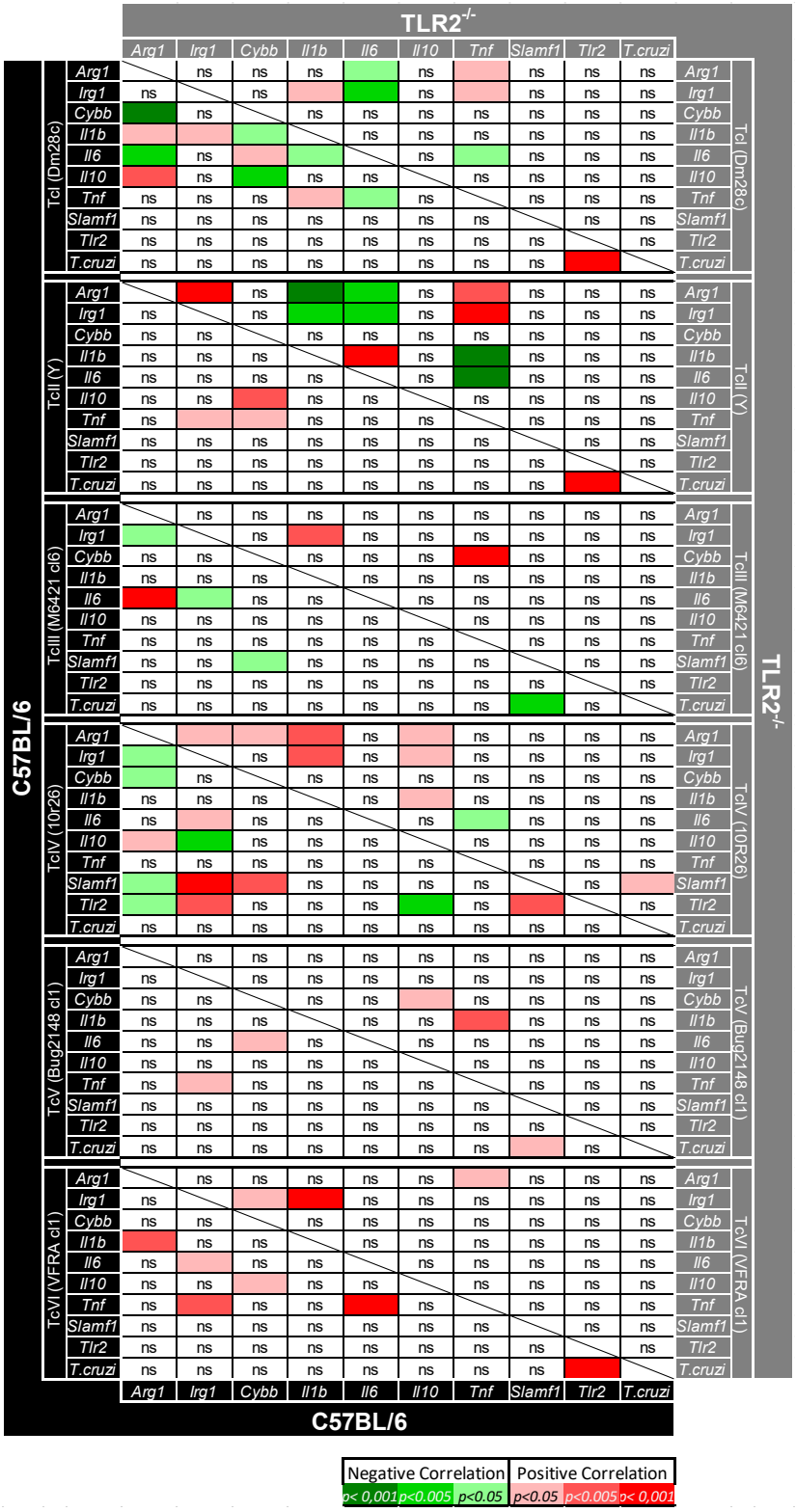

- 10R26: Positive correlations associated with the *Tlr2* deficiency were found in *Tlr2*$^{-/-}$ macrophages between *Arg1-Il1b, Irg1-Il1b, Il1b-Il10* and *Slamf1-T. cruzi,* and the negative correlation between *Il6-Tnf.* The correlations between *Arg1-Irg1, Arg1-Cybb* and *Irg1-Il10* changes from positive in C57BL/6 to negative in *Tlr2*$^{-/-}$ macrophages. The correlations that disappear from C57BL/6 to *Tlr2*$^{-/-}$ macrophages were the positive between *Irg1-Il6, Irg1-Slamf1, Irg1-Tlr2, Cybb-Slamf1* and *Slamf1-Tlr2,* and the negatives were *Arg1-Slamf1, Arg1-Tlr2* and *Il10-Tlr2.*
- Bug2148 cl1: Only positive correlations associated with the *Tlr2* deficiency were found in *Tlr2*$^{-/-}$ macrophages between *Cybb-Il10* and *Il1b-Tnf.* The correlations that disappear from C57BL/6 to *Tlr2*$^{-/-}$ macrophages were the positive between *Irg1-Tnf, Cybb-Il6* and *Slamf1-T. cruzi.*
- VFRA cl1: Only positive correlations associated with the *Tlr2* deficiency were found in *Tlr2*$^{-/-}$ macrophages between *Arg1-Tnf, Irg1-Cybb* and *Irg1-Il1b.* The correlations that disappear from C57BL/6 to *Tlr2*$^{-/-}$ macrophages were the positive between *Arg1-Il1b, Irg1 Il6, Irg-Tnf, Cybb-Il10, Il6-Tnf* and *Tlr2-Tnf.*

Table S **6** shows the correlation during the Internalization:

- Dm28c: Positive correlation associated with the *Tlr2* deficiency was found in *Tlr2*$^{-/-}$ macrophages between *Cybb-Il1b,* and a negative correlation between *Il1b-Il10.* The correlations between *Cybb-Il10* changes from positive in C57BL/6 to negative in *Tlr2*$^{-/-}$ macrophages. The correlations that disappear from C57BL/6 to *Tlr2*$^{-/-}$ macrophages were the positive between *Il10-Tnf* and *Slamf1-Tlr2,* and the negatives *Slamf1-T. cruzi* and *Tlr2-T. cruzi.*
- Y: Positive correlations associated with the *Tlr2* deficiency were found in *Tlr2*$^{-/-}$ macrophages between *Cybb-Irg1, Il1b-Irg1, Il1b-Cybb, Tnf-Irg1, Tnf-Cybb* and *Tnf-Il1b.* The correlations that disappear from C57BL/6 to *Tlr2*$^{-/-}$ macrophages were the positive between *Il6-Tnf,* and the negative *Arg1-Il10.*
- M6421 cl6: Positive correlation associated with the *Tlr2* deficiency was found in *Tlr2*$^{-/-}$ macrophages between *Il10-Irg1,* and the negatives *Il6-Cybb* and *Tnf-Il1b.* The correlations correlations that disappear from C57BL/6 to *Tlr2*$^{-/-}$ macrophages were the positive between *Il1b-Il6,* and the negative *Il6-Tlr2.*

Table S 6. Gene expression and parasite load correlation between C57BL/6 (Right) and Tlr2$^{-/-}$ (Left) Peritoneal macrophages infected with different strains of T. cruzi in the internalization (6h).

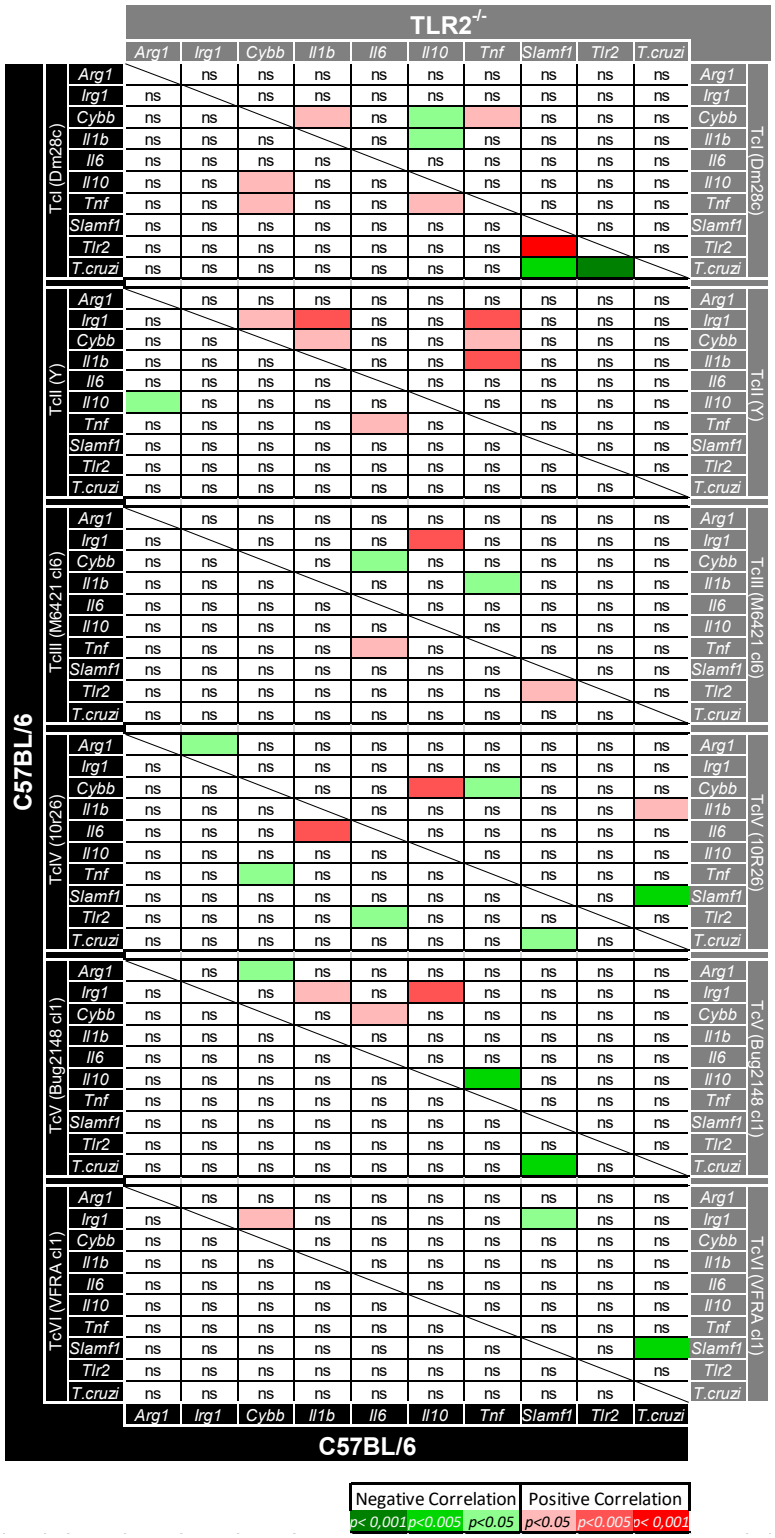

Table S 7 shows the correlation during the Intracellular proliferation:

- Dm28c: Positive correlations associated with the *Tlr2* deficiency were found in *Tlr2*$^{-/-}$ macrophages between *Arg1-Il1b* and *Il10-Tnf,* and the negatives *Arg1-Cybb* and *Arg1-Il6.* The correlation that disappear from C57BL/6 to *Tlr2*$^{-/-}$ macrophages was the positive between *Cybb-Il10,* and negative *Slamf1-Tlr2.*
- Y: Positive correlations associated with the *Tlr2* deficiency were found in *Tlr2*$^{-/-}$ macrophages between *Cybb-Il1b, Tnf-Cybb* and *Il1b-Tnf,* and a negative correlation between *Slamf1-Arg1.* The correlation that disappear from C57BL/6 to *Tlr2*$^{-/-}$ macrophages was the positive between *Slamf1-Tlr2,* and the negatives *Arg1-Irg1* and *Slamf1-T. cruzi.*
- M6421 cl6: Positive correlations associated with the *Tlr2* deficiency were found in *Tlr2*$^{-/-}$ macrophages between *Il1b-Cybb, Cybb-Tnf* and *Il1b-Tnf.* The correlations that disappear from C57BL/6 to *Tlr2*$^{-/-}$ macrophages were the positive between *Cybb-Il6, Il10-Tnf* and *Slamf1-T. cruzi.*
- 10R26: Positive correlations associated with the *Tlr2* deficiency were found in *Tlr2*$^{-/-}$ macrophages between *Il10-Cybb, Cybb-Tnf, Cybb-Slamf1* and *Tnf-Slamf1,* and the negatives *Arg1-Cybb, Arg1-Tnf* and *Arg1-Slamf1.* The correlations that disappear from C57BL/6 to *Tlr2*$^{-/-}$ macrophages were the positive between *Arg1-Il1b, Arg1-Il6, Arg-Tlr2* and *Il1b-Il6,* and the negative *Tlr2-T. cruzi.*
- Bug2148 cl1: Positive correlations associated with the *Tlr2* deficiency were found in *Tlr2*$^{-/-}$ macrophages between *Irg1-Cybb, Irg1-Il1b, Irg1-Il6* and *Cybb-Il1b.* The correlations that disappear from C57BL/6 to *Tlr2*$^{-/-}$ macrophages were the positive between *Arg1-Il6, Tnf-Tlr2* and *Slamf1-T. cruzi,* and the negatives *Il1b-Il10* and *Tlr2-T. cruzi.*
- VFRA cl1: Only a negative correlation associated with the *Tlr2* deficiency was found in *Tlr2*$^{-/-}$ macrophages between *Irg1-Slamf1.* The correlation that disappear from C57BL/6 to *Tlr2*$^{-/-}$ macrophages was the positive between *Cybb-Il1b,* and the negative *Slamf1-T. cruzi*

Table S 7. Gene expression and parasite load correlation between C57BL/6 (Right) and Tlr2$^{-/-}$ (Left) peritoneal macrophages infected with different strains of T. cruzi in the intracellular proliferation (24h).

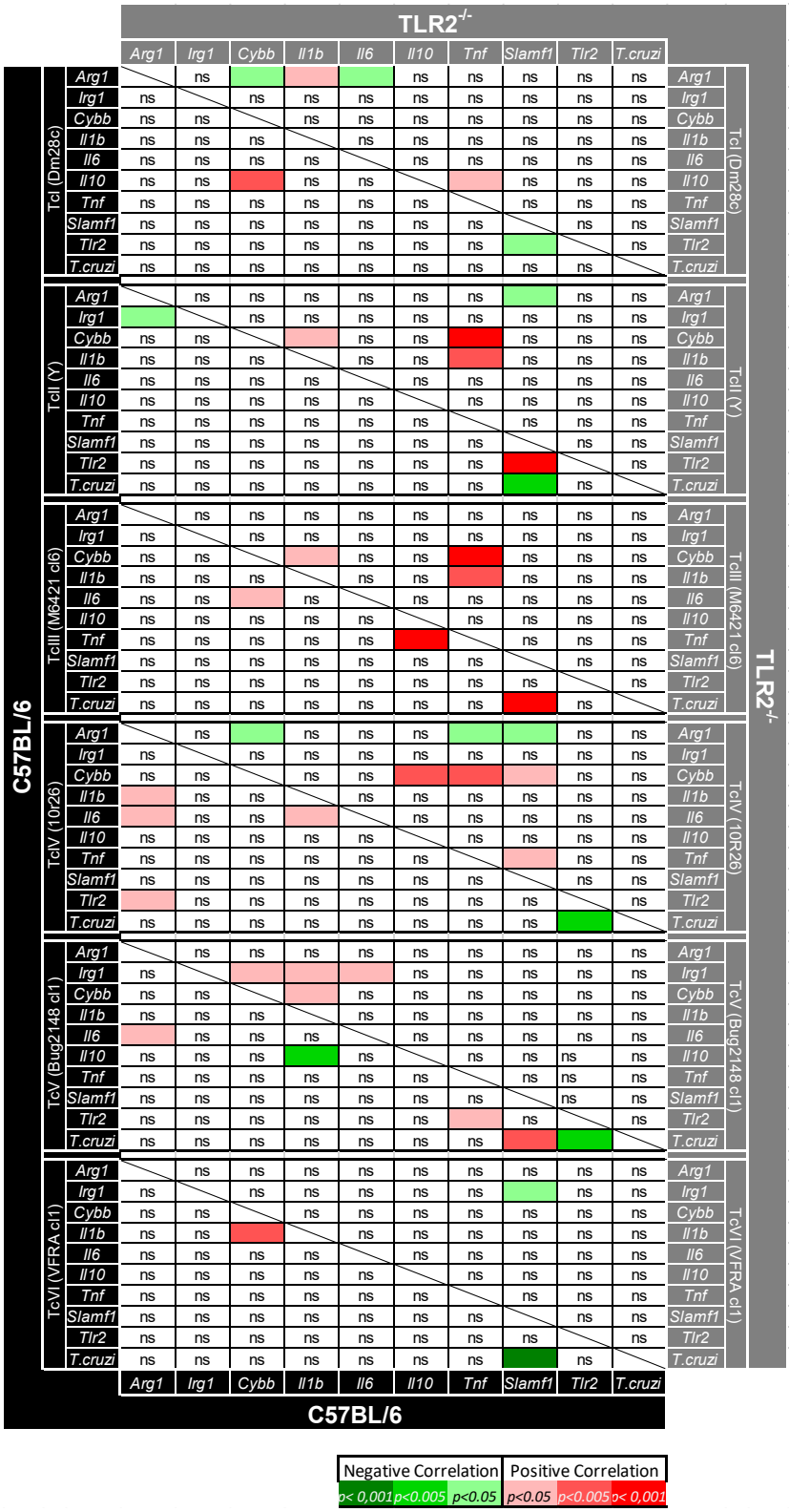

8.2.4 SLAMF1 in macrophages

Table S 8 shows the correlation during the Interaction:

- Dm28c) Positive correlations associated with the Slamf1 deficiency were found in *Slamf1*$^{-/-}$ macrophages between *Arg1-Irg1, Arg1-Cybb, Arg1-Tlr2, Irg1-Cybb, Irg1-Il6, Irg1-Tnf* and *Il6-Tlr2.* The correlations that disappear from BALB/c to *Slamf1*$^{-/-}$ macrophages were the positive between *Arg1-Il1b*, *Cybb-Il6, Cybb-Tnf, Il1b-Il6, Il1b-Il10* and *Il6-Il10*
- Y: Positive correlations associated with the Slamf1 deficiency were found in *Slamf1*$^{-/-}$ macrophages between *Irg1-Tnf, Cybb-Il6* and *Il10-T. cruzi,* and the negative *Tnf-Tlr2.* The correlation between *Arg1-Il6* changes from positive in BALB/c to negative in *Slamf1*$^{-/-}$ macrophages. The correlations that disappear from BALB/c to *Slamf1*$^{-/-}$ macrophages were the positive between *Arg1-Il1b, Arg1-Il10, Arg1-Tnf, Il1b-Il6, Il1b-Il10, Il1b-Tnf, Il6-Il10, Il6-Tnf, Il10-Tnf* and *Slamf1-Tlr2.*
- M6421 cl6: Positive correlations associated with the Slamf1 deficiency were found in *Slamf1*$^{-/-}$ macrophages between *Arg1-Cybb, Arg1-Il6, Arg1-Il10, Cybb-Il1b, Cybb-Il6, Cyb-Il10, Irg1-Tlr2, Il1b-Il6, Il1b-Il10, Il6-Il10, Il6-Tnf* and *Il10-Tnf.* The correlations that disappear from BALB/c to *Slamf1*$^{-/-}$ macrophages were the positive between *Arg1-Irg1* and *Cybb-T. cruzi.*
- 10R26: Positive correlations associated with the Slamf1 deficiency were found in *Slamf1*$^{-/-}$ macrophages between *Irg1-Cybb, Irg1-Il1b, Irg1-Il6, Irg1-Il10, Irg1-Tnf, Cybb-Il10, Cybb-Tnf, Il1b-Il10, Il6-Il10* and *Il10-Tnf.* The correlations that disappear from BALB/c to*Slamf1*$^{-/-}$ macrophages were the positive between *Arg1-Irg1, Irg1-Tlr2, Il1b-Tlr2* and *Il6-Tlr2,* and the negative *Slamf1-Tlr2.*
- Bug2148 cl1: Positive correlations associated with the Slamf1 deficiency were found in *Slamf1*$^{-/-}$ macrophages between *Arg1-Il10* and *Cybb-Il6.* The correlations that disappear from BALB/c to *Slamf1*$^{-/-}$ macrophages were the positive between *Irg1-Cybb, Irg1-Tnf* and *Cybb-Tnf,* and the negatives *Slamf1-T. cruzi* and *Tlr2-T. cruzi.*
- VFRA cl1: Positive correlation associated with the Slamf1 deficiency was found in *Slamf1*$^{-/-}$ macrophages between *Arg1-Il1b.* . The correlations that disappear from BALB/c to *Slamf1*$^{-/-}$ macrophages were the positive between *Arg1-Il6, Arg1-Tnf, Il1b-Il6, Il1b-Tnf, Il6-Il10, Il6-Tnf* and *Il10-Tnf.*

Table S 8. Gene Expression and parasite load correlations in BALB/c (Right) and Slamf1$^{-/-}$ (Left) peritoneal macrophages infected with different strains of T. cruzi in the interaction (1h).

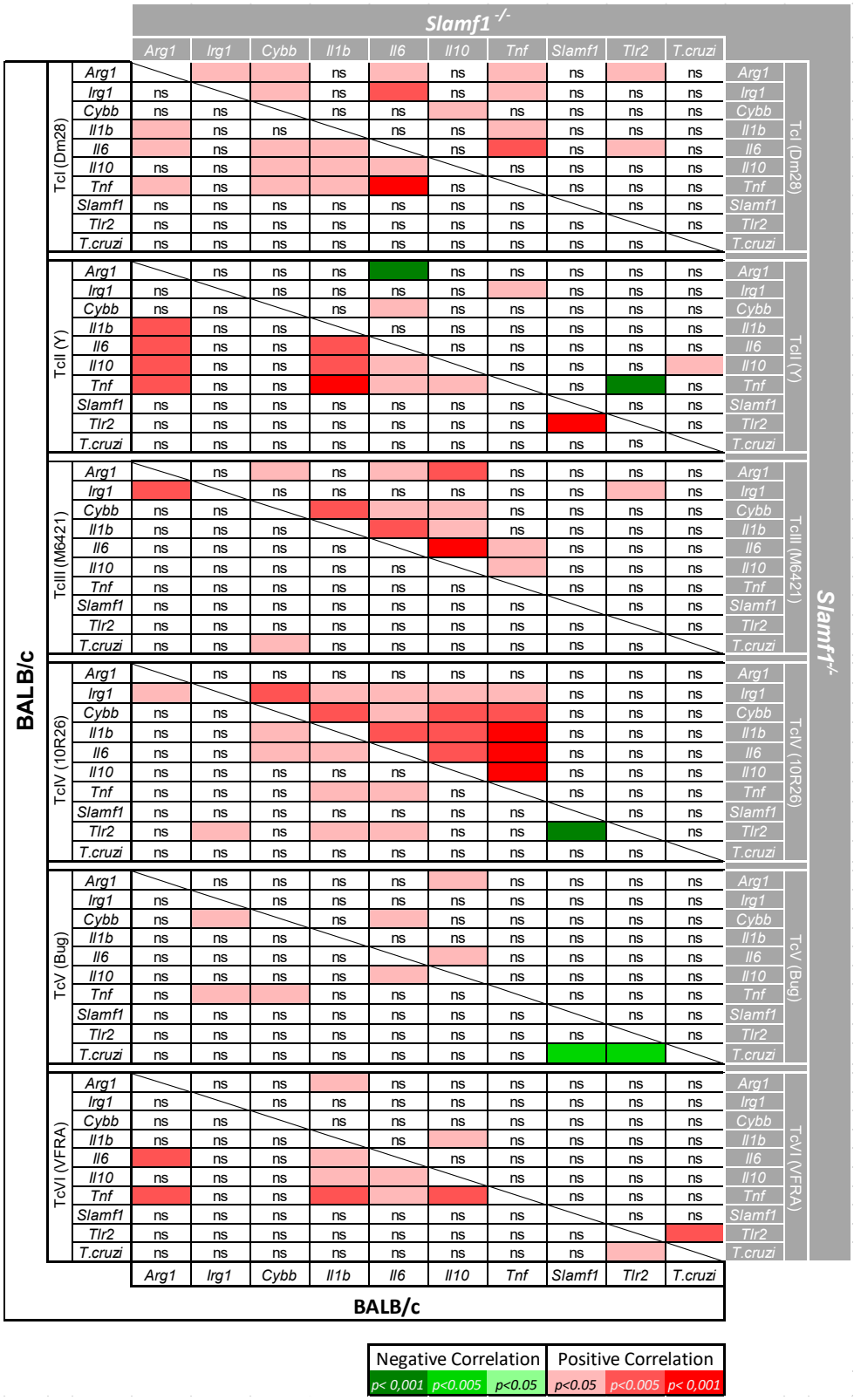

Table S 9. Gene Expression and parasite load correlations in BALB/c (Right) and Slamf1$^{-/-}$ (Left) peritoneal macrophages infected with different strains of T. cruzi in the internalization (6h).

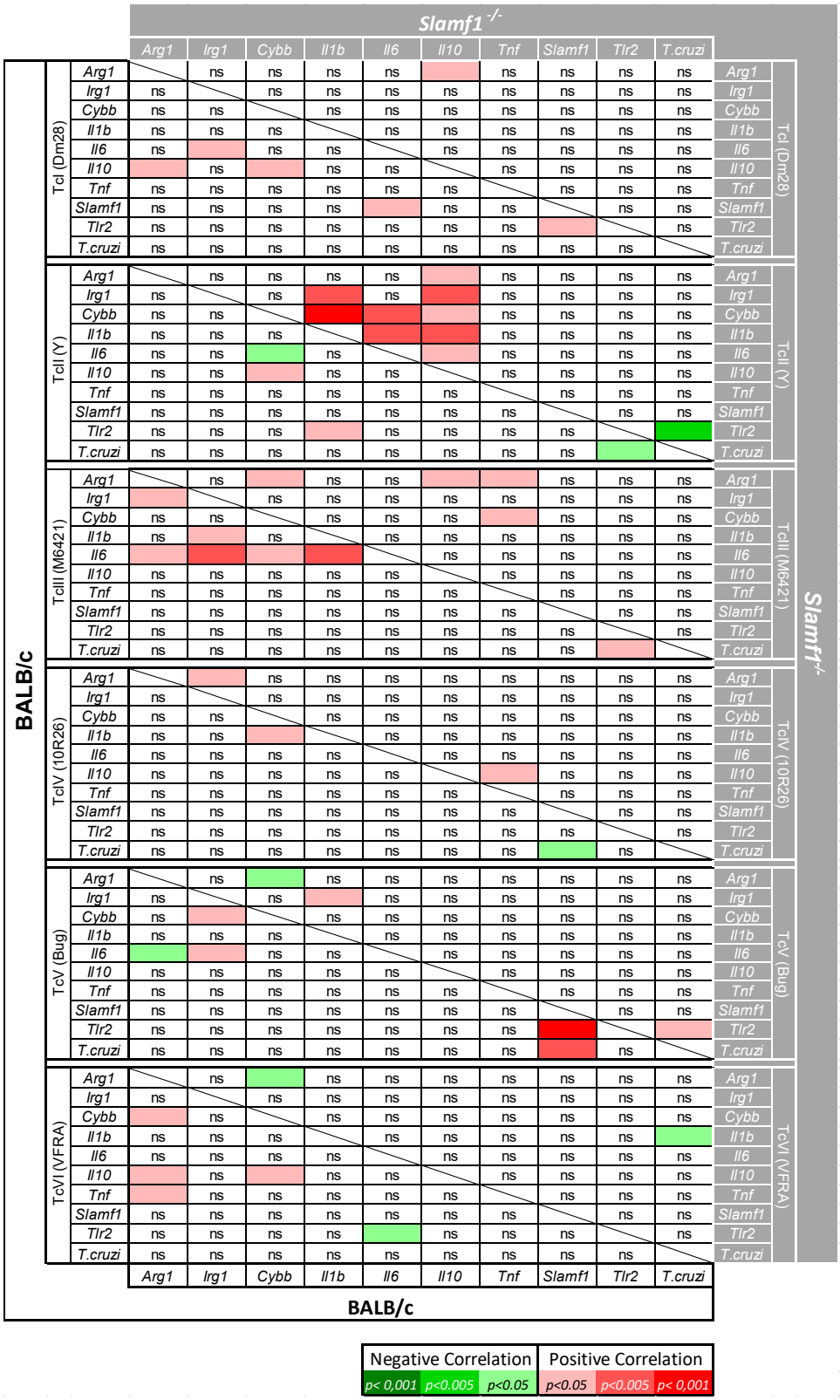

Table S 9 shows the correlation during the Internalization:

- Dm28c: The correlations that disappear from BALB/c to *Slamf1*$^{-/-}$ macrophages were the positive between *Irg1-Il6, Cybb-Il10, Il6-Slamf1* and *Slamf1-Tlr2.*
- Y: Positive correlations associated with the Slamf1 deficiency were found in *Slamf1*$^{-/-}$ macrophages between *Arg1-Il10, Irg1-Il1b, Irg1-Il10, Cybb-Il1b, Il1b-Il6, Il1b-Il10* and *Il6-Il10.* The correlation between *Cybb-Il6* changes from negative in BALB/c to positive in *Slamf1*$^{-/-}$ macrophages. The correlation that disappear from BALB/c to *Slamf1*$^{-/-}$ macrophages was the positive between *Il1b-Tlr2.*
- M6421 cl6: Positive correlations associated with the Slamf1 deficiency were found in *Slamf1*$^{-/-}$ macrophages between *Arg1-Cybb, Ag1-Il10, Arg1-Tnf* and *Cybb-Tnf.* The correlations that disappear from BALB/c to *Slamf1*$^{-/-}$ macrophages were the positive between *Arg1-Irg1, Arg1-Il6, Irg1-Il1b, Irg1-Il6, Cybb-Il6, Il1b-Il6* and *Tlr2-T. cruzi.*
- 10R26: Positive correlations associated with the Slamf1 deficiency were found in *Slamf1*$^{-/-}$ macrophages between *Arg1-Irg1* and *Il10-Tnf.* The correlation that disappear from BALB/c to *Slamf1*$^{-/-}$ macrophages was the positive between *Cybb-Il1b,* and the negative *Slamf1-T. cruzi.*
- Bug2148 cl1: Positive correlations associated with the Slamf1 deficiency were found in *Slamf1*$^{-/-}$ macrophages between *Irg1-Il1b* and *Tlr2-T. cruzi,* and the negative *Arg1-Cybb.*
- VFRA cl1: Negative correlation associated with the Slamf1 deficiency was found in *Slamf1*$^{-/-}$ macrophages between *Il1b-T. cruzi.* The correlation between *Arg1-Cybb* changes from positive in BALB/c to negative in *Slamf1*$^{-/-}$ macrophages. The correlations that disappear from BALB/c to *Slamf1*$^{-/-}$ macrophages were the positive between *Arg1-Il10, Arg1-Tnf* and *Cybb-Il10,* and the negative *Il6-Tlr2.*

Table S 10 shows the correlation during the Intracellular proliferation:

- Dm28c: Positive correlations associated with the Slamf1 deficiency were found in *Slamf1*$^{-/-}$ macrophages between *Arg1-Il6* and *Arg1-T. cruzi.*
- Y: Positive correlations associated with the Slamf1 deficiency were found in *Slamf1*$^{-/-}$ macrophages between *Irg1-Il6, Irg1-Il10, Il1b-Il10* and *Il1b-Tnf.* The correlations that disappear from BALB/c to *Slamf1*$^{-/-}$ macrophages were the positive between *Cybb-Tnf* and *Il6-Tnf.*The correlations that disappear from BALB/c to *Slamf1*$^{-/-}$ macrophages were the positive between *Irg1-Cybb, Irg1-Il6, Slamf1-Tlr2* and *Slamf1-T. cruzi,* and the negative *Arg1-Il6.*

Table S 10. Gene Expression and parasite load correlations in BALB/c (Right) and Slamf1$^{-/-}$ (Left) peritoneal macrophages infected with different strains of T. cruzi in the intracellular proliferation (24 h).

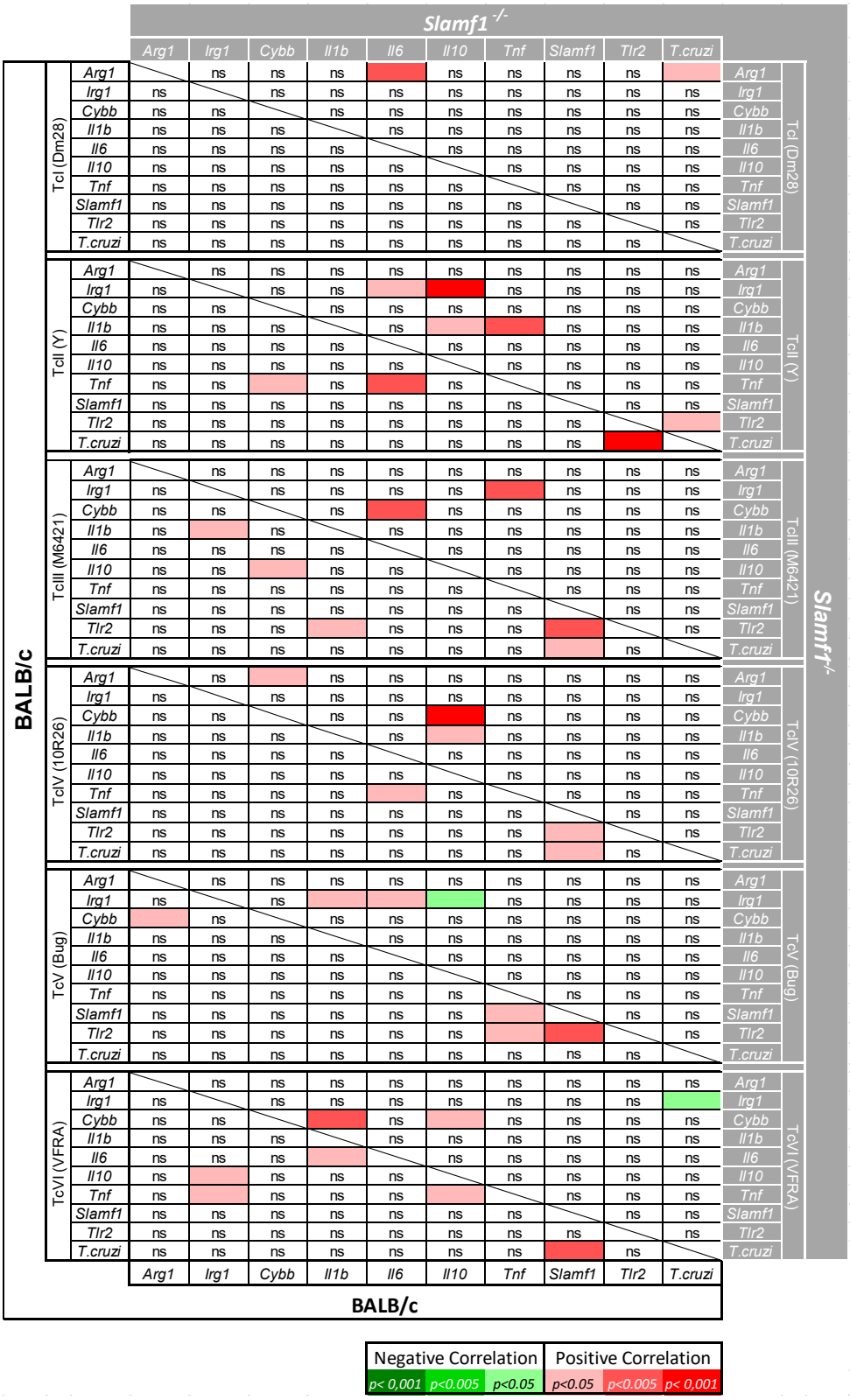

- M6421 cl6: Positive correlations associated with the Slamf1 deficiency were found in *Slamf1*$^{-/-}$ macrophages between *Irg1-Tnf* and *Cybb-Il6.* The correlations that disappear from BALB/c to *Slamf1*$^{-/-}$ macrophages were the positive between *Irg1-Il1b, Cybb-Il10, Il1b-Tlr2, Slamf1-Tlr2* and *Slamf1-T. cruzi.*
- 10R26: Positive correlations associated with the Slamf1 deficiency were found in *Slamf1*$^{-/-}$ macrophages between *Arg1-Cybb, Cybb-Il10* and *Il1b-Il10.* The correlations that disappear from BALB/c to *Slamf1*$^{-/-}$ macrophages were the positive between *Il6-Tnf, Slamf1-Tlr2* and *Slamf1-T. cruzi.*
- Bug2148 cl1: Positive correlations associated with the Slamf1 deficiency were found in *Slamf1*$^{-/-}$ macrophages between *Irg1-Il1b* and *Irg1-Il6,* and the negative *Irg1-Il10.* The correlations that disappear from BALB/c to *Slamf1*$^{-/-}$ macrophages were the positive between *Arg1-Cybb, Tnf-Slamf1, Tnf-Tlr2* and *Slamf1-Tlr2.*
- VFRA cl1: Positive correlations associated with the Slamf1 deficiency were found in *Slamf1*$^{-/-}$ macrophages between *Cybb-Il1b* and *Cybb-Il10,* and the negative *Irg1-T. cruzi.* The correlations that disappear from BALB/c to *Slamf1*$^{-/-}$ macrophages were the positive between *Irg1-Il10, Irg1-Tnf, Il1b-Il6, Il10-Tnf* and *Slamf1-T. cruzi.*

8.2.5 Spleen

Table S 11. Gene Expression and parasite load correlations in the spleens of BALB/c (Right) and Slamf1*$^{-/-}$ *(Left) mice infected with different strains of T. cruzi at 14 d.p.i. *Red Color positive correlation p<0.001.*

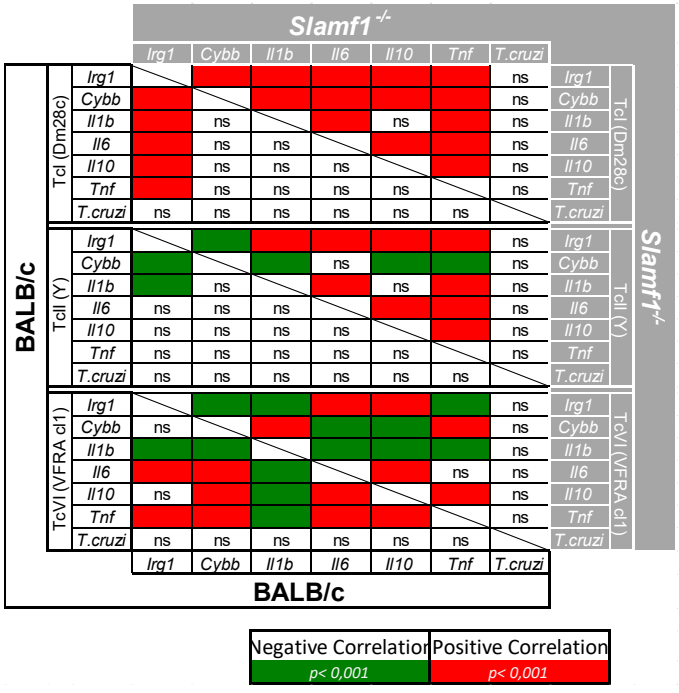

Appearance and disappearance in the correlations between the spleen of BALB/c and *Slamf1*$^{-/-}$ mice at 14d.p.i. indicate the role of SLAMF1 receptor in the infection with the different strains of *T. cruzi* (Table S 11).

- Dm28c: Positive correlations associated with the SLAMF1 deficiency were found in spleen of *Slamf1*$^{-/-}$ mice between *Cybb-Il1b, Cybb-Il6, Cybb-Il10, Cybb-Tnf, Il1b-Il6, Il1b-Tnf, Il6-Il10, Il6-Tnf* and *Il10-Tnf.*
- Y: Positive correlations associated with the SLAMF1 deficiency were found in spleen of *Slamf1*$^{-/-}$ mice between *Irg1-Il6, Irg1-Il10, Irg1-Tnf, Il1b-Il6, Il1b-Tnf, Il6-Il10, Il6-Tnf* and *Il10-Tnf,* and the negatives *Cybb-Il1b, Cybb-Il10* and *Cybb-Tnf.* The correlation between *Irg1-Il1b* changes from negative in BALB/c to positive in *Slamf1*$^{-/-}$ mice.
- VFRA cl1: Positive correlations associated with the SLAMF1 deficiency were found in spleen of *Slamf1*$^{-/-}$ mice between *Irg-Il10* and the negative *Irg1-Cybb.* The correlation that disappear from the spleen of BALB/c to *Slamf1*$^{-/-}$ mice was *Il6-Tnf.* The correlation between *Irg1-Tnf, Cybb-Il6* and *Cybb-Il10* changes from positive in BALB/c to negative in *Slamf1*$^{-/-}$ mice, and negative to positive was *Cybb-Il1b.*

Table S 12. Gene Expression and parasite load correlations in the spleens of BALB/c (Right) and Slamf1*$^{-/-}$ *(Left) mice infected with different strains of T. cruzi at 21 d.p.i. *Red Color positive correlation p<0.001.*

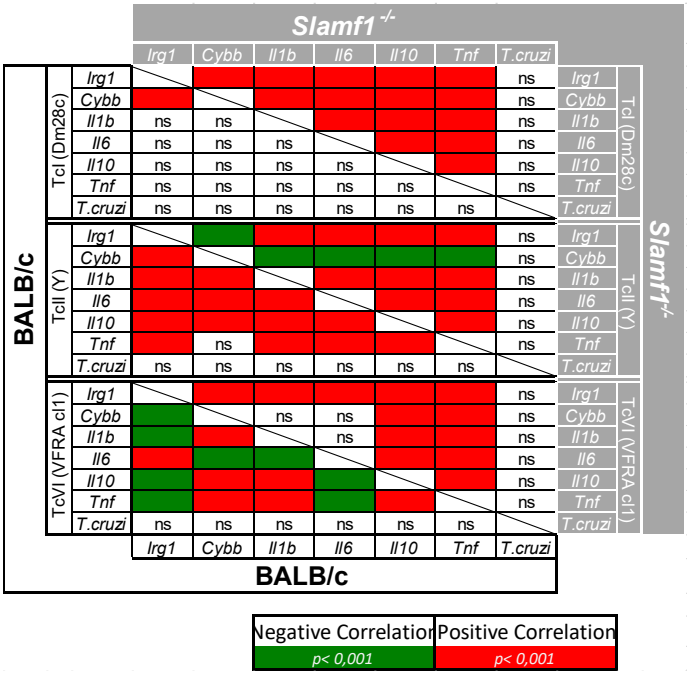

The correlation in the spleen at 21 d.p.i. are explained on Table S 12.

- Dm28c: Positive correlations associated with the SLAMF1 deficiency were found in spleen of *Slamf1*$^{-/-}$ mice between *Irg1-Il1b, Irg1-Il6, Irg1-Il10, Irg1-Tnf, Cybb-Il1b, Cybb-Il6, Cybb-Il10, Cybb-Tnf, Il1b-Il6, Il1b-Il10, Il1b-Tnf, Il6-Il10, Il6-Tnf* and *Il10-Tnf.*
- Y: Negative correlation associated with the Slamf1 deficiency was found in spleen of *Slamf1*$^{-/-}$ mice between *Cybb-Tnf.* The correlation between *Irg1-Cybb, Irg1-Il1b, Irg1-Il10, Irg1-Tnf, Il6-Il10* and *Il6-Tnf* changes from positive in BALB/c to negative in *Slamf1*$^{-/-}$ mice.
- VFRA cl1: The correlations that disappear from the spleen of BALB/c to *Slamf1*$^{-/-}$ mice were the positive between *Cybb-Il1b,* and the negative were *Cybb-Il6* and *Il1b-Il6.* The correlation between *Irg1-Tnf, Cybb-Il6* and *Cybb-Il10* changes from negative in BALB/c to positive in *Slamf1*$^{-/-}$ mice

8.2.6 Heart

Appearance and disappearance in the correlations between the heart of BALB/c and *Slamf1*$^{-/-}$ mice at 14 d.p.i. indicate the role of SLAMF1 receptor in the infection with the different strains of *T. cruzi* (Table S 13), all correlations were positive.

- Dm28c: The correlations that disappear from the heart of BALB/c to *Slamf1*$^{-/-}$ mice were the positive between *Irg1-Il10* and *Irg10-Tnf.*
- Y: Positive correlations associated with the Slamf1 deficiency were found in spleen of *Slamf1*$^{-/-}$ mice between *Irg1-Cybb, Cybb-Il1b* and *Cybb-Il10.* The correlations that disappear from the heart of BALB/c to *Slamf1*$^{-/-}$ mice were the positive between *Irg1-Il6* and *Il1b-Il6.*
- VFRA cl1: The correlations that disappear from the heart of BALB/c to *Slamf1*$^{-/-}$ mice were the positive between *Cybb-Il6, Cybb-Il10* and *Il6-Il10.*

Table S 13. Gene Expression and parasite load correlations in the hearts of BALB/c (Right) and Slamf1$^{-/-}$ (Left) mice infected with different strains of T. cruzi at 14 d.p.i. *Red Color positive correlation p<0.001.*

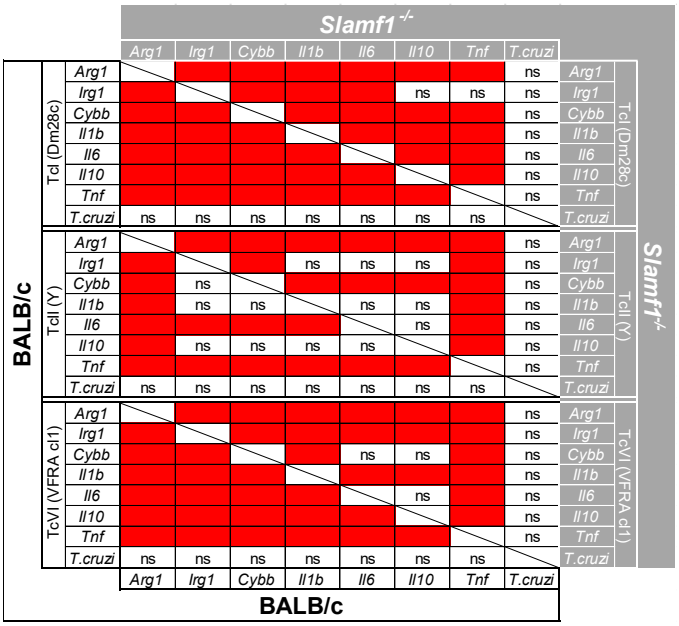

The correlation in the heart at 21 d.p.i. are explained on Table S 14.

- Dm28c: Negative correlation associated with the Slamf1 deficiency was found in heart of *Slamf1*$^{-/-}$ mice between *Irg1-Il1b.* The correlation between *Arg1-Ir1, Arg1-Il10, Cybb-Il6, Il1b-Il6,* and *Il6-Tnf* changes from negative in BALB/c to positive in *Slamf1*$^{-/-}$ mice, and the positive to negative *Arg1-Cybb, Arg1-Il1b, Arg1-Tnf* and *Irg1-Il6.*
- Y: The correlations that disappear from the heart of BALB/c to *Slamf1*$^{-/-}$ mice were the positive between *Arg1-Il6, Arg1-Il10, Irg1-Il6, Irg1-Il10, Cybb-Il1b, Cybb-Tnf, Il1b-Tnf* and *Il6-Il10* , and the negative *Arg1-Cybb, Arg1-Il1b, Arg1-Tnf, Irg1-Cybb, Irg1-Il1b, Irg1-Tnf, Cybb-Il6, Cybb-Il10, Il1b-Il6, Il1b-Il10, Il6-Tnf* and *Il10-Tnf.*
- VFRA cl1: Positive correlations associated with the SLAMF1 deficiency we found in spleen of *Slamf1*$^{-/-}$ mice between *Il1b-Tnf, Il6-Il10, Il6-Tnf* and *Il10-Tnf.* The correlations that disappear from the heart of BALB/c to *Slamf1*$^{-/-}$ mice was the negative between *Cybb-Il6.* The correlation between *Arg1-Il1b, Cybb-Il10, Cybb-Tnf, Il1b-Il6* and *Il1b-Il10* changes from negative in BALB/c to positive in *Slamf1*$^{-/-}$ mice, and positive to negative were *Irg1-Il10* and *Irg1-Tnf.*

Table S 14. Gene Expression and parasite load correlations in the hearts of BALB/c (Right) and Slamf1$^{-/-}$ (Left) mice infected with different strains of T. cruzi at 21 d.p.i. *Red Color positive correlation p<0.001.*

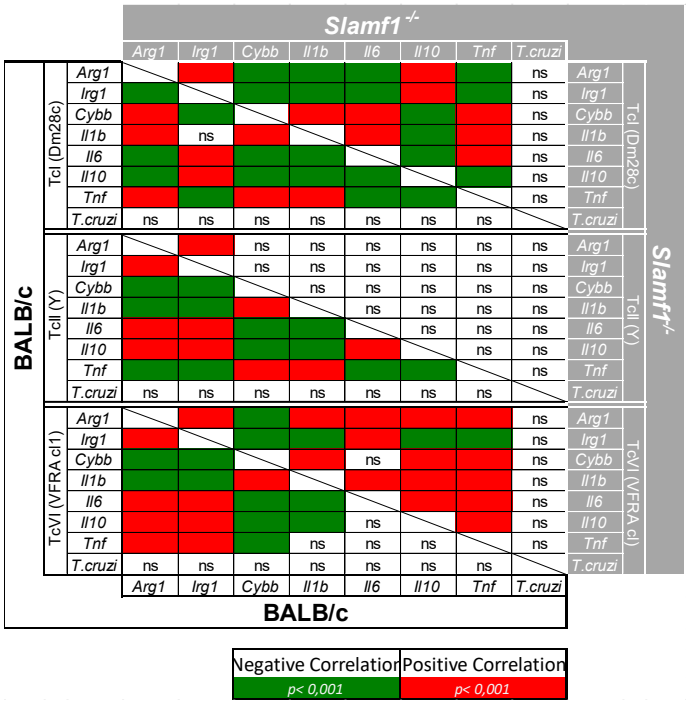

8.2.7 Liver

Appearance and disappearance in the correlations between the liver of BALB/c and *Slamf1*$^{-/-}$ mice at 14 d.p.i. indicate the role of SLAMF1 receptor in the infection with the different strains of *T. cruzi* (Table S 15) all correlations were positive.

- Dm28c: Positive correlations associated with the Slamf1 deficiency were found in spleen of *Slamf1*$^{-/-}$ mice between *Irg1-T. cruzi* and *Cybb-Il1b.*
- Y: The correlations that disappear from the liver of BALB/c to *Slamf1*$^{-/-}$ mice were the positive between *Irg1-Cybb, Irg1-Il1b, Irg1-Il6, Irg1-Il10, Irg1-Tnf, Cybb-Il1b, Cybb-Il10, Il1b-Il6, Il1b-Il10, Il1b-Tnf, Il6-Il10* and *Il10-Tnf.*
- VFRA cl1: Positive correlations associated with the Slamf1 deficiency were found in spleen of *Slamf1*$^{-/-}$ mice between *Irg1-Il10* and *Il1b-Il10.* The correlations that disappear from the liver of BALB/c to *Slamf1*$^{-/-}$ mice were the positive between *Irg1-Cybb, Irg1-Il6, Cybb-Il1b, Cybb-Il6* and *Il1b-Il6.*

Table S 15. Gene Expression and parasite load correlations in the livers of BALB/c (Right) and Slamf1$^{-/-}$ (Left) mice infected with different strains of T. cruzi at 14 d.p.i. *Red Color positive correlation p<0.001.*

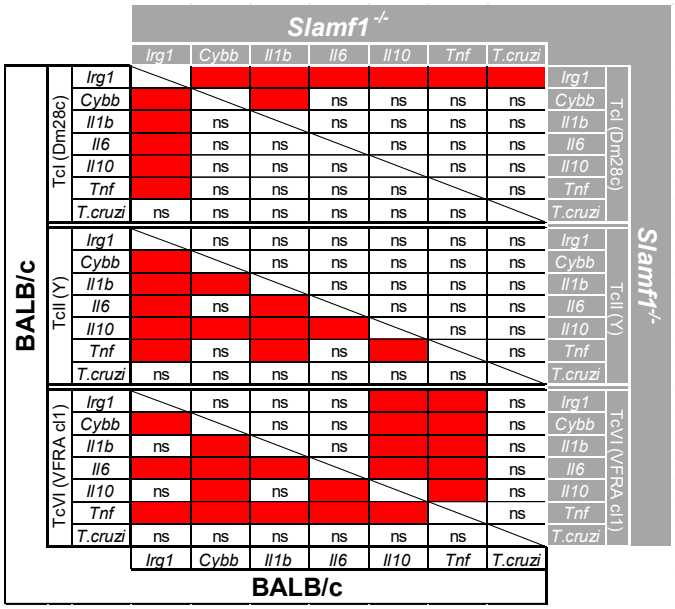

The correlation in the liver at 21 d.p.i. are explained on **Table S 16**.

Table S 16. Gene Expression and parasite load correlations in the livers of BALB/c (Right) and Slamf1$^{-/-}$ (Left) mice infected with different strains of T. cruzi at 21 d.p.i. *Red Color positive correlation p<0.001.*

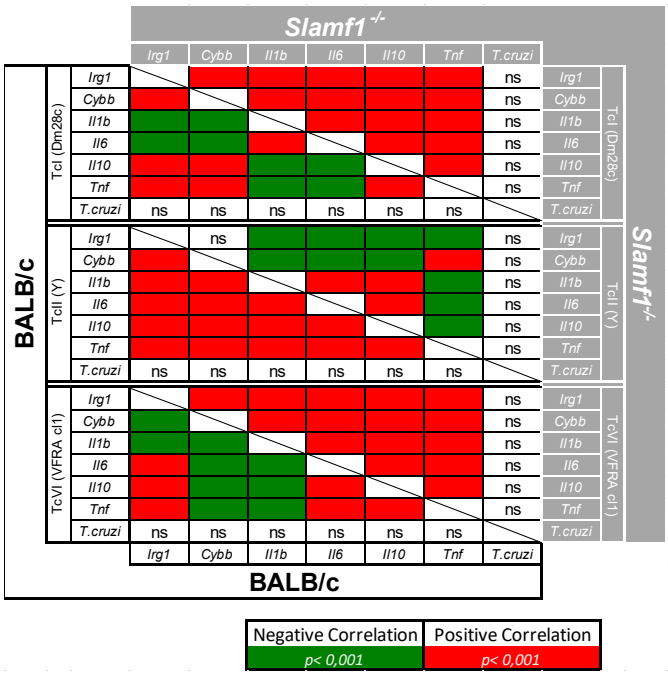

- Dm28c: The correlation between *Irg1-Il1b, Irg1-Il6, Cybb-Il1b, Cybb-Il6, Il1b-Il10, Il1b-Tnf, Il6-Il10* and *Il6-Tnf* changes from negative in BALB/c to positive in *Slamf1$^{-/-}$* mice.

- Y: The correlation that disappear from the liver of BALB/c to *Slamf1*$^{-/-}$ mice was the positive between *Irg1-Cybb.* The correlations that disappear from the heart of BALB/c to *Slamf1*$^{-/-}$ mice was the negative between *Cybb-Il6.* The correlation between *Irg1-Il1b, Irg1-Il6, Irg1-Il10, Irg1-Tnf, Cybb-Il1b, Cybb-Il6, Cybb-Il10, Il1b-Tnf* and *Il6-Tnf* changes from positive in BALB/c to negative in *Slamf1*$^{-/-}$ mice.
- VFRA cl1: The correlation between *Irg1-Cybb*, *Irg1-Il1b, Cybb-Il1b, Cybb-Il6,Cybb-Il10, Cybb-Tnf, Il1b-Il6, Il1b-Il10* and *Il1b-Tnf* changes from negative in BALB/c to positive in *Slamf1*$^{-/-}$ mice.

APPENDIX 2

Published articles

9 APPENDIX 2

Infection, Genetics and Evolution 21 (2014) 440–442

Contents lists available at ScienceDirect

Infection, Genetics and Evolution

journal homepage: www.elsevier.com/locate/meegid

Short communication

Distribution of *Trypanosoma cruzi* discrete typing units in Bolivian migrants in Spain

José A. Perez-Molina [a,*], Cristina Poveda [b], Angela Martinez-Perez [a], Felipe Guhl [b], Begoña Monge-Maillo [a], Manuel Fresno [c], Rogelio López-Velez [a], Juan D. Ramírez [b], Nuria Girones [c]

[a] Hospital Ramón y Cajal, Medicina Tropical y Parasitología Clínica, Servicio de Enfermedades Infecciosas, Madrid, Spain
[b] Centro de Investigaciones en Microbiología y Parasitología Tropical, CIMPAT, Universidad de los Andes, Cra 1 No. 18A-10, Bogotá, Colombia
[c] Centro de Biología Molecular Severo Ochoa, CSIC-UAM, Cantoblanco, Madrid, Spain

ARTICLE INFO

Article history:
Received 13 September 2013
Received in revised form 14 December 2013
Accepted 17 December 2013
Available online 3 January 2014

Keywords:
Trypanosoma cruzi
Discrete typing units
Chagas disease
Migration

ABSTRACT

Chagas disease is caused by the protozoan *Trypanosoma cruzi*. This parasite is transmitted to humans mainly through the faeces of infected triatomine "kissing" bugs, by blood transfusions or organ donation from infected donors, and can be transmitted from mother to child. This disease is endemic in the Americas, where Bolivia has up to 28.8% prevalence in general population. Increased migration to Europe has made it emerge in countries where it was previously unknown, being Spain the second country in number of patients after the United States. *T. cruzi* is an organism with a rich genetic diversity, what has been grouped into six discrete typing units (DTUs). Some authors have linked these DTUs either to specific geographical distribution or to the different clinical presentations. Nevertheless little is known about its distribution in migrant populations. Our aim was to describe the *T. cruzi* strains isolated from a population of chronically infected Bolivian patients attending our clinic in Madrid. Thirty-three consecutive patients meeting this condition were selected for the study. Molecular characterization was performed by an algorithm that combines PCR of the intergenic region of the mini exon-gene, the 24Sα and 18S regions of rDNA and the variable region of the satellite DNA. A descriptive analysis was performed and associations between epidemiological/clinical data and the different DTUs were tested. Twenty-seven out of thirty-three patients had their DTU detected. Mean age was 36 years (IQR 31–43.3) and 23 were women (76.7%). The median time since arrival to Spain was 60 months (IQR 43–81). The most common DTU were TcV, TcIV and TcI. Four patients had cardiac involvement: 2 had TcV and 2 could not have their DTU determined. TcIII was not isolated from any patient. DTUs distribution in migrant population seems to be similar to that observed in the patients' countries of origin.

1. Introduction

Chagas disease is caused by the protozoan parasite *Trypanosoma cruzi*. It has an acute initial form that is asymptomatic for most patients and a chronic form that manifests with cardiac, digestive, or cardiodigestive involvement after the acute infection. Patients can remain in a chronic indeterminate stage for decades, although every year 2–5% progress to a clinical stage. This disease is endemic in the Americas, and prevalence has reached 28.8% in the general population (Moncayo and Silveira, 2009). Increased migration to Europe means that Chagas disease has emerged in countries where it was previously unknown (Schmunis and Yadon, 2010). It is particularly frequent in Spain, which is the second country in number of cases after the US (Pérez-Molina et al., 2012). The increasing number of diagnoses made during the last decade have intensified the burden on the Spanish health system, which now has to streamline identification and treatment of a disease that was previously classed as tropical (Navarro et al., 2012). Many other European countries have faced a similar problem, and it is estimated that this disease goes undiagnosed in 92–96% of cases in its chronic indeterminate form (Basile et al., 2011).

Different typing methods have made it possible to identify several ancestral parasite lineages, and six near-clades (TcI to TcVI) have been identified. These near-clades are known as discrete typing units (DTU), which have been defined as "sets of stocks that are genetically more related to each other than to any other stock and that are identifiable by common genetic, molecular or immunological markers" (Zingales et al., 2009). DTUs have been linked to specific geographical distributions and various clinical presentations, and data on the isolation of *T. cruzi* in vectors, reservoirs, and human samples from different origins have added to our knowledge

* Corresponding author. Address: Medicina Tropical, Servicio de Enfermedades Infecciosas, Hospital Universitario Ramón y Cajal, Carretera de Colmenar Km 9,1, 28034 Madrid, Spain. Tel.: +34 913368108; fax: +34 913368238.
E-mail address: jose.perezmolina@gmail.com (J.A. Perez-Molina).

1567-1348/$ - see front matter © 2013 Elsevier B.V. All rights reserved.
http://dx.doi.org/10.1016/j.meegid.2013.12.018

of the evolution and distribution of the species in the Americas (Burgos et al., 2010; Ramírez et al., 2010; Zingales et al., 2012). Nevertheless, little is known about the exact distribution this species in the migrant population.

2. Objective

Our hypothesis was that the presence of the most common DTUs in a specific endemic area would be uniform in migrants from that area; however, we cannot predict whether biological characteristics such as degree of persistence in blood, tissue tropism, or absence of reinfection could modify the distribution of DTUs in non-endemic areas. Our aim was to describe the *T. cruzi* strains identified from a population of chronically infected Bolivian patients attending our clinic in Madrid.

3. Methods

We conducted a cross-sectional observational study. Thirty-three consecutive Bolivian patients who were chronically infected with *T. cruzi* were selected from those attended at our clinic during the period 2010–2011. They all had positive results in two serological tests: in-house IFAT and ELISA (ARCHITECT Chagas ELISA test, BiosChile, Abbott Laboratories, Wiesbaden, Germany). Our in-house IFAT was prepared with a combination of cultured epimastigote antigens (Mc, T, and Dm28), and human IgG (bioMérieux®) was used as a marker. Thirteen patients had a positive PCR result in blood. Molecular characterization was performed using an algorithm combining the PCR of the intergenic region of the mini-exon gene, the 24Sα and 18S regions of rDNA, and the variable region of the satellite DNA, as described elsewhere (Ramírez et al., 2013). The primers used were kinetoplast DNA (primers 121 [5′-AAATAATGTA CGGGKGAGATGCATGA-3′] and 122 [5′-GGTTCGATTGGGGTTGGT GTAATATA-3′]) and the tandem repeat satellite region from *T. cruzi* (primers cruzi1 [5′-ASTCGGCTGATCGTTTTCGA-3′] and cruzi2 [5′-AATTCCTCCAAGCAGCGGATA-3′] (Liarte et al., 2009). The molecular markers used were the intergenic region of the non-transcribed mini-exon gene (primers TCC [5′-CCC CCC TCC CAG GCC ACA CTG-3′], TC1 [5′-GTG TCC GCC ACC TCC TTCGGG CC-3′], and TC2 [5′-CCT GCA GGC ACA CGT GTG TGT G-3′]) (Souto et al., 1996). All mini-exon gene PCR assays were performed using two primers instead of a multiplex PCR assay to determine the presence of mixed infections. Thus, PCR was applied using the primers TCC-TC1 and TCC-TC2. Segments containing the D7 domain of LSU rDNA were amplified from genomic DNA by PCR using the trypanosomatid conserved primers D75 (5′-GCAGATCTTGGTTGGCGTAG-3′) and D76 (5′-GGTTCTCTGTTGCCCCTTTT-3) (Briones et al., 1999), as well as A10 with primers pr1 (5-CCGCTAAGCAGTTCTGTCCATA-3) and pr3 (5-GCTTTATTACCCCATGCCACAG-3) (Burgos et al., 2010).

We performed a descriptive analysis and tested associations between epidemiological and clinical data and the different DTUs. We specifically analyzed age, sex, cardiac or digestive involvement, and time since arrival in Spain. Qualitative data were analyzed using the χ^2 and Fisher exact tests; quantitative data were analyzed using the *t* test.

4. Results

DTUs were identified in 27 of the 33 patients. Mean age was 36 years (IQR, 31-43.3), and 23 patients were women (76.7%). The median time since arrival in Spain was 60 months (IQR, 43-81). These characteristics were similar to those of the population commonly attended at our clinic. DTU was not characterized in six patients. The most prevalent DTU was TcV ($n = 15$, 45.5%), followed by TcIV ($n = 5$, 15.2%) and TcI ($n = 1$, 3%). Six patients presented a combination of two different DTUs: two patients (6.1%) presented TcI in combination with TcIV, two (6.1%) had TcIV with TcV, one (3%) had TcI and TcV, and one (3%) had TcII and TcVI. TcIII was not identified in any patient (Fig. 1).

Cardiac involvement was detected in four patients. One patient had completed treatment during 2008 and presented right bundle branch block, which had been stable for five years of follow-up, although his DTU was not determined. Another patient also presented right bundle branch block; he received treatment in 2010, and his DTU was characterized as TcV. This TcV was also detected in a patient presenting ventricular extrasystoles, left anterior fascicular block, and incomplete right bundle branch block that had never been treated. Finally, DTUs were not characterized in a patient with a pacemaker for severe bradycardia. Findings regarding cardiac involvement were insufficient to test associations. Neither age nor sex nor time elapsed from arrival to Spain was significantly associated with any specific DTU. Similarly, no significant association was found with these three parameters when DTUs were grouped into TcV (whether alone or in combination with other DTUs) and non-TcV.

5. Discussion

In order of frequency, the most common DTUs identified in our sample were TcV, TcIV, and TcI. Consistent with published data on Bolivian patients (del Puerto et al., 2010), we also found a high number of mixed infections. TcII and TcVI coinfected only one patient; this finding seems reasonable, as both these DTUs are rarely reported in Bolivia. No TcIII was detected, maybe because it is associated with sylvatic cycles and is rarely present in human infection (Zingales et al., 2012).

The largest series characterizing DTUs in Bolivians to date found TcV and TcI to be the most common near-clades. However, this study excluded specific probes to detect TcIV (del Puerto et al., 2010). Using these specific probes, we found that TcIV was the second most frequent DTU. A study performed in Venezuela also found TcIV to be the second most common cause of human infection (Carrasco et al., 2012). TcIV has been linked to sylvatic cycles and has been reported in the context of acute oral outbreaks in tropical wet areas of Colombia and Brazil (Monteiro et al., 2012; Ramirez et al., 2013). A recent report also related this DTU to an oral outbreak in Bolivia (Santalla Vargas, 2012). Finally, TcIV has

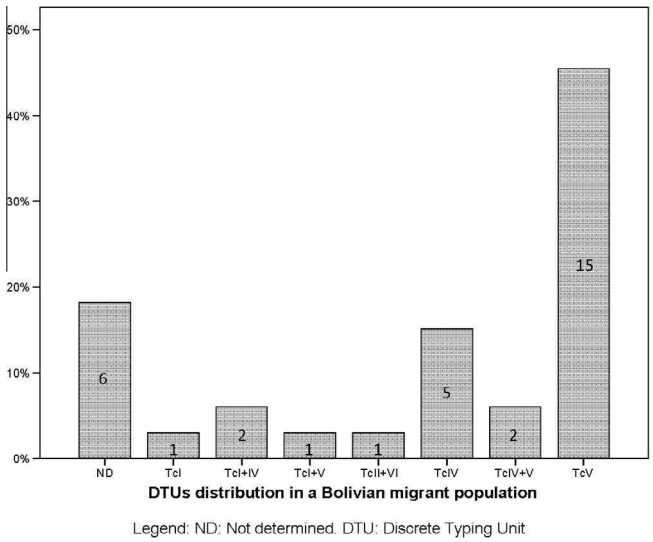

Fig. 1. DTUs distribution in a Bolivian population.

recently been detected in dogs, suggesting a potential role in domestic transmission (Ramírez et al., 2013).

Our study is limited by its small sample size and the fact that we did not record the exact geographical origin of our patients at the beginning of the study.

Ours is the first study to characterize the *T. cruzi* genome in an adult migrant population in Europe. Given that the distribution of DTUs in non-endemic countries could be comparable to that of endemic countries, the molecular genetics of the DTUs of *T. cruzi* and its potential associations with clinical outcomes warrant further study.

Acknowledgements

This work was carried out with the support provided by the programme on I+D+I 2008–2011, ISCIII-Subdirección General de Redes y Centros de Investigación Cooperativa (RICET), file no. RD12/0018/0019.

References

Basile, L., Jansa, J.M., Carlier, Y., Salamanca, D.D., Angheben, A, Seixas, J., Bartoloni, A., Van Gool, T., Cañavate, C., Flores-Chávez, M., Jackson, Y., Chiodini, P.L., Albajar-Viñas, P., 2011. Working group on chagas disease, chagas disease in European countries: the challenge of a surveillance system. Euro. Surveill. 16, pii=19968.

Briones, M.R., Souto, R.P., Stolf, B.S., Zingales, B., 1999. The evolution of two *Trypanosoma cruzi* subgroups inferred from rRNA genes can be correlated with the interchange of American mammalian faunas in the Cenozoic and has implications to pathogenicity and host specificity. Mol. Biochem. Parasitol. 104, 219–232.

Burgos, J.M., Diez, M., Vigliano, C., Bisio, M., Risso, M., Duffy, T., Cura, C., Brusses, B., Favaloro, L., Leguizamon, M.S., Lucero, R.H., Laguens, R., Levin, M.J., Favaloro, R., Schijman, A.G., 2010. Molecular identification of *Trypanosoma cruzi* discrete typing units in end-stage chronic chagas heart disease and reactivation after heart transplantation. Clin. Infect. Dis. 51, 485–495.

Carrasco, H.J., Segovia, M., Llewellyn, M.S., Morocoima, A., Urdaneta-Morales, S., Martínez, C., Martínez, C.E., Garcia, C., Rodríguez, M., Espinosa, R., de Noya, B.A., Díaz-Bello, Z., Herrera, L., Fitzpatrick, S., Yeo, M., Miles, M.A., Feliciangeli, M.D., 2012. Geographical distribution of *Trypanosoma cruzi* genotypes in Venezuela. PLoS Negl. Trop. Dis. 6, e1707.

del Puerto, R., Nishizawa, J.E., Kikuchi, M., Iihoshi, N., Roca, Y., Avilas, C., Gianella, A., Lora, J., Velarde, F.U., Renjel, L.A., Miura, S., Higo, H., Komiya, N., Maemura, K., Hirayama, 2010. Lineage analysis of circulating *Trypanosoma cruzi* parasites and their association with clinical forms of Chagas disease in Bolivia. PLoS Negl. Trop. Dis. 4, e687.

Liarte, D.B., Murta, S.M., Steindel, M., Romanha, A.J., 2009. *Trypanosoma cruzi*: multiplex PCR to detect and classify strains according to groups I and II. Exp. Parasitol. 123, 283–291.

Moncayo, Á., Silveira, A.C., 2009. Current epidemiological trends for Chagas disease in Latin America and future challenges in epidemiology, surveillance and health policy. Mem. Inst. Oswaldo Cruz 104, 17–30.

Monteiro, W.M., Magalhaes, L.K., de Sa, A.R., Gomes, M.L., Toledo, M.J., Borges, L., Pires, I., Guerra, J.A., Silveira, H., Barbosa, M., 2012. *Trypanosoma cruzi* IV causing outbreaks of acute Chagas disease and infections by different haplotypes in the Western Brazilian Amazonia. PLoS One 7, e41284.

Navarro, M., Norman, F.F., Pérez-Molina, J.A., López-Vélez, R., 2012. Benznidazole shortage makes Chagas disease a neglected tropical disease in developed countries: data from Spain. Am. J. Trop. Med. Hyg. 87, 489–490.

Pérez-Molina, J., Norman, F., López-Vélez, R., 2012. Chagas disease in non-endemic countries: epidemiology, clinical presentation and treatment. Curr. Infect. Dis. Rep. 14, 263–274. http://dx.doi.org/10.1007/s11908-012-0259-3.

Ramírez, J.D., Guhl, F., Rendón, L.M., Rosas, F., Marin-Neto, J.A., Morillo, C.A., 2010. Chagas cardiomyopathy manifestations and *Trypanosoma cruzi* genotypes circulating in chronic chagasic patients. PLoS Negl. Trop. Dis. 4, e899.

Ramirez, J.D., Montilla, M., Cucunuba, Z.M., Florez, A.C., Zambrano, P., Guhl, F., 2013. Molecular epidemiology of human oral Chagas disease outbreaks in Colombia. PLoS Negl. Trop. Dis. 7, e2041.

Ramírez, J.D., Turriago, B., Tapia-Calle, G., Guhl, F., 2013. Understanding the role of dogs (*Canis lupus familiaris*) in the transmission dynamics of *Trypanosoma cruzi* genotypes in Colombia. Vet. Parasitol.. http://dx.doi.org/10.1016/j.vetpar.2012.12.054.

Santalla Vargas, J., Oporto, P., Espinoza, E., Rios, T., Brutus, L., Garcia, L., 2012. Oral transmission of Chagas disease, first reported outbreak in Bolivia. In: Rozas-Dennis, G.S., Silva, M. (Ed.), Workshop internacional de la enfermedad de Chagas, vectores triatominos, *Trypanosoma cruzi* y triatoma virus Universidad Mayor de San Simón Cochabamba (BOL), 61. Available from: <http://www.documentation.ird.fr/hor/fdi:010059855>. (Last accessed 18 November 2013.).

Schmunis, G.A., Yadon, Z.E., 2010. Chagas disease: a Latin American health problem becoming a world health problem. Acta Trop. 115, 14–21. http://dx.doi.org/10.1016/j.actatropica.2009.11.003.

Souto, R.P., Fernandes, O., Macedo, A.M., Campbell, D.A., Zingales, B., 1996. DNA markers define two major phylogenetic lineages of *Trypanosoma cruzi*. Mol. Biochem. Parasitol. 83, 141–152.

Zingales, B. et al., 2009. A new consensus for *Trypanosoma cruzi* intra specific nomenclature: second revision meeting recommends TcI to TcVI. Mem. Inst. Oswaldo Cruz 104, 1051–1054.

Zingales, B. et al., 2012. The revised *Trypanosoma cruzi* subspecific nomenclature: rationale, epidemiological relevance and research applications. Infect. Genet. Evol. 12, 240–253.

OPEN ACCESS Freely available online

PLOS ONE

Cytokine Profiling in Chagas Disease: Towards Understanding the Association with Infecting *Trypanosoma cruzi* Discrete Typing Units (A BENEFIT TRIAL Sub-Study)

Cristina Poveda[1], Manuel Fresno[2], Núria Gironès[2], Olindo A. Martins-Filho[3], Juan David Ramírez[1], Julien Santi-Rocca[2], José A. Marin-Neto[4], Carlos A. Morillo[5], Fernando Rosas[6], Felipe Guhl[1]*

1 Centro de investigaciones en Microbiología y Parasitología Tropical (CIMPAT), Facultad de Ciencias, Universidad de los Andes, Bogotá, Colombia, **2** Centro de Biología Molecular Severo Ochoa, Consejo Superior de Investigaciones Científicas (CSIC), Universidad Autónoma de Madrid (UAM), Cantoblanco, Madrid, Spain, **3** Laboratory of Diagnostic and Monitoring Biomarkers, Centro de Pesquisas René Rachou, Fundação Oswaldo Cruz - FIOCRUZ, Belo Horizonte, MG, Brazil, **4** Cardiology Division, Internal Medicine Department, Medical School of Ribeirao Preto, Universidad de Sao Paulo, Sao Paulo, Brazil, **5** Department of Medicine, Cardiology Division, McMaster University, PHRI-HHSC, Hamilton, Ontario, Canada, **6** Electrofisiología, Clínica Abood Shaio, Bogotá, Colombia

Abstract

Background: Chagas disease caused by the protozoan *Trypanosoma cruzi* is an important public health problem in Latin America. The immunological mechanisms involved in Chagas disease pathogenesis remain incompletely elucidated. The aim of this study was to explore cytokine profiles and their possible association to the infecting DTU and the pathogenesis of Chagas disease.

Methods: 109 sero-positive *T. cruzi* patients and 21 negative controls from Bolivia and Colombia, were included. Flow cytometry assays for 13 cytokines were conducted on human sera. Patients were divided into two groups: in one we compared the quantification of cytokines between patients with and without chronic cardiomyopathy; in second group we compared the levels of cytokines and the genetic variability of *T. cruzi*.

Results: Significant difference in anti-inflammatory and pro-inflammatory cytokines profiles was observed between the two groups cardiac and non-cardiac. Moreover, serum levels of IFN-γ, IL-12, IL-22 and IL-10 presented an association with the genetic variability of *T.cruzi*, with significant differences in TcI and mixed infections TcI/TcII.

Conclusion: Expression of anti-inflammatory and pro-inflammatory cytokines may play a relevant role in determining the clinical presentation of chronic patients with Chagas disease and suggests the occurrence of specific immune responses, probably associated to different *T. cruzi* DTUs.

Citation: Poveda C, Fresno M, Gironès N, Martins-Filho OA, Ramírez JD, et al. (2014) Cytokine Profiling in Chagas Disease: Towards Understanding the Association with Infecting *Trypanosoma cruzi* Discrete Typing Units (A BENEFIT TRIAL Sub-Study). PLoS ONE 9(3): e91154. doi:10.1371/journal.pone.0091154

Editor: Aric Gregson, University of California Los Angeles, United States of America

Received July 16, 2013; **Accepted** February 10, 2014; **Published** March 7, 2014

Funding: This study was supported by grants from Ministerio de Ciencia e Innovación of Spain (SAF2010-18733), Chagas EpiNet from The European Union Seventh Framework Programme, contract no. 223034, RED RICET RD12/0018/0004 and Comunidad de Madrid S-2010/BMD-2332 to MF, and an institutional grant of Fundacion Ramon Areces and by Fondo de Investigaciones Sanitarias (PS09/00538), the Canadian Institute of Health Research (CIHR) and TDR/WHO. The authors thank the research fund of the faculty of sciences from the Universidad de los Andes and Centre of Molecular Biology "Severo Ochoa" from Universidad Autonoma de Madrid (Spain). The funders had no role in study design, data collection and analysis, decision to publish, or preparation of the manuscript.

Competing Interests: The authors have declared that no competing interests exist.

* E-mail: fguhl@uniandes.edu.co

Introduction

Chagas disease is considered by the World Health Organization (WHO) as one of the most important public health problems in Latin America, with an estimate of 7 million people infected and 110 million people at risk of contracting the disease [1,2]. Recent evidence has also indicated that Chagas disease has migrated to non-endemic regions posing a significant social threat [3]. This parasitic disease is caused by the protozoan *Trypanosoma cruzi*, transmitted by different routes: via the feces of infected triatomine bugs, contaminated blood transfusion, oral (contaminated food/juices), vertical transmission, organs transplantation and laboratory accidents. Approximately 60% of patients in the chronic phase are clinically asymptomatic, around 30% manifest cardiomyopathy, 8% megavisceral syndromes and the remaining 2% both cardiomyopathy and digestive involvement [4,5,6,7].

Two main hypotheses regarding the pathogenesis of Chagas disease have been proposed. One based on parasite persistence, and a second hypothesis based on adverse human host immune response to the infection, causing autoimmune aggression [8]. In the acute phase of the disease the host is able to control the infection in three different but complementary ways: i) Detection and direct destruction of the parasite by cells such as macrophages and dendritic cells, ii) activation of dendritic cells and macro-

phages that present antigen stimulation for the activation of the antigen-specific immune responses and iii) detection of infection by non-hematopoietic cells, which are the principal targets of the invasion by *T. cruzi* [9]. In the chronic phase, antigens that are elicited by the immune response are mediated by T cells, which play an important role in the progression of the disease. Studies in children with the indeterminate form have shown a high frequency of pro-inflammatory monocytes and regulatory cells compared with healthy subjects [10]. Thus, it is believed that expression of cytokines and their kinetics are important key factors influencing the development and progression of the disease. In fact, the balance between excessive pro-inflammatory cytokines and anti-inflammatory cytokines may be critical in the development of the chronic phase of the disease [5,8,11]. Studies on the specific role of cytokines in the immune response against *T. cruzi* have been recently reported and demonstrate that large amounts of Th1 pro-inflammatory cytokines such as Interferon Gamma (IFN-γ), Tumor Necrosis Factor Alpha (TNF-α) are related to cardiac disease [12]. It is also known that these cytokines are regulated by anti-inflammatory cytokines in low concentrations such as interleukin 10 and 5 (IL-10 and IL-5) [13]. Altogether, these data suggest a link between parasite infection, immune response polarization, and specific organ damage. Thus, cytokines may be used as biomarkers in order to identify the immune factors that influence disease progression has been carried out in different pathologies such as malaria, yellow fever, HIV infection, and also in Chagas disease [14,15,16]. It is believed that in these infectious diseases deregulation of host inflammatory responses play an important role and the profile of cytokines may be used as biomarkers of disease progression. Consequently, the characterization of these profiles may lead to future selection of treatment strategies targeting specific inflammatory pathways [17].

Several investigators have attempted to associate *T. cruzi* genetic variability and the different clinical manifestations of Chagas disease. The genetic variability within the *T. cruzi* taxon has been demonstrated using biological, biochemical and molecular markers, and has been grouped into six Discrete Typing Units (DTUs), TcI-TcVI [18,19]. TcI is mostly related to the sylvatic cycle in the Amazon region with sporadic cases in the domestic foci recently named TcI_{DOM} [20]. However, TcI has recently gained relevance since it has been associated with severe cardiomyopathic manifestations in patients from Argentina and Colombia [19,21,22,23]. TcII is the principal agent of Chagas disease in the Southern Cone of America and *Triatomainfestans* is the principal vector. TcV and TcVI, are derived from the hybridization between TcIII and TcII/TcIV and the cycle of transmission is mainly domestic [18,24]. These DTUs are related not only to heart disease but also to megavisceral syndromes [25,26]. TcIII and TcIV are mainly related to the sylvatic cycle of transmission and scarce evidence of human infection has been reported [27,28,29].

The aim of this study was to evaluate the different cytokine profiles in Chagasic patients with and without chronic cardiomyopathy to correlate these cytokine profiles in patients infected with the different *T.cruzi*DTUs in order to establish whether these factors may be involved in the pathogenesis of Chagas disease. Our results show that specific anti-inflammatory and pro-inflammatory cytokine modulation is correlated with the clinical presentation of chronic patients with Chagas disease and suggests the occurrence of specific immune responses, probably associated to different *T. cruzi* DTUs.

Results

Signature Profiles

Group I: CARD vs. NON-CARD. To identify possible markers of infection, and more specifically of cardiomyopathy, we measured seric cytokines in 16 patients with cardiomyopathy (CARD), 38 non-cardiac chagasic patients (NON-CARD), and 9 non-infected individuals (CONTROL). As expected in the case of immune responses against infection, cytokine production greatly varies among individuals, rendering inaccurate the use of the mean as central indicator. We thus used the mean of cytokine concentration, the latter being evaluated by the mean fluorescence intensity (MFI) of beads bound to cytokines recognized by immunofluorescence. The overall median of each individual MFI cytokine was calculated (IL-1β = 63.32, IL-2 = 49.28, IL-4 = 45.92, IL-5 = 58.24, IL-6 = 276, IL-9 = 181.4, IL-10 = 85.68, IL-12p70 = 54.6, IL-13 = 33.04, IL-17A = 44.8, IL-22 = 82.88, IFN-γ = 48.8 and TNF-α = 108.6) from patients of different clusters. These values were used as the cut-off mark to tag the cell population from each patient as being a high or low cytokine producer (Figure S1 in File S1). Then, in each group and for each cytokine, results were expressed as the frequency of individuals with a concentration of seric cytokine higher than the median of all samples (Figure 1). The assembling of the ascendant frequency of high cytokine producers for CONTROL generated the reference cytokine signature applied to identify changes in the overall cytokine signature from the CARD and NON-CARD groups. The results showed that the frequency of high cytokine producers in the CARD and NON-CARD groups was lower than in the CONTROL group.

A switch among anti-inflammatory and pro-inflammatory cytokines profiles in the CARD and NON-CARD groups of patients was observed. The NON-CARD patients showed higher frequency of anti-inflammatory cytokines and lower frequency of pro-inflammatory cytokines while the CARD displayed higher pro-inflammatory and lower anti-inflammatory cytokines. The cytokines involved in the anti-inflammatory profile were IL-13, IL-5 and IL-10 and those in the pro-inflammatory profile were: IL-2, IL-6, IL-9 and IL12 (FIGURE 2).

Group II: *T. cruzi* variability. As for Group I,overallmedian of each MFI cytokine wascalculated (IL-1β = 292,32, IL-2 = 224, IL-4 = 209.44, IL-5 = 251.44, IL-6 = 1197, IL-9 = 792.4, IL-10 = 369.6, IL-12p70 = 228.48, IL-13 = 160.16, IL-17A = 207.76, IL-22 = 547.12, IFN-γ = 198.24 and TNF-α = 465.92). These values were used as the cut-off mark to tag the cell population from each patient as being a high or low high cytokine producers(Figure S2 in File S1). Assembling of the ascendant frequency of high cytokine producers for CONTROL generated the reference cytokine signature applied to identify changes in the overall cytokine signature from all other groups: TcI, TcII and Mixed TcI/TcII (FIGURE 3).

A pro-inflammatory pattern was observed for all infected groups, but no particular pattern could be associated to the different DTUs. The frequency of cytokines in TcI, TcII and Mixed TcI/TcII showed lower frequency as compared with the CONTROL levels.

All the quantitative results provided by the cytometry system are included and can be found in Tables S1 and S2 in File S2.

Statistical Analysis

This analysis aimed to establish associations between levels of cytokines and the clinical manifestation (CARD or IND) and/or the genetic variability of *T.cruzi* (TcI, TcII and Mixed TcI/TcII). Analysis of principal components was performed with the 13

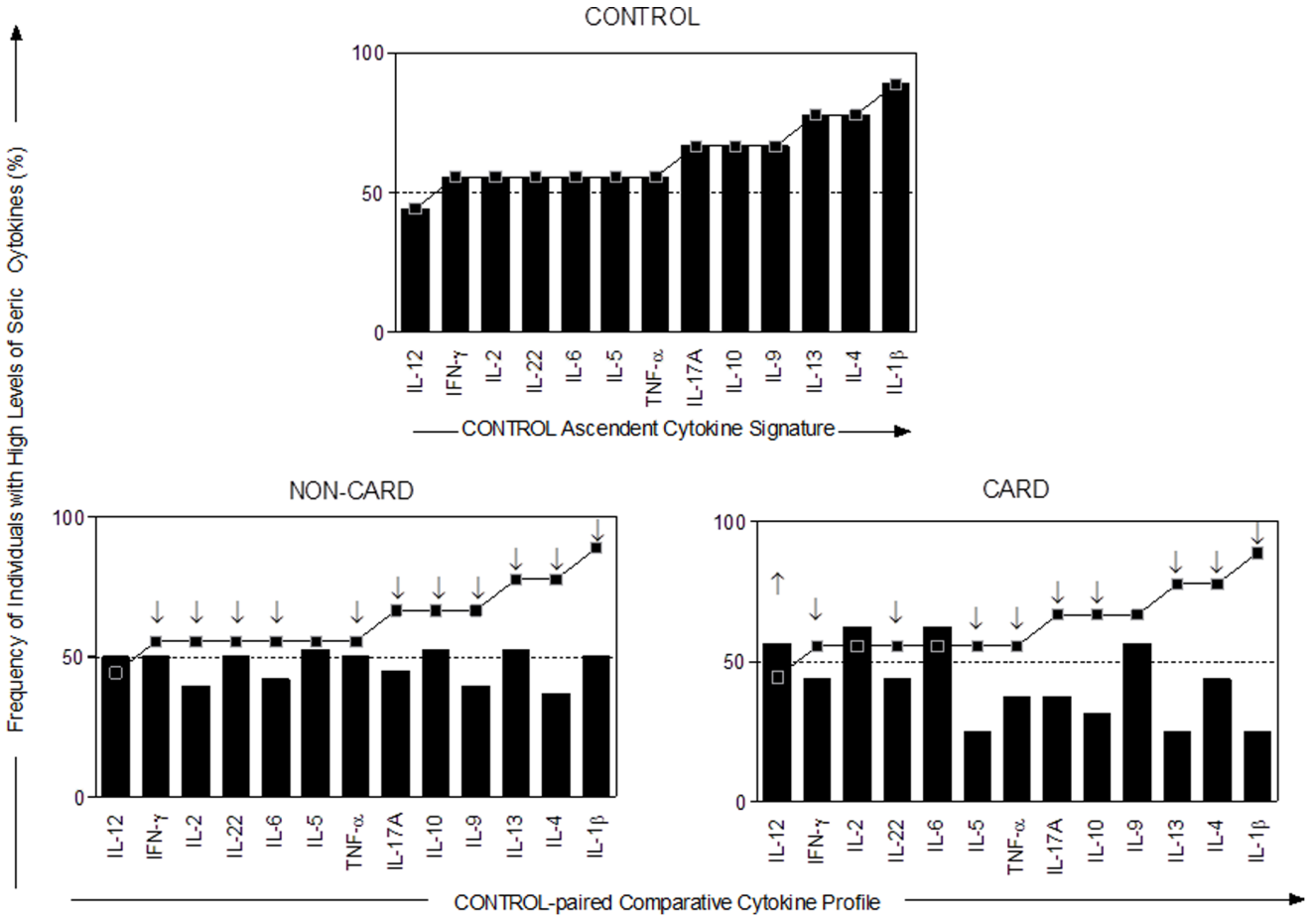

Figure 1. Cytokine Signatures with Frequency of Subjects with High Cytokine Levels. The diagrams were plotted using the global median of each MFI cytokine index as the cut-off mark to identify higher levels. The ascendant frequency of high cytokine producers at the with (CARD) and without Chagas cardiomyopathy (NON-CARD) was demonstrated by bar graphics. The ascendant frequency of high cytokine producers of the CONTROL group was used to generate the reference cytokine signature curves that were applied to identify changes in the overall cytokine signature from all other groups.
doi:10.1371/journal.pone.0091154.g001

cytokines studied. The principal components for the study group CARD vs NON-CARD were IL-12 = 0.990, IFN-γ = 0.990, IL-1 = 0.920, IL-6 = 0.915 and IL-9 = 0.895 which explained the model in 80.4% of the variation in the dataset; for the study group II *T. cruzi* DTUs the principal components were IFN-γ = 0.882, IL-12 = 0.822, IL-22 = 0.817 and IL-10 = 0.805 explaining 75.42% of variation (Tables S3 to S8 in File S2).

Finally, discriminant analysis was performed to observe which proportion of the selected components were actually able to group the study groups; for study group I (CARD vs NON-CARD) the components group in the right cluster (when both real and theory group coincide) : NON-CARD = 21/38 (55.3%), CAR = 16/16 (100%) and CONTROL = 5/9 (55.6%) (FIGURE 4 a); and for the study group II (*T. cruzi* DTUs) the components group in the right cluster TcI = 19/20 (95%), TcII = 3/20(15%), Mixed TcI/II = 13/15(86,7%) and CONTROL = 10/12(83,3%) (FIGURE 4 b). These results show a clear profile in patients with CARD, and an association between levels of cytokines and the variability of *T.cruzi* (TcI, TcII and Mix TcI/TcII)(Tables S9 and S10 in File S2.).

Discussion

An important finding of this study was a switch between the anti-inflammatory cytokines IL-13, IL-5 and IL-10 and pro-inflammatory cytokines IL-2, IL-6, IL-9 and IL-12 among CARD and NON-CARD groups. These findings suggest that regulation (differential regulation of cytokine synthesis) may play an important role in the development of Chagas cardiomyopathy.

The anti-inflammatory/pro-inflammatory cytokine profile switch found between patients with Chagas cardiomyopathy and those infected but still in the NON-CARD stage of the disease is compatible with the hypothesis that the progression of human Chagas disease from asymptomatic to severe forms, is related with a lack of adequate immune modulation [8]. While an appropriate, inflammatory, response may be beneficial in early stages of infection, the lack of control of this response later on the outcome of the disease will allow for the establishment of tissue damage. This hypothesis is in agreement with the finding that IL-10 levels were diminished in comparison to levels of TNF- α and IFN-γ in CARD patients, in contrast with the opposite profile (higher levels of IL-10 than levels of TNF- α and IFN-γ) in indeterminate form patients [8]. These findings are also in keeping with a recent report documenting increased matrix metalloproteinases 2 and 9 in *T. cruzi* seropositive subjects with and without Chagas cardiomyopa-

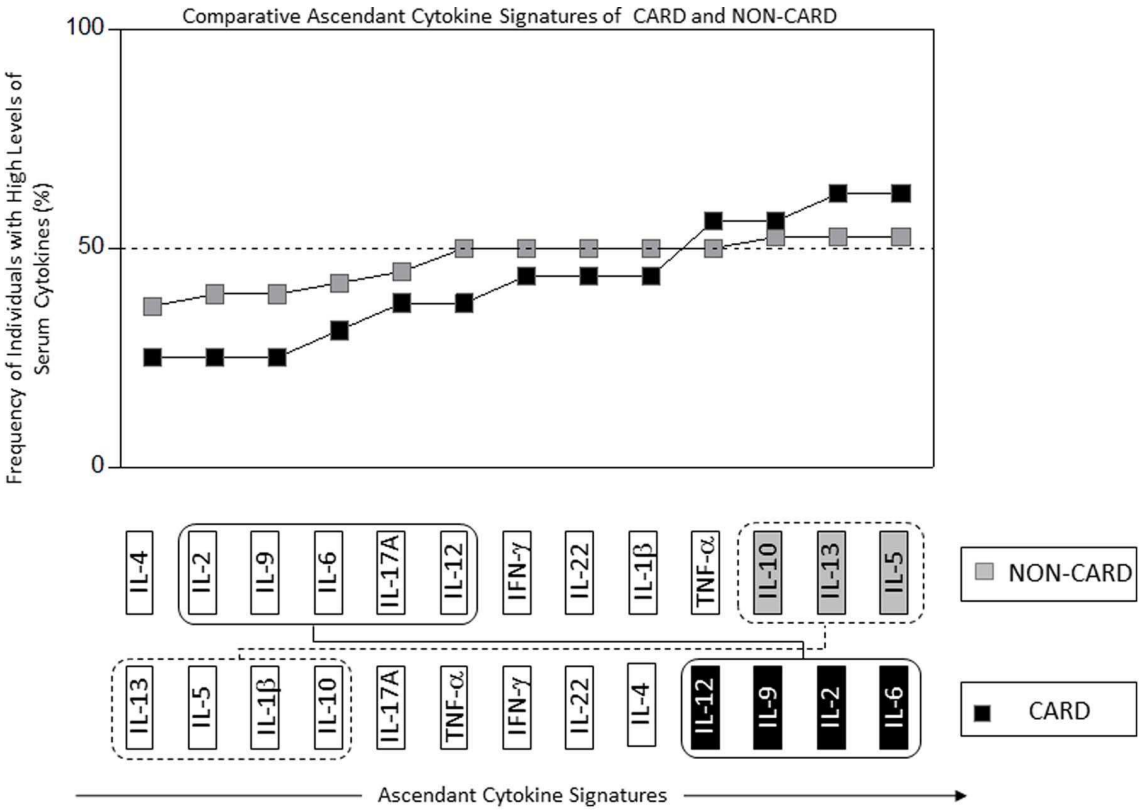

Figure 2. Comparative Cytokine Signatures of NON-CARD and CARD. The diagram is a comparison between the signing of the NON-CARD (■) and CARD (■). There is a switch between pro-inflammatory with the boxes in solid line (IL-6, IL-2, IL-9 and IL-12) and anti-inflammatory with the boxes in dashed line (IL-5,IL-13 and IL-10) cytokines; the CARD have higher frequencies of proinflammatory cytokines and lower levels of inflammatory cytokines, whereas the opposite occurs in the case of NON-CARD.
doi:10.1371/journal.pone.0091154.g002

thy manifestations [30]. However, previous reports have not documented that these pro-inflammatory cytokines play an important role in producing Chagas disease immunomodulation disequilibrium [8,31,32].

Pro-inflammatory cytokines involved in the switch were IL-2, IL-9, IL-6 and IL-12. The role of the last two cytokines has already been studied in Chagas disease. Thus, the presence of high levels of IL-6 in CARD patients was correlated with the severity of myocardium damage, in Peruvian and Colombian populations [33]. Another study determined the role of genetic polymorphism in the IL-12, and it was the C allele of IL-12B 3′UTR that acted as a risk factor and influenced the susceptibility to develop cardiomyopathy in Chagas disease [34]. Our results are in agreement with these studies and additionally document that these cytokines have higher levels in CARD patients compared to NON-CARD patients. On the other hand, the anti-inflammatory cytokines involved in the switch were IL-13, IL-5 and IL-10. IL-10 was the most important anti-inflammatory cytokine studied in the Chagas disease, and it has been shown that NON-CARD patients display higher levels of IL-10 in comparison to cardiac patients [8,35]. Other investigators evaluated the SNP's in indeterminate and CARD populations, and also divided the cardiac patients between those with non-dilated and dilated hearts, finding different allele and genotype frequencies among them; also, a correlation was found between the allele A of -1082G/A in the IL-10 and low levels in CARD patients [36].

On the other hand, the relationship of the genetic variability of the parasite and host characteristics with pathogenesis is increasingly recognized as an important factor in the understanding of Chagas disease. In all our groups independent of the genetic variability of the infecting *T.cruzi* DTUs a pro-inflammatory profile was observed. Moreover, all those groups manifested a pro-inflammatory profile similar to the one we found in the study group I (CARD and NON-CARD). However, the TcII and Mixed groups showed higher levels of cytokines compared to the TcI, where the levels did not exceed 50%. It is interesting to speculate that the lack of a highly specific profile associated to a particular infecting-DTU is likely due the pleiotropic and somewhat redundant role of many cytokines. For all DTUs groups the profile is pro-inflammatory, and probably this pro-inflammatory profile will eventually lead to the same clinical manifestation (cardiomyopathy), regardless of the different DTUs with which the patients were infected and of some particular cytokine responses which are DTU-dependent. Thus, we found higher levels of the cytokines IL-6 for TcI, IL-1 for TcII and of IL-22 for Mixed TcI/TcII. This is relevant, since it is known that IL-6 is secreted by T cells and macrophages, IL-1 by macrophages and lymphocytes, and IL-22 by dendritic cells and T cells [37].

Presumably, DTU-specific recognition by the immune system (Antibodies, B cells, or T cells), could lead to the differential responses observed. Thus the DTUs-differential recognition by host receptors, that recognized pathogen patterns and their cognate pathogen associated molecular patterns (PAMPs), could be linked with the observed different induction of pro-inflammatory cytokines. In this regard, previous reports, demonstrated that GPI-anchors from *T.cruzi* surface antigens triggered the synthesis

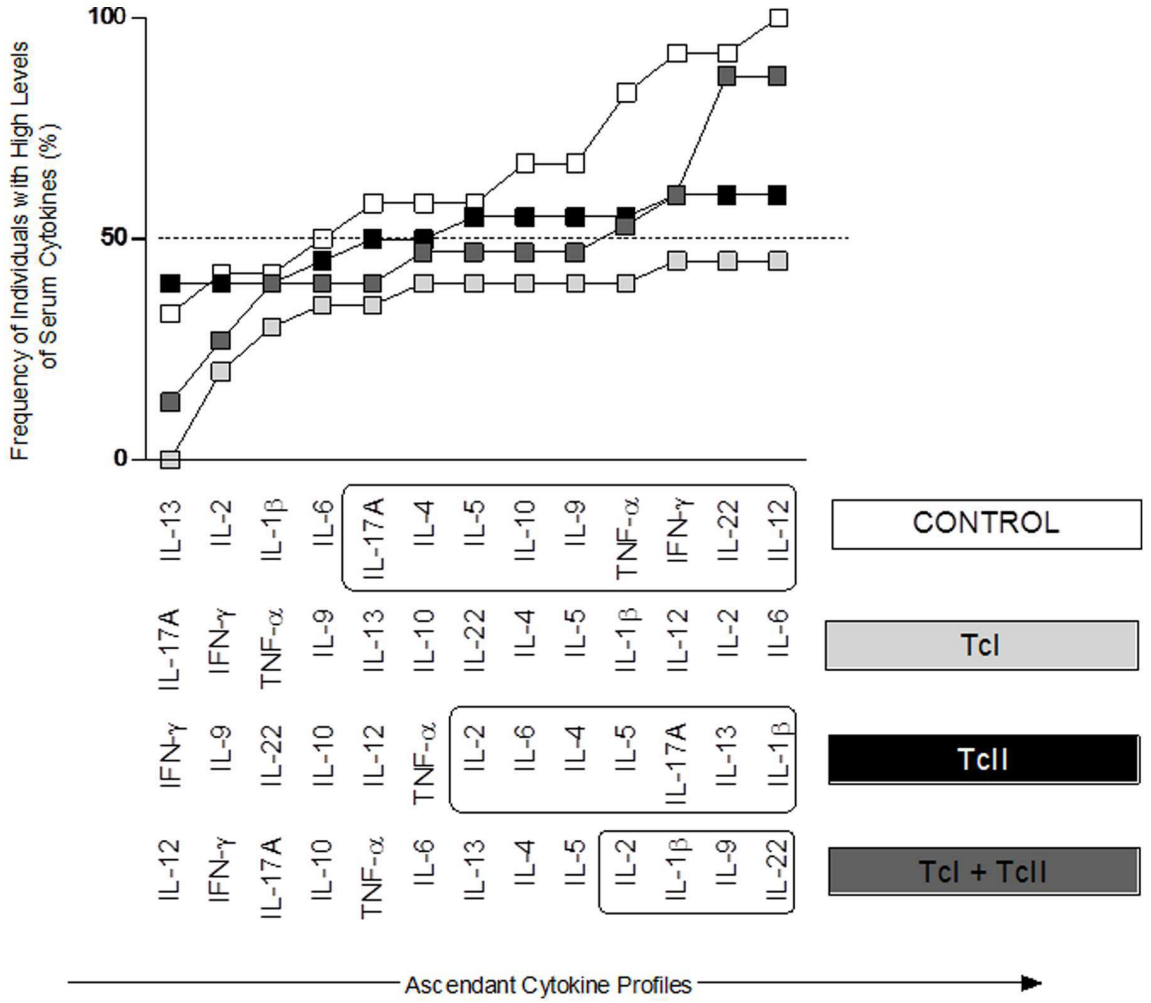

Figure 3. Comparison of Immunological Signatures between patients with chronic chagasic cardiomyopathy infected with different DTU's. The diagram is a comparison between the signing of the TcI (■), Tc II (■), Mixed TcI+TcII (■) and CONTROL (□). Cytokines with frequency equal or higher than 50% are in boxes.
doi:10.1371/journal.pone.0091154.g003

of IL-12 by macrophages and dendritic cells through toll-like receptor 2 (TLR-2) dependent activation [38]. In addition, TLR-9 that recognizes T. cruziCpG-rich DNA also stimulated the production of IL-12, IFN-γ and TNF-α by macrophages. The glycoinositolphospholipid from epimastigotes of *T. cruzi* is recognized as TLR-4 in which also trigger IL-12, IL-2 and TNF. In addition, other cells, known to be infected *T. cruzi,* as myocytes and adipocytes, may contribute to the cytokine profile observed. Since IL-6 is also produced by adipocytes [9].

The DAPC analysis showed a clear grouping for the CARD patients but not for NON-CARD patients. This result may be due to the fact that some patients in the NON-CARD group could be eventually more predisposed to develop cardiomyopathy or megaviscera syndrome explaining why cytokine levels are not homogeneous for this group. In the study group, the DAPC analysis suggests that there is association between the genetic variability of *T. cruzi* (Tc I, Tc II and Mixed TcI/TcII) and the levels of some cytokines. We found again in both groups, I and II, that IL-12, IFN-γ, IL-6 and IL-1 are the principal components and thus they may play an important role in Chagas disease pathophysiology. Also, differences in the frequency of high producers of IL-17 among in patients infected with different DTUs were found: 0% for TcI, 60% for TcII and 40% for mixed infection (TcI/TcII). Those differences may lead to slightly different outcomes of the disease. In this regard, previous studies showed that patients with less aggressive cardiomyopathy forms of the disease produce higher levels of IL-17 [39], suggesting that in our study the patients with more severe cardiomyopathy infection would be those with TcI followed by those with mixed infection and finally those infected with TcII.

In summary, pro-inflammatory profile is associated to CARD patients and anti-inflammatory profile to NON-CARD patients. The fact that the levels of cytokines were different for patients infected with different parasite DTUs suggests a specific immune response, probably associated to DTUs. A novel contribution of this study is the possibility of using IL-12, IFN-γ, IL-6 and IL-1 as prognostic biomarkers of Chagas Disease. Future studies should be carried out covering the geographical wide-range of DTUs and other human populations, in order to validate these cytokines as biomarkers as well as finding the plausible association between DTUs-epitope and Chagas Disease clinical manifestations.

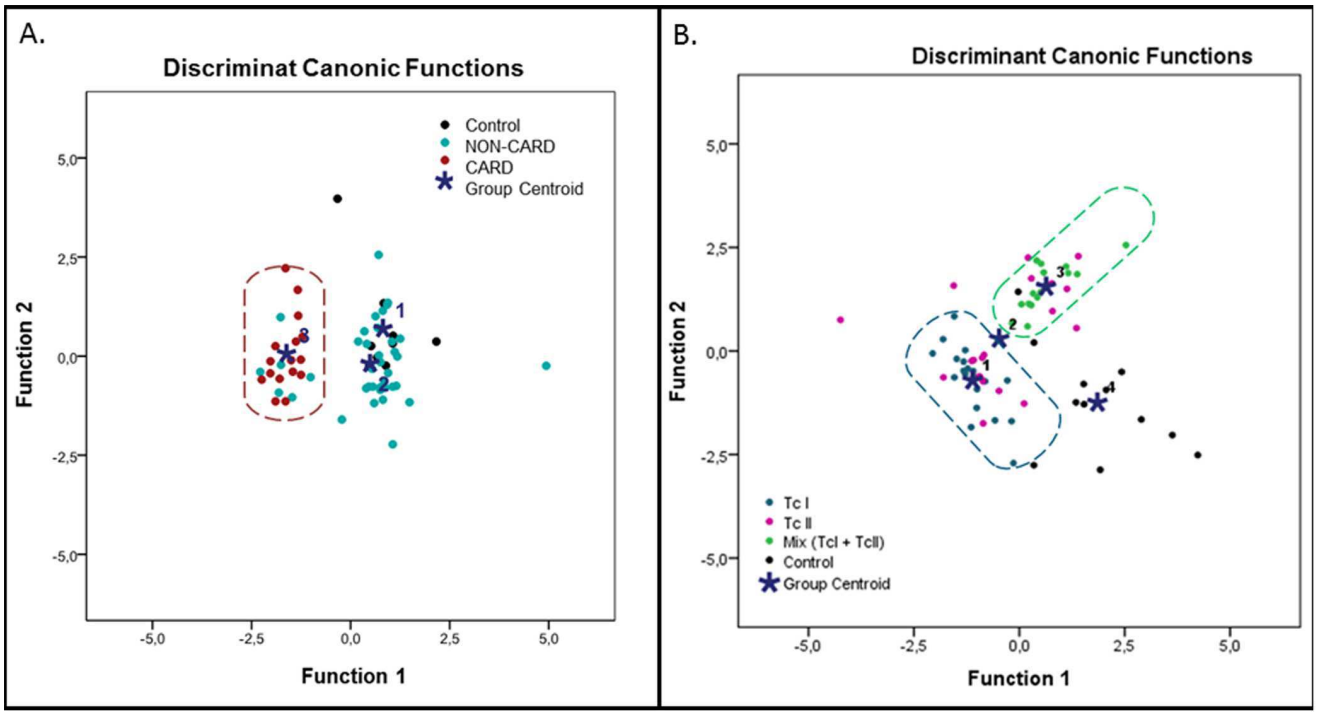

Figure 4. Discriminant Analysis of Principal Components (DAPC). 4A. DAPC for with and without cardiomyopathy Chagas patients and CONTROLS. The diagram show a cluster of 100% for CARD (Red circle), 55,3% for NON-CAR (Cian Circel) and 55,6% for the CONROL (●). 4B. DAPC of patients with chronic Chagas cardiomyopathy infected with different DTU's and CONTROLS: The diagram shows a cluster of 95% for TcI (Blue Circle), 15% for Tc II (Magenta Circle), 86,7% for mix TcI/TcII (Green Circle) and 83,3% for the CONTROL (●).
doi:10.1371/journal.pone.0091154.g004

Materials and Methods

Human Sera

Following WHO criteria for Chagas disease diagnosis, two serological tests (ELISA and IIF) were employed to enroll the patients. According to these diagnostic test results, a total of 109 serum samples from Chagas patients and 21 serum samples from healthy donors were assayed, aged 40 to 50 years living in rural areas of Colombia and Bolivia (77 individuals from Santander, Colombia and 53 from Cochabamba and Tarija, Bolivia). Chagas patients were classified as without cardiomyopathy (NON-CARD = 38) when they were seropositive with no evidence of cardiac disease (based on the absence of symptoms, physical signs and of normal X-ray, electrocardiogram and/or echocardiogram). Patients with chronic Chagas cardiomyopathy (CARD = 71) were characterized according to clinical criteria and abnormalities in chest X-ray, electrocardiogram and/or echocardiogram. The presence of other acute, hepatic, renal or psychiatric diseases were a motive for exclusion criteria.

The studies were conducted in two groups of individuals: the first one to compare the differences in the quantification of cytokines in patients with and without chronic cardiomyopathy and control individuals; and the second one to compare the differences between the levels of cytokines and the genetic variability of *T. cruzi*.

Group I (CARD and NON-CARD), included 54 serum samples from Chagas patients, 38 being classified as NON-CARD and 16 patients as CARD, and 9 serum samples from CONTROL individuals. The selection criteria of the patients groups were trying based on the assumption of obtaining the percentage to simulate the % of Chronic Chagasic manifestation reports 38/54 chagasicpatientes (70.37% NON-CARD) against not Chronic Chagasicmanifestationnd 16/54 (29.62% CARD).

Group II (*T. cruzi* DTUs), included 55 serum samples from Chagas patients with chronic cardiomyopathy and 12 CONTROL individuals. Twenty patients were typed as TcI, 20 as TcII and 15 mixed TcI/II. These sera were previously genotyped by Ramirez *et al.* 2010, where the initial sample size was 240 patients. Only 20/240 patients were genotyped as Mixed infection being TcI+ TcII (5/20 sera were contaminated with bacteria and subsequently excluded)we use the same sample size of patients for the others DTUs for optimal statistical analyzes.

Experimental ethics. Written and oral consent was obtained in all patients included as part of the BENEFIT trial (Benznidazole Evaluation for Interrupting Trypanosomiasis), the study is approved by all local and national Institutional Review Board (ClinicaAboodShaio, Hospital de la Policia, Fundacion Cardiovascular de San Gil Santander), the study is approved by the Ethics Research Committe of the World Health Organization as one of the funding agencies of the BENEFIT trial.

Cytokine Quantification and Flow Cytometry Acquisition

Fluorescent bead-based flow cytometry assays for 13 anti-inflammatory and pro-inflammatory cytokines was performed by duplicate (Human Th1/Th2/Th9/Th17/Th22 13plex FlowCytomix Multiplex, Bender MedSystems GmbH, eBioscience), on human sera (without *in-vitro* stimulation), following the manufacturer's protocol. Briefly, combining 2 different bead sizes and 6 or 7 fluorochrome densities for each population (thus fluorescence intensities, with an emission maximum in the far red range), 13 different bead populations are defined, each one associated to a specific antibody. Cytokines are trapped by these antibody-bead

complexes, and then recognized by another antibody in solution; the latter is previously bound to a secondary antibody coupled to phycoerythrin (PE).

Sample reading was performed in BIO FACS Canto II™ Becton Dickinson (BD) cytometer and analyzed with eFlowCytomix Pro software (Cat. No. BMS8402FF). After acquiring 30,000 events/microwell, cytokine concentration was analyzed according to manufacturer's recommendation. After gating the two bead sizes on a dot plot with forward scatter (FSC) and side scatter (SSC), events were plotted according to fluorescence emission at 700 nm (bead-contained fluorochrome, intensity corresponding to cytokine identity) and at 595 nm (PE emission peak, intensity corresponding to cytokine concentration). Fluorescence intensity will further refer to the intensity recorded at 595 nm.

Signatures Analyses

The cytokine profile was first assessed by identifying low and high cytokine producers, as previously reported [40]. Briefly, after the establishment of the overall median of Median of Fluorecence Intensity (MFI), each cytokine subsets from all sub-groups were tagged as they displayed low or high cytokine production. The percentage of sub-groups showing high cytokine indexes was calculated for each one. The ascendant frequency of high cytokine indexes of controls was then used as the reference cytokine curves to identify changes in the overall cytokine patterns from all other sub-groups. Each axis represents the frequency (%) of volunteers showing high cytokine indexes.

Statistical Analysis

Statistical analyses of the data were carried out using GraphPad Prism software 5.0 and Statistical Package for the Social Sciences 17, SPSS. Discriminant Analysis of Principal Components (DAPC) was performed, to assess the association between the different cytokines and the clinical manifestation of Chagas disease (CARD or NON-CARD) and/or the variability of *T.cruzi* (TcI, TcII and Mixed TcI/TcII). The totals of components considered were able to explain up to 80% of the model. The analysis of cytokine signatures was performed using the control cytokine signature as the reference curve, and significant differences were considered when the values emerged outside the quartile of the reference signature.

Supporting Information

File S1 File S1 includes the following: Figure S1. Ilustrative diagram of Chagasic patientes with and without chronic cardiomyopathy and control. The diagrams were plotted using the global median cytokine index as the cut-off mark to identify as a low (□) or high (■) cytokine producer. **Figure S2. Ilustrative diagram of patients with chronic Chagas cardiomyopathy infected with different DTU's and control.** The diagrams were plotted using the global median cytokine index as the cut-off mark to identify as a low (□) or high (■) cytokine producer.
(PDF)

File S2 File S2 includes the following: Table S1. MFI of with (CARD) and without (NON-CARD) chronic cardiomyopathy chagas patients and control. **Table S2**. MFI of patients with chronic Chagas cardiomyopathy infected with different DTU's and control **Table S3.** Kaiser-Meyer-Olkin and Barlett's Test for with and without chronic cardiomyopathy chagasic patients and control. **Table S4.** Communalities for with and without chronic cardiomyopathy chagasic patients and control. **Table S5**. Total Variance Explanied for with and without chronic cardiomyopathy chagasic patients and control. **Table S6.** Kaiser-Meyer-Olkin and Barlett's Test for patients with chronic Chagas cardiomyopathy infected with different DTU's and control. **Table S7.** Communalities for patients with chronic Chagas cardiomyopathy infected with different DTU's and control. **Table S8.** Total Variance Explanied for patients with chronic Chagas cardiomyopathy infected with different DTU's and control. **Table S9.** Classification Result for discriminant analyze for with and without chronic cardiomyopathy chagasic patients and control. **Table S10.** Classification Result for discriminant analyze for patients with chronic Chagas cardiomyopathy infected with different DTU's and control.
(DOCX)

Acknowledgments

We thank F. Quiroz, M. Florez at Fundación Cardiovascular, San Gil and Santander, Colombia. S. Navarrete at Hospital de la Policia, Bogotá, Colombia and J. Betancourt at ClínicaAboodShaio, Bogotá, Colombia for the recruitment of patients for the BENEFIT project in Colombia.

Author Contributions

Conceived and designed the experiments: CP JDR FG. Performed the experiments: CP JDR NG JSR. Analyzed the data: CP OAMF JDR. Contributed reagents/materials/analysis tools: CP MF NG JDR JSR JAMN CAM FR FG. Wrote the paper: CP JDR FG.

References

1. WHO (2007) World Health Organization Global health atlas. Available: http://wwwwhoint/globalatlas/Accessed 2008 Mar 2.
2. Rassi Jr A, Rassi A, Marcondes de Rezende J (2012) American Trypanosomiasis (Chagas Disease). Infectious Disease Clinics of North America 26: 275–291.
3. Schmunis GA, Yadon ZE (2010) Chagas disease: A Latin American health problem becoming a world health problem. Acta Tropica 115: 14–21.
4. Coura JR, Junqueira ACV, Fernandes O, Valente SAS, Miles MA (2002) Emerging Chagas disease in Amazonian Brazil. Trends in Parasitology 18: 171–176.
5. Pissetti CW, Correia D, de Oliveira RF, Llaguno MM, Balarin MAS, et al. (2011) Genetic and Functional Role of TNF-alpha in the Development *Trypanosoma cruzi* Infection. PLoS Negl Trop Dis 5: e976.
6. Macedo AM, Machado CR, Oliveira RP, Pena SDJ (2004) *Trypanosoma cruzi*: genetic structure of populations and relevance of genetic variability to the pathogenesis of chagas disease. Memerias do Instituto Oswaldo Cruz 99: 1–12.
7. Pissetti CW, Correia D, Braga T, Faria GEL, Oliveira RFd, et al. (2009) Associaco entre os niveis plasmaticos de TNF-α, IFN-γ, IL-10, Oxido nitrico e os isotipos de IgG especificos nas formas clinicas da doenca de Chagas cronica. Revista da Sociedade Brasileira de Medicina Tropical 42: 425–430.
8. Dutra WO, Menezes CAS, Villani FNA, Costa GCd, Silveira ABMd, et al. (2009) Cellular and genetic mechanisms involved in the generation of protective and pathogenic immune responses in human Chagas disease. Memórias do Instituto Oswaldo Cruz 104: 208–218.
9. Tarleton RL (2007) Immune system recognition of *Trypanosoma cruzi*. Current Opinion in Immunology 19: 430–434.
10. Vitelli-Avelar DM, Sathler-Avelar R, Massara RL, Borges JD, Lage PS, et al. (2006) Are increased frequency of macrophage-like and natural killer (NK) cells, together with high levels of NKT and CD4+CD25high T cells balancing activated CD8+ T cells, the key to control Chagas' disease morbidity? Clinical & Experimental Immunology 145: 81–92.
11. D'Ávila DA, Guedes PM, Castro AM, Gontijo ED, Chiari E, et al. (2009) Immunological imbalance between IFN-γ and IL-10 levels in the sera of patients with the cardiac form of Chagas disease. Memórias do Instituto Oswaldo Cruz 104: 100–105.
12. Ferreira RC, Ianni BM, Abel LC, Buck P, Mady C, et al. (2003) Increased plasma levels of tumor necrosis factor-α in asymptomatic/"indeterminate" and Chagas disease cardiomyopathy patients. Memórias do Instituto Oswaldo Cruz 98: 407–412.

13. Torres OA, Calzada JE, Beraún Y, Morillo CA, González A, et al. (2010) Role of the IFNG +874T/A polymorphism in Chagas disease in a Colombian population. Infection, Genetics and Evolution 10: 682–685.
14. Armah H, Wilson N, Sarfo B, Powell M, Bond V, et al. (2007) Cerebrospinal fluid and serum biomarkers of cerebral malaria mortality in Ghanaian children. Malaria Journal 6: 147.
15. Erdman LK, Dhabangi A, Musoke C, Conroy AL, Hawkes M, et al. (2011) Combinations of Host Biomarkers Predict Mortality among Ugandan Children with Severe Malaria: A Retrospective Case-Control Study. PLoS ONE 6: e17440.
16. Boulware DR, Meya DB, Bergemann TL, Wiesner DL, Rhein J, et al. (2010) Clinical Features and Serum Biomarkers in HIV Immune Reconstitution Inflammatory Syndrome after Cryptococcal Meningitis: A Prospective Cohort Study. PLoS Med 7: e1000384.
17. Ong'echa JM, Davenport GC, Vulule JM, Hittner JB, Perkins DJ (2011) Identification of Inflammatory Biomarkers for Pediatric Malarial Anemia Severity Using Novel Statistical Methods. Infection and Immunity 79: 4674–4680.
18. Zingales B, Andrade S, Briones M, Campbell D, Chiari E, et al. (2009) A new consensus for *Trypanosoma cruzi* intraspecific nomenclature: second revision meeting recommends TcI to TcVI. Memórias do Instituto Oswaldo Cruz 104: 1051–1054.
19. Zingales B, Miles MA, Campbell DA, Tibayrenc M, Macedo AM, et al. (2012) The revised Trypanosoma cruzi subspecific nomenclature: Rationale, epidemiological relevance and research applications. Infection, Genetics and Evolution 12: 240–253.
20. Ramírez JD, Guhl F, Messenger L, Lewis M, Montilla M, et al. (2012) Contemporary cryptic sexuality in *Trypanosoma cruzi*. Molecular Ecology 21: 4216–26.
21. Añez N, Crisante G, Silva FMd, Rojas A, Carrasco H, et al. (2004) Predominance of lineage I among *Trypanosoma cruzi* isolates from Venezuelan patients with different clinical profiles of acute Chagas' disease. Tropical Medicine & International Health 9: 1319–1326.
22. Burgos JM, Diez M, Vigliano C, Bisio M, Risso M, et al. (2010) Molecular Identification of *Trypanosoma cruzi* Discrete Typing Units in End-Stage Chronic Chagas Heart Disease and Reactivation after Heart Transplantation. Clinical Infectious Diseases 51: 485–495.
23. Ramírez JD, Guhl F, Rendón LM, Rosas F, Marin-Neto JA, et al. (2010) Chagas Cardiomyopathy Manifestations and *Trypanosoma cruzi* Genotypes Circulating in Chronic Chagasic Patients. PLoS Negl Trop Dis 4: e899.
24. Zafra G, Mantilla J, Valadares H, Macedo A, González C (2008) Evidence of *Trypanosoma cruzi* II infection in Colombian chagasic patients. Parasitology Research 103: 731–734.
25. Miguel BJ, Diez M, Vigliano C, Duffy T, Bisio M, et al. (2008) Molecular Diagnosis, Follow-up and Identification of Natural *Trypanosoma cruzi* Populations in Chagas Heart Disease Patients Undergoing Clinical Reactivation after Heart Transplantation. International Journal of Infectious Diseases 12, Supplement 2: S11–S12.
26. Diosque P, Barnabé, Padilla AM, Marco JD, Cardozo RnM, et al. (2003) Multilocus enzyme electrophoresis analysis of *Trypanosoma cruzi* isolates from a geographically restricted endemic area for Chagas disease in Argentina. International Journal for Parasitology 33: 997–1003.
27. Cura CI, Mejía-Jaramillo AM, Duffy Ts, Burgos JM, Rodriguero M, et al. (2010) *Trypanosoma cruzi* I genotypes in different geographical regions and transmission cycles based on a microsatellite motif of the intergenic spacer of spliced-leader genes. International Journal for Parasitology 40: 1599–1607.
28. Marcili A, Lima L, Valente VC, Valente SoA, Batista JS, et al. (2009) Comparative phylogeography of *Trypanosoma cruzi* TCIIc: New hosts, association with terrestrial ecotopes, and spatial clustering. Infection, Genetics and Evolution 9: 1265–1274.
29. Ramírez JD, Montilla M, Cucunubá ZM, Floréz AC, Zambrano P, et al. (2013) Molecular Epidemiology of Human Oral Chagas Disease Outbreaks in Colombia. PLoS Negl Trop Dis 7: e2041.
30. Bautista-López NL, Morillo CA, López-Jaramillo P, Quiroz R, Luengas C, et al. (2013) Matrix metalloproteinases 2 and 9 as diagnostic markers in the progression to Chagas cardiomyopathy. American heart journal 165: 558–566.
31. Gomes JAS, Bahia-Oliveira LMG, Rocha MOC, Martins-Filho OA, Gazzinelli G, et al. (2003) Evidence that Development of Severe Cardiomyopathy in Human Chagas' Disease Is Due to a Th1-Specific Immune Response. Infection and Immunity 71: 1185–1193.
32. Corrêa-Oliveira R, Gomes JdAS, Lemos EM, Cardoso GM, Reis DDÁ, et al. (1999) The role of the immune response on the development of severe clinical forms of human Chagas disease. Memórias do Instituto Oswaldo Cruz 94: 253–255.
33. López L, Arai K, Giménez E, Jiménez M, Pascuzo C, et al. (2006) C-Reactive Protein and Interleukin-6 Serum Levels Increase as Chagas Disease Progresses Towards Cardiac Failure. Revista Española de Cardiología 59: 50–56.
34. Zafra G, Morillo C, Martín J, González A, González CI (2007) Polymorphism in the 3' UTR of the IL12B gene is associated with Chagas disease cardiomyopathy. Microbes and Infection 9: 1049–1052.
35. Dutra WO, Rocha MOC, Teixeira MM (2005) The clinical immunology of human Chagas disease. Trends in Parasitology 21: 581–587.
36. Costa GC, da Costa Rocha MO, Moreira PR, Menezes AS, Silva MR, et al. (2009) Functional IL-10 Gene Polymorphism Is Associated with Chagas Disease Cardiomyopathy. Journal of Infectious Diseases 199: 451–454.
37. Satthaporn S, Eremin O (2001) Dendritic cells (I): Biological functions. J R Coll Surg Edinb 46: 9–19.
38. Campos MAS, Almeida IC, Takeuchi O, Akira S, Valente EP, et al. (2001) Activation of Toll-Like Receptor-2 by Glycosylphosphatidylinositol Anchors from a Protozoan Parasite. The Journal of Immunology 167: 416–423.
39. Guedes PMM, Gutierrez FRS, Silva GK, Dellalibera-Joviliano R, Rodrigues GJ, et al. (2012) Deficient Regulatory T Cell Activity and Low Frequency of IL-17-Producing T Cells Correlate with the Extent of Cardiomyopathy in Human Chagas' Disease. PLoS Negl Trop Dis 6: e1630.
40. Luiza-Silva M, Campi-Azevedo AC, Batista MA, Martins MA, Avelar RS, et al. (2011) Cytokine Signatures of Innate and Adaptive Immunity in 17DD Yellow Fever Vaccinated Children and Its Association With the Level of Neutralizing Antibody. Journal of Infectious Diseases 204: 873–883.

OPEN ACCESS Freely available online

PLOS | NEGLECTED TROPICAL DISEASES

Global Metabolomic Profiling of Acute Myocarditis Caused by *Trypanosoma cruzi* Infection

Núria Gironès[1,2]*, Sofía Carbajosa[1], Néstor A. Guerrero[1¤], Cristina Poveda[1], Carlos Chillón-Marinas[1], Manuel Fresno[1,2]

1 Centro de Biología Molecular Severo Ochoa, CSIC-UAM, Madrid, Spain, **2** Instituto de Investigación Sanitaria de la Princesa, Madrid, Spain

Abstract

Chagas disease is caused by *Trypanosoma cruzi* infection, being cardiomyopathy the more frequent manifestation. New chemotherapeutic drugs are needed but there are no good biomarkers for monitoring treatment efficacy. There is growing evidence linking immune response and metabolism in inflammatory processes and specifically in Chagas disease. Thus, some metabolites are able to enhance and/or inhibit the immune response. Metabolite levels found in the host during an ongoing infection could provide valuable information on the pathogenesis and/or identify deregulated metabolic pathway that can be potential candidates for treatment and being potential specific biomarkers of the disease. To gain more insight into those aspects in Chagas disease, we performed an unprecedented metabolomic analysis in heart and plasma of mice infected with *T. cruzi*. Many metabolic pathways were profoundly affected by *T. cruzi* infection, such as glucose uptake, sorbitol pathway, fatty acid and phospholipid synthesis that were increased in heart tissue but decreased in plasma. Tricarboxylic acid cycle was decreased in heart tissue and plasma whereas reactive oxygen species production and uric acid formation were also deeply increased in infected hearts suggesting a stressful condition in the heart. While specific metabolites allantoin, kynurenine and p-cresol sulfate, resulting from nucleotide, tryptophan and phenylalanine/tyrosine metabolism, respectively, were increased in heart tissue and also in plasma. These results provide new valuable information on the pathogenesis of acute Chagas disease, unravel several new metabolic pathways susceptible of clinical management and identify metabolites useful as potential specific biomarkers for monitoring treatment and clinical severity in patients.

Citation: Gironès N, Carbajosa S, Guerrero NA, Poveda C, Chillón-Marinas C, et al. (2014) Global Metabolomic Profiling of Acute Myocarditis Caused by *Trypanosoma cruzi* Infection. PLoS Negl Trop Dis 8(11): e3337. doi:10.1371/journal.pntd.0003337

Editor: Herbert B. Tanowitz, Albert Einstein College of Medicine, United States of America

Received July 25, 2014; **Accepted** October 12, 2014; **Published** November 20, 2014

Data Availability: The authors confirm that all data underlying the findings are fully available without restriction. All relevant data are within the paper and its Supporting Information files

Funding: This work was supported by "Ministerio de Ciencia e Innovación" (SAF2010-17833); "Fondo de Investigaciones Sanitarias" (PS09/00538 and PI12/00289); "Red de Investigación de Centros de Enfermedades Tropicales" (RICET RD12/0018/0004); European Union (HEALTH-FE-2008-22303, ChagasEpiNet); "Universidad Autónoma de Madrid" and "Comunidad de Madrid" (CC08-UAM/SAL-4440/08); AECID Cooperation with Argentine (A/025417/09 and A/031735/10), Comunidad de Madrid (S-2010/BMD-2332) and "Fundación Ramón Areces". SC was recipient of a FPI fellowship financed by Spanish "Ministerio de Ciencia y Tecnología". The funders had no role in study design, data collection and analysis, decision to publish, or preparation of the manuscript.

Competing Interests: The authors have declared that no competing interests exist.

* Email: ngirones@cbm.csic.es

¤ Current address: CPTP, Centre de Physiopathologie de Toulouse-Purpan Inserm UMR1043 - CNRS UMR5282, Université Toulouse III, CHU Purpan, Toulouse, France

Introduction

Chagas disease, caused by the protozoan parasite *Trypanosoma cruzi*, affects approximately 8 million people worldwide [1] and kills more than 15,000 each year, thus representing a major cause of morbidity and mortality in endemic countries [2]. Chagasic cardiomyopathy is the most serious and frequent manifestation in *T. cruzi* infected patients in the chronic phase of the disease. Acute Chagas disease is an often nonspecific and frequently unrecognized condition, but acute infection associated to congenital cases and oral transmission can have a fatal outcome in humans [3]. Myocarditis, although uncommonly reported and difficult to diagnose, is uniformly present during acute infection. Moreover, endomyocardial biopsies taken when patients are diagnosed during this phase of the disease consistently reveal acute myocarditis, even if the patient is asymptomatic [4]. The ranges of acute cardiac pathogenesis are characterized by pericardial effusion, pericarditis, ventricular enlargement with dysfunction or congestive heart failure or both [5]. In the chronic phase, myocardial inflammation associated to mononuclear infiltrate is a common finding in histological sections, although the spatial association between parasites and inflammatory infiltrate is controversial and manifests as heart failure, arrhythmia, heart block, thromboembolism, stroke, and sudden death. Chronic Chagasic Cardiomyopathy is characterized by its severity, as well as by a worse prognosis when compared with other cardiomyopathies [6].

T. cruzi has a complex life cycle involving several stages in both vertebrates and insect vectors. It infects and replicates in macrophages and cardiomyocytes as well as many other cell types [2]. However, the pathogenesis is thought to be dependent on an immune-inflammatory reaction to a low-grade infection [7,8]. To date no vaccine is available [9] and current drugs have many side effects [10]. Some chronic asymptomatic patients are currently treated with those drugs, although its efficacy has not been clearly demonstrated yet, basically because there is no useful surrogate

Author Summary

Chagas disease, caused by *Trypanosoma cruzi*, is the most common cause of cardiomyopathy in Latin America. After the acute phase myocarditis, the disease becomes asymptomatic, and many years later some patients may develop Chagas cardiomyopathy. Treatment is available, but causes side effects. Thus, new drugs are needed, but there are no good tools to assess treatment efficacy. We performed the first global metabolomics analysis in heart tissue and plasma from mice infected with *T. cruzi* along the infection. We have identified more than 200 biochemicals (around 2/3 of total) that significantly differed in heart and 100 (around 1/3) in plasma. Some of those show extremely marked and highly significant differences. More importantly, our results unravel many new aspects of metabolic alterations that can be useful for: a) better understanding the pathogenesis of this disease; b) provide new clinic-pathological data of *T. cruzi* infection that can be potentially used for a better clinical management of Chagasic patients; c) define several metabolites as potential biomarkers of this disease. Thus, our study identifies common biomarkers of cardiomyopathy but more importantly specific candidate biomarkers of acute Chagas Disease Cardiomyopathy, not observed in a clinically similar disease Idiopathic Dilated Cardiomiopathy. Allantoin, kynurenine and p-cresol sulfate, that can be easily detected in serum, are highly promising candidates. In summary, we think our results would help to better understand the pathogenesis and management of the disease and offer new candidate biomarkers for monitoring the severity of the disease and treatment efficacy.

marker for clinical improvement and therapeutic efficacy. In the meantime, follow up of the treated patients by PCR turned out to be the only way to guide physicians to deal with the disease [11,12]. Several studies on biomarkers of cure have been proposed based on seronegativization of antibodies, lytic antibodies, hemostatic parameters, natriuretic peptides, recombinant antigens and proteomic assays [13] but none of them seems to be particularly sensitive. Thus, new biomarkers are needed to monitor responses to treatment.

Global metabolomic analysis is a powerful tool to understand the pathophysiology of parasite infection as well as to identify biomarkers of disease, as it has been done for dilated cardiomyopathy [14]. Thus, identification of metabolic conditions could provide a deeper knowledge of the pathophysiology and the immunopathology as well of being of clinical value, since restoration of those metabolites to basal levels could be beneficial for the host during acute infection. On the other hand, they could be also useful as biomarkers. The current paucity of effective preventive or therapeutic options is another strong motivation for the study of host-parasite metabolism interplay.

Moreover, metabolic function can clearly affect the activity of the immune system [15,16,17]. In this regard, in acute *T. cruzi* infection there are major immunological changes [18], that in some cases are linked to the production of amino acid metabolites, as kynurenine, a product of indolamine 2,3 dioxygenase (IDO) enzymatic activity from tryptophan, which is supposed to control parasite growth [19,20]. In addition, the levels of L-arginine, modulated by Arginase enzymatic activity, deeply affect the activity of T lymphocytes in experimental *T. cruzi* infection in mice [21]. Thus, the knowledge of the metabolic alterations will help to understand the course of the infection.

Since *T. cruzi* is able to replicate intracellularly, it will likely affect infected host cell metabolism. Thus, metabolic changes were observed *in vitro* after infection with the parasite in endothelial cells [22]. In addition, Garg et al performed microarray analysis of the cardiomyocyte mitochondrial metabolism during *in vivo* infection showing deficiencies in mitochondrial oxidative phosphorylation-mediated ATP generation that plays an important role in cardiac homeostasis [23]. More recently, Caradonna et al. using a genome-scale functional screen identified interconnected metabolic networks centered around host energy production, nucleotide metabolism, pteridine biosynthesis, and fatty acid oxidation as key processes that fuel intracellular *T. cruzi* growth in HeLa cells *in vitro* [24].

However, there are no reports to date on global metabolomic analysis during *in vivo T. cruzi* infection. Moreover, metabolite levels during infection may reflect not only host metabolism but also the possible contribution of parasite-derived metabolites, which has never been assessed before. Thus, here we studied the metabolic profile in heart and plasma from *T. cruzi* infected mice. The results unravel many new aspects of metabolic alterations that can be useful for better understanding the pathogenesis of this disease and to better control *T. cruzi* infection as well as showing the potential of particular metabolites as biomarkers of this disease.

Materials and Methods

Mice and parasites

Young adult (6 to 8-week-old) BALB/c female mice were transported from Charles River Laboratories and hosted in a controlled environment. *In vivo* infections performed with Y *T. cruzi* strain (obtained from Dr. John David, Department of medicine, Harvard Medical School, Boston, Massachusetts, U.S.A.). Blood trypomastigotes were routinely maintained by infecting IFNγ receptor-deficient mice (129 Ifngrttm1Agt/J) [25] purifying them from their blood. These mice were a gift from Manfred Kopf (Max-Planck-Institute for Immunobiology, Freiburg). Parasitemia levels were checked every two-three days by microscopic inspection and counting of parasites in a 5 µl drop of the tail vein blood as described [26]. Real time qPCR was performed as described [27].

Ethics statement

This study was carried out in strict accordance with the European Commission legislation for the protection of animals used for scientific purposes (Directive 2010/63/EU). Mice were maintained under pathogen-free conditions at the Centro de Biología Molecular Severo Ochoa (CSIC-UAM) animal facility. The protocol for the treatment of the animals was approved by the "Comité de Ética de Investigación de la Universidad Autónoma de Madrid", Spain (permit CEI-47-899). Animals had unlimited access to food and water. They were euthanized in a CO_2 chamber and all efforts were made to minimize their suffering.

Experimental design

Global biochemical profiles were determined in methanol extracts derived from mouse heart tissue and plasma from two independent experiments including uninfected mice (n = 6) and mice infected with 2,000 blood trypomastigotes of the Y strain of *T. cruzi* (see supplemental experimental information for details), and sacrificed at 14 (n = 6) and 21 days post-infection (n = 6). Plasma and heart tissue were elicited. To prevent blood coagulation, syringes were impregnated with heparin, and plasma was obtained from the supernatant immediately after centrifugation of the blood and frozen at −80°C. Hearts were perfused with

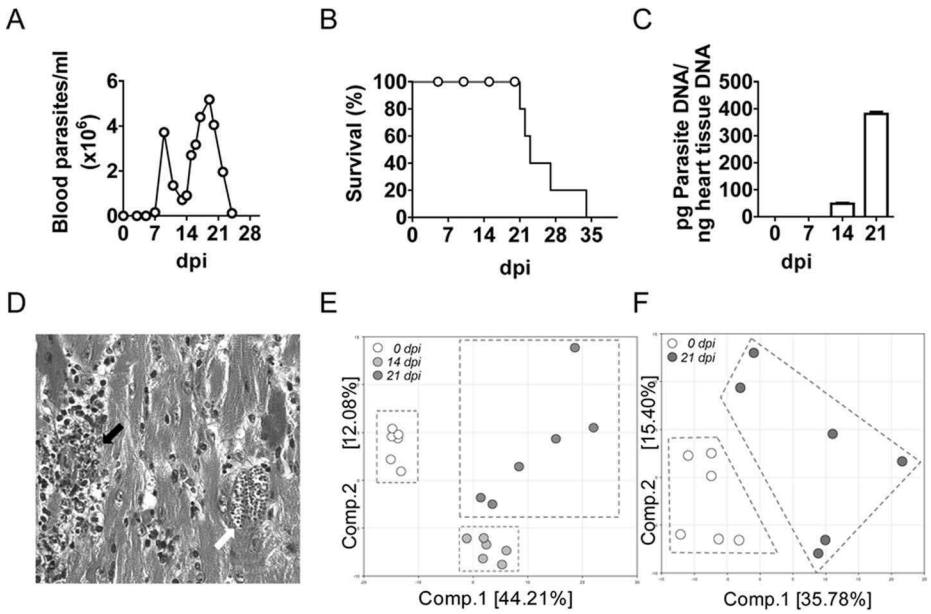

Figure 1. Parasite burden and mice survival during *T. cruzi* infection. Parasite burden in blood and survival were monitored every two-three days as described in material and methods section. (A) Parasitemia. (B) Parasite DNA quantification by qPCR as described in the methods. (C) Mice survival. (D) Representative heart tissue section stained with H&E showing amastigote nests (white arrow) and mononuclear cell infiltration (black arrow). (E) Principal component analysis in heart tissue samples. (F) Principal component analysis in plasma samples.
doi:10.1371/journal.pntd.0003337.g001

10 ml of phosphate buffered saline (PBS) and heparin to remove blood and immediately frozen at −80°C. Samples were prepared following instructions from Metabolon (see supplemental experimental information for details).

Parasite DNA quantitative real time PCR

At different days post infection mice were euthanized in a CO_2 chamber and blood and heart tissue were collected. Hearts were perfused with PBS and heparin (1 U/ml) and were minced into small pieces with a sterile scalpel and DNA was isolated with High PurePCR Template preparation Kit, Roche. For *T. cruzi* detection, we followed the qPCR assay described by [27]. Briefly, 100, 10, 1, 0.1 and 0.01 pg of DNA purified from Y strain epimastigotes were used to generate the standard curve. Experimental heart tissue qPCR reactions contained 100 ng of genomic DNA. Murine *Tnf* gene qPCR reactions were set up for normalization and expressed as pg Parasite DNA/ng heart tissue DNA.

Biochemical sample preparation

Samples were prepared following Metabolon's instructions. Briefly, heart tissue was defrosted at room temperature (RT) and cut with sterile surgical blade. Approximately 80 mg of tissue were weighed and disposed in 2 ml eppendorf tubes. Heart tissue was heat-inactivated at 50°C for 30 min. 1600 µl of the extraction methanol solvent A (containing standards resuspended in 80% HPLC grade Methanol; Sigma Aldrich 494291, CAS 67-56-1) were added to the sample. Plasma was defrosted at RT. 100 µl of plasma was transferred to a new tube and any parasites present in plasma were heat-inactivated at 50°C for 30 min. Then, plasma was combined with 450 ul of extraction Metabolon solvent B (containing standards resuspended in 100% HPLC grade Methanol; Sigma Aldrich 494291, CAS 67-56-1). After incubation for 24 h at RT, samples were stored at −80°C until shipment in dry ice.

Metabolomic analysis

The extracted samples were split into equal parts for analysis on the gas chromatography (GC)/mass spectrometry (MS) and liquid chromatography (LC)/MS platforms. Instrument variability was determined by calculating the median relative standard deviation (RSD) for the internal standards that were added to each sample prior to injection into the mass spectrometers. Overall process variability was determined by calculating the median RSD for all endogenous metabolites (i.e., non-instrument standards) present in 100% of the Matrix samples, which are technical replicates of pooled samples. Values were normalized in terms of raw area counts (OrigScale). For a single day run, this is equivalent to the raw data. Each biochemical in OrigScale is rescaled to set the median equal to 1 and expressed as imputed normalized counts for each biochemical (ScaledImpData).

Principal components analysis

Principal component analysis (PCA) is a mathematical procedure that uses an orthogonal transformation to convert a set of observations of possibly correlated variables into a set of values of linearly uncorrelated variables called principle components. This transformation is defined in such a way that the first principal component has the largest possible variance (that is, accounts for as much of the variability in the data as possible), and the second component in turn has the highest variance possible under the constraint that it is orthogonal to (i.e., uncorrelated with) the preceding component. Thus, data set interpretation is that the stratification of metabolites by component 1 may have the greatest contribution to separating the metabolic signature of these samples followed by component 2.

Statistical analysis

Pair-wise comparisons of data from infected mice respect non-infected (0 dpi) were performed by Welch's two sample t-tests using the program "R" http://cran.r-project.org/.

Results

Experimental *T. cruzi* infection

Infection of BALB/c mice with the Y strain of *T. cruzi* produced high parasitemia in the second and third week post-infection (Figure 1A) and no survival was observed by 34 dpi (Figure 1B). In a simultaneous experiment parasite DNA in heart tissue increased up to 21 days post-infection (dpi), the last day analyzed before the end of the experiment (Figure 1C). Besides, histological analysis of the heart at 21 dpi showed heart damage, with intense myocarditis and amastigote nests (Figure 1D).

Metabolic changes

We selected samples at 14 dpi and 21 dpi from heart tissue and plasma 21 dpi for metabolic analysis, corresponding to the acute phase of infection. We performed a global metabolomic analysis and we detected a total of 325 compounds of known identity (named biochemicals) in heart extract and 306 compounds in plasma extract (Table S1). Following log transformation and imputation with minimum observed values for each compound, Welch's two-sample *t*-test was used to identify biochemicals that differed significantly between experimental groups. Our analysis identified more than 200 biochemicals (around 2/3) that differed significantly in heart and 100 (around 1/3) in plasma.

Multiple metabolites were altered upon *T. cruzi* infection, and Principal component analysis (PCA) revealed that, in heart tissue, *T. cruzi* infection was accompanied by distinct biochemical changes compared to control animals (Figure 1E). Components 1 and 2 could be decomposed into several metabolite levels that explained 44.21% and 12.08% of the total variation, respectively. Thus, samples from control and infected mice at 14 dpi grouped separately in the analysis, although more heterogeneity was observed by day 21 post-infection in heart tissue (Figure 1E). Similarly, in plasma, components 1 and 2 explained 35.71% and 15.40%, respectively, and discriminated biochemicals in control and infected mice at 21 dpi, despite the greater heterogeneity observed in this case between individual mice (Figure 1F). PCA components used for the heart and plasma are shown in supplementary tables S2 and S3, respectively, which list the metabolites contributing to the stratification of the PCA profiles. In this files, the coefficient value of each metabolite for component 1 and component 2 are represented. The larger the positive or negative coefficients value for a given metabolite, the greater its contribution to separating the metabolic profiles and thus the better candidate it may be as a biomarker. We will highlight below the more relevant changes in several pathways.

Glucose metabolism

Compared to uninfected counterparts, glucose levels were elevated in heart tissue by days 14 and 21 post-infection (Figure 2A). This observation likely reflects an increase in glucose uptake considering glucose levels declined in infected plasma over time (Figure 2B). This also agrees with the observed increase of the sorbitol pathway metabolites, sorbitol and fructose, in the heart. Besides, multiple glycolytic intermediates including glucose-6 phosphate and fructose-6-phosphate and the end products pyruvate and lactate were also significantly elevated in infected heart tissue, but not in plasma (Figure 2A and B, respectively). In contrast, reduced glucose shuttling to the pentose phosphate pathway (PPP) was observed in response to infection as marked by lower levels of ribulose and sedoheptulose-7-phosphate. Thus, infected hearts have increased glycolysis.

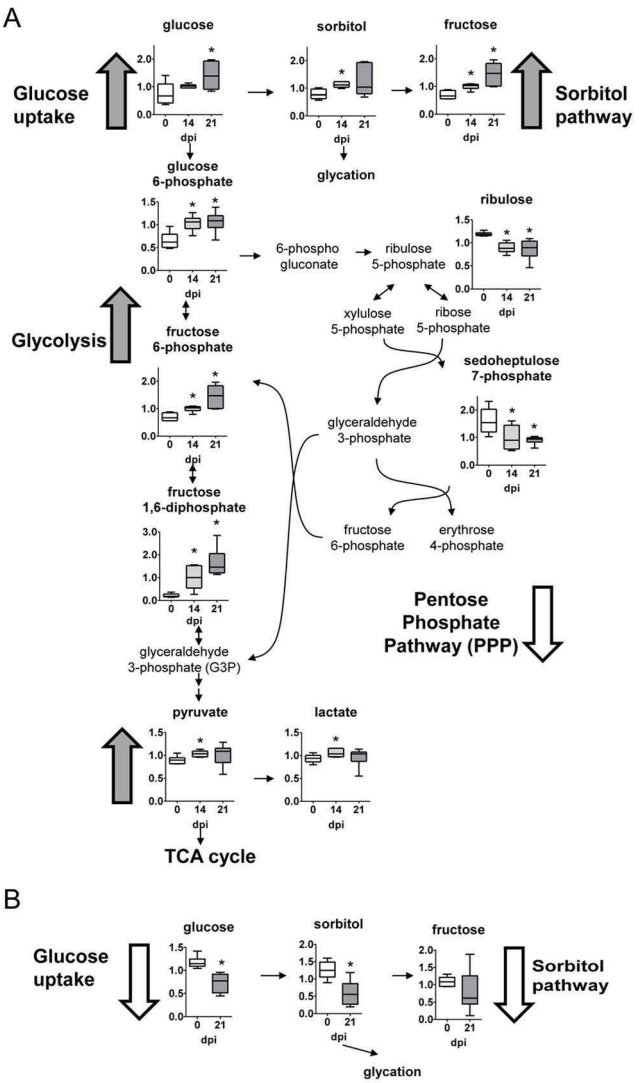

Figure 2. Carbohydrate pathways. (A) Graphs represent the ScaledImpData of different biochemicals of the glycolytic, sorbitol and pentose phosphate pathways from heart tissue. (B) Same as in A from plasma samples. Samples from control uninfected mice are in white boxes, from mice sacrificed at 14 dpi in light gray boxes and from mice sacrificed at 21 dpi in dark grey boxes. Statistically significant differences respect to uninfected mouse samples are denoted, $*p \leq 0.05$.
doi:10.1371/journal.pntd.0003337.g002

Tricarboxylic acid cycle (TCA)

In infected heart tissue, the TCA cycle intermediates, succinylcarnitine and fumarate decreased (Figure 3A). This TCA cycle imbalance in the heart may be indicative of decreased oxidative metabolism, potentially resulting from succinate dehydrogenase (SDH) and electron transport complex II dysfunction. However, all of the TCA cycle metabolites, including succinate, were diminished in plasma of infected mice (Figure 3B).

Lipid metabolism

Following infection, long chain fatty acids such as palmitate, stearate and oleate increased in heart tissue, but reduced in the plasma (Figure 4A and 4B, respectively). Although changes in fatty acid levels may be indicative of a difference in synthesis, malonylcarnitine levels were significantly diminished in infected tissue, suggesting a limited capacity for lipid biogenesis. Instead,

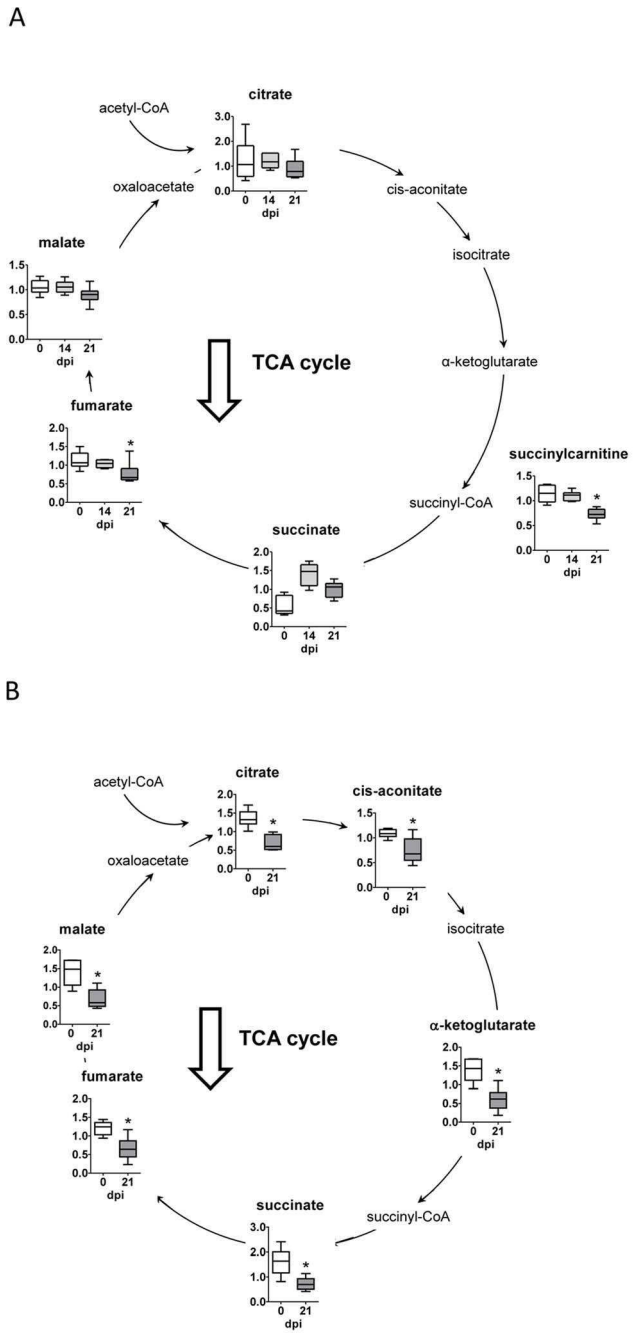

Figure 3. Tricarboxyilic acid cycle. (A) Graphs represent the ScaledImpData of different biochemicals of the tricarboxyilic acid cycle from heart tissue samples. (B) Same as in A from plasma samples. Samples from control uninfected mice are in white boxes, from mice sacrificed at 14 dpi in light gray boxes and from mice sacrificed at 21 dpi in dark grey boxes. Statistically significant differences respect to uninfected mouse samples are denoted, *p≤0.05.
doi:10.1371/journal.pntd.0003337.g003

uptake of lipids from plasma and fatty acid β-oxidation in the heart tissue may be altered considering that long chain carnitine conjugate lipids such as palmitoylcarnitine and oleoylcarnitine were much higher in infected animals and may reflect increased lipid transport into the mitochondria, as evidenced by lower levels of carnitine.

Phospholipid metabolism

The phospholipid catabolite glycerophosphorylcholine (GPC) was elevated in heart tissue after infection (Figure 4C). This may be indicative of a change in phospholipid dynamics since it was accompanied by much higher levels of multiple lysolipids such as 1-linoleoylglycerophosphoethanolamine and 1-palmitoleoylglycerophosphocholine that may reflect enhanced hydrolysis of phospholipids or lipid bodies. In contrast, these metabolites were diminished or unaltered in the plasma of infected animals (Figure 4D). Additionally, phospholipid precursors as choline, choline phosphate, ethanolamine, and phosphoethanolamine especially at late time points also accumulated in infected heart tissue and may be indicative of an increased capacity for phospholipid synthesis, and thus very high accumulation of phospholipids in the heart of infected animals.

Branched chain amino acid metabolism (BCAA)

Heart tissue from *T. cruzi* infected mice possessed higher levels of the BCAAs leucine, isoleucine and valine (Figure 5A). Differences in BCAA levels can reflect changes in their degradation and utilization. In this sense, the downstream products 2-methylbutyrylcarnitine, isovalerylcarnitine and alpha-keto acids (3-methyl-2-oxovalerate and 4-methyl-2-oxopentanoate) were significantly elevated in heart. Additionally, BCAA catabolites including the alpha-keto acids were also increased in plasma (Figure 5B).

Nucleotide metabolism

Compared to uninfected controls, heart tissue from *T. cruzi* infected mice dramatically exhibited much lower levels of multiple purine nucleotides and related metabolites such as adenine, inosine, and hypoxanthine being the levels of adenine almost depleted (Figure 6A). Such metabolites indicate severe alterations in redox homeostasis. In addition, heme, another product of redox activity increased 20–30 times in the infected heart (Figure 6B). In contrast, higher levels of xanthosine, xanthine, urate and allantoin were found in heart tissue from infected mice (Figure 6A). Similar to heart tissue, lower levels of inosine and increased allantoin were found in plasma (Figure 6C). These results may reflect a decrease in synthesis as supported by lower levels of pentose phosphate pathway metabolism. However, more likely purine degradation may be strongly enhanced as evidenced by the great accumulation of the downstream catabolic products xanthosine, urate, and allantoin in infected hearts.

Tryptophan metabolism

Tryptophan and some of its metabolites as kynurenine, c-glycosyltryptophan and 3-indoxyl sulfate were increased in heart tissue (Figure 7A) as well as kynurenine and c-glycosyltryptophan in plasma from infected mice (Figure 7B).

p-Cresol sulfate

p-Cresol sulfate is part of the phenylalanine and tyrosine metabolism, and it was found strongly increased both in heart tissue and plasma from infected mice (Figure **7C** and **7D**, respectively). p-Cresol sulfate is likely a microbial metabolite that is found in urine and blood and likely derives from secondary metabolism of p-Cresol.

Discussion

Chagas is a complex disease with acute and chronic phases showing cardiac alterations. Although, the immunopathogenesis is relatively well established, there are still several issues poorly

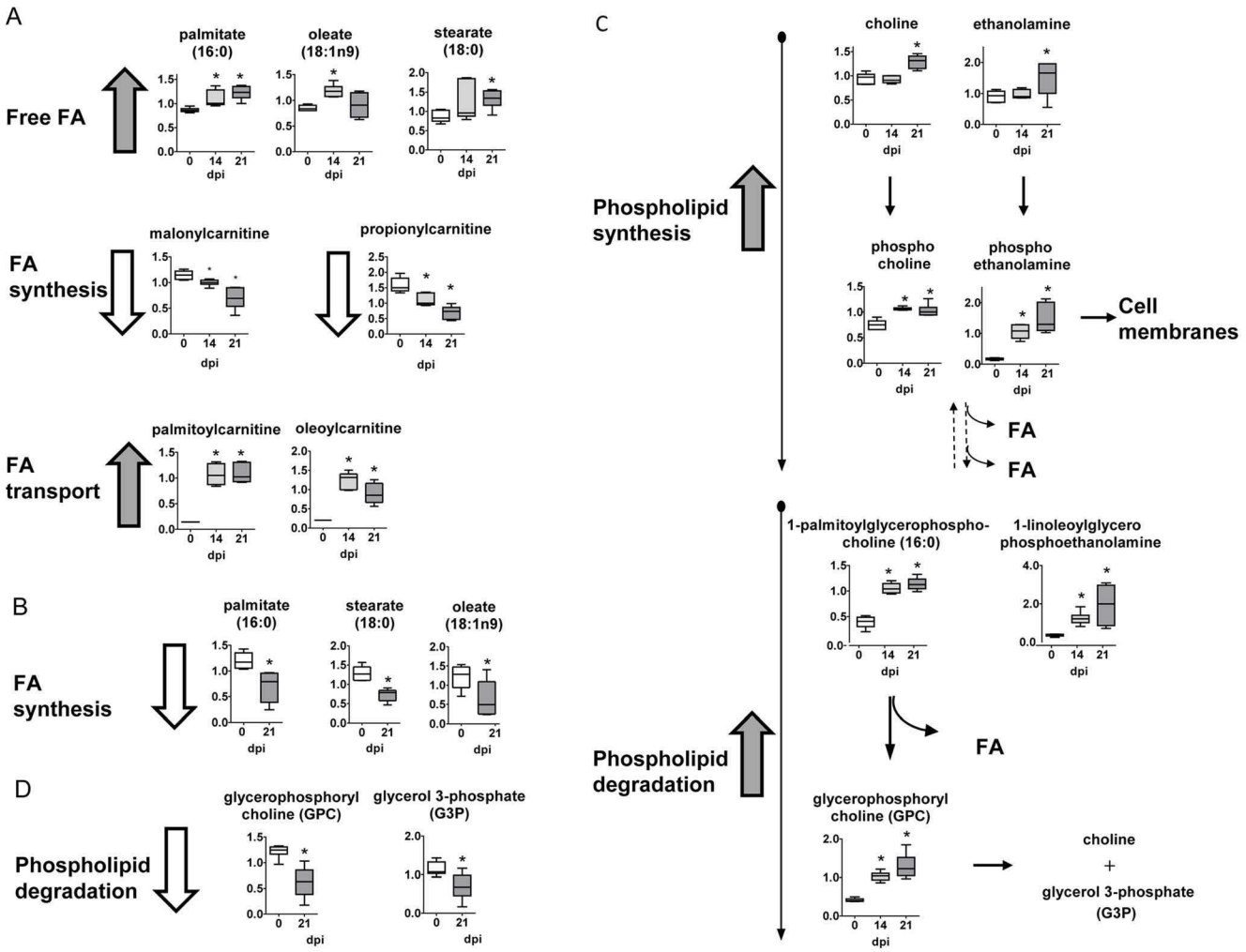

Figure 4. Fatty acid and phospholipid metabolism. (A) Graphs represent the ScaledImpData of different biochemicals of fatty acid metabolism from heart tissue. (B) Same as in A from plasma samples. (C) Same as in A of different biochemicals of phospholipid metabolism from heart tissue samples. (D) Same as in C from plasma samples. Samples from control uninfected mice are in white boxes, from mice sacrificed at 14 dpi in light gray boxes and from mice sacrificed at 21 dpi in dark grey boxes. Statistically significant differences respect to uninfected mouse samples are denoted, *$p \leq 0.05$.

doi:10.1371/journal.pntd.0003337.g004

understood. Among those: why a minority of asymptomatic patients become symptomatic after several years?; and which is the reason for the different clinical manifestations?. Besides, few drugs are available to date, which present adverse effects that many patients cannot tolerate. Thus, new drugs are urgently needed, and to achieve that, a deeper knowledge of clinical pathophysiology is required. In this respect, metabolomics may help to better characterize the pathophysiology of the disease as well as to define new biomarkers.

In an unprecedented study, we performed global metabolomic analysis in plasma and heart of mice infected with the *T. cruzi* Y strain. This parasite strain has been considered reticulotropic by many authors in the field. However, other authors claim that the strain might have suffered a change from reticulotropic to myotropic/cardiotropic through time [28]. In agreement with the last, in our experimental model it infects cardiomyocytes [29], produces a characteristic histologic alterations as homogeneous pancarditis with inflammatory infiltrates along epicardium, a high epicardial and sub-epicardial inflammation that was homogenous in auricles and ventricles, myeloid and lymphoid infiltration and intra-myocardial perivasculitis [30] resembling damage observed in Chagasic patients [31]. Moreover, Our analysis revealed that following infection there are many significant biochemical alterations in heart and plasma of infected animals, which are much more evident both in number of changes and in fold variations in the heart, the target organ of *T. cruzi* infection. Our results have identified more than 200 biochemicals (around 2/3) that differed significantly in heart and 100 (around 1/3) in plasma. Some of those showed extremely marked and highly significant differences. More importantly, our results unravel many new aspects of metabolic alterations that can be useful for better understanding the pathogenesis of this disease and to better control *T. cruzi* infection as well as showing the potential of particular metabolites as biomarkers. Our study identifies common biomarkers of cardiomyopathy but more importantly specific candidate biomarkers of acute Chagas Disease Cardiomyopathy, not observed in a clinically similar disease as Idiopathic Dilated Cardiomyopathy.

Alterations include amino acid metabolism, glucose utilization, the TCA cycle, nucleotide catabolism, and membrane lipid

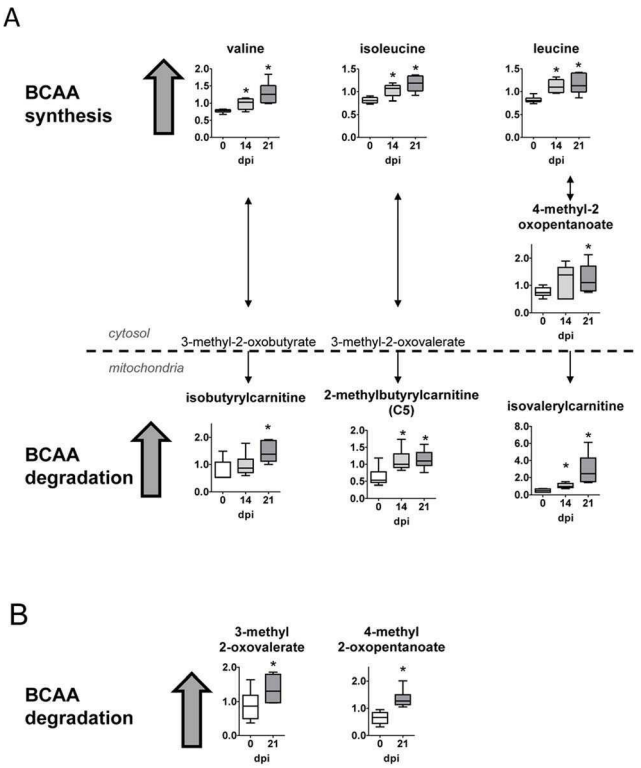

Figure 5. Branched chain amino acid metabolism. (A) Graphs represent the ScaledImpData of different biochemicals of the branched chain amino acid metabolism from heart tissue samples. (B) Same as in A from plasma samples. Samples from control uninfected mice are in white boxes, from mice sacrificed at 14 dpi in light gray boxes and from mice sacrificed at 21 dpi in dark grey boxes. Statistically significant differences respect to uninfected mouse samples are denoted, *$p \leq 0.05$.
doi:10.1371/journal.pntd.0003337.g005

pathways. Glucose can be utilized to support a variety of physiological processes including energy generation, fatty acid synthesis, and nucleotide biogenesis. Our results show that compared to control uninfected animals, glucose levels were elevated in heart tissue by days 14 and 21 post-infection. This observation may reflect an increase in glucose uptake considering that glucose levels declined in infected plasma over time. Furthermore, the accumulation of the sorbitol pathway metabolites (sorbitol and fructose) in the heart, but not in plasma, may be an indication of enhanced glucose uptake since excess glucose is often reduced to sorbitol by aldose reductase. Consequently, higher levels of sorbitol can contribute to the generation of advanced glycation end products (AGE) that have been associated with the development of heart failure in other diseases [32]. In addition, multiple glycolytic intermediates including glucose-6 phosphate and fructose-6-phosphate and the end products lactate and pyruvate were significantly elevated in infected heart tissue and may be indicative of increased glycolysis. In this regard, accelerated rates of glycolysis can be indicative of hypertrophy of the heart [33] that accompanies many forms of heart dysfunction, a hallmark of Chagas disease [34]. Thus, these alterations in glycolytic metabolism may be associated with increased cardiac stress in *T. cruzi* infected hearts and require further investigation. In contrast, reduced glucose shuttling to the pentose phosphate pathway (PPP) was observed in response to infection, which is required for the biogenesis of nucleotides and the regeneration of NADPH necessary for glutathione reduction and anabolic reactions. Thus, diminished PPP metabolism may restrict the biosynthetic capacity of the heart and contribute to altered redox homeostasis.

Altered glycolytic metabolism suggested that the TCA cycle may also differ following *T. cruzi* infection. In fact, in *T. cruzi* infected mice an imbalanced TCA cycle in the heart is likely indicative of decreased oxidative metabolism, potentially resulting from succinate dehydrogenase (SDH) and electron transport complex II dysfunction. This would be in agreement with previous studies where chagasic hearts showed mitochondrial respiratory chain impairment [35]. Since the heart has perpetually high energy demands related to the maintenance of processes such as ion transport, calcium homeostasis, and sarcomeric function, the fact that TCA cycle mediated oxidative metabolism may be diminished following infection may ultimately induce metabolic stress in cardiac tissue. In this respect, disruption of the Krebs cycle is often implicated in energetic imbalances characteristic of myocardial ischemia [36,37]. Alternatively, those selective differences in succinate may be explained by interference of those metabolites by *T. cruzi* metabolism due to fumarate reductase and succinate dehydrogenase enzymatic activities expressed by this parasite [38].

In addition to protein synthesis, branched chain amino acids (BCAA) can be degraded to replenish the TCA cycle and facilitate fatty acid synthesis. Furthermore, diverse injuries and heart diseases are reported to increase consumption of BCAAs. In agreement, heart tissue from *T. cruzi* infected mice possessed higher levels of the BCAAs isoleucine, leucine and valine. Differences in BCAA levels can reflect changes in degradation and amino acid utilization. Additionally, multiple BCAA catabolites including the alpha-keto acids 3-methyl-2-oxovalerate and 4-methyl-2-oxopentanoate and the downstream products 2-methylbutyrylcarnitine and isovalerylcarnitine were significantly elevated in these tissues as well as plasma. Thus, these observations may reflect an increase in amino acid and muscle turnover following infection.

Fatty acids are a critical source of energy for mitochondrial oxidation and cellular ATP generation. Following infection, long chain fatty acids such as palmitate, stearate, and oleate were elevated in heart tissue, but reduced in plasma. Although changes in fatty acid levels may be indicative of a difference in synthesis, malonylcarnitine levels were significantly diminished in infected tissue, suggesting a limited capacity for lipid synthesis. On the contrary, long chain carnitine conjugate lipids such as palmitoylcarnitine and oleoylcarnitine were high suggesting that lipid transport into the mitochondria may be increased. Collectively, these observations suggest that lipid accumulation due to fatty acid uptake in this tissue may not promote intracellular parasite replication by enhancing lipid oxidation as described [24], but instead, by producing a great deal of host cell lipid bodies, a characteristic trait in *T. cruzi* infection [39]. Interestingly, cardiac lipotoxicity results from elevated palmitoly-L-carnitine [40], which we found elevated in hearts of *T. cruzi* infected mice. On the contrary, propionyl-carnitine is considered a cardiac protector [41] and we found it decreased in infected heart.

Phospholipids are essential components of the membrane lipid bilayer. In comparison to control heart tissue, the phospholipid catabolite glycerophosphorylcholine (GPC) was elevated following infection. It may be indicative of a change in phospholipid dynamics and were accompanied by strikingly higher levels of multiple lysolipids such as 1-linoleoylglycerophosphoethanolamine and 1-palmitoleoylglycerophosphocholine that may reflect enhanced hydrolysis of phospholipids or production of lipid bodies. Additionally, the phospholipid precursors choline, choline

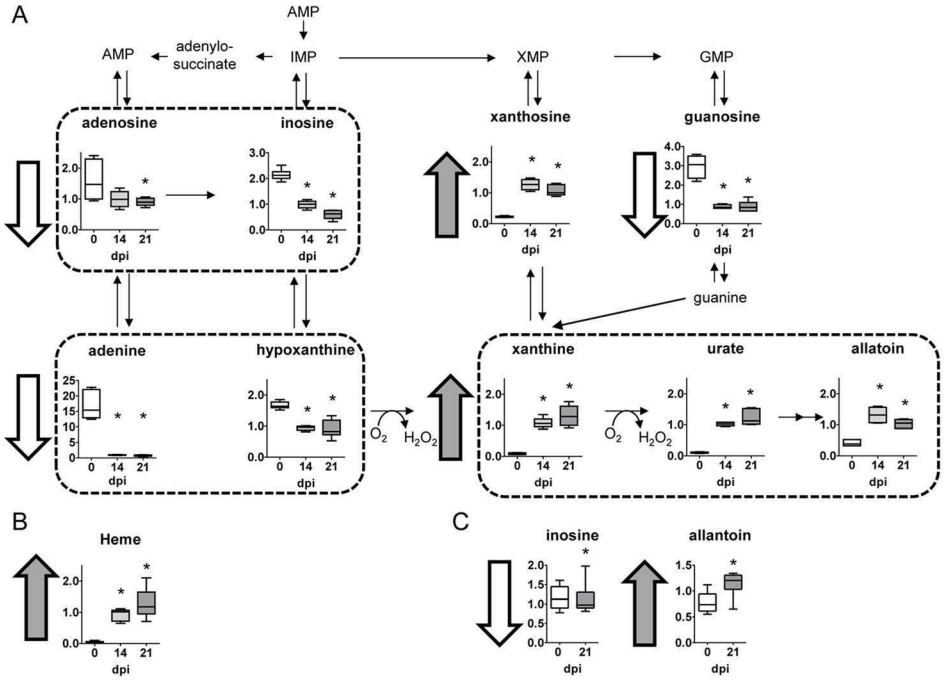

Figure 6. Nucleotide metabolism. (A) Graphs represent the ScaledImpData of different biochemicals of the nucleotide metabolism from heart tissue samples. (B) Same as in A from plasma samples. Samples from control uninfected mice are in white boxes, from mice sacrificed at 14 dpi in light gray boxes and from mice sacrificed at 21 dpi in dark grey boxes. Statistically significant differences respect to uninfected mouse samples are denoted, *p≤0.05.
doi:10.1371/journal.pntd.0003337.g006

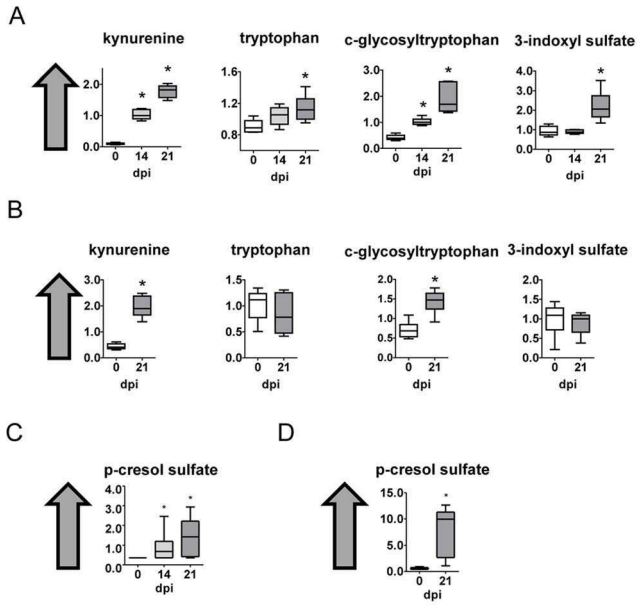

Figure 7. Tryptophan, phenylalanine and tyrosine metabolism. (A) Graphs represent the ScaledImpData of different biochemicals of the tryptophan metabolism from heart tissue samples. (B) Same as in A from plasma samples (C) A Graphs represent the ScaledImpData of different biochemicals of the phenylalanine and tyrosine metabolism from heart tissue samples. (D) Same as in C from plasma samples. Samples from control uninfected mice are in white boxes, from mice sacrificed at 14 dpi in light gray boxes and from mice sacrificed at 21 dpi in dark grey boxes. Statistically significant differences respect to uninfected mouse samples are denoted, *p≤0.05.
doi:10.1371/journal.pntd.0003337.g007

phosphate, ethanolamine, and phosphoethanolamine also accumulated in infected heart tissue and may be indicative of an increased capacity for phospholipid synthesis. Differences in these metabolites may reflect tissue remodeling during infection.

Noteworthy, heart tissue from *T. cruzi* infected mice was almost depleted of adenine and had much lower levels of purine nucleotides and metabolites such as adenosine, guanosine, inosine, and hypoxanthine, compared to uninfected controls. Lower levels of these metabolites may reflect a decrease in synthesis as supported by lower levels of pentose phosphate pathway metabolism. But more likely, purine degradation may be enhanced as evidenced by a strong accumulation of the downstream catabolic products xanthosine, xanthine, urate, and allantoin in infected hearts. Differences in the levels of these metabolites may also reflect a change in redox homeostasis since the generation of xanthine and urate are accompanied by the production of hydrogen peroxide (H_2O_2). Thus, differences in purine metabolism may contribute to altered redox homeostasis in cardiac tissue. In addition, it has been described that the parasite scavenges purines and pteridine for amastigote replication in HeLa cells [24]. Thus, the decreased levels of adenine observed in heart tissue may reflect both phenomena: decreased synthesis and parasite utilization.

Interestingly, xantine oxidase (XOS) the enzyme responsible for reactive oxygen species (ROS) generation has been considered responsible for cardiac dysfunction in *T. cruzi* infection [42]. Thus, allopurinol, a xanthine oxidase inhibitor, is being considered for treating Chagasic patients [43]. Inhibition of ROS generation ameliorates myocarditis during Chagas disease, although parasite burden in the heart was not significantly decreased [44]. Interestingly, the effect of ROS inhibition seems to be related with the levels of metabolites as substrates of immune-related

enzymes and thus their imbalances can be targeted to combat infectious diseases.

Besides, the fact that uric acid is so strongly elevated and adenine so depleted may indicate that ROS production in the heart should be very high (Figure 6A). ROS also increase the ability of *T. cruzi* to replicate intracellularly [45]. Uric acid is linked to several cardiovascular diseases [46,47,48], although there is still discrepancy on whether it is really the cause or the effect of the disease [49]. The increase in uric acid is also associated to elevated fructose [50], also shown in our analysis. Uric acid is able to activate inflammasome NLRP3, being a danger signal in many pathological processes and in inflammation. Higher signaling through NLRP3 has been recently related to adverse outcome in other forms of cardiac dysfunction as idiopathic dilated cardiomyopathy [51]. However, in apparent contrast, it has been recently demonstrated a protective role of NLRP3 inflammasome in the control of *T.cruzi* infection through caspase-1-dependente IL-1R-independent nitric oxide (NO) production [52]. Thus, it would be worth testing the role of NLRP3 in Chagas disease cardiomyopathy and not only relative to infection.

In addition, Heme, a product involved in redox homeostasis, was increased in infected heart, and is also able to increase *T. cruzi* growth [53]. Increased heme levels are found in failing hearts [54] associated to ROS production. In this regard, it is also worth mentioning that allopurinol, that inhibits XOS, has been used effectively against *T. cruzi* in mouse models [43,55] and also to prevent cardiovascular dysfunction (CVD) [48].

Lysoglycerol-phosphocholines, that increased very significantly in *T. cruzi* infected heart, may also contribute to immunosuppression associated to Chagas disease [56], since they inhibit T-cell proliferation in response to activation and induce apoptosis [57].

Kynurenine is not usually found in heart tissue, and acts as an endothelium-derived relaxing factor produced during inflammation [58]. It can also control dendritic cell immunogenicity [59]. Notably, this metabolite has been implicated in resistance to *T. cruzi* infection [19,20]. Furthermore, the serum levels of IDO enzymatic activity in Chagas disease symptomatic patients decrease with therapeutic treatment [60]. Since, IDO activity is often elevated in response to inflammatory cytokines such as TNFα and IFNγ, elevated in cardiac patients [12], these findings may reflect immune cell activation in response to *T. cruzi* infection.

p-Cresol sulfate and indoxyl sulfate are considered uremic toxins [61]. Although they are generally associated to dialysis disturbances they have an emerging role in cardiovascular disease and mortality in renal patients. Serum p-Cresol sulfate predicts cardiovascular disease and mortality in elderly hemodialysis patients [62]. In patients with chronic renal failure p-cresol sulphate accumulation in plasma is due to renal dysfunction and cause endothelial dysfunction increasing the cardiovascular risk [63]. We found it highly increased in heart tissue as well as serum of infected mice. The levels of p-cresol sulphate can be also predictive of clinical outcome. Our work, if confirmed in Chagas disease patients, may suggest that p-cresol sulphate could be useful a marker of *T. cruzi* infection and further studies are needed to check if it also correlates with disease outcome.

Recently, a global metabolomic analysis in an experimental hamster model of idiopathic dilated cardiomyopathy (DCM) has been described [14]. By comparison with our data some specific biomarkers, and by extension pathogenic mechanism(s), can be inferred, that can help to distinguish among those clinically similar but etiologically distinct dilated cardiomyopathies. In that study, only 180 metabolites were detected and variations were found in 62 of them. Their results suggest that the glycolysis and the TCA cycle energy pathways are attenuated in cardiac tissue during the symptomatic phase. In contrast, hearts from *T. cruzi* infected mice have increased glycolysis, despite having the TCA cycle decreased. Similar to our results they observed increased oxidative stress in the DCM. Thus, the rest of alterations we found can be considered specific, so far, of cardiomyopathy associated to *T. cruzi* infection. Among those, much higher lipid (and specially phospholipids) accumulation in *T. cruzi* infected hearts as well as stronger depletion of adenine and increase in allantoin and uric acid.

Previous studies on metabolic alterations caused by *T. cruzi* infection were based only on host enzymatic expression *in vitro* [24]. Thus our work greatly expands those results by detecting their metabolites *in vivo* in a mouse model of infection. Our findings suggest that *T. cruzi* infection disrupts multiple biochemical pathways in heart tissue that may ultimately contribute to cardiac failure. In particular, increased glycolysis and decreased oxidative metabolism may predispose heart muscle to energetic imbalances characteristic of heart failure [64]. Furthermore, altered glucose utilization may limit the anabolic capacity of the heart and therefore the ability to repair damaged tissue and to detoxify free radicals. Consequently, evidence of altered redox homeostasis, inflammation, and tissue remodeling were observed in response to infection.

In summary, we have found many metabolic alterations in experimental acute Chagas disease. Many of these suggest a stressful condition in the heart such as: a) increased glycolysis, b) respiratory chain impairment, c) lipid accumulation, d) ROS production and uric acid formation. All of those could be related with heart hypertrophy. Noteworthy, some of those metabolites have much stronger variations than reported in other cardiac pathologies. Probably more interestingly, we found elevated p-cresol sulfate, which is associated to infections, and kynurenine and allantoin in serum that, either individually or in combination, may be specific biomarkers in this disease. Moreover, p-cresol sulfate, kynurenine and allantoin presented very high positive coefficients in the PCA analysis in plasma reinforcing its value as possible biomarkers. Very importantly, in the evaluation of new drugs against Chagas disease, a biomarker of cardiac function recovery is urgently needed to assess the efficacy of new treatments in the clinic-pathological symptoms and not only for determining parasitological cure. Despite that our study spans only the acute Chagas disease, taking into account that acute and chronic phases share some similarities, the possibility that any of the candidate biomarkers may apply to the chronic phase cannot be excluded. Thus, future studies may benefit from examining metabolic differences induced by acute versus chronic infection to determine the long-term risk factors associated with *T. cruzi* infection, as well as exploring the usefulness of the ones described here as biomarkers of clinical improvement.

Supporting Information

Table S1 Summary of the significantly altered biochemicals. 325 biochemical were identified in heart extracts and 306 in plasma extract. Following log transformation and imputation with minimum observed values for each compound, Welch's two-sample t-test was used to identify biochemicals that differed significantly between experimental groups. Biochemicals that achieved statistical significance ($p \leq 0.05$), as well as those approaching significance ($0.05 < p < 0.10$), is shown. Increased levels of biochemicals are in red and decreased levels in green.
(DOCX)

Table S2 Contribution of the heart tissue individual biochemicals to the Principal components analysis

(PCA). List of the calculated coefficients of heart tissue biochemicals ordered from higher to lower. The higher positive and negative coefficients are the ones that have more contribution for the PCA analysis. Component 1 may have the greatest contribution to separating the metabolic signature followed by component 2. Plasma candidate biomarkers as p-cresol sulphate, kynurenine and allantoin, which increase with the infection are highlighted.
(DOCX)

Table S3 Contribution of the plasma individual biochemicals to the Principal components analysis (PCA). List of the calculated coefficients of heart tissue biochemicals ordered from higher to lower. The higher positive and negative coefficients are the ones that have more contribution for the PCA analysis. Component 1 may have the greatest contribution to separating the metabolic signature followed by component 2. Plasma candidate biomarkers as p-cresol sulphate, kynurenine and allantoin, which increase with the infection, with very high positive coefficients are highlighted.
(DOCX)

Acknowledgments

The authors would like to thank Ryan Michalek for the analysis of the data, Julien Santi-Rocca for his suggestions, Beatriz Barrocal for the care of the animals and Maria A. Chorro for her technical assistance.

Author Contributions

Conceived and designed the experiments: NG MF. Performed the experiments: SC NAG CP CCM. Analyzed the data: NG MF. Wrote the paper: NG MF.

References

1. WHO (2013) Chagas disease (American trypanosomiasis). Factsheets.
2. Telleria J, Tibayrenc M (2010) American Trypanosomiasis. Chagas Disease: One hundred years of research. Elsevier: 848.
3. Sanchez LV, Ramirez JD (2013) Congenital and oral transmission of American trypanosomiasis: an overview of physiopathogenic aspects. Parasitology 140: 147–159.
4. Henao-Martinez AF, Schwartz DA, Yang IV (2012) Chagasic cardiomyopathy, from acute to chronic: is this mediated by host susceptibility factors? Trans R Soc Trop Med Hyg 106: 521–527.
5. Parada H, Carrasco HA, Anez N, Fuenmayor C, Inglessis I (1997) Cardiac involvement is a constant finding in acute Chagas' disease: a clinical, parasitological and histopathological study. Int J Cardiol 60: 49–54.
6. Ribeiro AL, Nunes MP, Teixeira MM, Rocha MO (2012) Diagnosis and management of Chagas disease and cardiomyopathy. Nat Rev Cardiol 9: 576–589.
7. Girones N, Fresno M (2003) Etiology of Chagas disease myocarditis: autoimmunity, parasite persistence, or both? Trends Parasitol 19: 19–22.
8. Marin-Neto JA, Cunha-Neto E, Maciel BC, Simoes MV (2007) Pathogenesis of chronic Chagas heart disease. Circulation 115: 1109–1123.
9. Quijano-Hernandez I, Dumonteil E (2011) Advances and challenges towards a vaccine against Chagas disease. Hum Vaccin 7: 1184–1191.
10. Pinazo MJ, Munoz J, Posada E, Lopez-Chejade P, Gallego M, et al. (2010) Tolerance of benznidazole in treatment of Chagas' disease in adults. Antimicrob Agents Chemother 54: 4896–4899.
11. Murcia L, Carrilero B, Munoz MJ, Iborra MA, Segovia M (2010) Usefulness of PCR for monitoring benznidazole response in patients with chronic Chagas' disease: a prospective study in a non-disease-endemic country. J Antimicrob Chemother 65: 1759–1764.
12. Poveda C, Fresno M, Girones N, Martins-Filho OA, Ramirez JD, et al. (2014) Cytokine profiling in Chagas disease: towards understanding the association with infecting Trypanosoma cruzi discrete typing units (a BENEFIT TRIAL substudy). PLoS One 9: e91154.
13. Requena-Mendez A, Lopez MC, Angheben A, Izquierdo L, Ribeiro I, et al. (2013) Evaluating Chagas disease progression and cure through blood-derived biomarkers: a systematic review. Expert Rev Anti Infect Ther 11: 957–976.
14. Maekawa K, Hirayama A, Iwata Y, Tajima Y, Nishimaki-Mogami T, et al. (2013) Global metabolomic analysis of heart tissue in a hamster model for dilated cardiomyopathy. J Mol Cell Cardiol 59: 76–85.
15. Mathis D, Shoelson SE (2011) Immunometabolism: an emerging frontier. Nat Rev Immunol 11: 81.
16. Arpaia N, Campbell C, Fan X, Dikiy S, van der Veeken J, et al. (2013) Metabolites produced by commensal bacteria promote peripheral regulatory T-cell generation. Nature 504: 451–455.
17. Macia L, Thorburn AN, Binge LC, Marino E, Rogers KE, et al. (2012) Microbial influences on epithelial integrity and immune function as a basis for inflammatory diseases. Immunol Rev 245: 164–176.
18. Sanoja C, Carbajosa S, Fresno M, Girones N (2013) Analysis of the dynamics of infiltrating CD4(+) T cell subsets in the heart during experimental Trypanosoma cruzi infection. PLoS One 8: e65820.
19. Knubel CP, Martinez FF, Acosta Rodriguez EV, Altamirano A, Rivarola HW, et al. (2011) 3-Hydroxy kynurenine treatment controls T. cruzi replication and the inflammatory pathology preventing the clinical symptoms of chronic Chagas disease. PLoS One 6: e26550.
20. Knubel CP, Martinez FF, Fretes RE, Diaz Lujan C, Theumer MG, et al. (2010) Indoleamine 2,3-dioxigenase (IDO) is critical for host resistance against Trypanosoma cruzi. FASEB J 24: 2689–2701.
21. Cuervo H, Guerrero NA, Carbajosa S, Beschin A, De Baetselier P, et al. (2011) Myeloid-derived suppressor cells infiltrate the heart in acute Trypanosoma cruzi infection. J Immunol 187: 2656–2665.
22. Morris SA, Tanowitz HB, Bilezikian JP, Wittner M (1991) Modulation of host cell metabolism by Trypanosoma cruzi. Parasitol Today 7: 82–87.
23. Garg N, Gerstner A, Bhatia V, DeFord J, Papaconstantinou J (2004) Gene expression analysis in mitochondria from chagasic mice: alterations in specific metabolic pathways. Biochem J 381: 743–752.
24. Caradonna KL, Engel JC, Jacobi D, Lee CH, Burleigh BA (2013) Host metabolism regulates intracellular growth of Trypanosoma cruzi. Cell Host Microbe 13: 108–117.
25. Huang S, Hendriks W, Althage A, Hemmi S, Bluethmann H, et al. (1993) Immune response in mice that lack the interferon-gamma receptor. Science 259: 1742–1745.
26. Brener Z (1962) Therapeutic activity and criterion of cure on mice experimentally infected with Trypanosoma cruzi. Rev Inst Med Trop Sao Paulo 4: 389–396.
27. Cuervo H, Pineda MA, Aoki MP, Gea S, Fresno M, et al. (2008) Inducible nitric oxide synthase and arginase expression in heart tissue during acute Trypanosoma cruzi infection in mice: arginase I is expressed in infiltrating CD68+ macrophages. J Infect Dis 197: 1772–1782.
28. de Diego JA, Penin P, del Rey J, Mayer R, Gamallo C (1991) A comparative pathological study of three strains of Trypanosoma cruzi in an experimental model. Histol Histopathol 6: 199–206.
29. Calderon J, Maganto-Garcia E, Punzon C, Carrion J, Terhorst C, et al. (2012) The receptor Slamf1 on the surface of myeloid lineage cells controls susceptibility to infection by Trypanosoma cruzi. PLoS Pathog 8: e1002799.
30. Rodriguez HO, Guerrero NA, Fortes A, Santi-Rocca J, Girones N, et al. (2014) Trypanosoma cruzi strains cause different myocarditis patterns in infected mice. Acta Trop 139C: 57–66.
31. Bastos CJ, Aras R, Mota G, Reis F, Dias JP, et al. (2010) Clinical outcomes of thirteen patients with acute chagas disease acquired through oral transmission from two urban outbreaks in northeastern Brazil. PLoS Negl Trop Dis 4: e711.
32. Hartog JW, Voors AA, Bakker SJ, Smit AJ, van Veldhuisen DJ (2007) Advanced glycation end-products (AGEs) and heart failure: pathophysiology and clinical implications. Eur J Heart Fail 9: 1146–1155.
33. Leong HS, Brownsey RW, Kulpa JE, Allard MF (2003) Glycolysis and pyruvate oxidation in cardiac hypertrophy–why so unbalanced? Comp Biochem Physiol A Mol Integr Physiol 135: 499–513.
34. Rassi A, Jr., Rassi A, Marin-Neto JA (2010) Chagas disease. Lancet 375: 1388–1402.
35. Wen JJ, Garg N (2004) Oxidative modification of mitochondrial respiratory complexes in response to the stress of Trypanosoma cruzi infection. Free Radic Biol Med 37: 2072–2081.
36. Cross HR, Clarke K, Opie LH, Radda GK (1995) Is lactate-induced myocardial ischaemic injury mediated by decreased pH or increased intracellular lactate? J Mol Cell Cardiol 27: 1369–1381.
37. Neely JR, Morgan HE (1974) Relationship between carbohydrate and lipid metabolism and the energy balance of heart muscle. Annu Rev Physiol 36: 413–459.
38. Christmas PB, Turrens JF (2000) Separation of NADH-fumarate reductase and succinate dehydrogenase activities in Trypanosoma cruzi. FEMS Microbiol Lett 183: 225–228.
39. D'Avila H, Freire-de-Lima CG, Roque NR, Teixeira L, Barja-Fidalgo C, et al. (2011) Host cell lipid bodies triggered by Trypanosoma cruzi infection and enhanced by the uptake of apoptotic cells are associated with prostaglandin E(2) generation and increased parasite growth. J Infect Dis 204: 951–961.
40. Tominaga H, Katoh H, Odagiri K, Takeuchi Y, Kawashima H, et al. (2008) Different effects of palmitoyl-L-carnitine and palmitoyl-CoA on mitochondrial function in rat ventricular myocytes. Am J Physiol Heart Circ Physiol 295: H105–112.

41. Broderick TL, Paulson DJ, Gillis M (2004) Effects of propionyl-carnitine on mitochondrial respiration and post-ischaemic cardiac function in the ischaemic underperfused diabetic rat heart. Drugs R D 5: 191–201.
42. Gupta S, Dhiman M, Wen JJ, Garg NJ (2011) ROS signalling of inflammatory cytokines during Trypanosoma cruzi infection. Adv Parasitol 76: 153–170.
43. Perez-Mazliah DE, Alvarez MG, Cooley G, Lococo BE, Bertocchi G, et al. (2013) Sequential combined treatment with allopurinol and benznidazole in the chronic phase of Trypanosoma cruzi infection: a pilot study. J Antimicrob Chemother 68: 424–437.
44. Dhiman M, Garg NJ (2011) NADPH oxidase inhibition ameliorates Trypanosoma cruzi-induced myocarditis during Chagas disease. J Pathol 225: 583–596.
45. Paiva CN, Feijo DF, Dutra FF, Carneiro VC, Freitas GB, et al. (2012) Oxidative stress fuels Trypanosoma cruzi infection in mice. J Clin Invest 122: 2531–2542.
46. Harzand A, Tamariz L, Hare JM (2012) Uric acid, heart failure survival, and the impact of xanthine oxidase inhibition. Congest Heart Fail 18: 179–182.
47. Higgins P, Dawson J, Lees KR, McArthur K, Quinn TJ, et al. (2012) Xanthine oxidase inhibition for the treatment of cardiovascular disease: a systematic review and meta-analysis. Cardiovasc Ther 30: 217–226.
48. Kelkar A, Kuo A, Frishman WH (2011) Allopurinol as a cardiovascular drug. Cardiol Rev 19: 265–271.
49. Brunet P, Gondouin B, Duval-Sabatier A, Dou L, Cerini C, et al. (2011) Does uremia cause vascular dysfunction? Kidney Blood Press Res 34: 284–290.
50. Lanaspa MA, Tapia E, Soto V, Sautin Y, Sanchez-Lozada LG (2011) Uric acid and fructose: potential biological mechanisms. Semin Nephrol 31: 426–432.
51. Luo B, Wang F, Li B, Dong Z, Liu X, et al. (2013) Association of nucleotide-binding oligomerization domain-like receptor 3 inflammasome and adverse clinical outcomes in patients with idiopathic dilated cardiomyopathy. Clin Chem Lab Med 51: 1521–1528.
52. Goncalves VM, Matteucci KC, Buzzo CL, Miollo BH, Ferrante D, et al. (2013) NLRP3 controls Trypanosoma cruzi infection through a caspase-1-dependent IL-1R-independent NO production. PLoS Negl Trop Dis 7: e2469.
53. Nogueira NP, de Souza CF, Saraiva FM, Sultano PE, Dalmau SR, et al. (2011) Heme-induced ROS in Trypanosoma cruzi activates CaMKII-like that triggers epimastigote proliferation. One helpful effect of ROS. PLoS One 6: e25935.
54. Khechaduri A, Bayeva M, Chang HC, Ardehali H (2013) Heme levels are increased in human failing hearts. J Am Coll Cardiol 61: 1884–1893.
55. Gobbi P, Lo Presti MS, Fernandez AR, Enders JE, Fretes R, et al. (2007) Allopurinol is effective to modify the evolution of Trypanosoma cruzi infection in mice. Parasitol Res 101: 1459–1462.
56. Goni O, Alcaide P, Fresno M (2002) Immunosuppression during acute Trypanosoma cruzi infection: involvement of Ly6G (Gr1(+))CD11b(+)immature myeloid suppressor cells. Int Immunol 14: 1125–1134.
57. Foulds LM, Boysen RI, Crane M, Yang Y, Muir JA, et al. (2008) Molecular identification of lyso-glycerophosphocholines as endogenous immunosuppressives in bovine and rat gonadal fluids. Biol Reprod 79: 525–536.
58. Wang Y, Liu H, McKenzie G, Witting PK, Stasch JP, et al. (2010) Kynurenine is an endothelium-derived relaxing factor produced during inflammation. Nat Med 16: 279–285.
59. Nguyen NT, Kimura A, Nakahama T, Chinen I, Masuda K, et al. (2010) Aryl hydrocarbon receptor negatively regulates dendritic cell immunogenicity via a kynurenine-dependent mechanism. Proc Natl Acad Sci U S A 107: 19961–19966.
60. Maranon C, Egui A, Fernandez-Villegas A, Carrilero B, Thomas MC, et al. (2013) Benznidazole treatment reduces the induction of indoleamine 2,3-dioxygenase (IDO) enzymatic activity in Chagas disease symptomatic patients. Parasite Immunol 35: 180–187.
61. Raff AC, Meyer TW, Hostetter TH (2008) New insights into uremic toxicity. Curr Opin Nephrol Hypertens 17: 560–565.
62. Lin CJ, Pan CF, Chuang CK, Sun FJ, Wang DJ, et al. (2014) P-cresyl sulfate is a valuable predictor of clinical outcomes in pre-ESRD patients. Biomed Res Int 2014: 526932.
63. Guida B, Cataldi M, Riccio E, Grumetto L, Pota A, et al. (2013) Plasma p-cresol lowering effect of sevelamer in peritoneal dialysis patients: evidence from a Cross-Sectional Observational Study. PLoS One 8: e73558.
64. Pouleur H (1990) Diastolic dysfunction and myocardial energetics. Eur Heart J 11 Suppl C: 30–34.

PLOS | NEGLECTED TROPICAL DISEASES

RESEARCH ARTICLE

Cyclooxygenase-2 and Prostaglandin E_2 Signaling through Prostaglandin Receptor EP-2 Favor the Development of Myocarditis during Acute *Trypanosoma cruzi* Infection

Néstor A. Guerrero[1¤], Mercedes Camacho[2], Luis Vila[2], Miguel A. Íñiguez[1,3], Carlos Chillón-Marinas[1], Henar Cuervo[1,4], Cristina Poveda[1], Manuel Fresno[1,3‡], Núria Gironès[1,3‡*]

1 Centro de Biología Molecular Severo Ochoa, CSIC-UAM, Madrid, Spain, **2** Institut de Recerca de l'Hospital de la Santa Creu i de Sant Pau, Barcelona, Spain, **3** Instituto de Investigación Sanitaria de la Princesa, Madrid, Spain, **4** Department of Obstetrics/Gynecology, Columbia University Medical Center, Columbia University, New York, New York, United States of America

¤ Current address: CPTP, Centre de Physiopathologie de Toulouse-Purpan, Inserm UMR1043—CNRS UMR5282—Université Toulouse III, CHU Purpan, Toulouse, France
‡ Both authors equally contributed to the direction of this work
* ngirones@cbm.csic.es

OPEN ACCESS

Citation: Guerrero NA, Camacho M, Vila L, Íñiguez MA, Chillón-Marinas C, Cuervo H, et al. (2015) Cyclooxygenase-2 and Prostaglandin E_2 Signaling through Prostaglandin Receptor EP-2 Favor the Development of Myocarditis during Acute *Trypanosoma cruzi* Infection. PLoS Negl Trop Dis 9 (8): e0004025. doi:10.1371/journal.pntd.0004025

Editor: Herbert B. Tanowitz, Albert Einstein College of Medicine, UNITED STATES

Received: March 10, 2015

Accepted: August 2, 2015

Published: August 25, 2015

Data Availability Statement: All relevant data are within the paper and its Supporting Information files.

Funding: This work was supported by (NG) grants from "Fondo de Investigaciones Sanitarias" (PS09/00538 and PI12/00289); "Universidad Autónoma de Madrid" and "Comunidad de Madrid" (CC08-UAM/SAL-4440/08); by (MF) grants from "Ministerio de Ciencia e Innovación" (SAF2010-17833); "Red de Investigación de Centros de Enfermedades Tropicales" (RICET RD12/0018/0004); European Union (HEALTH-FE-2008-22303, ChagasEpiNet);

Abstract

Inflammation plays an important role in the pathophysiology of Chagas disease, caused by *Trypanosoma cruzi*. Prostanoids are regulators of homeostasis and inflammation and are produced mainly by myeloid cells, being cyclooxygenases, COX-1 and COX-2, the key enzymes in their biosynthesis from arachidonic acid (AA). Here, we have investigated the expression of enzymes involved in AA metabolism during *T*. *cruzi* infection. Our results show an increase in the expression of several of these enzymes in acute *T*. *cruzi* infected heart. Interestingly, COX-2 was expressed by $CD68^+$ myeloid heart-infiltrating cells. In addition, infiltrating myeloid $CD11b^+Ly6G^-$ cells purified from infected heart tissue express COX-2 and produce prostaglandin E_2 (PGE_2) *ex vivo*. *T*. *cruzi* infections in COX-2 or PGE_2-dependent prostaglandin receptor EP-2 deficient mice indicate that both, COX-2 and EP-2 signaling contribute significantly to the heart leukocyte infiltration and to the release of chemokines and inflammatory cytokines in the heart of *T*. *cruzi* infected mice. In conclusion, COX-2 plays a detrimental role in acute Chagas disease myocarditis and points to COX-2 as a potential target for immune intervention.

Author Summary

The role of prostanoids, products of the arachidonic acid pathway, during *Trypanosoma cruzi* infection has been studied by inhibiting key enzymes in prostanoid synthesis as cyclooxygenases (COX-1 and COX-2), with opposed results. Here we analyzed the expression of cyclooxygenases, prostanoid synthases and receptors in the heart of mice susceptible and non-susceptible to *T*. *cruzi* infection and found that they were highly increased

AECID Cooperation with Argentine (A/025417/09 and A/031735/10), Comunidad de Madrid (S-2010/BMD-2332) and "Fundación Ramón Areces". NAG was recipient of a ISCIII Ph.D. fellowship financed by the Spanish "Ministerio de Sanidad". CCM and HC were recipients of contracts from SAF2010-17833 and PI060388, respectively. The funders had no role in study design, data collection and analysis, decision to publish, or preparation of the manuscript.

Competing Interests: The authors have declared that no competing interests exist.

respect to non-infected mice. We previously identified the presence of myeloid-derived suppressor cells expressing arginase-1 (Arg-1). Further analysis showed that COX-2 was expressed in Arg-1$^-$ myeloid cells in heart tissue, suggesting the existence of different myeloid populations involved in the leukocyte infiltration (COX-2$^+$Arg-1$^-$) and tissue repair (COX-2$^-$Arg-1$^+$). Mice deficient in the expression of COX-2 and the prostaglandin PGE_2 receptor EP-2 infected with *T. cruzi* showed a marked reduction in the cardiac inflammatory infiltration in comparison with infected wild type mice, indicating an adverse effect of COX-2 and PGE_2 signaling through EP-2 receptor in the development of myocarditis during acute *T. cruzi* infection, suggesting the possibility of immune intervention using COX inhibitors.

Introduction

Chagas disease is a multisystemic disorder caused by *Trypanosoma cruzi* infection that affects more than 8 million people worldwide, being endemic in Latin America. Due to the scarcity of preventive and therapeutic tools and population at risk, it is considered as a neglected tropical disease [1, 2]. More than 40,000 new infected people and 12,550 deaths per year are estimated. The high rate of migration towards non-endemic countries has spread the boundaries of the infection to other continents. Non-vectorial transmission is possible through oral ingestion, blood transfusion, organ transplantation and during pregnancy. The risk of infection is related to the country of origin of the migrants and the rate of prevalence in a given country [3].

Chagas disease is characterized by acute and chronic phases. Death occurs occasionally in the acute phase (<5–10% of symptomatic cases) as a result of severe myocarditis, meningoencephalitis, or both. The experimental model of infection in mice recapitulates many clinical features observed in human infection, although different strains of mice and parasites produce different disease outcomes [4].

Heart inflammation during the acute phase of *T. cruzi* experimental infection is initiated by lymphoid and myeloid mononuclear cell infiltration [5]. We have isolated from infected hearts an infiltrating monocytic CD11b$^+$Ly6C$^+$Ly6G$^-$ population expressing both classical (M1) and alternatively (M2) activated macrophage markers that is able to suppress T cell proliferation *ex vivo*, characteristics that define them as myeloid-derived suppressor cells (MDSCs) [6, 7].

Myeloid cells are thought to be the major source of prostanoids, end products of cell membrane arachidonic acid (AA) catabolism, which include prostaglandins, prostacyclin and thromboxanes [8]. Enzymes implicated in prostanoid production have been investigated for many years [9]. All these lipid mediators have important roles in homeostasis and immune response regulation [10]. Cyclooxygenases, COX-1 and COX-2, are principal enzymes in prostanoid production. COX-1 expression is involved in homeostasis while COX-2 is induced by several factors, including infection [9]. However, the specific role of COX-2 and downstream enzymes in the context of infection varies depending on the infectious agent [11–13].

PGE_2, a product of terminal PGE_2 synthases (PGES) has pro-inflammatory properties [14] but also immunosuppressive properties [15] by signaling through G-protein coupled PGE receptors (EP), termed EP-1, EP-2, EP-3 and EP-4. PGE_2 also decreases the ability of macrophages to phagocytize and kill microorganisms [16, 17], and is required for monocyte migration in response to chemokines [18, 19].

There are few studies about the role of prostanoids in human chagasic pathology [20, 21], but it has been described that monocyte inflammatory mediators inhibit cellular proliferation and enhance cytokine production in patients [22]. In rodent models of acute infection, the

levels of $PGF_{2\alpha}$, TXB_2, 6-oxo-$PGF_{1\alpha}$ [23] and PGE_2 [24] in plasma, were increased. Macrophages from infected rats show an increased number of lipid bodies, where COX-2 produces PGE_2 [25]. Recently, it has been shown that the absence of Phospholipase A2γ, an enzyme implicated in AA release from membranes, decreases mice survival [26].

The role of COX in mice infected with *T. cruzi* has been studied using non-selective inhibitors of COX-1 and COX-2, as well as COX-2-selective inhibitors (NSAIDs), with conflicting results. Thus, it has been described that COX inhibitors cause an increase in mortality and parasitism [27] in *T. cruzi* infection, but contrarily, other reports claim that COX-2 inhibition decreases the level of parasitism [28, 29]. In addition, both beneficial and adverse effects of COX inhibitors have been reported, depending on the phase of *T. cruzi* infection and the mice strain used [30]. Discrepancies between these studies could be explained by the different ability of BALB/c and C57BL/6 mouse strains to produce PGE_2 [31]; the presence of distinct levels of cytokines in serum [32] or because of differences in cardiac cytokine expression profile [6].

Thus, in order to clarify the role of prostanoids in acute cardiac inflammation, we infected susceptible and non-susceptible mice, as well as COX-2 and EP-2 deficient mice with *T. cruzi* and analyzed cardiac inflammation, leukocyte infiltration and expression of cytokines, chemokines and inflammatory mediators in the infected mice.

Results

Prostanoid-synthesizing enzymes in the heart tissue of *T. cruzi* infected mice

We infected mice with the Y strain of *T. cruzi*. Immunopathology caused by this parasite strain is characterized by cardiac inflammatory damage. As we previously reported [33], C57BL/6, but not BALB/c, infected mice recovered from infection and survived (S1A Fig). Parasitemia was detectable between 9 and 21 d.p.i. and was higher in BALB/c mice (S1B Fig). Hearts of BALB/c infected mice showed more leukocyte infiltration and parasite nests than C57BL/6 mice (S1C Fig). We next studied the expression level of enzymes involved in the AA pathway in the heart of both strains after infection (Fig 1A). COX-2 gene expression (*Ptgs2*), but not COX-1 (*Ptgs1*), was increased in heart tissue during the acute phase of *T. cruzi* infection similarly in both mouse strains. *Ptges* (microsomal prostaglandin E2 synthase, mPGES-1), *Hpgds* (leucocyte type PGD synthase) and *Tbxas1* (thromboxane synthase) mRNA expression levels were also incremented. However, *Ptgds* (lipocalin-type prostaglandin D synthase) mRNA basal level of expression in heart tissue did not change upon *T. cruzi* infection. These results indicate that *T. cruzi* infection promoted the selective up-regulation of some of the enzymes involved in prostanoid production in heart tissue, including COX-2 and mPGES-1.

Myeloid cells in inflamed cardiac tissue express COX-2

Since COX-2 plays a key role in the synthesis of PGs in inflammatory processes, we aimed to identify the cells expressing this enzyme in the heart of *T cruzi* infected mice. Hearts from C57BL/6 (Fig 1B) and BALB/c (Fig 1C) mice were immunostained for COX-2 and myeloid and lymphoid markers, and imaged by confocal microscopy. Cells expressing COX-2 were abundant in the infected hearts of both mice strains, showing a strong staining in the perinuclear region of both myeloid CD68 positive and non-myeloid CD68 negative infiltrating cells. Interestingly, there was no co-localization of COX-2 and Arg-1, a marker of M2 macrophages and MDSCs (Fig 1D). Although COX-2 expression by activated lymphocytes has been previously described [34], CD4 staining was not detected in infiltrating $COX\text{-}2^+$ cells in hearts of

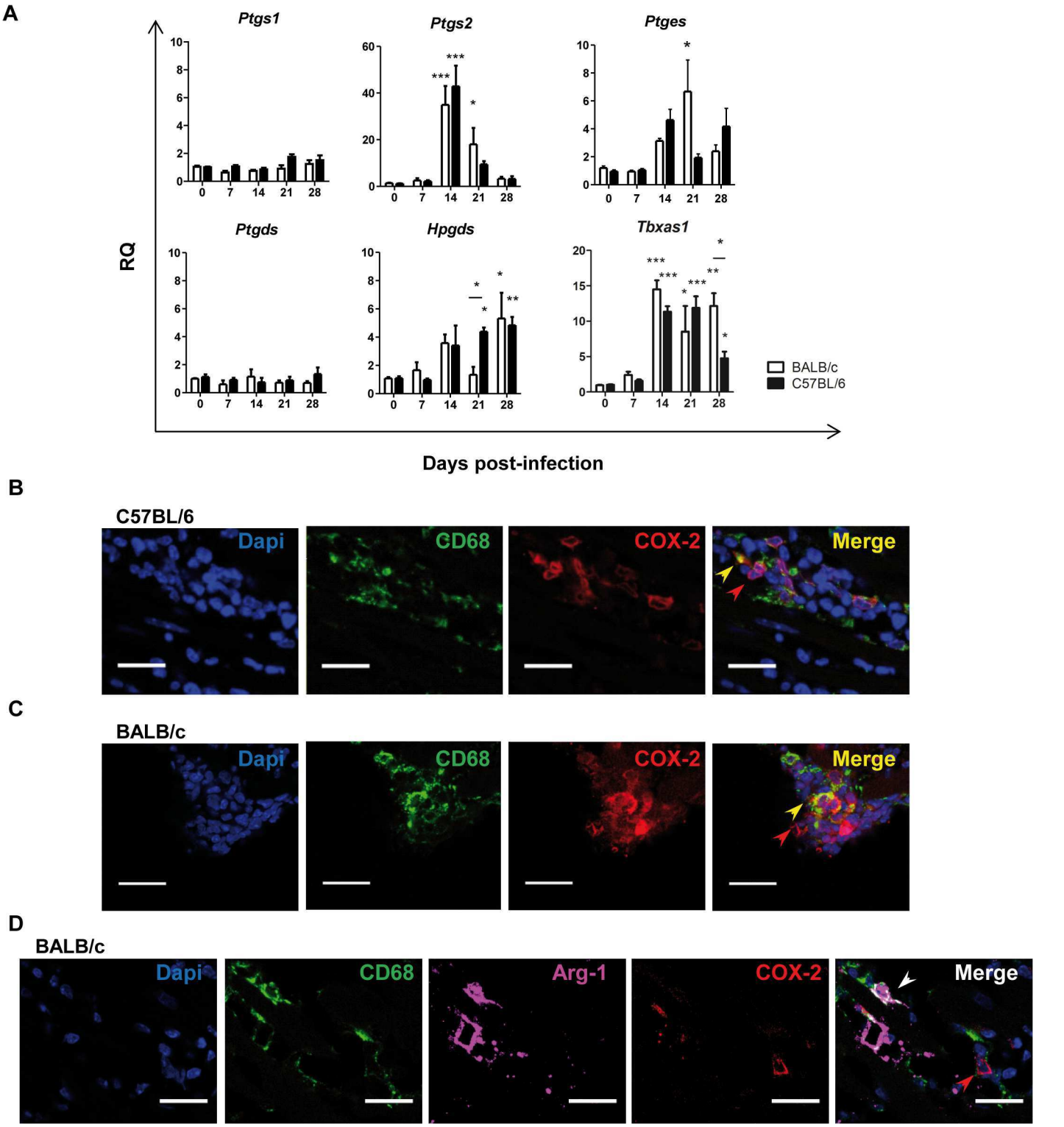

Fig 1. Expression of prostanoid synthases in *T. cruzi* infected cardiac tissue. (A) Expression of *Ptgs1*, *Ptgs2*, *Ptges* (mPGES1), *Ptgds*, *Hpgds* and *Tbxas1* in heart tissue of, either non-infected (0) or at different d.p.i. (7 to 28), BALB/c and C57BL/6 mice. Means ± SEM from three independent experiments (n = 9) are shown. Statistical comparisons are indicated * $p< 0.05$, *** $p< 0.001$. (B) Heart tissue samples from C57BL/6 mice at 14 d.p.i. and (C) BALB/c mice at 21 d.p.i., were stained with DAPI for nuclei (Blue) and specific antibodies for the macrophage marker CD68 (green) and the enzyme COX-2 (red). (D) Heart tissue from BALB/c mice at 21 d.p.i. stained for COX-2 (red), CD68 (green) and Arg-1 (magenta). In the merge of B, C and D, red, yellow and white arrows point to $COX\text{-}2^+$, $CD68^+COX\text{-}2^+$ and $CD68^+Arg\text{-}1^+$ cells, respectively. Pictures are representative of several sections analyzed in 3 different mice from three independent experiments; the scale bar is 20 μm.

doi:10.1371/journal.pntd.0004025.g001

infected C57BL/6 (S2A Fig) nor BALB/c mice (S2C Fig). No staining was observed in negative control sections incubated with secondary antibodies alone (S2B, S2D and S2E Fig).

We next isolated myeloid cells from hearts of *T. cruzi* infected C57BL/6 and BALB/c mice at the times,14 and 21 d.p.i. respectively, when maximum Arg-1 and inducible nitric oxide synthase (iNOS) expression is observed [7]. Using anti-Ly6G antibody labeled magnetic microbeads we obtained the $Ly6G^+$ population. $CD11b^+$ cells were selected from the remaining $Ly6G^-$ population, (Fig 2A). As previously described [7], the $CD11b^+Ly6G^-$ cell population expressed iNOS and Arg-1, and here we show that they also expressed COX-2 (Fig 2A). Interestingly, COX-2 gene expression was much higher in $CD11b^+$ cells obtained from infected cardiac tissue than those from the blood (Fig 2B), pointing to infiltrating myeloid cells in inflamed tissue as the source of COX-2.

$CD11b^+Ly6G^-$ cells from infected cardiac tissue produce PGE_2

In agreement with the increase in COX-2 expression, a significant increase in the production of prostanoids as PGE_2 and 6-oxo PGF1α in infected hearts was detected by mass spectrometry analysis on total heart extracts (Fig 2C). Further *ex vivo* analysis on $Ly6G^+$ and $CD11b^+Ly6G^-$ purified heart infiltrating myeloid cells cultured in the presence of radiolabeled AA, showed that $Ly6G^+$ cells did not produce any detectable prostanoid (Fig 2D). In contrast, $CD11b^+$ $Ly6G^-$ cells produced high levels of PGE_2 and low amounts of $PGF_{2\alpha}$ (Fig 2E). These results indicate that the $CD11b^+Ly6G^-$ myeloid population is able to synthesize high levels of PGE_2 from AA, while other cell types in heart tissue are likely producing PGE_2 and 6-oxo PGF1α.

Cardiac inflammation is reduced in $COX\text{-}2^{-/-}$ mice

In order to study the role of COX-2 in the development of cardiac leukocyte infiltration, we infected $COX\text{-}2^{+/+}$ and $COX\text{-}2^{-/-}$ mice with the Y strain of the parasite. $COX\text{-}2^{-/-}$ mice showed 30% reduction in blood parasite number compared to $COX\text{-}2^{+/+}$ mice at the peak of parasitemia (Fig 3A). However, COX-2 deficiency did not significantly affect cardiac parasite burden compared to $COX\text{-}2^{+/+}$ infected mice (Fig 3B). No mortality was observed neither in $COX\text{-}2^{+/+}$ nor in $COX\text{-}2^{-/-}$ infected mice up to 42 d.p.i.

Inflammatory infiltrates were analyzed and quantified in *T. cruzi* infected hearts from $COX\text{-}2^{+/+}$ and $COX\text{-}2^{-/-}$ mice. Fig 3C shows the extent of leukocyte infiltration calculated from several tissue sections as described in Methods. We observed significant less inflammatory infiltration in infected $COX\text{-}2^{-/-}$ than in $COX\text{-}2^{+/+}$ mice. Representative images corresponding to the quantification of cell infiltration are shown in Fig 3D.

We next analyzed the cellular composition of the immune inflammatory infiltrate by determining gene expression of surface markers characteristic of various immune cell populations by qRT-PCR and normalizing the data from infected animals respect to non-infected controls. In agreement with histological findings, infection in $COX\text{-}2^{-/-}$ mice compared to $COX\text{-}2^{+/+}$ mice, led to lower expression of the common leukocyte marker *Ptprc* (CD45) as well as of *Cd4*, *Cd8*, *Cd68*, and *Itgax* (CD11c) as markers of T helper cells, cytotoxic T cells, macrophages and dendritic cells, respectively (Fig 4A).

To characterize the immune response in hearts of $COX\text{-}2^{-/-}$ infected mice, gene expression of chemokines and cytokines were analyzed. mRNA levels of chemokines (*Ccl2*, *Ccl5* and *Cxcl9*) and cytokines (*Ifng*, *Tnf*, *Il4*, *Il6* and *Il10)* were significantly increased during *T. cruzi* infection in hearts of both $COX\text{-}2^{+/+}$ and $COX\text{-}2^{-/-}$ mice (Fig 4B and 4C). However, chemokine expression presented different patterns in $COX\text{-}2^{+/+}$ and $COX\text{-}2^{-/-}$ mice. *Ccl2* and *Ccl5* expression, but not *Cxcl9*, was significantly higher in $COX\text{-}2^{+/+}$ mice than in $COX\text{-}2^{-/-}$ mice (Fig 4B). Induction of pro-inflammatory cytokines *Ifng*, *Tnf* and *Il6* was lower, whereas *Il4* expression

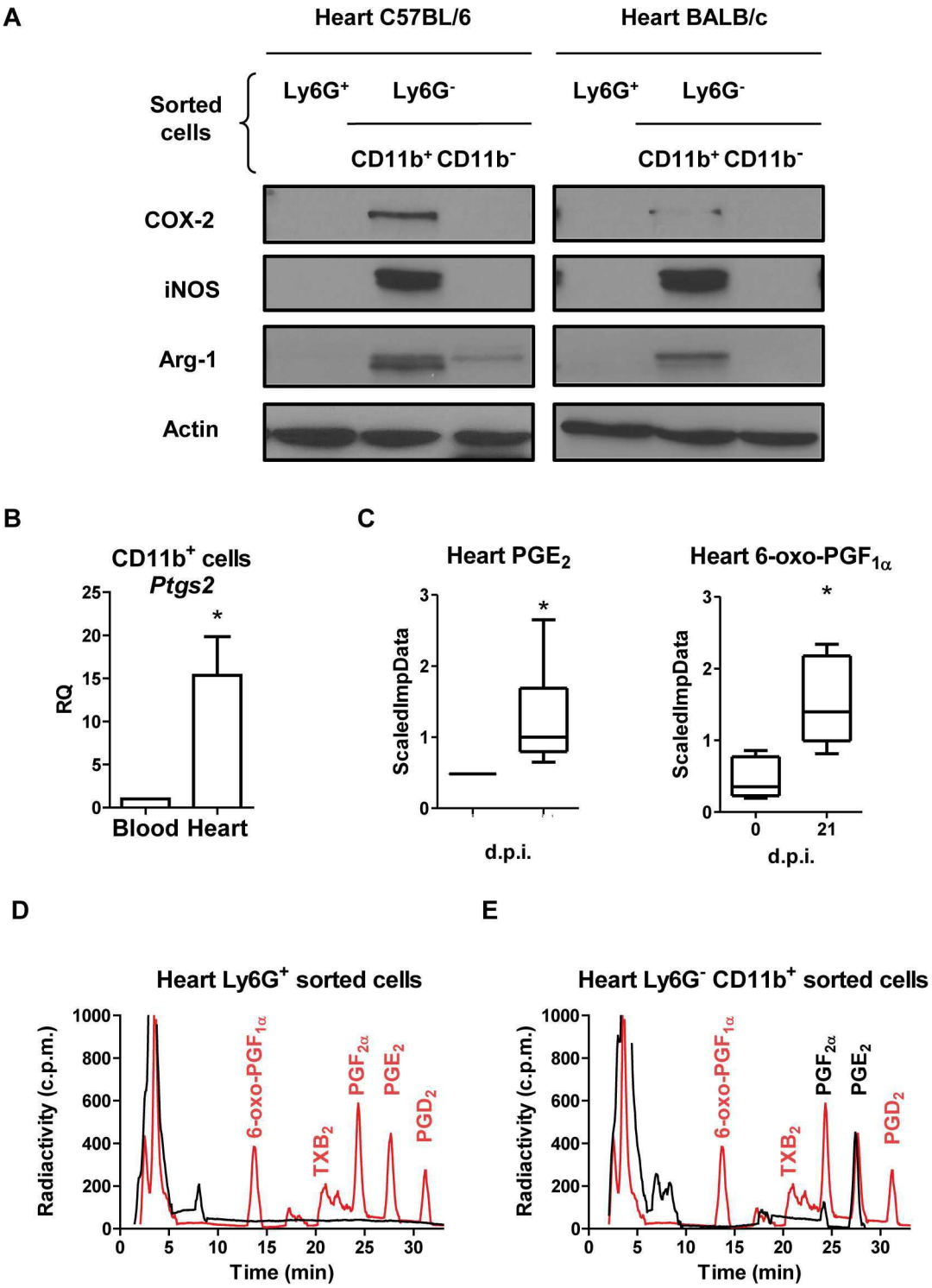

Fig 2. COX-2 expression and activity in heart and infiltrating myeloid cells during *T. cruzi* infection. (A) Purified Ly6G$^+$, Ly6G$^-$CD11b$^+$and Ly6G$^-$CD11b$^-$ cells were obtained from infected C57BL/6 (14 d.p.i.) and BALB/c (21 d.p.i.) mice hearts, by magnetic cell separation. Arg-1, iNOS and COX-2 levels were analyzed by Western blot. Protein levels of Actin are shown as loading control. A representative experiment of the two performed is shown. (B) CD11b$^+$ cells were obtained from pooled infected BALB/c mouse hearts or blood at 21 d.p.i (n = 15). *Ptgs2* (COX-2) expression in blood and heart tissue was determined by real time qRT-PCR. Mean ± SEM of two independent experiments is shown. (C) PGE_2 and 6-oxo-$PGF_{1\alpha}$ levels in total heart extracts of BALB/c from non-infected (0 d.p.i.) and 21 d.p.i., were determined as described in Methods and represented as scaled imputed data (ScaledImpData) after normalizing raw data values respect to median values of each day run (*p<0.05). Prostanoid production in purified Ly6G$^+$ (D) and Ly6G$^-$ CD11b$^+$ (E) cells

from BALB/c mice hearts at 21 d.p.i. was determined by incubation with labeled 25 μM [C^{14}] AA and analysis by HPLC (black line and text). Prostanoid standards (red line and text) were run in parallel as described in Methods. A representative experiment out of two performed is shown.

doi:10.1371/journal.pntd.0004025.g002

was higher, in COX-$2^{-/-}$ compared to COX-$2^{+/+}$ mice (Fig 4C). The anti-inflammatory cytokine *Il10* showed lower expression in the COX-$2^{-/-}$ infected mice. There were no significant differences in *Arg1* expression between COX-$2^{+/+}$ or COX-$2^{-/-}$ mice (Fig 4D), but induction of *Nos2* mRNA (iNOS) was significantly lower in COX-$2^{-/-}$ infected mice (Fig 4D). There was no induction of *Ptgs1* (COX-1) expression that could compensate for the COX-$2^{-/-}$ deficiency (Fig 4D). *Ptges* (mPGES-1) expression was increased upon infection, with lower levels in heart tissue from COX-$2^{-/-}$ mice compared to COX-$2^{+/+}$ mice (Fig 4D). Nevertheless, protein analysis by western blot showed lower expression of both iNOS and Arg-1 in infected COX-$2^{-/-}$ respect to COX-$2^{+/+}$ mice (Fig 5). Analysis of TNF-α levels in plasma showed a similar increase in both COX-$2^{+/+}$ and COX-$2^{-/-}$ infected mice, indicating that the effect of COX-2 deficiency is not systemic but specific of the heart (S3A Fig). Basal levels of gene expression did not significantly change between COX-$2^{+/+}$ and COX-$2^{-/-}$ mice (S4 Fig).

Cardiac inflammation is reduced in EP-$2^{-/-}$ mice

We found increased levels of PGE_2 in heart tissue and cardiac infiltrating cells after *T. cruzi* infection. Since the effector function of PGE_2 produced by myeloid cells depends on its binding to EP receptors, we studied gene expression of its 4 receptors, EP-1 (*Ptger1*), EP-2 (*Ptger2*), EP-3 (*Ptger3*) and EP-4 (*Ptger4*), in hearts of mice during infection. The results show that in control infected mice the overall expression of EP receptors is higher than in non-infected hearts, except for *Ptger3* (Fig 6A). However, in C57BL/6 infected hearts *Ptger2* expression showed the highest increases suggesting a potential role of this receptor in *T.cruzi* infection. Thus, we used mice deficient in the expression of the EP-2 (in the C57BL/6 background), which has been involved in inflammation [35], and also in an autocrine loop of macrophage activation by PGE_2 [36], in order to study the role of this receptor during *T. cruzi* infection. The results show that EP-$2^{+/+}$ and EP-$2^{-/-}$ mice survived infection and no significant differences in parasitemia or in heart parasite burden were observed between them (Fig 6B and 6C). These results suggest that EP-2 signaling does not play an essential role in parasite elimination.

However, significant less heart inflammatory infiltrates were observed in infected EP-$2^{-/-}$ in comparison with EP-$2^{+/+}$ mice at 14 d.p.i. (Fig 6D). Representative images of cardiac tissue and inflammatory infiltration are shown in Fig 6E. The expression of the common leukocyte marker *Ptprc* (CD45) was lower in the heart of infected EP-$2^{-/-}$ mice respect to EP-$2^{+/+}$, whereas mRNA levels of cell markers as *Cd4* (Th cells), *Cd8* (Tc cells), and *Itgax*- (CD11c; DCs), did not show significant differences. However, the expression of *Cd68*, a macrophage marker, significantly increased in EP-$2^{-/-}$ respect to EP-$2^{+/+}$ mice (Fig 7A). Regarding chemokines, *Ccl2* expression, but not *Ccl5* and *Cxcl9*, was significantly reduced in the EP-$2^{-/-}$ compared to EP-$2^{+/+}$ infected mice (Fig 7B). Induction of pro-inflammatory cytokines *Ifng* and *Il6*, the Th2 cytokine *Il4* and the anti-inflammatory cytokine *Il10*, but not *Tnf*, was lower in EP-$2^{-/-}$ compared with EP-$2^{+/+}$ (Fig 7C). Similarly to COX-$2^{-/-}$, no differences were observed in TNF-α plasma levels in EP-$2^{-/-}$ as compared to EP-$2^{+/+}$ infected mice (S3B Fig). *Ptgs2* (COX-2) gene expression was significantly lower in EP-$2^{-/-}$ infected mice (Fig 7D). There were no differences between mouse strains in *Nos2* mRNA (iNOS) expression (Fig 7D), but *Arg1* mRNA expression was higher in EP-$2^{-/-}$ mice (Fig 7D). Western blot analysis showed a significant increase in EP-$2^{-/-}$ respect to EP-$2^{+/+}$ mice, in the protein levels of these enzymes involved in L-arginine metabolism (Fig 8). Basal levels of gene expression did not significantly change between EP-$2^{+/+}$ and EP-$2^{-/-}$ mice (S5 Fig).

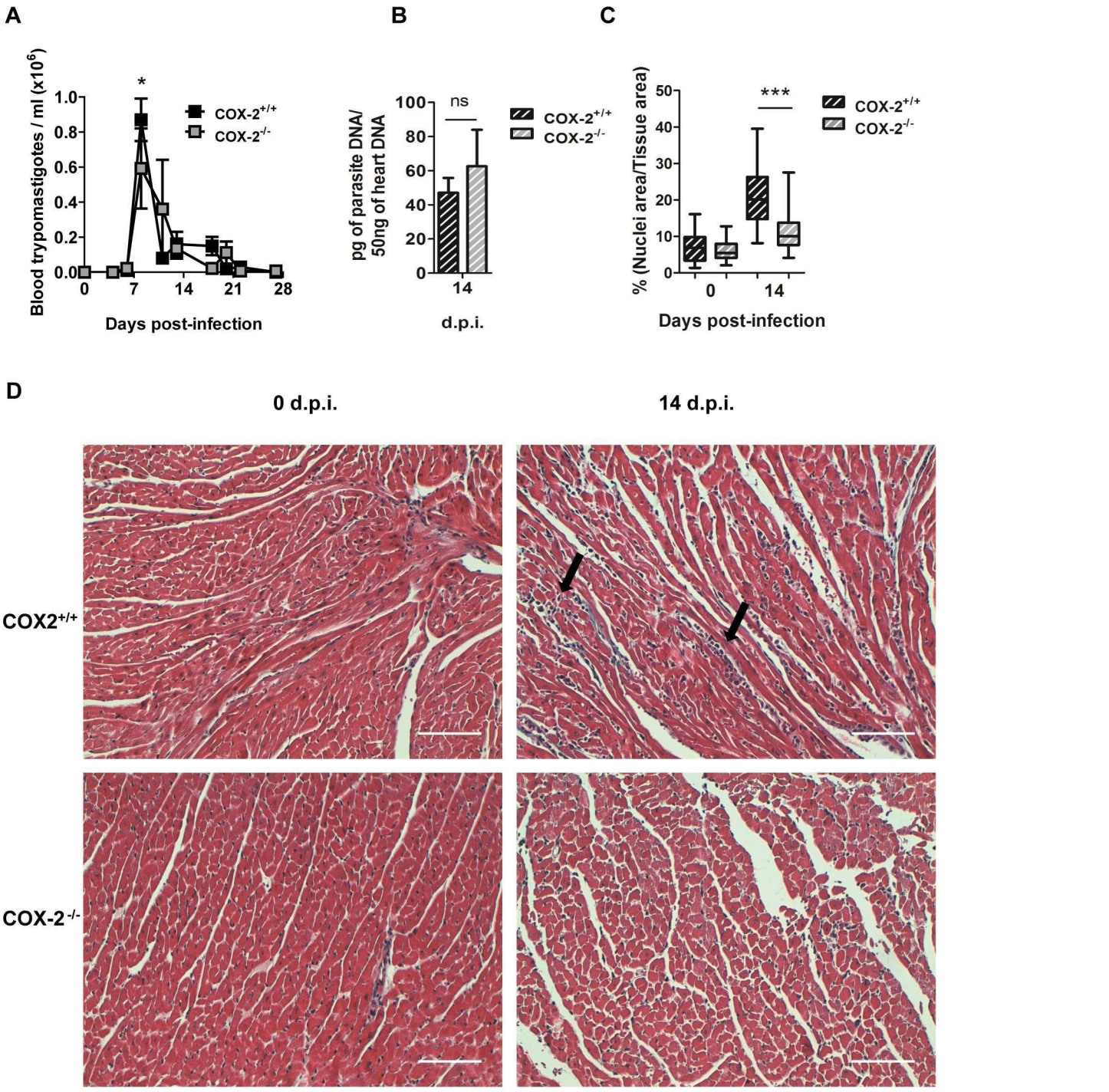

Fig 3. Parasite burden and heart inflammation in *T. cruzi* infected COX-2$^{+/+}$ and COX-2$^{-/-}$ mice. (A) The presence of parasites in the blood of COX-2$^{+/+}$ or COX-2$^{-/-}$ mice at different d.p.i. was quantified by direct counting under optical microscopy. (B) DNA from heart tissue was isolated and qPCR using *T. cruzi* DNA standard was performed to determine parasite burden in COX-2$^{+/+}$ or COX-2$^{-/-}$ infected mice at 14 d.p.i. Means ± SEM from three independent experiments are shown (n = 4). (C) Heart tissue sections of COX-2$^{+/+}$ and COX-2$^{-/-}$ mice either non-infected (0 d.p.i.) or 14 d.p.i., were stained with Masson's Trichrome and inflammatory cell infiltration was quantified as described in Methods. (D) Representative pictures of heart tissue sections described in C. Arrows indicate inflammatory infiltration. Scale bar is 100 μm. (ns = non-significant; *p<0.05; **p< 0.01; ***p<0.001).

doi:10.1371/journal.pntd.0004025.g003

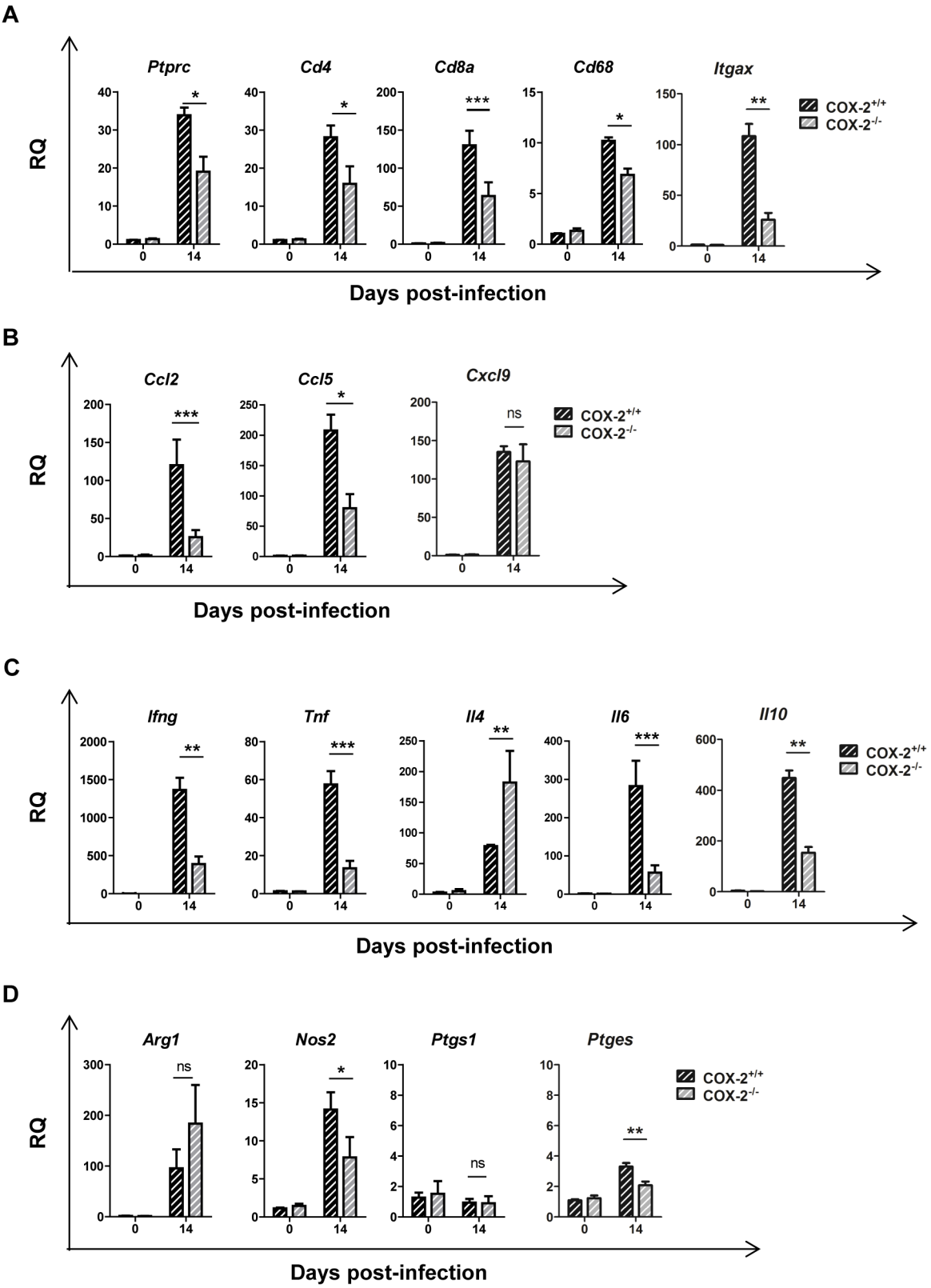

Fig 4. Gene expression of cell markers, chemokines, cytokines and inflammatory enzymes during *T. cruzi* infection in the heart of COX-2$^{+/+}$ and COX-2$^{-/-}$ mice. mRNA levels of the different genes analyzed was determined by qRT-PCR in heart tissue RNA samples isolated from non-infected (0 d.p.i.) or 14 d.p.i. COX-2$^{+/+}$ or COX-2$^{-/-}$ mice. Data are expressed as RQ calculated from CT values as described in Methods. Gene expression of lymphoid and

myeloid cell markers as *Ptprc*, *Cd4*, *Cd8a*, *Cd68* and *Itgax* (A), chemokines as *Ccl2*, *Ccl5* and *Cxcl9* (B), cytokines as *Ifng*, *Tnf*, *Il4*, *Il6* and *Il10* (C) and enzymes as *Arg1*, *Nos2*, *Ptgs1* and *Ptges* (mPGES1) (D) is shown. Means ± SEM from one representative experiment (n = 3) out of four is shown (n = 5; * p<0.05; **p<0.01; ***p<0.001).

doi:10.1371/journal.pntd.0004025.g004

Methods

Parasites and mice

BALB/c and C57BL/6 mice (6 to 8-week-old) were purchased from Harlan, Interfauna Iberica. B6;129S7-*Ptgs2*$^{tm1Jed/J}$ (COX-2$^{-/-}$) mice were purchased from The Jackson Laboratory. C57BL/6 *Ptger2*^{tm1Sna} (EP-2$^{-/-}$) mice were a gift form Dr. Shu Narumiya, (Faculty of Medicine, University of Kyoto). Wild type B6/129S (COX-2$^{+/+}$) and C57BL/6 (EP-2$^{+/+}$) mice were obtained by breeding heterozygote pairs.

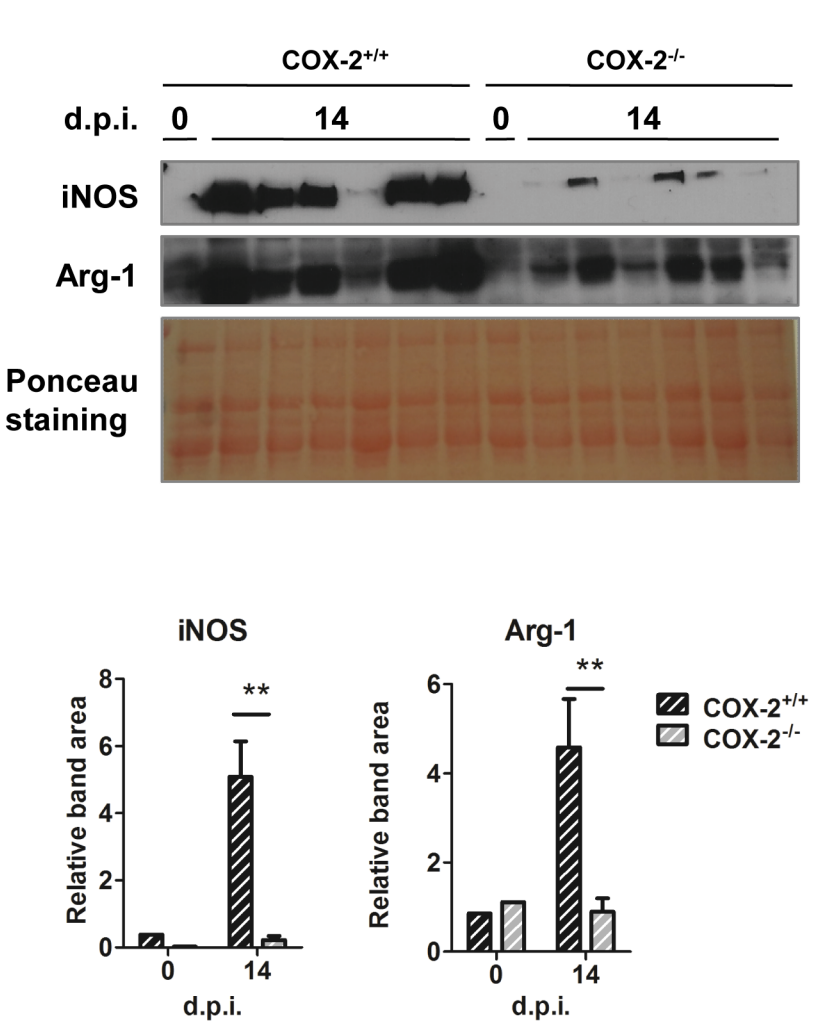

Fig 5. iNOS and Arg-1 expression in *T. cruzi* infected cardiac tissue of COX-2$^{+/+}$ and COX-2$^{-/-}$ mice. (A) Western blot analysis of iNOS and Arg-1 protein in extracts from hearts of COX-2$^{+/+}$ and COX-2$^{-/-}$ from non-infected mice (0 d.p.i.) and at 14 d.p.i. Ponceau staining of the blot is shown as a loading control. Samples for 6 different infected mice are shown. (B) Quantification of iNOS and Arg-1 band areas relative to the Ponceau staining from COX-2$^{+/+}$ (dashed black bars) and COX-2$^{-/-}$ (dashed gray bars) is represented as means ± SEM in arbitrary units. A representative experiment (n = 5) out of two is shown (**p<0.01).

doi:10.1371/journal.pntd.0004025.g005

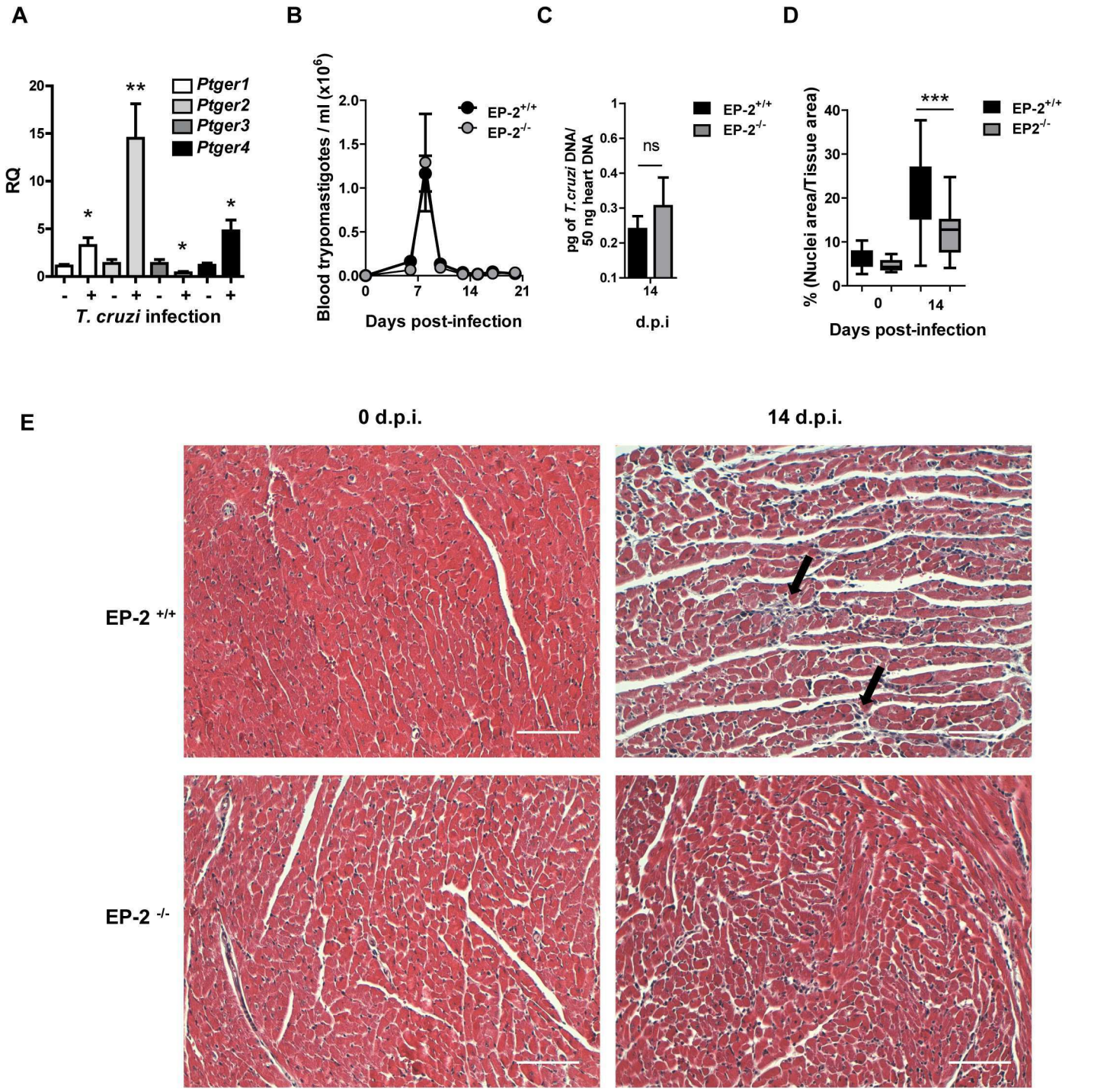

Fig 6. Parasite burden and heart inflammation in *T. cruzi* infected EP-2$^{+/+}$ and EP-2$^{-/-}$ mice. (A) mRNA levels of EP receptors (*Ptger1*, *Ptger2*, *Ptger3* and *Ptger4*) was determined by qRT-PCR in heart tissue RNA samples isolated from C57BL/6 mice non-infected (0 d.p.i.) and at 14 days post-infection (n = 5). (B) The presence of the parasites in the blood of EP-2$^{+/+}$ or EP-2$^{-/-}$ mice at different d.p.i. was quantified by direct counting under optical microscopy. (C) DNA from heart tissue was isolated and qPCR using *T. cruzi* DNA standard was performed to determine parasite burden in EP-2$^{+/+}$ or EP-2$^{-/-}$ infected mice at 14 d.p.i. Means ± SEM from a representative experiment (n = 4) from three independent experiments are shown (n = 4). (D) Heart tissue sections of EP-2$^{+/+}$ and EP-2$^{-/-}$ from non-infected mice (0 d.p.i.) and at 14 d.p.i., were stained with Masson's Trichrome and inflammatory cell infiltration was quantified as described in Methods. (***p<0.001). (E) Representative pictures of heart sections described in C. Arrows indicate inflammatory infiltration. Scale bar is 100 μm.

doi:10.1371/journal.pntd.0004025.g006

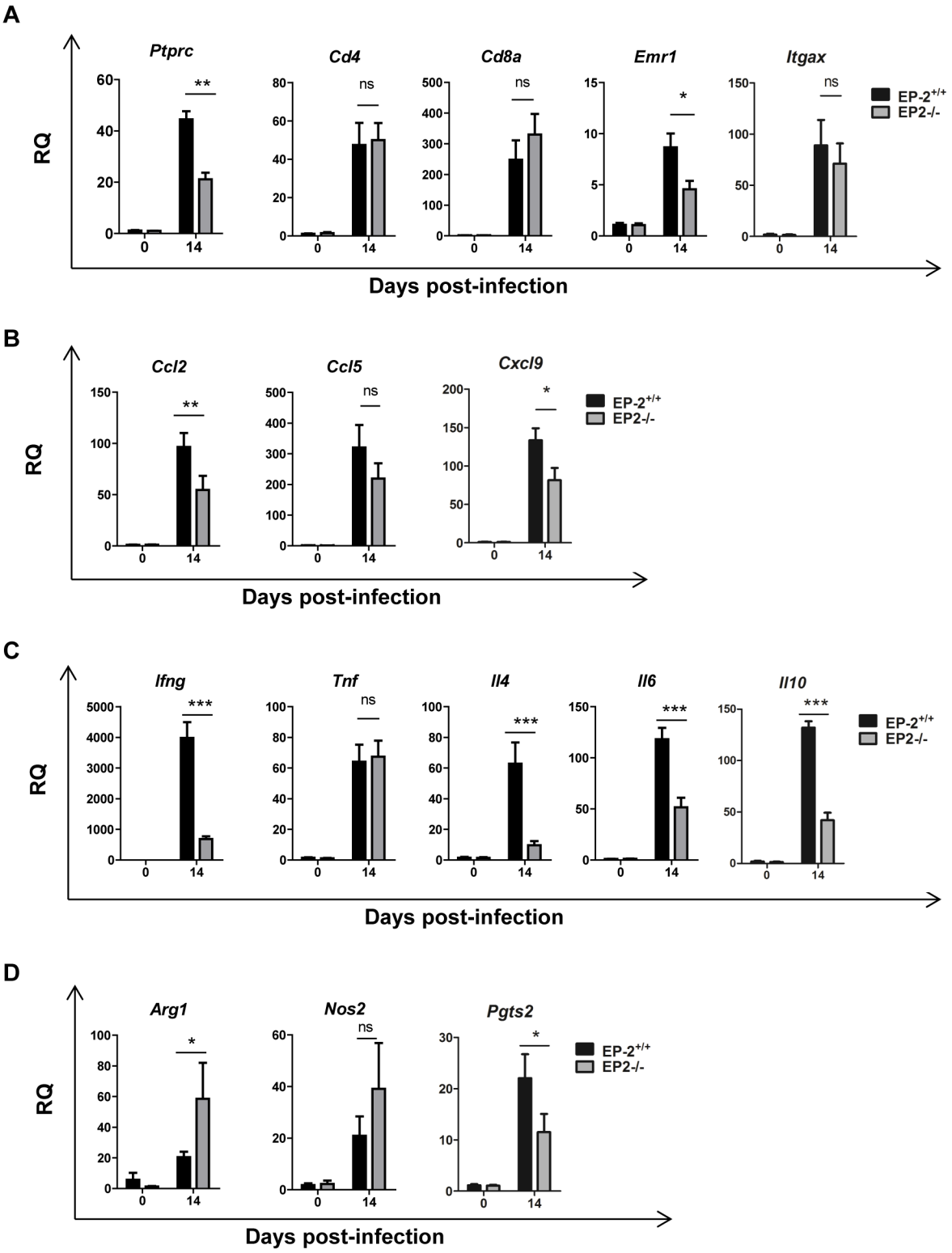

Fig 7. Gene expression of cell markers, chemokines, cytokines and inflammatory enzymes during *T. cruzi* infection in the heart of EP-2$^{+/+}$ and EP-2$^{-/-}$ mice. Expression of the different genes was analyzed by qRT-PCR in RNA samples of heart tissue isolated from EP-2$^{+/+}$ and EP-2$^{-/-}$ non-infected mice (0 d.p.i.) and at 14 d.p.i. Data are expressed as RQ calculated from CT values as described in Methods. Gene expression of lymphoid and myeloid cell markers as *Ptprc*, *Cd4*, *Cd8a*, *Cd68* and *Itgax* (A), chemokines as *Ccl2*, *Ccl5* and *Cxcl9* (B), cytokines as *Ifng*, *Tnf*, *Il4*, *Il6* and *Il10* (C) and enzymes as *Nos2*, *Ptgs2* and *Arg1* (D) is shown. Means ± SEM from a representative experiment (n = 3) out of two is shown (n = 4;* p<0.05; **p<0.01; ***p<0.001).

doi:10.1371/journal.pntd.0004025.g007

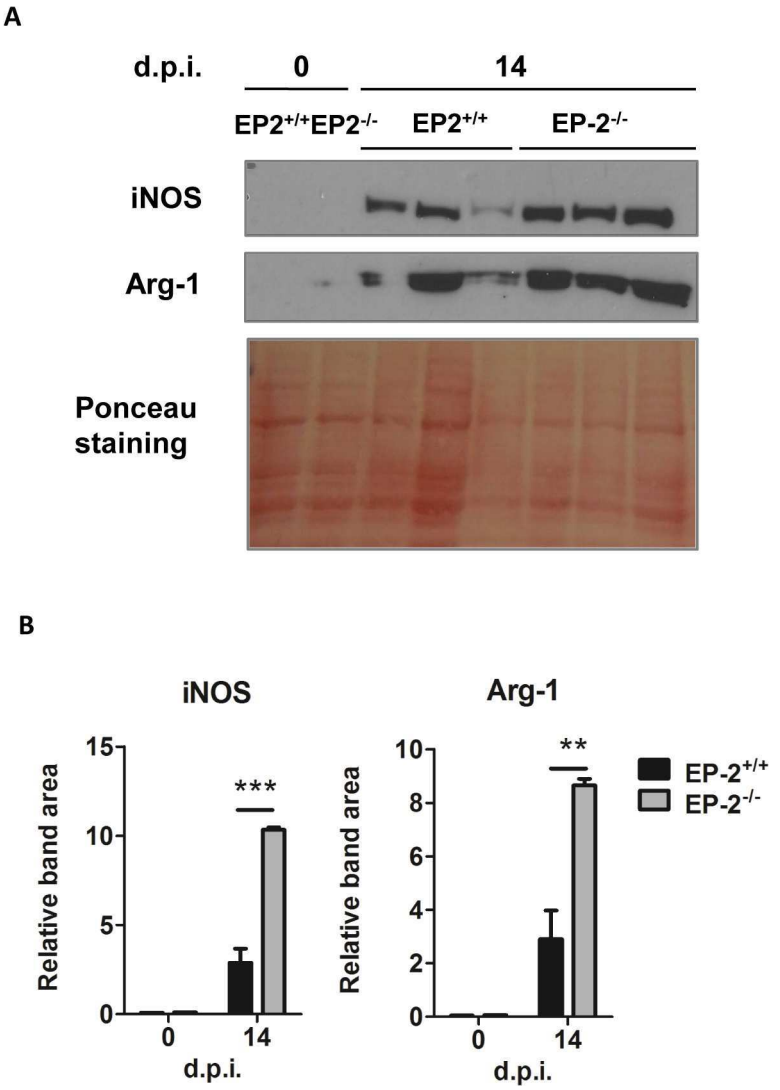

Fig 8. iNOS and Arg-1 expression in *T. cruzi* infected cardiac tissue of EP-2$^{+/+}$ and EP-2$^{-/-}$ mice. (A) Western blot analysis of iNOS and Arg-1 protein in extracts from hearts of EP-2$^{+/+}$ and EP-2$^{-/-}$ non-infected mice (0 d.p.i.) and at 14 d.p.i. Ponceau staining of the blot is shown as a loading control. Extracts from 3 different infected mice were loaded. (B) Quantification of iNOS and Arg-1 band areas relative to the Ponceau staining from EP-2$^{+/+}$ (black bars) and EP-2$^{-/-}$ (gray bars) is represented as means ± SEM in arbitrary units. A representative experiment out of two is shown (**p<0.01; ***p<0.001).

doi:10.1371/journal.pntd.0004025.g008

In vivo infections were performed with Y *T. cruzi* strain as described [6, 7]. Groups of 3–15 mice were infected with 2,000 trypomastigotes per mice by intraperitoneal injection. Groups of 3–6 non-infected mice were included in the experiments as a control. Survival was monitored daily and parasitemia levels were checked every 2–3 days. Mice blood and tissues were collected at 0 (non-infected), 14 and 21 days post-infection (d.p.i.), as indicated.

Ethics statement

This study was carried out in strict accordance with the European Commission legislation for the protection of animals used for scientific purposes (Directives 86/609/EEC and 2010/63/EU).

Mice were maintained under pathogen-free conditions at the Centro de Biología Molecular Severo Ochoa (CSIC-UAM) animal facility. The protocol for the treatment of the animals was approved by the "Comité de Ética de Investigación de la Universidad Autónoma de Madrid", Spain (permits CEI-14-283 and CEI-47-899). Animals had unlimited access to food and water. They were euthanized in a CO_2 chamber and all efforts were made to minimize their suffering.

Quantitative PCR

Hearts were perfused with Phosphate buffered saline (PBS) solution containing 1UI/ml of heparin, minced into small pieces with a sterile scalpel and DNA was isolated with High PurePCR Template preparation Kit (Roche). For *T. cruzi* detection, we used the quantitative PCR (qPCR) assay described by Piron et al. [37]. 100, 10, 1, 0.1 and 0.01 pg of DNA purified from Y strain epimastigotes were used to generate the standard curve. qPCR reactions were performed with 100 ng of genomic DNA and murine *Tnf* gene primers were used as DNA loading control.

mRNA analysis by quantitative RT-PCR

For RNA extraction, heart tissue was perfused with PBS containing 1UI/ml of heparin, cut in small pieces using a sterile scalpel blade, followed by mechanical disruption using a PT 1300 D homogenizer (Kinematica Polytron, Fisher Scientific) in TRIzol reagent (Invitrogen) as indicated by the manufacturer. Gene expression was analyzed by quantitative reverse transcription PCR (qRT-PCR). Reverse transcription of total RNA was performed using the components of the High Capacity cDNA Archive Kit (Applied Biosystems. Life Sciences) or the SuperScript Enzyme (Invitrogen, Life Sciences). Amplification were performed using TaqMan MGB probes (S1 Table) and the TaqMan Universal PCR Master Mix (Applied Biosystems) on an ABI PRISM 7900 HT instrument (Applied Biosystems. Life Sciences). For cultured cells, samples were treated as mentioned above except for the mechanical disruption. All samples were assayed in triplicate. Quantification of gene expression by real-time PCR was calculated by the comparative threshold cycle (CT) method as described in [38] ($RQ = 2^{-\Delta\Delta CT}$). All quantifications were normalized to the ribosomal *18S* control to account for the variability in the initial concentration of RNA and in the conversion efficiency of the reverse transcription reaction.

Protein expression analysis

Protein extracts were prepared from heart tissue perfused with PBS containing 1UI/ml of heparin, cut in small pieces using a sterile scalpel blade followed by mechanical disruption in Triton X-100 based protein lysis buffer. Protein concentration was determined by the bicinchoninic acid method (BCA, Pierce) using Bovine Serum Albumin (BSA) for the standard curve. Western blot analyses were performed as follows: 15 or 50 μg of cell or tissue extract were fractionated on SDS polyacrylamide gel and transferred to a Nitrocellulose membrane Hybond-ECL (Amersham Biosciences) and blocked in 5% fat free dry milk or 5% BSA in 0,1% Tween-20 Tris Buffered Saline. Membranes were incubated overnight with diluted primary antibodies (S2 Table) at 4–8°C. The membranes were incubated with horseradish peroxidase conjugated secondary antibodies (S2 Table) and detection was carried out with Supersignal detection reagent (Pierce) followed by photographic film exposure. Fiji package software was used to quantify band intensity normalizing band areas of the sample to their respective loading control.

Histological studies

Cardiac tissues from mice were placed in 10% neutral buffered formalin for at least 4 hours at room temperature followed by incubation in 70% ethanol overnight. Samples were then embedded in paraffin (Tissue Embedding Station Leica EG1160), and 5 μm tissue sections were prepared (Microtome Leica RM2155). Samples were deparaffinized and rehydrated using a Tissue Processing Station Leica TP1020. Slides were stained with Masson´s Trichrome staining and mounted permanently in Eukitt´s quick hardening mounting medium (Biochemika, Fluka analytical). The sections were microscopically analyzed in a Leica microscope (DMD 108, Leica microsystems Wetzlar GmbH, Germany) using the 20x magnification objective lens and Lamp intensity 10 and f/Stop 12. Ventricular myocardium micrographs were taken avoiding pericardium, endocardium, atria and big vessels. Nine pictures of different sections, separated by at least 50 μm, per heart were taken. The degree of inflammatory-cell infiltration was quantified using the Fiji package [39] and the plugin Trainable Weka Segmentation developed by Ignacio Arganda Carreras (Versailles, France) [39] (Image J macro used for automated image analysis is detailed in S1 File) and expressed as the percentage of the nuclei/tissue area ratio.

Confocal immunofluorescence

Organs were removed from mice at different d.p.i., cut and fixed in a 4% paraformaldehyde PBS buffered solution for 2h at room temperature, followed by incubation in a 30% sucrose solution at 4°C overnight. Tissues were then embedded in Tissue-Tek OCT in Cryomolds (Sakura) and frozen. 10 μm sections were cut using a cryostat Leica CM1900. Slides were fixed in acetone for 10 min at room temperature and incubated 10 min with NH_4Cl to reduce autofluorescence. Then, slides were washed with PBS, permeabilized with 0,1% Triton X-100, blocked and incubated over night at 4°C with primary antibodies (S2 Table) in blocking buffer (PBS 0,1% Triton X-100, 5% BSA). The samples were washed with PBS and secondary antibodies (S2 Table) were added in blocking buffer and incubated overnight at 4°C. Blocking of unspecific secondary antibody binding was achieved by addition of 2% of normal serum of the species in which the secondary antibody was raised. As a negative control, sections were treated in the same manner, except that incubation with primary antibody was omitted. Nuclei were stained using 1 μg/ml of DAPI (268298, Merck). Prolong Gold Antifade Reagent (Invitrogen) was used to mount the slides that were kept at 4°C until observation. Stained slides were observed with the confocal laser scanning microscope LSM710, coupled to an AxioimagerM2 microscope (Zeiss). The micrographs were processed using the software ZEN (Zeiss) or the Fiji Package.

Isolation of $Ly6G^+$ and $CD11b^+Ly6G^-$ cells by magnetic sorting

BALB/c (n = 15) or C57BL/6 mice (n = 15) were infected i.p. with 2,000 trypomastigotes of the Y strain. At 21 d.p.i. for BALB/c and 14 d.p.i. for C57BL/6, mice were euthanized in a CO_2 chamber and hearts were aseptically removed, perfused with 10 ml PBS containing 1UI/ml of heparin, and kept in cold Hank´s balanced saline solution (HBSS). Then, hearts were pooled in a cell culture dish, washed thoroughly with HBSS and minced into small pieces with a sterile surgery blade. Mouse hearts (maximum 4 per tube) were transferred into the gentleMACS C tube containing 4,7 mL of HBSS. 300μL of Collagenase II solution (600 U/ml) and 10 μl DNase I solution (60U/ml) were added. Then tissue was disrupted with GentleMACS Dissociator (Miltenyi Biotec GMbH). To obtain cell suspensions, a 70 μm cell strainer (Falcon BD) was used. After red blood cells lysis, the cells were magnetically sorted. For $Ly6G^+$ cell sorting, anti Ly-6G MicroBead kit was used with MACS LS columns and MACS Separators (Miltenyi Biotec

GmbH), following manufacturer instructions. Ly6G$^-$ fraction of the cell suspension was afterwards processed for CD11b$^+$ cell sorting using CD11b Microbeads kit.

Analysis of prostanoids

Prostanoid levels were determined in mouse tissue extracts from 0 (non-infected) and 21 d.p.i. by Metabolon Inc., and expressed as ScaledImpData as previously described [40]. To determine *in vitro* prostanoid production, heart infiltrating cells were magnetically sorted as described above and incubated 30 minutes at 37°C in 500 μl of RPMI without Fetal bovine serum (FBS) in the presence of 25 μM [^{14}C] AA, PerkinElmer (Massachusetts, USA). 500 μl of 2% acetic acid in cold methanol was added to extract and preserve AA derivatives. Samples were vortexed and the air inside the tube was substituted by inert nitrogen gas. Samples were kept frozen at -80°C until HPLC was performed. HPLC device was composed by a Beckman Solvent Module 126 with the column Ultraphere ODS (C-18, Beckman-Coulter) 5 μm diameter sphere particle, 4.5 mm and 25 cm column diameter and length respectively and a Beckman 171 Radioisotope Detector. Scintillation liquid Ecoscint H was purchased from National Diagnostics. Prostanoids were resolved with the isocratic flow (1ml/min) of the mobile phase: Acetonitrile/water/acetic acid 33:67:0.1 v/v/v. Standards were produced using [^{14}C] Arachidonic Acid and different cell types expressing the respective enzymes, and [^{14}C] Arachidonic Acid incubated in medium was used as input control as described [41].

Statistical analysis

For *in vivo* experiments, data are shown as means ± SEM. All the *in vitro* experiments were performed at least three times. Significance was evaluated by Student's t-test when two groups were compared. ANOVA one way followed by Tukey post-test was used when groups of samples from an experiment had different time points. ANOVA two way followed by Bonferroni post-test were used when the experiment included time and mice strain as variables. For survival analysis, we used Gehan-Breslow-Wilcoxon method. GraphPad Prism 5.00 software (La Jolla, CA, USA) was used for statistical analysis.

Discussion

In order to clarify the role of prostanoids in the outcome of T. cruzi infection we first analyzed the expression of prostanoid-synthesizing enzymes in cardiac tissue from T. cruzi susceptible (BALB/c) and non-susceptible (C57BL/6) mice. Our results showed an increase of COX-2/mPGES-1/PGE_2 axis in heart tissue upon infection in both strains of mice, indicating that it has no direct effect on susceptibility to infection. Confocal microscopy analysis showed the presence of CD68$^+$Arg-1$^+$COX-2$^-$ cells and CD68$^+$Arg-1$^-$COX-2$^+$, suggesting that there are at least two subpopulations of monocytic infiltrating cells with mutually exclusive expression of those enzymes. Thus, our results show that the myeloid population infiltrating the heart in *T. cruzi* infection is more complex than previously described [7], and suggests a difference in the function of these two myeloid populations. Macrophages can rapidly change their phenotype and function in response to local microenvironmental signals, playing key roles in the initiation and resolution of inflammation and tissue homeostasis [42] and could be involved in tissue repair and fibrosis [43]. Thus, myeloid cardiac infiltration could inhibit parasite replication and also facilitate the repair of damaged muscular tissue [44]. A suggestive hypothesis is that COX-2 expressing macrophages could be linked to inflammation meanwhile Arg-1$^+$ macrophages could be involved in tissue repair.

Immunostaining of heart tissue sections showed the presence of myeloid and non-myeloid cells positive for COX-2 in heart tissue sections of both BALB/c and C57BL/6 mice. However,

after purification of myeloid cells from heart tissue, we found that only a particular subset expressed COX-2, being the levels of COX-2 expression higher in C57BL/6 than BALB/c mice. Likely, non-myeloid COX-2 positive cells are lost in the purification process, a fact that might account for the apparent contrary results.

Interestingly, we demonstrated that PGE_2 and 6-oxo-$PGF_{1\alpha}$ (stable hydrolysis product of PGI_2) were elevated in infected heart tissue. Furthermore, monocytes ($CD11b^+Ly6G^-$) isolated from infected heart express COX-2, and are able to produce high levels of PGE_2 *ex vivo*. The differences in metabolites detected in total heart extracts *versus* purified myeloid cells are likely due to their synthesis by other cell types and/or enrichment after cell purification. In agreement with this, we have previously reported that *T. cruzi* infection induces COX-2 in cardiomyocytes, leading to $PGF_{2\alpha}$ and TXA_2 production [45]. Although COX-2 expression can be induced in $CD4^+$ T cells upon activation [34], heart infiltrating $CD4^+$ cells did not express detectable levels of COX-2.

On the other hand, the increase of *Tbxas1* and *Hpgds* gene expression observed upon *T. cruzi* infection in both C57BL/6 and BALB/c mice suggests the production of their respective TXA_2 and PGD_2 metabolites in infected cardiac tissue. *Tbxas1* was elevated up to 28 d.p.i. and its product, TXA_2, besides its vascular functions [46], could have a pro-inflammatory role for monocytes [47]. In contrast, *Hpgds* expression showed a gradual increase during the acute phase, and its product, PGD_2, could be involved in resolution of inflammation, as described in other settings [48–50]. Resistant C57BL/6 mice showed significantly higher expression of *Hpgds* at 21 d.p.i. and lower expression of *Tbxas1* at 28 d.p.i. than the susceptible BALB/c mice, suggesting that C57BL/6 may resolve inflammation earlier than BALB/c infected mice. However, TXA_2 and PGD_2 metabolites were not detected in purified $Ly6G^+$ nor in $CD11b^+Ly6G^-$ cells, suggesting that they could be produced by other infiltrating cell types or by infected cardiomyocytes [45].

Previous reports using COX-2 inhibitors in *T. cruzi* infection showed discordant results [30]. Moreover, COX-2 inhibitors may interfere with the immune response [34], but more importantly, many COX-2 inhibitors have effects independent of their ability to inhibit cyclooxygenase activity [51–53]. For those reasons, we analyzed the contribution of COX-2 by using a mouse model deficient for its expression. We found a small variation in parasitemia (30% reduction at the peak of parasitemia) in $COX\text{-}2^{-/-}$ respect to the $COX\text{-}2^{+/+}$ mice, which cannot be taken as indicative of resistance. In addition, no changes were observed in cardiac parasite burden, in spite that $COX\text{-}2^{-/-}$ mice expressed less iNOS than $COX\text{-}2^{+/+}$ mice, considered to be key for resistance in *T. cruzi* infection [54], indicating that heart parasite load is not affected by the lack of COX-2 expression. Interestingly, we found that COX-2 was required for leukocyte infiltration and inflammation in the heart upon *T. cruzi* infection, but it did not affect systemic inflammation. However, $COX\text{-}2^{-/-}$ mice are resistant to death in sepsis, indicating that in this case COX-2 has a systemic pro-inflammatory role [55]. An important role of endogenous COX-2 derived PGs in migration of immune cells to infected tissues or lymphoid organs is becoming evident [19]. Thus, the decrease in cardiac inflammation and in local production of cytokines and chemokines observed in $COX\text{-}2^{-/-}$ infected mice, indicate a pro-inflammatory role of prostanoids as PGE_2 in acute myocarditis.

We have previously described that PGE_2 induces COX-2 and mPGES-1 expression in an autocrine loop required for full activation of macrophages [36]. Thus, the fact that $COX\text{-}2^{-/-}$ mice showed a reduced *Ptges* mRNA expression (mPGES-1) suggest a blockade of the autocrine loop that may impair full activation of macrophages, resulting in the reduced cardiac infiltration observed. In the same direction, lack of PGE_2 signaling through EP-2 receptor in $EP\text{-}2^{-/-}$ infected mice, resulted in reduced *Ptgs* (COX-2) mRNA expression that may also block the autocrine loop, impairing macrophages to infiltrate the cardiac tissue. This is in agreement

with the observed decrease in *Ccl2* mRNA expression in COX-2$^{-/-}$ and EP-2$^{-/-}$ infected mice respect to wild type infected mice, since this chemokine is required for migration of monocytes to the inflamed infected tissue [56]. Moreover, PGE_2 also affects migration of myeloid cells potentiating CCL2 activity [19]. Therefore, the reduction of cardiac infiltration in both animal models suggest a detrimental pro-inflammatory role of COX-2 in the onset of cardiac inflammation.

Strikingly, Arg-1 and iNOS expression, markers of MDSCs, was higher in hearts of infected EP-2$^{-/-}$ mice than in those from COX-2$^{-/-}$ infected mice hearts, indicating that infiltrating cells from EP-2$^{-/-}$ mice present a more marked MDSCs phenotype. In addition, the effect of EP-2 deficiency on cytokine and chemokine production in heart, was milder than the observed in COX-2$^{-/-}$ infected mice. In the hearts of C57BL/6 mice, infection caused a greater significant increase in the expression of *Ptger2*, which validates the use of EP-2$^{-/-}$ mice in the C57BL/6 background. But still *Ptger1* and *Ptger4* were significantly increased although in a minor extent. Thus in EP-2$^{-/-}$ infected mice PGE_2 can still signal through *Ptger1* and *Ptger4* causing this milder effect in EP-2$^{-/-}$ mice in comparison to the observed in COX-2$^{-/-}$ infected hearts. In contrast, in COX-2$^{-/-}$ infected mice, mPGES1 synthase expression is substantially reduced and PGH_2 substrate for PGE_2 production likely relies on constitutive COX-1 activity. Thus, the decreased levels of PGE_2 may affect signaling through all PGE_2 receptors, having a broader effect on leukocyte infiltration. The response to *T. cruzi* infection in mice deficient in other enzymes and products of the AA pathway has been scarcely studied [26, 27]. Sharma *et al.* described that deficiency of $iPLA_2$-γ (Ca^{++} independent PLA_2 isoform-γ), which is involved in AA membrane release, aggravated infection and decreased survival, while Mukherjee *et al.* described that COX-1$^{-/-}$ mice showed higher parasitemia than wild type infected mice, but no difference in survival was noted [27]. In our hands, interference within the AA pathway at a different level, as COX-2 mediated production of prostanoids or PGE_2/EP-2 signaling, results in decreased inflammation in heart of *T. cruzi* infected mice, with low incidence in parasite burden and survival. Altogether, these results point to an essential role of the AA pathway in heart inflammation during *T. cruzi* infection.

In the other hand, related with the prostanoid pathway, 5-lipoxygenase (5-LO) has been shown to play a detrimental role during T. cruzi infection by potentiating heart parasitism and inflammation [57, 58] through the regulation of iNOS activity [59]. However, further studies are needed to elucidate the crosstalk between LO and COX pathways during infection."

Besides, we have previously showed that monocytic $CD11b^+Ly6G^-$ heart infiltrating cells (MDSCs), expressing iNOS and Arg-1 suppressed *ex vivo* T cell proliferation [7]. Since some of these infiltrating cells also express COX-2 and produce PGE_2 it is possible that COX-2-derived PGs could contribute to immune suppression, a possibility that should be addressed in the future.

In conclusion, during acute *T. cruzi* infection there is an increase in the expression of many enzymes of the AA metabolism, including COX-2 and mPGES-1 that leads to an increase in their metabolite PGE_2, partially due to infiltrating myeloid cells in the heart. Besides, we have identified a new myeloid infiltrating population characterized by the expression of COX-2. Thus, so far there are at least three different myeloid populations infiltrating the *T. cruzi* infected heart: granulocytes, monocytic MDSCs expressing iNOS and Arg-1 and monocytic cells expressing COX-2. COX-2 activity likely increases PGE_2 levels in heart tissue, which play a pro-inflammatory role by signaling through EP-2. However, the phenotype of EP-2$^{-/-}$ is not as strong as COX-2$^{-/-}$ infected mice probably due to PGE_2 signaling through alternative EP receptors. Our findings suggest that COX-2 plays a detrimental role in acute Chagas disease myocarditis. Further research of the AA pathway is needed to completely understand its role during *T. cruzi* infection for immune intervention approaches.

Supporting Information

S1 Fig. Survival, parasite burden and inflammation of BALB/c and C57BL/6 mice infected with *T. cruzi*. (A) Survival was checked every day during the infection in BALB/c and C57BL/6 mice (n = 5). (B) The presence of the parasites in the blood of BALB/c and C57BL/6 mice was quantified by direct counting under optical microscopy. Means ± SEM of a representative experiment (n = 4) from two independent experiments are shown. (* $p< 0.05$; ** $p< 0.01$). (C) Histology of cardiac tissue in non-infected (0 d.p.i.) or 21 d.p.i *T. cruzi* infected BALB/c and C57BL/6 mice. Representative pictures of heart tissue sections of each group, processed for Masson`s Trichrome histology staining, are shown. Black arrows point to the infiltrating leukocytes and red arrows point to parasite nests. Scale bar is 100 μm.
(TIF)

S2 Fig. COX-2 and CD4 expression in *T. cruzi* infected mouse cardiac tissue. (A) Heart tissue was isolated at 14 d.p.i. from infected C57BL/6 mice and sections were stained with DAPI for nuclei (Blue), the lymphocyte marker CD4 (green) or COX-2 (red). A representative picture of several sections analyzed in at least three different mice from two independent experiments is shown. (B) Control sample from heart of C57BL/6 mice at 14 d.p.i. incubated with secondary antibodies coupled to Alexa Fluor (AF) 488, and 647 in the absence of primary antibodies. (C) Same as in A from heart of BALB/c mice at 21 d.p.i.. (D) Same as in B from heart of BALB/c mice at 21 d.p.i. (E) Control samples from heart of BALB/c mice at 21 d.p.i. incubated with secondary antibodies coupled to Alexa Fluor (AF) 488, 555 and 647 in the absence of primary antibodies. Scale bar is 20 μm.
(TIF)

S3 Fig. Serum levels of TNFα in COX-$2^{+/+}$, COX-$2^{-/-}$, EP-$2^{+/+}$ and EP-$2^{-/-}$ mice during *T. cruzi* infection. TNFα concentration in non-infected mice (0 d.p.i.) and at 14 d.p.i. in blood serum of (A) COX-$2^{+/+}$ and COX-$2^{-/-}$ and (B) EP-$2^{+/+}$ and EP-$2^{-/-}$ mice. Representative means ± SEM from two independent experiments are shown (n = 6) (ns = non-significant).
(TIF)

S4 Fig. Comparison of the gene expression of cell markers, chemokines, cytokines and inflammatory enzymes basal levels in the heart of COX-$2^{+/+}$ and COX-$2^{-/-}$ mice. mRNA levels of the different genes analyzed was determined by qRT-PCR in heart tissue RNA samples isolated from non-infected (0 d.p.i.) COX-$2^{+/+}$ or COX-$2^{-/-}$ mice. Data are expressed as RQ calculated from CT values as described in Methods. Gene expression of lymphoid and myeloid cell markers as *Ptprc*, *Cd4*, *Cd8a*, *Cd68* and *Itgax* (A), chemokines as *Ccl2*, *Ccl5* and *Cxcl9* (B), cytokines as *Ifng*, *Tnf*, *Il4*, *Il6* and *Il10* (C) and enzymes as *Arg1*, *Nos2*, *Ptgs1* and *Ptges* (mPGES1) (D) is shown. Means ± SEM from one representative experiment (n = 3) out of four is shown (n = 5; * $p<0.05$).
(TIF)

S5 Fig. Comparison of the gene expression of cell markers, chemokines, cytokines and inflammatory enzymes basal levels in the heart of EP-$2^{+/+}$ and EP-$2^{-/-}$ mice. mRNA levels of the different genes analyzed was determined by qRT-PCR in heart tissue RNA samples isolated from non-infected (0 d.p.i.) EP-$2^{+/+}$ or EP-$2^{-/-}$ mice. Data are expressed as RQ calculated from CT values as described in Methods. Gene expression of lymphoid and myeloid cell markers as *Ptprc*, *Cd4*, *Cd8a*, *Cd68* and *Itgax* (A), chemokines as *Ccl2*, *Ccl5* and *Cxcl9* (B), cytokines as *Ifng*, *Tnf*, *Il4*, *Il6* and *Il10* (C) and enzymes as *Nos2*, *Ptgs2* and *Arg1* (D) is shown. Means ± SEM from one representative experiment (n = 3) out of four is shown (n = 5; * $p<0.05$).
(TIF)

S1 Table. Taqman probes. List of the Taqman Probes from Applied Biosystems (A&B) used in the mRNA analysis by quantitative RT-PCR, including reference of the manufacturer, gene symbol and protein name.
(PDF)

S2 Table. Antibodies. List of antibodies from different providers used in confocal immunofluorescence and western blot analysis including the reference from each provider, the application and the dilution utilized.
(PDF)

S1 File. Image J macro used for automated image analysis. Plugin Trainable Weka Segmentation developed by Ignacio Arganda Carreras (Versailles, France).
(PDF)

Acknowledgments

The authors would like to thank Beatriz Barrocal for taking care of the animals and Maria A. Chorro and Maria C. Maza for their excellent technical assistance. We thank Dr. Alejandro Pascual and Dr. Laura García-Bermejo from the Ramón y Cajal Hospital for their precious help with the histologic analysis. We also thank the personal of the Confocal Microscopy Service (S.M.O.C.) at the CBMSO for their excellent assistance.

Author Contributions

Conceived and designed the experiments: NAG NG MF MAÍ. Performed the experiments: NAG NG HC MC CCM CP. Analyzed the data: NAG NG MF. Contributed reagents/materials/analysis tools: MC LV. Wrote the paper: NAG MC MAÍ NG MF.

References

1. Hotez PJ, Molyneux DH, Fenwick A, Kumaresan J, Sachs SE, Sachs JD, et al. Control of neglected tropical diseases. The New England journal of medicine. 2007; 357(10):1018–27. PMID: 17804846.
2. Morillo CA. Infection with Trypanosoma cruzi and progression to cardiomyopathy: what is the evidence and is the tide finally turning? Circulation. 2013; 127(10):1095–7. doi: 10.1161/CIRCULATIONAHA.113.000891 PMID: 23393009.
3. Moncayo A, Silveira AC. Current epidemiological trends for Chagas disease in Latin America and future challenges in epidemiology, surveillance and health policy. Memorias do Instituto Oswaldo Cruz. 2009; 104 (Suppl 1):17–30. PMID: 19753454.
4. Rodriguez HO, Guerrero NA, Fortes A, Santi-Rocca J, Girones N, Fresno M. Trypanosoma cruzi strains cause different myocarditis patterns in infected mice. Acta Trop. 2014; 139:57–66. Epub 2014/07/16. doi: 10.1016/j.actatropica.2014.07.005 S0001-706X(14)00227-7 [pii]. PMID: 25017312.
5. Molina HA, Kierszenbaum F. Kinetics of development of inflammatory lesions in myocardial and skeletal muscle in experimental Trypanosoma cruzi infection. J Parasitol. 1988; 74(3):370–4. Epub 1988/06/01. PMID: 3132546.
6. Cuervo H, Pineda MA, Aoki MP, Gea S, Fresno M, Girones N. Inducible nitric oxide synthase and arginase expression in heart tissue during acute Trypanosoma cruzi infection in mice: arginase I is expressed in infiltrating CD68+ macrophages. The Journal of infectious diseases. 2008; 197(12):1772–82. PMID: 18473687. doi: 10.1086/529527
7. Cuervo H, Guerrero NA, Carbajosa S, Beschin A, De Baetselier P, Girones N, et al. Myeloid-derived suppressor cells infiltrate the heart in acute Trypanosoma cruzi infection. J Immunol. 2011; 187 (5):2656–65. PMID: 21804013. doi: 10.4049/jimmunol.1002928
8. Wymann MP, Schneiter R. Lipid signalling in disease. Nat Rev Mol Cell Biol. 2008; 9(2):162–76. Epub 2008/01/25. doi: 10.1038/nrm2335 nrm2335 [pii]. PMID: 18216772.
9. Dubois RN, Abramson SB, Crofford L, Gupta RA, Simon LS, Van De Putte LB, et al. Cyclooxygenase in biology and disease. Faseb J. 1998; 12(12):1063–73. PMID: 9737710.

10. Harris SG, Padilla J, Koumas L, Ray D, Phipps RP. Prostaglandins as modulators of immunity. Trends in immunology. 2002; 23(3):144–50. PMID: 11864843.

11. Carey MA, Bradbury JA, Seubert JM, Langenbach R, Zeldin DC, Germolec DR. Contrasting effects of cyclooxygenase-1 (COX-1) and COX-2 deficiency on the host response to influenza A viral infection. J Immunol. 2005; 175(10):6878–84. PMID: 16272346.

12. Goldmann O, Hertzen E, Hecht A, Schmidt H, Lehne S, Norrby-Teglund A, et al. Inducible cyclooxygenase released prostaglandin E2 modulates the severity of infection caused by Streptococcus pyogenes. J Immunol. 2010; 185(4):2372–81. PMID: 20644176. doi: 10.4049/jimmunol.1000838

13. Takahashi T, Zhu SJ, Sumino H, Saegusa S, Nakahashi T, Iwai K, et al. Inhibition of cyclooxygenase-2 enhances myocardial damage in a mouse model of viral myocarditis. Life sciences. 2005; 78(2):195–204. PMID: 16107267.

14. Krause P, Bruckner M, Uermosi C, Singer E, Groettrup M, Legler DF. Prostaglandin E(2) enhances T-cell proliferation by inducing the costimulatory molecules OX40L, CD70, and 4-1BBL on dendritic cells. Blood. 2009; 113(11):2451–60. PMID: 19029446. doi: 10.1182/blood-2008-05-157123

15. van der Pouw Kraan TC, Boeije LC, Smeenk RJ, Wijdenes J, Aarden LA. Prostaglandin-E2 is a potent inhibitor of human interleukin 12 production. The Journal of experimental medicine. 1995; 181(2):775–9. PMID: 7836930.

16. Aronoff DM, Canetti C, Peters-Golden M. Prostaglandin E2 inhibits alveolar macrophage phagocytosis through an E-prostanoid 2 receptor-mediated increase in intracellular cyclic AMP. J Immunol. 2004; 173(1):559–65. PMID: 15210817.

17. Weinberg DA, Weston LK, Kaplan JE. Influence of prostaglandin I2 on fibronectin-mediated phagocytosis in vivo and in vitro. Journal of leukocyte biology. 1985; 37(2):151–9. PMID: 2981944.

18. Panzer U, Uguccioni M. Prostaglandin E2 modulates the functional responsiveness of human monocytes to chemokines. European journal of immunology. 2004; 34(12):3682–9. PMID: 15484190.

19. Diaz-Munoz MD, Osma-Garcia IC, Iniguez MA, Fresno M. Cyclooxygenase-2 deficiency in macrophages leads to defective p110gamma PI3K signaling and impairs cell adhesion and migration. J Immunol. 2013; 191(1):395–406. Epub 2013/06/05. doi: 10.4049/jimmunol.1202002 jimmunol.1202002 [pii]. PMID: 23733875.

20. de Barros-Mazon S, Guariento ME, da Silva CA, Coffman RL, Abrahamsohn IA. Differential regulation of lymphoproliferative responses to Trypanosoma cruzi antigen in patients with the cardiac or indeterminate form of Chagas disease. Clinical immunology (Orlando, Fla. 2004; 111(1):137–45. PMID: 15093563.

21. Sousa AS, Xavier SS, Freitas GR, Hasslocher-Moreno A. Prevention strategies of cardioembolic ischemic stroke in Chagas' disease. Arquivos brasileiros de cardiologia. 2008; 91(5):306–10. PMID: 19142374.

22. Gomes JA, Molica AM, Keesen TS, Morato MJ, de Araujo FF, Fares RC, et al. Inflammatory mediators from monocytes down-regulate cellular proliferation and enhance cytokines production in patients with polar clinical forms of Chagas disease. Hum Immunol. 2014; 75(1):20–8. Epub 2013/09/28. doi: 10.1016/j.humimm.2013.09.009 S0198-8859(13)00530-2 [pii]. PMID: 24071371.

23. Cardoni RL, Antunez MI. Circulating levels of cyclooxygenase metabolites in experimental Trypanosoma cruzi infections. Mediators of inflammation. 2004; 13(4):235–40. PMID: 15545053.

24. Celentano AM, Gorelik G, Solana ME, Sterin-Borda L, Borda E, Gonzalez Cappa SM. PGE2 involvement in experimental infection with Trypanosoma cruzi subpopulations. Prostaglandins. 1995; 49 (3):141–53. PMID: 7652183.

25. D'Avila H, Freire-de-Lima CG, Roque NR, Teixeira L, Barja-Fidalgo C, Silva AR, et al. Host cell lipid bodies triggered by Trypanosoma cruzi infection and enhanced by the uptake of apoptotic cells are associated with prostaglandin E(2) generation and increased parasite growth. The Journal of infectious diseases. 2011; 204(6):951–61. PMID: 21849292. doi: 10.1093/infdis/jir432

26. Sharma J, Eickhoff CS, Hoft DF, Ford DA, Gross RW, McHowat J. The absence of myocardial calcium-independent phospholipase A2gamma results in impaired prostaglandin E2 production and decreased survival in mice with acute Trypanosoma cruzi infection. Infect Immun. 2013; 81(7):2278–87. Epub 2013/02/23. doi: 10.1128/IAI.00497-12 IAI.00497-12 [pii]. PMID: 23429536; PubMed Central PMCID: PMC3697611.

27. Mukherjee S, Machado FS, Huang H, Oz HS, Jelicks LA, Prado CM, et al. Aspirin treatment of mice infected with Trypanosoma cruzi and implications for the pathogenesis of Chagas disease. PloS one. 2011; 6(2):e16959. PMID: 21347238. doi: 10.1371/journal.pone.0016959

28. Freire-de-Lima CG, Nascimento DO, Soares MB, Bozza PT, Castro-Faria-Neto HC, de Mello FG, et al. Uptake of apoptotic cells drives the growth of a pathogenic trypanosome in macrophages. Nature. 2000; 403(6766):199–203. PMID: 10646605.

29. Hideko Tatakihara VL, Cecchini R, Borges CL, Malvezi AD, Graca-de Souza VK, Yamada-Ogatta SF, et al. Effects of cyclooxygenase inhibitors on parasite burden, anemia and oxidative stress in murine Trypanosoma cruzi infection. FEMS immunology and medical microbiology. 2008; 52(1):47–58. PMID: 18031539.

30. Machado FS, Mukherjee S, Weiss LM, Tanowitz HB, Ashton AW. Bioactive lipids in Trypanosoma cruzi infection. Advances in parasitology. 2011; 76:1–31. PMID: 21884885. doi: 10.1016/B978-0-12-385895-5.00001-3

31. Kuroda E, Yamashita U. Mechanisms of enhanced macrophage-mediated prostaglandin E2 production and its suppressive role in Th1 activation in Th2-dominant BALB/c mice. J Immunol. 2003; 170(2):757–64. PMID: 12517938.

32. Roggero E, Perez A, Tamae-Kakazu M, Piazzon I, Nepomnaschy I, Wietzerbin J, et al. Differential susceptibility to acute Trypanosoma cruzi infection in BALB/c and C57BL/6 mice is not associated with a distinct parasite load but cytokine abnormalities. Clinical and experimental immunology. 2002; 128 (3):421–8. PMID: 12067296.

33. Sanoja C, Carbajosa S, Fresno M, Girones N. Analysis of the dynamics of infiltrating CD4(+) T cell subsets in the heart during experimental Trypanosoma cruzi infection. PloS one. 2013; 8(6):e65820. Epub 2013/06/19. doi: 10.1371/journal.pone.0065820 PONE-D-13-02620 [pii]. PMID: 23776551; PubMed Central PMCID: PMC3679147.

34. Iniguez MA, Punzon C, Fresno M. Induction of cyclooxygenase-2 on activated T lymphocytes: regulation of T cell activation by cyclooxygenase-2 inhibitors. J Immunol. 1999; 163(1):111–9. PMID: 10384106.

35. Narumiya S. Prostanoids and inflammation: a new concept arising from receptor knockout mice. Journal of molecular medicine (Berlin, Germany). 2009; 87(10):1015–22. PMID: 19609495.

36. Diaz-Munoz MD, Osma-Garcia IC, Fresno M, Iniguez MA. Involvement of PGE2 and the cAMP signalling pathway in the up-regulation of COX-2 and mPGES-1 expression in LPS-activated macrophages. Biochem J. 2012; 443(2):451–61. Epub 2012/01/25. doi: BJ20111052 [pii] doi: 10.1042/BJ20111052 PMID: 22268508.

37. Piron M, Fisa R, Casamitjana N, Lopez-Chejade P, Puig L, Verges M, et al. Development of a real-time PCR assay for Trypanosoma cruzi detection in blood samples. Acta Trop. 2007; 103(3):195–200. PMID: 17662227.

38. Schmittgen TD, Livak KJ. Analyzing real-time PCR data by the comparative C(T) method. Nat Protoc. 2008; 3(6):1101–8. Epub 2008/06/13. PMID: 18546601.

39. Schindelin J, Arganda-Carreras I, Frise E, Kaynig V, Longair M, Pietzsch T, et al. Fiji: an open-source platform for biological-image analysis. Nature methods. 2012; 9(7):676–82. PMID: 22743772. doi: 10.1038/nmeth.2019

40. Girones N, Carbajosa S, Guerrero NA, Poveda C, Chillon-Marinas C, Fresno M. Global Metabolomic Profiling of Acute Myocarditis Caused by Trypanosoma cruzi Infection. PLoS Negl Trop Dis. 2014; 8 (11):e3337. Epub 2014/11/21. doi: 10.1371/journal.pntd.0003337 PNTD-D-14-01266 [pii]. PMID: 25412247.

41. Sola J, Godessart N, Vila L, Puig L, de Moragas JM. Epidermal cell-polymorphonuclear leukocyte cooperation in the formation of leukotriene B4 by transcellular biosynthesis. J Invest Dermatol. 1992; 98 (3):333–9. Epub 1992/03/01. PMID: 1312107.

42. Murray PJ, Wynn TA. Protective and pathogenic functions of macrophage subsets. Nature reviews. 2011; 11(11):723–37. PMID: 21997792. doi: 10.1038/nri3073

43. Wynn TA, Barron L. Macrophages: master regulators of inflammation and fibrosis. Seminars in liver disease. 2010; 30(3):245–57. PMID: 20665377. doi: 10.1055/s-0030-1255354

44. Arnold L, Henry A, Poron F, Baba-Amer Y, van Rooijen N, Plonquet A, et al. Inflammatory monocytes recruited after skeletal muscle injury switch into antiinflammatory macrophages to support myogenesis. The Journal of experimental medicine. 2007; 204(5):1057–69. PMID: 17485518.

45. Corral RS, Guerrero NA, Cuervo H, Girones N, Fresno M. Trypanosoma cruzi Infection and Endothelin-1 Cooperatively Activate Pathogenic Inflammatory Pathways in Cardiomyocytes. PLoS Negl Trop Dis. 2013; 7(2):e2034. PMID: 23409199. doi: 10.1371/journal.pntd.0002034

46. Cheng Y, Austin SC, Rocca B, Koller BH, Coffman TM, Grosser T, et al. Role of prostacyclin in the cardiovascular response to thromboxane A2. Science (New York, NY. 2002; 296(5567):539–41. PMID: 11964481.

47. Caughey GE, Pouliot M, Cleland LG, James MJ. Regulation of tumor necrosis factor-alpha and IL-1 beta synthesis by thromboxane A2 in nonadherent human monocytes. J Immunol. 1997; 158(1):351–8. PMID: 8977210.

48. Bellows CF, Alder A, Wludyka P, Jaffe BM. Modulation of macrophage nitric oxide production by prostaglandin D2. The Journal of surgical research. 2006; 132(1):92–7. PMID: 16289592.

49. Kanaoka Y, Urade Y. Hematopoietic prostaglandin D synthase. Prostaglandins, leukotrienes, and essential fatty acids. 2003; 69(2–3):163–7. PMID: 12895599.

50. Rajakariar R, Hilliard M, Lawrence T, Trivedi S, Colville-Nash P, Bellingan G, et al. Hematopoietic prostaglandin D2 synthase controls the onset and resolution of acute inflammation through PGD2 and 15-deoxyDelta12 14 PGJ2. Proceedings of the National Academy of Sciences of the United States of America. 2007; 104(52):20979–84. doi: 10.1073/pnas.0707394104 PMID: 18077391; PubMed Central PMCID: PMC2409252.

51. Schror K. Pharmacology and cellular/molecular mechanisms of action of aspirin and non-aspirin NSAIDs in colorectal cancer. Best Pract Res Clin Gastroenterol. 2011; 25(4–5):473–84. Epub 2011/11/30. doi: 10.1016/j.bpg.2011.10.016 S1521-6918(11)00104-1 [pii]. PMID: 22122764.

52. Iniguez MA, Punzon C, Cacheiro-Llaguno C, Diaz-Munoz MD, Duque J, Cuberes R, et al. Cyclooxygenase-independent inhibitory effects on T cell activation of novel 4,5-dihydro-3 trifluoromethyl pyrazole cyclooxygenase-2 inhibitors. Int Immunopharmacol. 2010; 10(10):1295–304. Epub 2010/08/17. doi: 10.1016/j.intimp.2010.07.013 S1567-5769(10)00240-7 [pii]. PMID: 20709632.

53. Xu H, Izon DJ, Loftin C, Spain LM. The COX-2 inhibitor NS-398 causes T-cell developmental disruptions independent of COX-2 enzyme inhibition. Cell Immunol. 2001; 214(2):184–93. Epub 2002/06/29. doi: S0008-8749(01)91891-X [pii] doi: 10.1006/cimm.2001.1891 PMID: 12088417.

54. Holscher C, Kohler G, Muller U, Mossmann H, Schaub GA, Brombacher F. Defective nitric oxide effector functions lead to extreme susceptibility of Trypanosoma cruzi-infected mice deficient in gamma interferon receptor or inducible nitric oxide synthase. Infect Immun. 1998; 66(3):1208–15. PMID: 9488415; PubMed Central PMCID: PMC108035.

55. Ejima K, Layne MD, Carvajal IM, Kritek PA, Baron RM, Chen YH, et al. Cyclooxygenase-2-deficient mice are resistant to endotoxin-induced inflammation and death. Faseb J. 2003; 17(10):1325–7. PMID: 12738799.

56. Paiva CN, Figueiredo RT, Kroll-Palhares K, Silva AA, Silverio JC, Gibaldi D, et al. CCL2/MCP-1 controls parasite burden, cell infiltration, and mononuclear activation during acute Trypanosoma cruzi infection. Journal of leukocyte biology. 2009; 86(5):1239–46. PMID: 19641038. doi: 10.1189/jlb.0309187

57. Borges CL, Cecchini R, Tatakihara VL, Malvezi AD, Yamada-Ogatta SF, Rizzo LV, et al. 5-Lipoxygenase plays a role in the control of parasite burden and contributes to oxidative damage of erythrocytes in murine Chagas' disease. Immunol Lett. 2009; 123(1):38–45. doi: 10.1016/j.imlet.2009.02.002 PMID: 19428550.

58. Pavanelli WR, Gutierrez FR, Mariano FS, Prado CM, Ferreira BR, Teixeira MM, et al. 5-lipoxygenase is a key determinant of acute myocardial inflammation and mortality during Trypanosoma cruzi infection. Microbes Infect. 2010; 12(8–9):587–97. doi: 10.1016/j.micinf.2010.03.016 PMID: 20381637.

59. Panis C, Mazzuco TL, Costa CZ, Victorino VJ, Tatakihara VL, Yamauchi LM, et al. Trypanosoma cruzi: effect of the absence of 5-lipoxygenase (5-LO)-derived leukotrienes on levels of cytokines, nitric oxide and iNOS expression in cardiac tissue in the acute phase of infection in mice. Experimental parasitology. 2011; 127(1):58–65. doi: 10.1016/j.exppara.2010.06.030 PMID: 20599987.

Acta Tropica 157 (2016) 145–150

Contents lists available at ScienceDirect

Acta Tropica

journal homepage: www.elsevier.com/locate/actatropica

Prevalence of *Trypanosoma cruzi*'s Discrete Typing Units in a cohort of Latin American migrants in Spain

Angela Martinez-Perez[a,1], Cristina Poveda[b,1], Juan David Ramírez[c], Francesca Norman[a], Núria Gironés[b], Felipe Guhl[d], Begoña Monge-Maillo[a], Manuel Fresno[b], Rogelio López-Vélez[a,*]

[a] National Referral Unit for Tropical Diseases, Infectious Diseases Department, Ramón y Cajal University Hospital, IRICYS, Madrid, Spain
[b] Centro de Biología Molecular Severo Ochoa, CSIC-UAM, Madrid, Spain
[c] Grupo de Investigaciones Microbiológicas—UR (GIMUR), Facultad de Ciencias Naturales y Matemáticas, Universidad del Rosario, Bogotá, Colombia
[d] Centro de Investigaciones en Microbiología y Parasitología Tropical, CIMPAT, Universidad de los Andes, Cra 1 No. 18A-10, Bogotá, Colombia

ARTICLE INFO

Article history:
Received 5 May 2015
Received in revised form
27 November 2015
Accepted 31 January 2016
Available online 2 February 2016

Keywords:
Chagas disease
Trypanosoma cruzi
Migration
Discrete Typing Units
Genome

ABSTRACT

Chagas disease is caused by the protozoan *Trypanosoma cruzi*. This is an endemic disease in the Americas, but increased migration to Europe has made it emerge in countries where it was previously unknown, being Spain the second non endemic country in number of patients. *T. cruzi* is a parasite with a wide genetic diversity, which has been grouped by consensus into 6 Discrete Typing Units (DTUs) affecting humans. Some authors have linked these DTUs either to a specific epidemiological context or to the different clinical presentations. Our main objective was to describe the *T. cruzi* DTUs identified from a population of chronically infected Latin American migrants attending a reference clinic in Madrid. 149 patients meeting this condition were selected for the study. Molecular characterization was performed by an algorithm that combines PCR of the intergenic region of the mini exon-gene, the 24Sα and 18S regions of rDNA and the variable region of the satellite DNA. A descriptive analysis was performed and associations between geographical/clinical data and the different DTUs were tested. DTUs could be determined in 105 out of 149 patients, 93.3% were from Bolivia, 67.7% were women and median age was 35 years (IQR 29–44). The most common DTU found was TcV (58; 55.2%), followed by TcIV (17; 16.2%), TcII (10; 9.5%) and TcI (4; 3.8%). TcIII and TcVI were not identified from any patient, and 15.2% patients presented mixed infections. In addition, we determined DTUs after treatment in a subset of patients. In 57% patients had different DTUs before and after treatment. DTUs distribution from this study indicates active transmission of *T. cruzi* is occurring in Bolivia, in both domestic and sylvatic cycles. TcIV was confirmed as a cause of chronic human disease. The current results indicate no correlation between DTU and any specific clinical presentation associated with Chagas disease, nor with geographical origin. Treatment with benznidazole does not always clear *T. cruzi's* genetic material from blood, and DTUs detected in the same patient may vary over time indicating that polyparasitism is frequent.

1. Introduction

Trypanosoma cruzi is a protozoan parasite transmitted by many species of triatomine vectors which can infect over 70 different genera of mammalian hosts. Chagas disease is the name given to the human infection, which can produce cardiac and/or digestive disorders in up to 30% of infected individuals. This disease is endemic in Latin America, where up to 8–9 million people are thought to be infected and between 25 to 90 million are at risk of acquiring the disease according to the Pan American Health Organization (2008). Increased migration has made Chagas disease emerge in areas where it was previously not known, with Spain having the largest number of imported cases after the United States (Schmunis and Yadon, 2010).

T. cruzi presents great genetic diversity and is classified by consensus into six Discrete Typing Units (DTUs) named TcI to TcVI (Zingales, 2009). The relevance of *T. cruzi* genetic diversity in Chagas disease should be examined further but existing evidence supports the importance of this diversity in terms of epiology and its association with clinical presentation and outcomes.

* Corresponding author at: National Referral Centre for Tropical Diseases, Infectious Diseases Department, Ramón y Cajal University Hospital, IRICYS, Ctra Colmenar, Km 9,100, 28034 Madrid, Spain.
E-mail address: rogelio.lopezvelez@salud.madrid.org (R. López-Vélez).
[1] Equal contribution.

http://dx.doi.org/10.1016/j.actatropica.2016.01.032
0001-706X/

Different DTUs are associated with different biological cycles of transmission and seem to have varying geographical distributions (Zingales et al., 2012). TcI, the most frequent and widely distributed DTU, has been found from the South of the US to the North of Chile and Argentina, and can be transmitted both in sylvatic and domestic cycles. TcIII and TcIV have been more frequently associated with sylvatic cycles, and have been implicated as a cause of acute outbreaks in the Amazon basin (Marcili et al., 2009b; Monteiro et al., 2012). TcIII has also been found in armadillos (Yeo et al., 2005), although it has been identified from domestic dogs as well (Cardinal et al., 2008), and associated to the terrestrial niche even in the Chaco region (Llewellyn et al., 2009; Marcili et al., 2009a). While TcIV seemed to have an arboreal ecotope (Cardinal et al., 2008) and is the second most frequent DTU detected in Venezuela (Carrasco et al., 2012). TcII, TcV and TcVI have been more often associated with domestic cycles in the Southern Cone countries (Zingales et al., 2012). However, the majority of these data have been obtained from *T. cruzi* parasites cultured in laboratory media, which may alter the composition of *T. cruzi* populations by eliminating or reducing some near-clades of the parasite (Deane et al., 1984; Venegas et al., 2013).

Some authors have identified a differential tissue tropism among these DTUs and linked some of them to specific clinical presentations. For instance, TcI has been associated with cardiac disease in Colombia, Argentina, Venezuela and Brazil (Burgos et al., 2010; Miles et al., 1981; Ramírez et al., 2010); TcII, TcV and TcVI can cause both cardiac and digestive disease, even causing megasyndromes. In addition, *T. cruzi's* genetic diversity seems to confer different drug susceptibility both "in vitro" (Moraes et al., 2014; Zingales et al., 2014), although this does not seem to influence the clinical outcome (Moreno et al., 2010), and "in vivo" (Teston et al., 2013).

The aim of this study was to identify the *T. cruzi* near-clades from a population of chronically infected Latin American migrant patients, and to describe their association with geographical origin and specific clinical manifestations. In addition the persistence and temporal variation of these DTUs after treatment were investigated.

2. Methods

2.1. Population and selection criteria

Participation in the study was offered to Latin American migrants attending the Tropical Medicine Referral Centre of the Ramon y Cajal Hospital (Madrid, Spain) between January 2009 and February 2011. Adult patients diagnosed with chronic *T. cruzi* infection who were willing to attend follow up visits and were able to understand and sign informed consent were selected. Exclusion criteria were: acute infection (discarded in recently arrived subjects by clinical findings and direct parasitological methods), age below 18 years and refusal to sign informed consent.

Diagnosis was established by two positive serological tests: an in-house IFAT and an ELISA (ARCHITECT Chagas ELISA test. BiosChile, Abbott lab. Wiesbaden, Germany). The in-house IFAT was prepared with a combination of cultured epimastigote antigens (Mc, T and Dm28), using a human IgG from bioMérieux® as a marker. EDTA tubes were used for collection and transport and samples were stored at −80 °C.

The study was approved by the Ramón y Cajal Hospital Ethics committee.

2.2. T. cruzi *molecular detection and molecular characterization*

Double blind molecular characterization was performed at the CIMPAT laboratory in Bogotá (Colombia) using an algorithm, as previously reported (Ramírez et al., 2010). The algorithm combines PCR of the intergenic region of the mini exon-gene, the 24Sα and 18S regions of rDNA and the variable region of the satellite DNA as described. Molecular markers include the intergenic region of the non-transcribed mini-exon gene using primers TCC (5′CCC CCCCCC TCC CAG GCC ACA CTG3′), TC1 (5′GTG TCC GCC ACC TCC TTCGGG CC3′) and TC2 (5′CCT GCA GGC ACA CGT GTG TGT G 3′). All mini-exon gene PCR assays were performed using two primers instead of a multiplex PCR assay to determine the presence of mixed infections. Thus, PCR reactions were set separately using TCC-TC1 and TCC-TC2 primers. In order to increase the number of genotyping assays, in some cases PCRs were performed 3 times in triplicate. We used segments containing the variable domain D7 of the rDNA 24Sα subunit using D75 (5′GCAGATCTTGGTTGGCGTAG3′) and D76 (5′GGTTCTCTGTTGCCCCTTTT3′), and the A10 with primers pr1 (5′CCGCTAAGCAGTTCTGTCCATA3′) and pr3 (5′GCTTTATTACCCCATGCCACAG3′) (Burgos et al., 2007). The reference strains used to compare size of amplified fragments were: TcI: Silvio X10, TcII: ESM, TcIII: Arma, TcIV: CanIII, TcV: Bug and, TcVI: Cl Brener.

2.3. Statistical analysis

Qualitative variables were expressed as total number of observations and relative frequencies, and were analyzed with the χ^2 and Fisher exact tests. Quantitative variables were expressed as medians and interquartile ranges (IQR), or mean and standard deviations if they were normal. Unpaired Student's *t*-test or Wilcoxon test were used for associations of quantitative data. Associations were tested between demographic characteristics and clinical data, and the different DTUs among those patients in whom a DTU could be determined. Age, gender, geographical origin, serological titres and presence of specific visceral involvement during a three year follow-up period were analyzed. Additionally, DTU determination was repeated after treatment in 19 cases.

2.4. Description of visceral involvement

Every patient had a 12-lead electrocardiogram (ECG) and echocardiogram performed at baseline. Other examinations (cardiac Holter, cardiac MRI, oesophageal manometry or barium enema) were requested if clinical symptoms were present or according to the results found in the baseline examinations. Cardiac involvement was considered to be present when at least one of the following was found: left or right bundle branch block, left anterior fascicular block, left posterior fascicular block, any degree of atrioventricular block, sinus bradycardia, primary ST-T changes, abnormal q waves, atrial fibrillation, ventricular arrhythmias, reduced global left ventricular function or evidence of regional wall motion abnormality. Digestive involvement was diagnosed when at least one of the following was present: loss of peristaltic activity of the esophagus, synchronic waves and failure or incomplete aperture of the lower esophageal sphincter with ingestion, low amplitude waves; decreased bowel haustrae or a dilated, atonic colon.

3. Results

3.1. Overall demographic data and geographical distribution

One hundred and forty-nine consecutive patients were selected for the study, 101 (67.7%) were women and median age was 35 years (IQR 29–44). Median time living in Spain was 5 years (IQR 3–5). DTUs could be determined in 105 patients (70.4%), 70 were women (66.6%) and median age was 36 years (IQR 29–45). Overall, the most common DTU found was TcV (58; 55.2%), followed by TcIV (17; 16.2%), TcII (10; 9.5%) and TcI (4; 3.8%). Additionally, 16

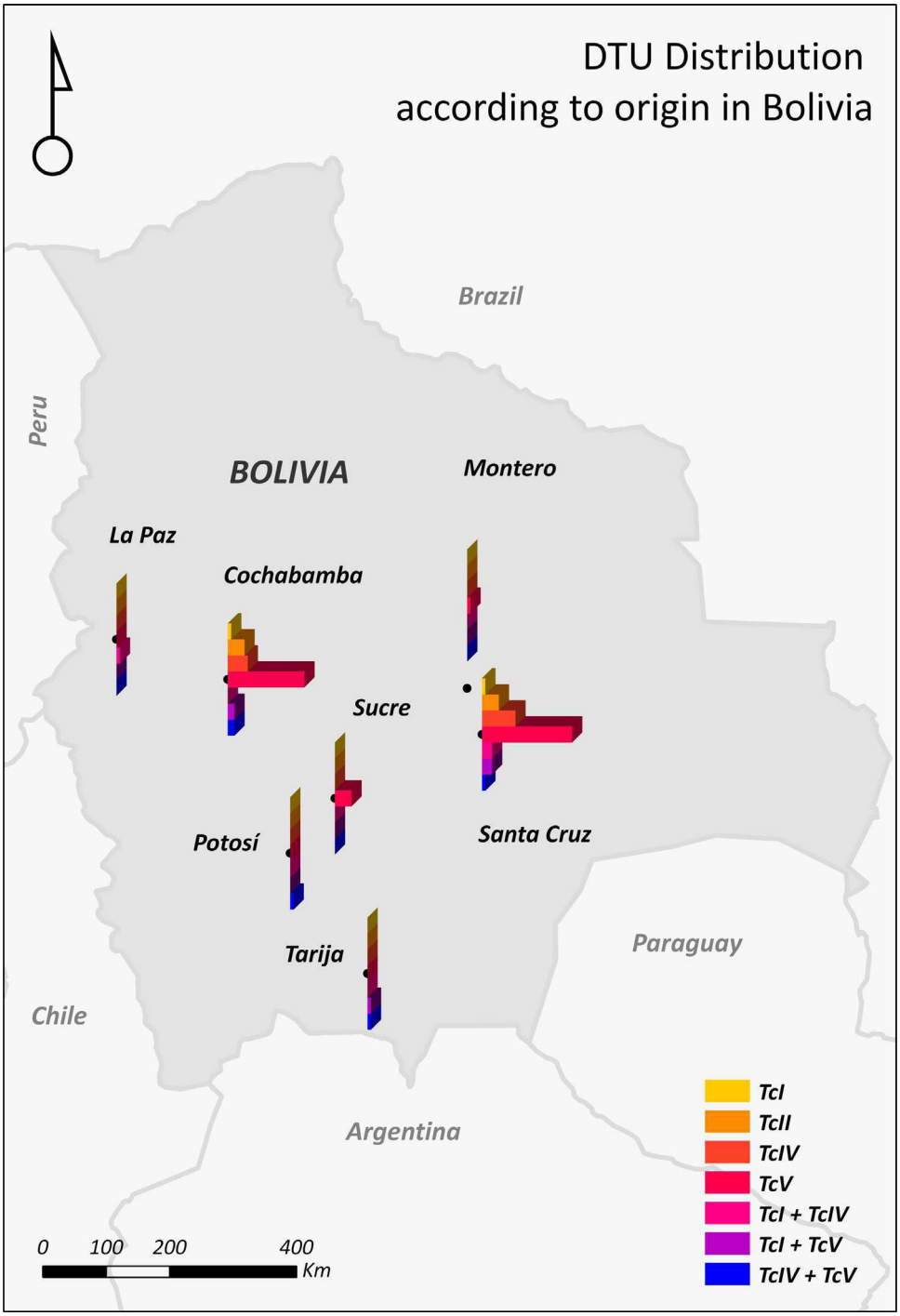

Fig. 1. Distribution of Discrete Tying Units according to patients' geographical origin in Bolivia.

Table 1
Baseline characteristics of patients in whom DTU was determined.

DTU	Number of patients (%)	Mean Age (SD)	Female n(%)	ELISA Mean (SD)	IFAT Mean (SD)	Visceral involvement N (%)
TcI	4(3.8%)	37.2(8.73)	2(50%)	2.14(.17)	130(60)	4(100%)
TcII	10(9.5%)	37.3(12.78)	6(60%)	2.33(.21)	195.55(70.5)	3(30%)
TcIV	17(16.2%)	35.5(9.27)	8(47%)	2.39(.29)	176.47(76.2)	7(41.1%)
TcV	58(55.2%)	36.8(9.16)	43(74.14%)	2.34(.29)	181.42(63.8)	15(25.8%)
TcI + TcIV	4(3.8%)	35.7(6.29)	4(100%)	2.36(.27)	160(113.1)	1(25%)
TcI + TcV	7(6.6%)	38.7(10.32)	4(57.14%)	2.22(.29)	194.28(90.7)	3(42.8%)
TcIV + TcV	5(4.7%)	37(12.28)	3(60%)	2.5(0)	224(87.6)	1(20%)
Total	105(100%)	36.8(9.44)	70(66.66%)	2.34(.28)	181.9(71.1)	34(32.3%)

DTU: Discrete Typing Unit. SD: standard deviation. ELISA: enzyme-linked immunosorbent assay. IFAT: immuno fluorescent antibody test.

(15.2%) patients presented mixed infections, namely with TcI + TcV (7; 6.6%), TcIV + TcV (5; 4.7%) or TcI + TcIV (4; 3.8%). No TcIII or TcVI were found in our samples.

Most of the patients who had their DTU determined came from Bolivia (98; 93.3%), one came from Paraguay and another came from Ecuador. No geographical origin was reported in 5 patients. The distribution of DTUs according to geographical origin in Bolivia is shown in Fig. 1. The geographical origin is the one reported by the patients as either their place of birth or the place where they spent most of their lives before coming to Spain (at least five years of residency were considered). When DTU types were analyzed according to geographical origin, no statistically significant differences were observed (p = 0.266).

3.2. Clinical signs and visceral involvement

Among the 105 patients whose DTU could be determined, 53 (50.5%) referred symptoms suggestive of Chagas disease. The tests performed confirmed visceral involvement in 34 (32.3%): 28 had cardiac involvement [16 (10.73%) had ECG abnormalities, 17 (16.3%) had cardiac ultrasound abnormalities, no Holter or cardiac MRI abnormalities were described]; 5 had digestive involvement [3 out of 56 (5.3%) had oesophageal disease detected by manometry, and 2 out of 17 (11.7%) had an abnormal barium enema] and 1 had both cardiac and digestive involvement. Some patients presented more than one abnormality. Despite this, no association was found between a particular DTU and the presence of symptoms or visceral involvement (p = 0.998 and p = 0.101, respectively), or between DTU and the type of visceral involvement (cardiac or digestive). DTU distribution and associated demographic and clinical characteristics are listed in Table 1.

3.3. Serum titration and correlation with molecular characterization of T. cruzi infection

The mean ELISA titres were 2.34 (SD 0.28), while mean IFAT titres were 181.9 (SD 71.1). No statistically significant correlation was found between the IFAT or ELISA titres and DTUs (p = 0.641 and p = 0.941, respectively). These serum titres remained stable during a three year follow up period both in treated and untreated patients. DTU distribution and associated ELISA and IFAT titres are listed in Table 1.

3.4. Molecular characterization of T. cruzi before and after treatment

A subset of 19 patients had a second DTU determination performed once they had completed treatment (the median time until the second determination was 3 months). Details on specific DTU determined before and after therapy are listed in Table 2. Patients were treated with standard anti-parasitic therapy with benznidazole 5 mg/kg for 60 days, although one patient (patient 11) presented an adverse reaction and therapy was changed to nifurtimox 10 mg/kg for 90 days.

For one patient, no DTU could be detected before treatment (patient 15) and in another 4 (patients 16, 17, 18, 19) no DTU could be detected after treatment. In the remaining 14 (77.7%) a DTU was determined before and after treatment. In 4 out of these 14 cases (28.6%) the DTU found after the treatment was the same as the one found previously. There were 2 cases of mixed infections, where one of the DTUs remained after treatment while the other apparently cleared from peripheral blood. The other 8 (57%) patients had different DTUs before and after treatment.

Table 2
Discrete Typing Units variability before and after treatment.

Patient number	DTU Before treatment[a]	DTU After treatment
1	V	I
2	V	II
3	V	II
4	V	III
5	V	IV
6	I + IV	IV
7	V	IV
8	IV	V
9	V	V
10	V	V
11	I + V	V
12	V	V
13	V	V
14	IV	V
15	ND	IV
16	V	ND
17	IV	ND
18	V	ND
19	V	ND

DTU: Discrete Typing Unit. ND: not detected.
[a] Benznidazole 5 mg/kg for 60 days, or nifurtimox 10 mg/kg for 90 days in patient 11.

4. Discussion

Advances in the field of *T. cruzi* genetic diversity include a recent consensus to standardize the diverse results found in different settings (Zingales, 2009). However, different algorithms and characterization techniques are in use and their development is ongoing, which add complexity to the interpretation of findings. In addition, fluctuant parasitemia and suspected differential tissue tropisms make it difficult to establish clear associations between DTU type and clinical manifestations.

To the authorsí knowledge this is the largest study performing DTU characterization in human patients outside endemic areas (where re-infection does not occur). In addition, visceral involvement was fully described. A limitation of this study is that the mode of infection could not be fully determined. Nevertheless, most patients probably acquired the infection through vectorial transmission, and secondary through congenital transmission.

Our group published a previous study presenting epidemiological data on *T. cruzi*'s DTUs obtained from 33 patients (Perez-Molina et al., 2014). The current study presents the results of other larger set of patients for whom this determination was made and our current sample size allowed us to test statistical associations between DTU type and visceral involvement. In the current study, a mean of 4 years follow-up has passed, allowing for a broader clinical evaluation including early visceral involvement. In addition, this follow up period allowed us to take a second sample for DTU identification in patients who had fulfilled complete treatment.

T. cruzi's DNA was characterized in 105 out of 149 patients, a high sensitivity not reached in previous studies, probably because PCRs were performed 3 times in triplicate. This was done in purpose to increase the detection rate of DNA in samples. In addition, the youngest the patient the commonest it is to have a detectable parasitemia, and mean age in our population was 35 years old. The most common DTUs detected in our samples were, in order of frequency, TcV, TcIV, TcII and TcI, as well as many mixed infections. DTU distribution and the presence of mixed infections confirms previous findings from our group among Bolivian patients (Perez-Molina et al., 2014). In this work, our bigger sample size and a regular follow up with exhaustive clinical examination allowed us to detect any visceral involvement and to relate it to the DTUs identified. No correlation was observed between these DTUs and the specific geo-

graphical origin of the patients, nor the presence of specific visceral involvement.

In this study, TcV was confirmed to be the main cause of human infection and disease among Bolivians, what is concordant with previous works from Brenière et al. where this DTU was named clonet 39 (Breniere et al., 1998, 1989). However, we have detected a number of Bolivian patients with TcII and TcIV, indicating more heterogeneity than previously reported in Bolivia. This might be because the probes used for DNA characterization in previous studies among humans excluded TcIII and TcIV DTUs as these were considered to be sylvatic, (del Puerto et al., 2010) or had a very small sample size (Barnabé et al., 2011). TcIV had been previously associated with acute oral outbreaks in tropical areas (Monteiro et al., 2012; Ramirez et al., 2013), and has been described as the second most common DTU in human samples from Venezuela and the fourth most frequent in human samples from Colombia (Carrasco et al., 2012; Ramírez et al., 2010). The current results confirm that this DTU is also an important cause of chronic Chagas disease with visceral involvement (5 had cardiac involvement and 2 had digestive involvement) in Bolivian patients as for Colombians (Ramírez et al., 2010), and therefore should be considered as a preferent strain to be tested in future drug development, according to recent expert claims on other DTUs (Zingales et al., 2014). TcII, which has been rarely reported in Bolivia, was found in less than 10% of our patients as expected, while it has been reported as a the more common DTU in Venezuela and Colombia (Carrasco et al., 2012; Ramírez et al., 2010; Ramirez et al., 2013). TcI has previously been reported as a major cause of infection in Bolivia and our data confirm TcI as a cause of chronic human infection, although it is less frequent. Nevertheless, it is worth noting that all 4 patients who were infected with TcI had visceral involvement. TcIII was not found in our sample population, although beings mainly transmitted in sylvatic cycles of *T. cruzi* (Brenière et al., 2012; Zingales et al., 2012), has been also found in domestic *Triatoma infestans* from Bolivia (Perez et al., 2012). TcVI has rarely been found outside the Gran Chaco region. Our findings are concordant with DTUs found in vectors and reservoirs in the same areas, except for the absence of TcIII in our samples.

Another important finding was the high proportion of mixed infections (up to 15.2% of the baseline determinations), what was similar to the one found in a previous work by our group (Perez-Molina et al., 2014) and concordant with other authors' findings in Latin America (Cura et al., 2012). A previous study in the Bolivian Gran Chaco region found mixed infections in up to 13% of the *T. infestans* vectors examined (Perez et al., 2013). Mixed infections have also been detected in other vectors and reservoirs in the American region (Noireau et al., 2009; Ramirez et al., 2012).

Since most of our patients were Bolivian (93.3%), the DTU distribution and the presence of mixed infections observed in this study could be representative of *T. cruzi's* epidemiology only in this endemic area. The lack of correlation between DTU and specific geographical origin might be due to the fact that patients reported the place where they lived mainly before migrating. Cities known to receive internal migration are overrepresented in our sample, and probably do not reflect the areas where the infection was most likely acquired considering that most infections are due to vectorial transmission. In addition, congenital transmission is also frequent in Bolivia, allowing the spread of any DTU to urban areas.

Although some authors have identified differential tissue tropism for different DTUs (Burgos et al., 2010; del Puerto et al., 2010; Ramírez et al., 2010) we found no correlation between DTU and specific visceral involvement, in accordance with other published studies (Poveda et al., 2014; Zafra et al., 2011). This might be because the number of certain DTUs detected in samples was too low to achieve statistical significance.

Treatment with Benznidazole 5 mg/kg for 60 days did not clear *T. cruzi* genetic material from blood samples, and this has also been reported by other authors (Murcia et al., 2010), although the significance of this finding with respect to parasite clearance is unclear. The presence of *T. cruzi's* genetic material in blood suggests either failure to treatment or maybe the presence of DNA fragments able to hybridize. DTU I, II, III, IV and V were all detected after treatment, while only TcIII was not identified prior to treatment. Some authors have shown, by means of a qualitative PCR assay that *T. cruzi's* genetic material can appear in blood up to 420 days after correct treatment (Murcia et al., 2010), what in a clinical setting translates failure to treatment. In our work we detected parasite DNA in 14 out of 19 patients who had received treatment, we also identified different *T. cruzi's* near clades before and after treatment.

Up to 22.9% (24/105) of patients had polyparasitism: 16 mixed infections were detected before treatment was administered and another 8 patients out of 14 who had a second DTU determination after treatment presented a DTU that was different from the previous one. As mentioned above, a different DTU was found after treatment in 8 cases. Cryptic mixed infections and heterogeneous drug response might be responsible for this finding. *T. cruzi* is believed to present intermittent parasitemia in the host, a recent study showed that diverse DTUs can be detected from a single individual at a different time point in the absence of treatment (Sanchez et al., 2013); In addition, strains and clones tested in vitro have shown differential response to nitrohetercyclic compounds as the ones used in our clinical practice (Moraes et al., 2014). Therefore, mixed infections in Chagas diseases is a natural phenomenon and could be more frequent than expected (Perez et al., 2014). Assuming that mixed infections are the natural process, the correlation of DTUs with visceral involvement would be confusing. Anyway, this phenomenon has to be confirmed and its implications in clinical management clarified.

In conclusion, the DTU distribution found in this study may be indicative of where active transmission of *T. cruzi*, in both domestic and sylvatic cycles, is occurring in Bolivia. TcIV was confirmed as a cause of chronic human disease. Some experts believe research efforts should be focused on developing new drugs only against those DTUs known to cause human disease (Zingales et al., 2014), but our results indicate any DTU may be transmitted to humans and cause visceral involvement. The current results appear to indicate there is no significant correlation between DTU and any specific clinical presentation associated with Chagas disease. In order to identify temporal changes before disease appears, field studies following patients in the indeterminate stage of the disease should be performed, but this way of procedure is difficult as once an infected patient is detected the antiparasitic treatment follows and the natural course of the disease is broken. Treatment with benznidazole does not always clear *T. cruzi's* genetic material from blood as this may be detected up to three months after completing treatment, what suggests either failure to treatment or maybe the presence of DNA fragments able to hybridize. Finally, DTUs detected in the same patient may vary over time indicating that polyparasitism is frequent.

Acknowledgements

This study has been supported by the Spanish Collaborative Network for Research in Tropical Diseases (VI PN de I+D +I 2008–2011, ISCIII—Subdirección General de Redes y Centros de Investigación Cooperativa, expediente RD12/0018/0019).

We would like to thank Jesús Garrido Rubio from the Institute for Regional Development, University of Castilla-La Mancha, for his help with figure editing.

References

Barnabé, C., De MeeÛs, T., Noireau, F., Bosseno, M.-F., Monje, E.M., Renaud, F., Brenière, S.F., 2011. *Trypanosoma cruzi* discrete typing units (DTUs): microsatellite loci and population genetics of DTUs TcV and TcI in Bolivia and Peru. Infect. Genet. Evol. 11 (7), 1752–1760.

Brenière, S.F., Aliaga, C., Waleckx, E., Buitrago, R., Salas, R., Barnabé, C., Tibayrenc, M., Noireau, F., 2012. Genetic characterization of *Trypanosoma cruzi* DTUs in wild triatoma infestans from Bolivia: predominance of TcI. PLoS Negl. Trop. Dis. 6 (5), e1650.

Breniere, S.F., Carrasco, R., Revollo, S., Aparicio, G., Desjeux, P., Tibayrenc, M., 1989. Chagas' disease in Bolivia: clinical and epidemiological features and zymodeme variability of *Trypanosoma cruzi* strains isolated from patients. Am. J. Trop. Med. Hyg. 41 (5), 521–529.

Breniere, S.F., Bosseno, M.F., Telleria, J., Bastrenta, B., Yacsik, N., Noireau, F., Alcazar, J.L., Barnabe, C., Wincker, P., Tibayrenc, M., 1998. Different behavior of two *Trypanosoma cruzi* major clones: transmission and circulation in young Bolivian patients. Exp. Parasitol. 89 (3), 285–295.

Burgos, J.M., Altcheh, J., Bisio, M., Duffy, T., Valadares, H.M., Seidenstein, M.E., Piccinali, R., Freitas, J.M., Levin, M.J., Macchi, L., Macedo, A.M., Freilij, H., Schijman, A.G., 2007. Direct molecular profiling of minicircle signatures and lineages of *Trypanosoma cruzi* bloodstream populations causing congenital Chagas disease. Int. J. Parasitol. 37 (12), 1319–1327.

Burgos, J.M., Diez, M., Vigliano, C., Bisio, M., Risso, M., Duffy, T., Cura, C., Brusses, B., Favaloro, L., Leguizamon, M.S., Lucero, R.H., Laguens, R., Levin, M.J., Favaloro, R., Schijman, A.G., 2010. Molecular identification of *Trypanosoma cruzi* discrete typing units in end-stage chronic Chagas heart disease and reactivation after heart transplantation. Clin. Infect. Dis. 51 (5), 485–495.

Cardinal, M.V., Lauricella, M.A., Ceballos, L.A., Lanati, L., Marcet, P.L., Levin, M.J., Kitron, U., Gurtler, R.E., Schijman, A.G., 2008. Molecular epidemiology of domestic and sylvatic *Trypanosoma cruzi* infection in rural northwestern Argentina. Int. J. Parasitol. 38 (13), 1533–1543.

Carrasco, H.J., Segovia, M., Llewellyn, M.S., Morocoima, A., Urdaneta-Morales, S., Martínez, C., Martínez, C.E., Garcia, C., Rodríguez, M., Espinosa, R., de Noya, B.A., Díaz-Bello, Z., Herrera, L., Fitzpatrick, S., Yeo, M., Miles, M.A., Feliciangeli, M.D., 2012. Geographical distribution of *Trypanosoma cruzi* genotypes in Venezuela. PLoS Negl. Trop. Dis. 6 (6), e1707.

Cura, C.I., Lucero, R.H., Bisio, M., Oshiro, E., Formichelli, L.B., Burgos, J.M., Lejona, S., BrusÉS, B.L., HernÁNdez, D.O., Severini, G.V., Velazquez, E., Duffy, T., Anchart, E., Lattes, R., Altcheh, J., Freilij, H., Diez, M., Nagel, C., Vigliano, C., Favaloro, L., Favaloro, R.R., Merino, D.E., Sosa-Estani, S., Schijman, A.G., 2012. *Trypanosoma cruzi* Discrete Typing Units in Chagas disease patients from endemic and non-endemic regions of Argentina. Parasitology 139 (4), 516–521.

Deane, M.P., Sousa, M.A., Pereira, N.M., Goncalves, A.M., Momen, H., Morel, C.M., 1984. *Trypanosoma cruzi*: inoculation schedules and re-isolation methods select individual strains from doubly infected mice, as demonstrated by schizodeme and zymodeme analyses. J. Protozool. 31 (2), 276–280.

del Puerto, R., Nishizawa, J.E., Kikuchi, M., Iihoshi, N., Roca, Y., Avilas, C., Gianella, A., Lora, J., Gutierrez Velarde, F.U., Renjel, L.A., Miura, S., Higo, H., Komiya, N., Maemura, K., Hirayama, K., 2010. Lineage analysis of circulating *Trypanosoma cruzi* parasites and their association with clinical forms of Chagas disease in Bolivia. PLoS Negl. Trop. Dis. 4 (5), e687.

Llewellyn, M.S., Lewis, M.D., Acosta, N., Yeo, M., Carrasco, H.J., Segovia, M., Vargas, J., Torrico, F., Miles, M.A., Gaunt, M.W., 2009. *Trypanosoma cruzi* IIc: phylogenetic and phylogeographic insights from sequence and microsatellite analysis and potential impact on emergent Chagas disease. PLoS Negl. Trop. Dis. 3 (9), e510.

Marcili, A., Lima, L., Valente, V.C., Valente, S.A., Batista, J.S., Junqueira, A.C., Souza, A.I., da Rosa, J.A., Campaner, M., Lewis, M.D., Llewellyn, M.S., Miles, M.A., Teixeira, M.M., 2009a. Comparative phylogeography of *Trypanosoma cruzi* TCIIc: new hosts, association with terrestrial ecotopes, and spatial clustering. Infect. Genet. Evol. 9 (6), 1265–1274.

Marcili, A., Valente, V.C., Valente, S.A., Junqueira, A.C., da Silva, F.M., Pinto, A.Y., Naiff, R.D., Campaner, M., Coura, J.R., Camargo, E.P., Miles, M.A., Teixeira, M.M., 2009b. Trypanosoma cruzi in Brazilian Amazonia: lineages TCI and TCIIa in wild primates, *Rhodnius* spp. and in humans with Chagas disease associated with oral transmission. Int. J. Parasitol. 39 (5), 615–623.

Miles, M.A., Cedillos, R.A., Povoa, M.M., de Souza, A.A., Prata, A., Macedo, V., 1981. Do radically dissimilar *Trypanosoma cruzi* strains (zymodemes) cause Venezuelan and Brazilian forms of Chagas' disease? Lancet 1 (8234), 1338–1340.

Monteiro, W.M., Magalhaes, L.K., de Sa, A.R., Gomes, M.L., Toledo, M.J., Borges, L., Pires, I., Guerra, J.A., Silveira, H., Barbosa, M., 2012. *Trypanosoma cruzi* IV causing outbreaks of acute Chagas disease and infections by different haplotypes in the Western Brazilian Amazonia. PLoS One 7 (7), e41284.

Moraes, C.B., Giardini, M.A., Kim, H., Franco, C.H., Araujo-Junior, A.M., Schenkman, S., Chatelain, E., Freitas-Junior, L.H., 2014. Nitroheterocyclic compounds are more efficacious than CYP51 inhibitors against *Trypanosoma cruzi*: implications for Chagas disease drug discovery and development. Sci. Rep. 4, 4703.

Moreno, M., D'Avila, D.A., Silva, M.N., Galvao, L.M., Macedo, A.M., Chiari, E., Gontijo, E.D., Zingales, B., 2010. *Trypanosoma cruzi* benznidazole susceptibility in vitro does not predict the therapeutic outcome of human Chagas disease. Mem. Inst. Oswaldo Cruz 105 (7), 918–924.

Murcia, L., Carrilero, B., Muñoz, M.J., Iborra, M.A., Segovia, M., 2010. Usefulness of PCR for monitoring benznidazole response in patients with chronic Chagas disease: a prospective study in a non-disease-endemic country. J. Antimicrob. Chemother. 65 (8), 1759–1764.

Noireau, F., Diosque, P., Jansen, A.M., 2009. *Trypanosoma cruzi*: adaptation to its vectors and its host. Vet. Res. 40 (2), 26.

PAHO, 2008. Chagas Disease (American Trypanosomiasis). Pan American Health Organization Web site, 2008. Available online: http://www.paho.org/english/ad/dpc/cd/chagas.htm (Last accessed 11.11.15.).

Perez, E., Monje, M., Chang, B., Buitrago, R., Parrado, R., Barnabe, C., Noireau, F., Breniere, S.F., 2013. Predominance of hybrid discrete typing units of *Trypanosoma cruzi* in domestic *Triatoma infestans* from the Bolivian Gran Chaco region. Infect. Genet. Evol. 13, 116–123.

Perez, C.J., Lymbery, A.J., Thompson, R.C., 2014. Chagas disease: the challenge of polyparasitism? Trends Parasitol. 30 (4), 176–182.

Perez-Molina, J.A., Poveda, C., Martinez-Perez, A., Guhl, F., Monge-Maillo, B., Fresno, M., Lopez-Velez, R., Ramirez, J.D., Girones, N., 2014. Distribution of *Trypanosoma cruzi* discrete typing units in Bolivian migrants in Spain. Infect. Genet. Evol. 21, 440–442.

Poveda, C., Fresno, M., Girones, N., Martins-Filho, O.A., Ramirez, J.D., Santi-Rocca, J., Marin-Neto, J.A., Morillo, C.A., Rosas, F., Guhl, F., 2014. Cytokine profiling in Chagas disease: towards understanding the association with infecting *Trypanosoma cruzi* discrete typing units (a BENEFIT TRIAL sub-study). PLoS One 9 (3), e91154.

Ramírez, J.D., Guhl, F., Rendón, L.M., Rosas, F., Marin-Neto, J.A., Morillo, C.A., 2010. Chagas cardiomyopathy manifestations and *Trypanosoma cruzi* genotypes circulating in chronic chagasic patients. PLoS Negl. Trop. Dis. 4 (11), e899.

Ramirez, J.D., Guhl, F., Messenger, L.A., Lewis, M.D., Montilla, M., Cucunuba, Z., Miles, M.A., Llewellyn, M.S., 2012. Contemporary cryptic sexuality in *Trypanosoma cruzi*. Mol. Ecol. 21 (17), 4216–4226.

Ramirez, J.D., Montilla, M., Cucunuba, Z.M., Florez, A.C., Zambrano, P., Guhl, F., 2013. Molecular epidemiology of human oral Chagas disease outbreaks in Colombia. PLoS Negl. Trop. Dis. 7 (2), e2041.

Sanchez, L.V., Bautista, D.C., Corredor, A.F., Herrera, V.M., Martinez, L.X., Villar, J.C., Ramirez, J.D., 2013. Temporal variation of *Trypanosoma cruzi* discrete typing units in asymptomatic Chagas disease patients. Microbes Infect. 15 (10–11), 745–748.

Schmunis, G.A., Yadon, Z.E., 2010. Chagas disease: a Latin American health problem becoming a world health problem. Acta Trop. 115 (1–2), 14–21.

Teston, A.P., Monteiro, W.M., Reis, D., Bossolani, G.D., Gomes, M.L., de Araujo, S.M., Bahia, M.T., Barbosa, M.G., Toledo, M.J., 2013. In vivo susceptibility to benznidazole of *Trypanosoma cruzi* strains from the western Brazilian Amazon. Trop. Med. Int. Health 18 (1), 85–95.

Venegas, J., Diaz, F., Rojas, T., Miranda, S., Jercic, M.I., Gonzalez, C., Conoepan, W., Vargas, A., Pichuantes, S., Gajardo, M., Rodriguez, J., Sanchez, G., 2013. Microsatellite loci-based distribution of *Trypanosoma cruzi* genotypes from Chilean chronic Chagas disease patients and *Triatoma infestans* is concordant with a specific host-parasite association hypothesis. Acta parasitol. 58 (2), 139–148.

Yeo, M., Acosta, N., Llewellyn, M., Sanchez, H., Adamson, S., Miles, G.A., Lopez, E., Gonzalez, N., Patterson, J.S., Gaunt, M.W., de Arias, A.R., Miles, M.A., 2005. Origins of Chagas disease: didelphis species are natural hosts of *Trypanosoma cruzi* I and armadillos hosts of *Trypanosoma cruzi* II, including hybrids. Int. J. Parasitol. 35 (2), 225–233.

Zafra, G., Mantilla, J.C., Jacome, J., Macedo, A.M., Gonzalez, C.I., 2011. Direct analysis of genetic variability in *Trypanosoma cruzi* populations from tissues of Colombian chagasic patients. Hum. Pathol. 42 (8), 1159–1168.

Zingales, B., Miles, M.A., Campbell, D.A., Tibayrenc, M., Macedo, A.M., Teixeira, M.M.G., Schijman, A.G., Llewellyn, M.S., Lages-Silva, E., Machado, C.R., Andrade, S.G., Sturm, N.R., 2012. The revised *Trypanosoma cruzi* subspecific nomenclature: rationale, epidemiological relevance and research application. Infect. Genet. Evol. 12 (2), 240–253.

Zingales, B., 2009. A new consensus for *Trypanosoma cruzi* intraespecific nomenclature: second revision meeting recomends TcI to TcVI. Mem. Inst. Oswaldo Cruz 104.

Zingales, B., Miles, M.A., Moraes, C.B., Luquetti, A., Guhl, F., Schijman, A.G., Ribeiro, I., 2014. Drug discovery for Chagas disease should consider *Trypanosoma cruzi* strain diversity. Mem. Inst. Oswaldo Cruz 109 (6), 828–833.